TRANSPORTATION RESEARCH RECORD 1043

Pavement System Analysis

TRB
TRANSPORTATION RESEARCH BOARD
NATIONAL RESEARCH COUNCIL
WASHINGTON, D.C. 1985

Transportation Research Record 1043
Price $18.40
Editor: Elizabeth W. Kaplan
Compositor: Harlow A. Bickford
Layout: Betty L. Hawkins

modes
1 highway transportation
4 air transportation

subject areas
24 pavement design and performance
40 maintenance
62 soil foundations

Transportation Research Board publications are available by ordering directly from TRB. They may also be obtained on a regular basis through organizational or individual affiliation with TRB; affiliates or library subscribers are eligible for substantial discounts. For further information, write to the Transportation Research Board, National Research Council, 2101 Constitution Avenue, N.W., Washington, D.C. 20418.

Printed in the United States of America

Library of Congress Cataloging-in-Publication Data
National Research Council. Transportation Research Board.

Pavement system analysis.

(Transportation research record ; 1043)
1. Pavements–Performance. 2. Pavements–Design and construction. I. National Research Council (U.S.). Transportation Research Board. II. Series.
TE7.H5 no. 1043 380.5 s 86-8788
[TE251.5] [625.8]
ISBN 0-309-03959-2 ISSN 0361-1981

Sponsorship of Transportation Research Record 1043

GROUP 2–DESIGN AND CONSTRUCTION OF TRANSPORTATION FACILITIES
Robert C. Deen, University of Kentucky, chairman

Pavement Management Section
W. Ronald Hudson, University of Texas at Austin, chairman

Committee on Rigid Pavements
Richard A. McComb, Federal Highway Administration, chairman Ernest J. Barenberg, William E. Brewer, Larry Joe Burton, Albert J. Bush III, Richard N. Cochrane, Bert E. Colley, Raymond A. Forsyth, Ray H. Fowler, James L. Greene, Yang H. Huang, Michael P. Jones, Walter P. Kilareski, T. J. Larsen, B. Frank McCullough, Dennis W. Miller, John Minor, Robert G. Packard, Surendra K. Saxena, Gary Wayne Sharpe, Joe P. Sheffield, William A. Yrjanson

Committee on Flexible Pavements
R. G. Hicks, Oregon State University, chairman
James A. Sherwood, Federal Highway Administration, secretary
R. N. Doty, David C. Esch, Wade L. Gramling, Douglas I. Hanson, Newton C. Jackson, Dallas N. Little, Dennis B. Luhrs, J. W. Lyon, Jr., Joe P. Mahoney, Adrian Pelzner, William A. Phang, James A. Scherocman, James F. Shook, Eugene L. Skok, Jr., Herbert F. Southgate, William T. Stapler, Harvey J. Treybig, Harry H. Ulery, Jr., Cecil J. Van Til, Loren M. Womack, Richard J. Worch

Committee on Strength and Deformation Characteristics of Pavement Sections
Amir N. Hanna, Portland Cement Association, chairman
Gilbert Y. Baladi, Richard D. Barksdale, Stephen F. Brown, George R. Cochran, Billy G. Connor, Gaylord Cumberledge, Jacob Greenstein, Jim W. Hall, Jr., R. G. Hicks, Mario S. Hoffman, Ignat V. Kalcheff, William J. Kenis, Thomas W. Kennedy, Erland Lukanen, Michael S. Mamlouk, Lufti Raad, J. Brent Rauhut, Quentin L. Robnett, Gary Wayne Sharpe, James F. Shook, Eugene L. Skok, Jr., R. N. Stubstad, Marshall R. Thompson, Mian-Chang Wang

Lawrence F. Spaine, Transportation Research Board staff

Sponsorship is indicated by a footnote at the end of each paper. The organizational units, officers, and members are as of December 31, 1984.

NOTICE: The Transportation Research Board does not endorse products or manufacturers. Trade and manufacturers' names appear in this Record because they are considered essential to its object.

Contents

Addresses of Authors

Al-Sanad, Hasan, Department of Civil Engineering, Kuwait University, Kuwait
Anderson, D. A., Pennsylvania Transportation Institute, Pennsylvania State University, University Park, Pa. 16802
Anderson, Mark, Transportation Research Program, University of Kentucky, Lexington, Ky. 40506-0043
Barenberg, E. J., Department of Civil Engineering, University of Illinois at Urbana-Champaign, Urbana, Ill. 61801
Bissada, Amir F., Department of Civil Engineering, Kuwait University, Kuwait
Brown, Danny, Pavement & Physical Research Branch, Office of Materials and Research, Georgia Department of Transportation, 15 Kennedy Drive, Forest Park, Ga. 30050
Carmichael, R. F. III, ARE, Inc., 2600 Dellana Lane, Austin, Tex. 78746
Chua, Koon Meng, Texas Transportation Institute, Texas A&M University, College Station, Tex. 77843
Deen, Robert C., Transportation Research Program, University of Kentucky, Lexington, Ky. 40506-0043
Elliott, Robert P., Department of Civil Engineering, University of Arkansas, Fayetteville, Ark. 72701
George, K. P., Department of Civil Engineering, University of Mississippi, University, Miss. 38677
Gulden, Wouter, Pavement & Physical Research Branch, Office of Materials and Research, Georgia Department of Transportation, 15 Kennedy Drive, Forest Park, Ga. 30050
Husain, Shakir, Department of Civil Engineering, University of Mississippi, University, Miss. 38677
Ioannides, A. M., Department of Civl Engineering, University of Illinois at Urbana-Champaign, Urbana, Ill. 61801
Jackson, Newton, Washington State Department of Transportation, Highway Administration Building, Olympia, Wash. 98504
Khedr, Safwan, Department of Civil Engineering, University of Kansas, Lawrence, Kans. 66045
Kilareski, W. P., Pennsylvania Transportation Institute, Pennsylvania State University, University Park, Pa. 16802
Lary, Jo A., Dames & Moore, 155 N.E. 100th Street, Seattle, Wash. 98125
Lee, Clyde E., Department of Civil Engineering, University of Texas at Austin, Austin, Tex. 78712
Lytton, Robert L., Texas Transportation Institute, Texas A&M University, College Station, Tex. 77843
Mahoney, Joe P., Department of Civil Engineering, University of Washington, Seattle, Wash. 98105
Mamlouk, Michael S., Department of Civil Engineering, Arizona State University, Tempe, Ariz. 85287
McCullough, B. Frank, Center for Transportation Research, University of Texas at Austin, Austin, Tex. 78712-1075
Ozbeki, Mohammed A., Department of Civil Engineering, Pennsylvania State University, University Park, Pa. 16802
Perl, Mordechai, Department of Mechanical Engineering, Technion-Israel Institute of Technology, Haifa, Israel
Roberts, Freddy L., Texas Transportation Institute, Texas A&M University, College Station, Tex. 77843
Rosson, Barry T., Ellisor and Tanner, Inc., 12750 Merit Drive, Dallas, Tex. 75251
Saraf, Chhote L., Center for Transportation Research, University of Texas at Austin, Austin, Tex. 78712-1075
Shankar, P. R., Department of Civil Engineering, University of Texas at Austin, Austin, Tex. 78712
Sharma, Jay, Department of Civil Engineering, University of Washington, Seattle, Wash. 98105
Sharpe, Gary W., Transportation Research Program, University of Kentucky, Lexington, Ky. 40506-0043
Sides, Arieh, Department of Civil Engineering, Technion-Israel Institute of Technology, Haifa, Israel
Southgate, Herbert F., Transportation Research Program, University of Kentucky, Lexington, Ky. 40506-0043
Stuart, E., Geotechnical and Materials Technology Section, U.S.D.A. Forest Service, Pleasant Hills, Calif. 94523
Thompson, Marshall R., Department of Civil Engineering, University of Illinois at Urbana-Champaign, Urbana, Ill. 61801
Uzan, Jacob, Department of Civil Engineering, Technion-Israel Institute of Technology, Haifa, Israel
Wang, M. C., Department of Civil Engineering, Pennsylvania State University, University Park, Pa. 16802

Evaluation Methodology for Jointed Concrete Pavements

MOHAMMED A. OZBEKI, W. P. KILARESKI, and D. A. ANDERSON

ABSTRACT

Many Interstate and other major highways that were constructed with jointed portland cement concrete pavements have reached their design life and consequently are deteriorating significantly. Few transportation agencies have an effective method for evaluating the structural adequacy of transverse joints. Most pavement rehabilitation programs now under way are based on subjective engineering judgment. A more objective evaluation procedure is presented. A newly developed finite element program, JSLAB, was used in a parametric study to determine which variables have the most significant effect on the performance of transverse joints. It was concluded that the variables that most significantly affect pavement deflections and stresses are the modulus of subgrade reaction and the modulus of dowel-concrete interaction. On the basis of this study, it was concluded that a rigid pavement system can be structurally evaluated if the modulus of subgrade reaction and the dowel-concrete modulus are known. Charts were developed to determine these moduli and subsequently to evaluate in-service pavements.

Many of the Interstate and other major highways in the United States were constructed with jointed portland cement concrete (PCC) pavements. Although these pavements have provided good serviceability, the design life of many of them has been exceeded and they have deteriorated significantly. In most cases the predominant distress associated with these pavements is the deterioration of the transverse joints rather than of the slab itself. Spalling, cracking, and faulting are the most serious types of distress found at the joints.

Many transportation agencies do not have an effective method for evaluating the structural adequacy of transverse joints. Most of the pavement rehabilitation programs now under way were undertaken on the basis of subjective engineering judgment. Typically an engineer will "walk" a project to determine the type of repairs or rehabilitation needed. The engineer will visually select the joints that should be removed and the joints that should remain in place. This type of evaluation can lead to the removal of sound joints or the acceptance of joints that are deteriorated. Without the proper evaluation of each joint it is difficult to select the appropriate rehabilitation procedure. Because repair and rehabilitation of major highways across the nation are important from an economic as well as an engineering point of view, a more objective scheme must be used to evaluate the condition of joints and their expected future performance.

The purpose of ths paper is to discuss the development of a methodology for evaluating the structural behavior of jointed concrete with a nondestructive testing device (NDT). A newly developed finite element computer program, JSLAB, was used for the analysis of the rigid pavement joints.

PCC EVALUATION REQUIREMENTS

There are several repair or rehabilitation schemes available for PCC pavements. They include resealing of joints, partial concrete removal and patching, joint removal and replacement, subsealing, overlays, and complete reconstruction. The selection of the wrong rehabilitation scheme will result in a loss of both time and money because the repairs may not perform for the expected design period or because a repair scheme may be selected that is not needed. Deterioration of the transverse joints contributes most to the poor performance of PCC pavements; therefore, an effective evaluation methodology must address the condition of these joints.

Spalling and cracking at joints is of concern to engineers; however, faulting of the slabs is the largest contributor to the loss of serviceability of a PCC pavement. This faulting can be due to a loss of subgrade support (voids) or deterioration of the load transfer system, or both. An evaluation methodology should be able to distinguish the various causes of deterioration because the rehabilitation scheme is different for each type of distress. For example, subsealing is needed to correct a loss of subgrade support, whereas establishment of load transfer is required for a deteriorated load transfer system.

FINITE ELEMENT MODEL

Most jointed PCC pavements are analyzed and designed by assuming continuous slabs that are infinite in length. Different types of joints with various load transfer systems will affect, in different ways, the structural response of jointed concrete pavements under the applied load. Therefore, any structural model used for design or analysis should consider the entire pavement structure with all its components, such as joints, load transfer systems, subbase support, and loading configuration. It should also consider loss of subgrade support, nonuniform slab thickness, and nonuniform subgrade modulus.

A number of finite element models have been developed for the analysis of concrete pavement systems. These may be divided into the following major classes: plane-strain models, three-dimensional models, and slab models. The most desirable model for concrete pavement analysis is probably the three-dimensional one in which the geometry of the entire system can be taken into consideration. There are computer programs that employ three-dimensional finite element models, such as the SAP program de-

veloped by Wilson (1), but the amount of input and the computational costs required to use these programs make them impractical.

The two-dimensional plane-strain representation of the concrete pavement system is rather simplistic. The pavement system is represented as a transverse slice of pavement with a unit thickness. These models, because of their simplifying assumptions, are not suited to the analysis of such concrete pavement features as joints, cracks, and load transfer devices.

The slab models are based on the classical theory of a medium-thick plate supported by a Winkler foundation. Slab models have been developed by Tabatabaie and Barenberg (2), Huang and Wang (3,4), and Bhatia (5). Although a number of structural models have been available for the analysis of concrete pavement systems, none of these contains all of the features that are essential to adequate representation of the pavement system.

The finite element model used in this study is called JSLAB. It was developed by Tayabji and Colley at the Construction Technology Laboratory, a division of the Portland Cement Association. The JSLAB program has many practical features and has the ability to allocate stiffness parameters to the load transfer device (LTD). Thus LTD stiffness allocation is not done at each set of nodes along a joint as is the case with programs such as ILLI-SLAB (1) and the program developed by Huang and Wang (3,4). This feature is useful for the analysis of jointed slabs with nonuniformly spaced LTDs at joints.

The specific capabilities of JSLAB are

1. Stresses and deflections in concrete pavement sections of up to nine slabs with longitudinal and transverse joints can be determined;
2. A two-layer system, in which the layers may be bonded or unbonded, can be analyzed;
3. Load transfer can be modeled with dowels, aggregate interlock, or keys;
4. Concrete pavement slabs with full or partial subgrade contact can be analyzed, and the effect of thermal gradients on curling stresses can be analyzed, both independently and in combination with traffic loads; and
5. The effect of joints with nonuniformly spaced load transfer devices can be analyzed.

The JSLAB finite element model (6,7) is represented by an assemblage of subdivided or discrete bodies called finite elements. These elements are interconnected at specified locations that are called nodes or nodal points. Simple functions are chosen to approximate the distribution of displacements over each finite element. These assumed functions are called displacement functions or shape functions and are used to express continuous displacements in terms of discrete nodal displacements. Relationships are then established between nodal displacement (u) and nodal forces (p) applied at the nodes using the principle of virtual work or some other variational principle. These element force-displacement relationships are expressed in the form of an element stiffness matrix (k), which incorporates the material and geometric properties of the element, namely,

$$[k]\{u\} = \{p\} \tag{1}$$

where {u} is element displacement and {p} is element applied force.

The overall or global structural stiffness matrix [K] for the entire system is formulated by superimposing the individual element stiffness matrices using element connectivity properties of the structure. The overall stiffness matrix is used to assemble a set of simultaneous equations of the form:

$$[K]\{U\} = \{P\} \tag{2}$$

where

[K] = overall stiffness matrix,
{U} = global displacement, and
{P} = global applied forces.

The solution to Equation 2 results in nodal displacements for the entire system.

JSLAB COMPUTER PROGRAM

The JSLAB computer program was written in FORTRAN for a CDC computer. The program was modified for use on an IBM computer, to include graphic capabilities. The input to the program is

1. Geometry of the concrete slab, stabilized base or overlay, and load transfer system;
2. Elastic properties of the concrete slab, stabilized base or overlay, load transfer system, and subgrade; and
3. Loading configuration.

The output given by the program is

1. Dowel shear and moment at each node along the joint (for nondoweled joints this output is omitted);
2. Stresses in the concrete pavement, stabilized base, or overlay;
3. Deformations of the pavement system, which consist of vertical deflection and rotation; and
4. Applied loads, which consist of vertical components of applied load and moments about the x- and y-axis, respectively, at each node.

Because JSLAB is a relatively new program, a comparison was made of the results obtained from the program and those obtained from other solutions. Interior stresses and edge and corner deflections were calculated using JSLAB and Westergaard's equations (8) as follows:

$$\sigma = 0.275\,(1+\nu)\,(P/h^2)\left\{4[\log(\ell/b)] + 1.069\right\} \tag{3}$$

$$\Delta = (1/6^{1/2})\,(1 + 0.4\,\nu)\,(P/k\ell^2) \quad \text{(edge deflection)} \tag{4}$$

$$\Delta = (P/k\ell^2)\,[1.1 - 0.88\,(a/\ell)] \quad \text{(corner deflection)} \tag{5}$$

where

σ = maximum stress under the load;
Δ = maximum deflection under the load;
P = applied load;
a = radius of a circular loaded area;
b = $(1.6a^2 + H^2 - 0.675h)^{1/2}$, for a < 1.724h;
b = a, for a > 1.724h;
k = modulus of subgrade support;
ℓ = radius of relative stiffness of the pavement with respect to subgrade given by $\ell = 4[Eh^3/12(1-\nu^2)K]$;
h = thickness of the concrete slab;
E = modulus of elasticity of the concrete slab; and
ν = Poisson's ratio of the concrete slab.

A comparison of the stresses and deflections obtained from the JSLAB program and Westergaard's equation is shown in Figure 1. The solid line in the figure represents Westergaard's exact solution,

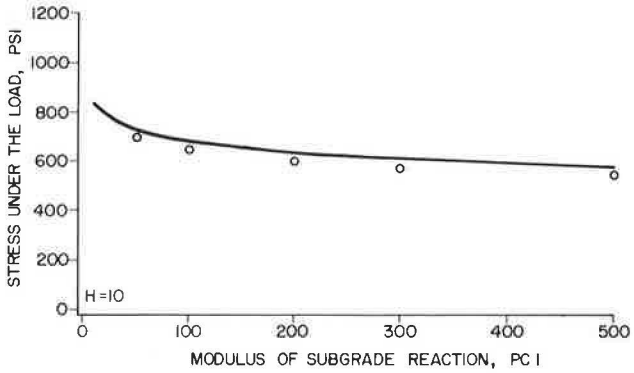

FIGURE 1 Comparison of finite element solutions and Westergaard's equation for interior loading.

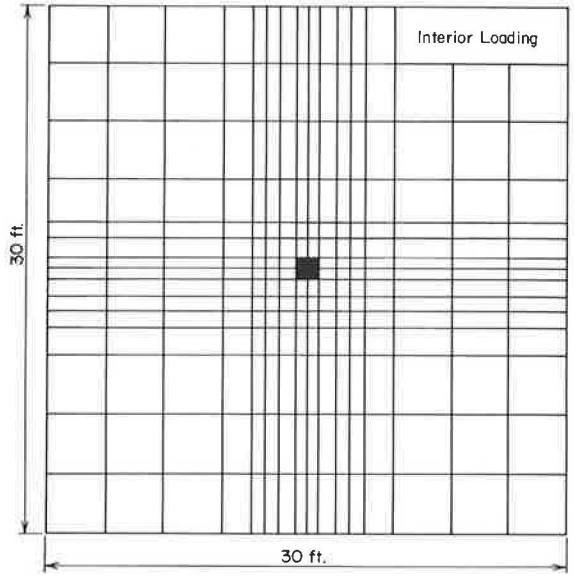

FIGURE 2 Slab used in finite element analysis.

while the small circles represent the finite element solutions. Because Westergaard's exact solutions are for an infinite slab, a large 30-ft (9.14-m) square slab (Figure 2) was used in the finite element analysis. Westergaard assumed that the load was distributed uniformly over the area of a small circle. The loaded area for Westergaard's solution, therefore, was assumed to be a circle with a diameter of 15 in. (38.10 cm), and a 15-in. (38.10-cm) square was selected to represent the loading condition in the finite element analysis. A single load of 50 kips (222 kN) was used for the loading configurations. Figure 2 also shows the mesh of the finite element models used in this comparison. The modulus of elasticity and the Poisson's ratio of the concrete slab were assumed to be 5×10^6 psi (34.5 GPa) and 0.15, respectively. The comparison was made for a slab thickness of 10 in. (25.4 cm) and five moduli of subgrade reaction: 50, 100, 200, 300, and 500 pci (13.6, 27.1, 54.3, 81.4, and 135.7 N/cm^3).

The agreement between the results obtained with JSLAB and those obtained with Westergaard's equation was quite good. In general the differences between the two solutions were small as shown in Figure 1 for an interior load. Corner and edge loading cases also have the same results.

PARAMETRIC STUDY OF PCC PAVEMENT PROPERTIES

A parametric study was conducted to determine the influence of selected design variables on the structural response of a typical jointed pavement as constructed in Pennsylvania. The responses, which were calculated using JSLAB, were the surface deflection of the loaded slab along the transverse joint, and the tensile bending stresses in the concrete under the tire along the longitudinal x-axis. The influence of the design variables on the efficiency of the transverse joint was also studied. Joint efficiency was defined as the vertical deflection of Point B divided by the vertical deflection of Point A (Figure 3).

The loading used in the parametric study consisted of an 18-kip single-axle truck. (This was the truck configuration used at the Pennsylvania Transportation Research Facility.) The contact area of the tire was converted to a uniformly loaded area with a tire pressure of 80 psi (9).

The following jointed pavement system, which is typical of pavements constructed in Pennsylvania in the 1960s, was used as a reference in the parametric study:

Slab thickness = 10 in. (25.4 cm)
Concrete modulus of elasticity = 4,500,000 psi (31.0 GPa)
Modulus of subgrade reaction = 200 pci (54.2 N/cm^3)
Poisson's ratio of concrete = 0.20
Twelve uniformly spaced dowels
Dowel diameter = 1 1/4 in. (3.2 cm)
Dowel spacing = 12 in. (30.5 cm)

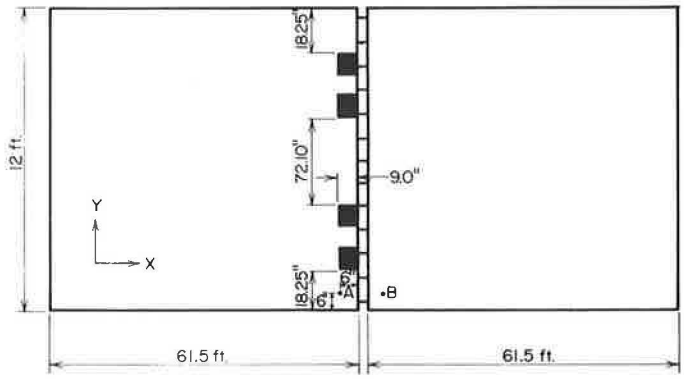

FIGURE 3 Loading configuration used in the parametric study.

Modulus of dowel-concrete interaction = 2 million pci (542.8 kN/cm³)
Dowel modulus of elasticity = 29 million psi (199.8 GPa)
Poisson's ratio of dowel material (steel) = 0.30
Joint opening = 0.25 in. (6.4 mm)
Slab length = 61.5 ft (18.7 m)

In considering the effect of a particular design variable, only one of the input values was changed while all other design variables were kept constant. The results are discussed in the following sections.

Dowel Size

The dowel diameters considered were 3/4, 1, 1 1/4, and 1 1/2 in. (19, 25.4, 32, and 38 mm). As shown in Figures 4(a) and 4(c), dowel diameter has no major influence on corner deflection and joint efficiency. However, larger dowel sizes increase the tensile bending stresses along the x-axis (longitudinal) in the vicinity of the joint, as shown in Figure 4(b). However, it can be shown that larger dowel size decreases the stresses along the y-axis (transverse), which is the critical stress in this case.

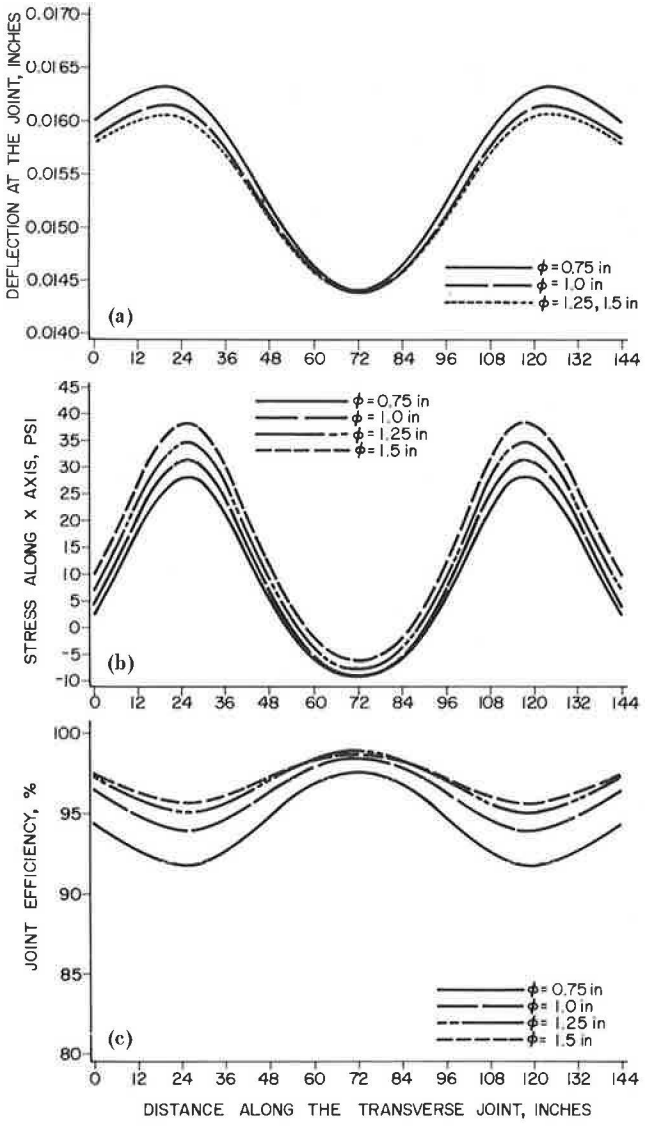

FIGURE 4 Effect of dowel diameter on pavement response: (a) deflection at the joint under the tires, (b) stresses along the x-axis under the tires, and (c) percentage joint efficiency.

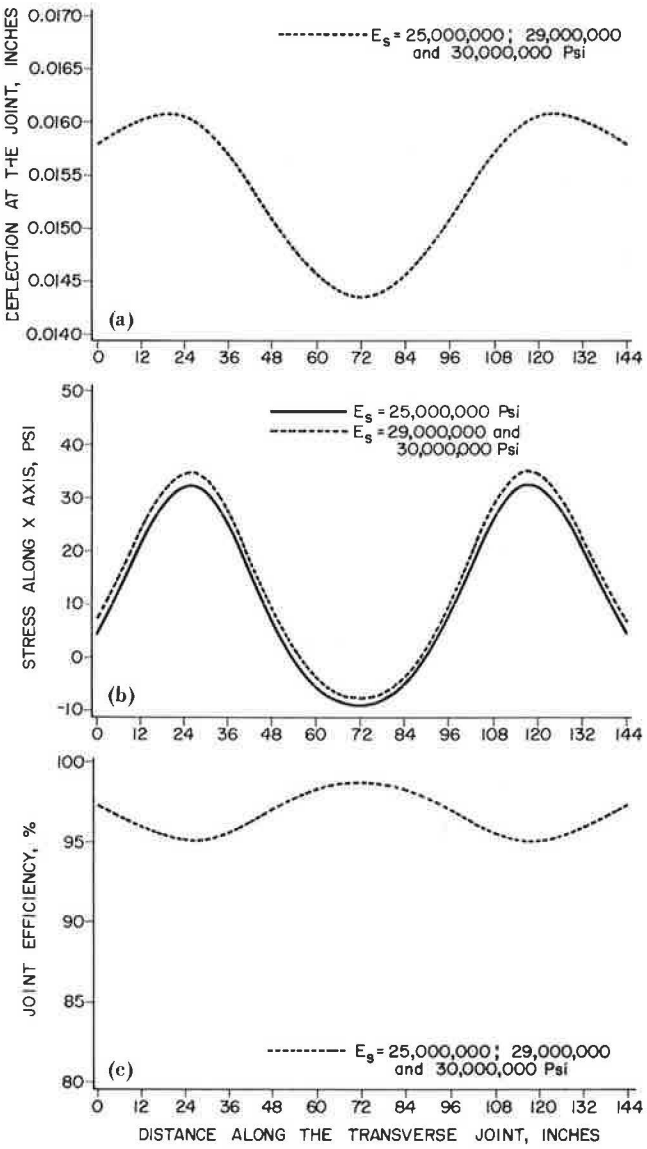

FIGURE 5 Effect of dowel modulus of elasticity on pavement response: (a) deflection at the joint under the tires, (b) stresses along the x-axis under the tires, and (c) percentage joint efficiency.

Dowel Modulus of Elasticity

The dowel modulus of elasticity values considered were 25×10^6, 29×10^6, and 30×10^6 psi (172.25, 199.8, and 206.7 GPa). As shown in Figure 5, responses are essentially the same in all cases.

Joint Width

The joint widths considered were 0.1, 0.2, 0.25, and 0.5 in. (2.5, 5.1, 6.4, and 12.3 mm). It was found that corner deflections, tensile bending stresses, and joint efficiencies are the same in all four cases.

Concrete Modulus of Elasticity

The concrete modulus of elasticity values considered were 4×10^6, 4.5×10^6, and 5×10^6 psi (27.6, 31.0,

and 41.4 GPa). The tensile stresses along the x-axis and the joint efficiency are relatively unaffected by these changes in modulus. As the modulus increases, the deflection decreases slightly. However, this decrease in deflection is not significant because the variation is less than 5 percent.

Modulus of Subgrade Reaction

The modulus of subgrade reaction values considered were 100, 200, 300, and 500 pci (27.2, 54.2, 81.6, and 135.5 N/cm³). As shown in Figure 6, as the modulus of subgrade reaction increases, the corner deflection of the pavement slabs decreases significantly. This increase in subgrade reaction does not significantly change the tensile bending stresses along the x-axis, as shown in Figure 6(b). Joint efficiencies do vary, however, as shown in Figure 6(c).

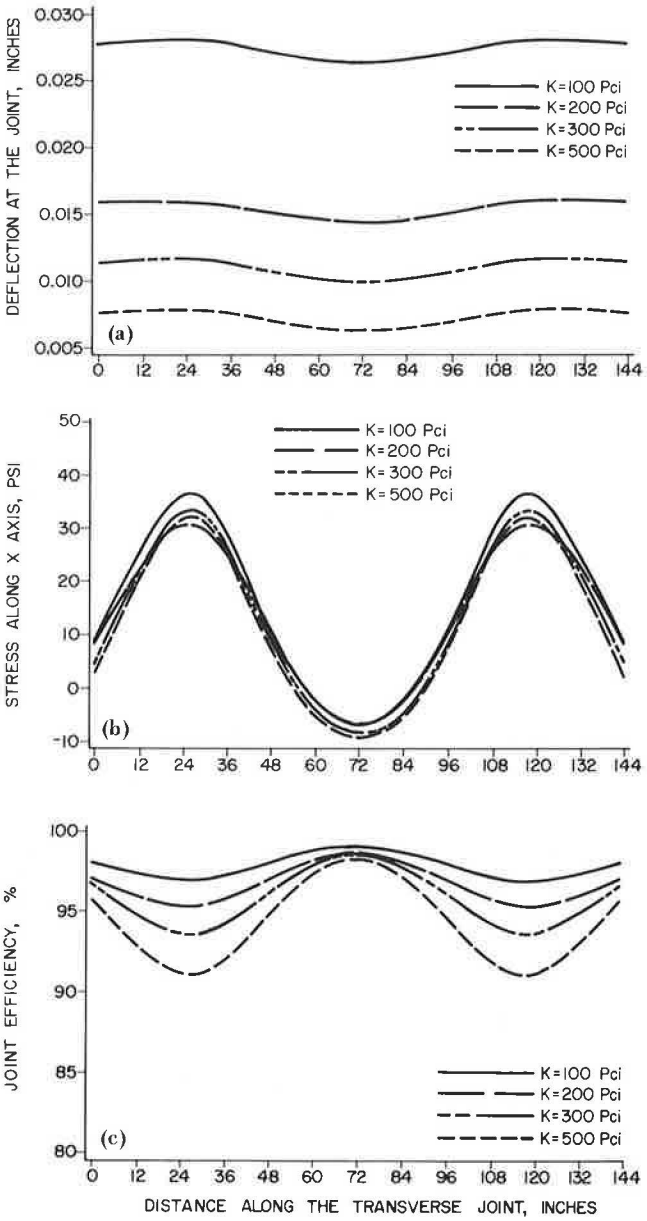

FIGURE 6 Effect of modulus of subgrade reaction on pavement response: (a) deflection at the joint under the tires, (b) stresses along the x-axis under the tires, and (c) percentage joint efficiency.

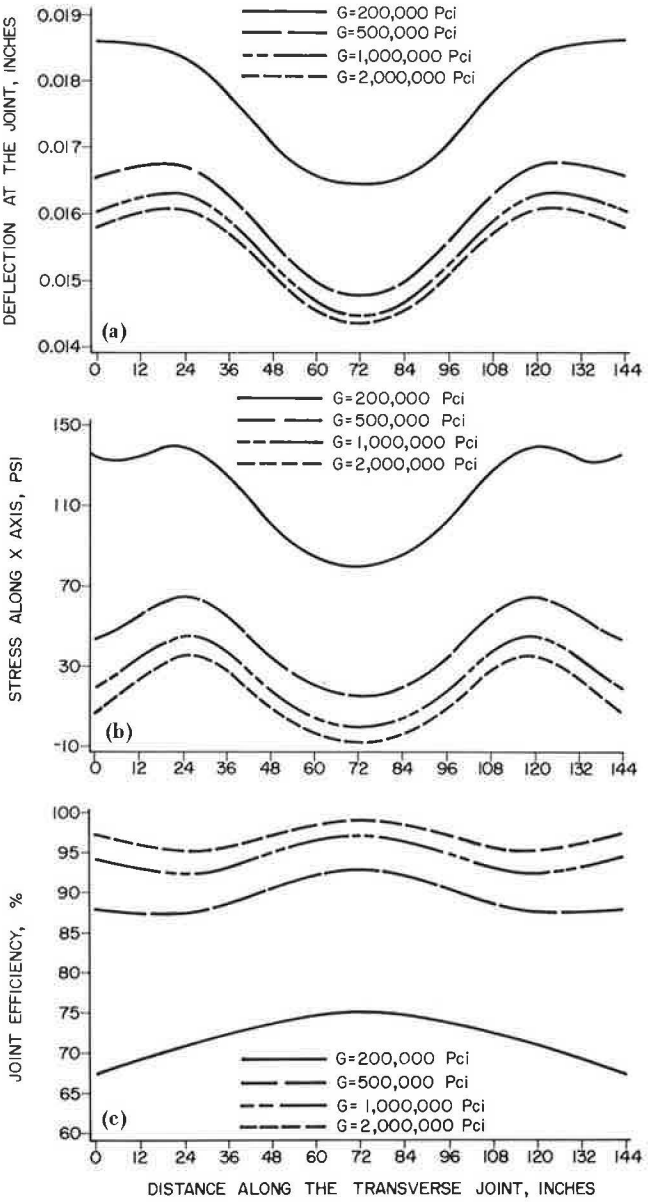

FIGURE 7 Effect of modulus of dowel-concrete interaction on pavement response: (a) deflection at the joint under the tires, (b) stresses along the x-axis under the tires, and (c) percentage joint efficiency.

Modulus of Dowel-Concrete Interaction

The modulus values of dowel-concrete interaction considered were 2×10^5, 5×10^5, 10×10^5, and 20×10^5 pci (54.3, 135.7, 271.4, and 678.6 kN/cm³). As shown in Figure 7, the effect of these changes in modulus is significant for all of the structural responses. It should be noted that many researchers assume a value of 1.5×10^6 pci (407.1 kN/cm³) for the modulus of dowel-concrete interaction. In this analysis the modulus values covered a wide range. The significance of the change in modulus will be discussed in detail later.

It was concluded that the variables that appreciably affect calculated pavement response are the modulus of subgrade reaction (k) and the modulus of dowel-concrete interaction (G). The influence of these parameters on pavement behavior was studied further.

SENSITIVITY ANALYSIS FOR MODULUS OF SUBGRADE REACTION AND MODULUS OF DOWEL-CONCRETE INTERACTION

The parametric study showed that a loss in the modulus of subgrade reaction (low k) or a loss in the modulus of dowel-concrete interaction (low G) can increase pavement deflections and stresses enough to cause deterioration and eventual failure of the joint system. Therefore a sensitivity analysis was conducted to determine the effect of variations in k and G on the corner deflection of the pavement slab (the deflection at Point A shown in Figure 3) and joint efficiency (the deflection at Point B divided by the deflection at Point A). These responses were chosen because they are easily obtained with an NDT device such as the Road Rater, falling weight deflectometer, or Benkelman beam. Thus the theoretical analysis can be verified by field measurements.

For the pavement system analyzed, surface deflections and joint efficiencies were computed by varying one modulus (k or G) while keeping the other constant. All other parameters and the loading configuration were kept the same as for the typical pavement section defined in the previous section.

Figures 8 and 9 show, respectively, the absolute deflection and the joint efficiency versus the modulus of dowel-concrete interaction (G) for four different moduli of subgrade reaction (k): 200, 300, 400, and 500 pci (54.4, 81.6, 108.8, and 135.5 N/cm³). As shown in these figures, for all practical cases in which the pavement support is in good condition, the change in pavement response becomes insignificant for values of G greater than approximately 200,000 pci (54.3 kN/cm³). A pavement is considered to have a good support condition when k is greater than 200 pci (10). However, the response of the pavement changes appreciably for values of G less than 200,000 pci (54.30 kN/cm³). Therefore the limiting criterion selected for the modulus of dowel-concrete interaction, for pavements with good support (k > 200 pci), was 200,000 pci (54.30 kN/cm³).

It can also be seen in Figures 8 and 9 that the changes in pavement deflections and joint efficiencies become insignificant for values of k greater than 200 pci (54.4 N/cm³) as long as the load transfer is adequate (G > 200,000 pci). Thus the limiting criterion selected for the modulus of subgrade reaction was 200 pci (54.4 N/cm³).

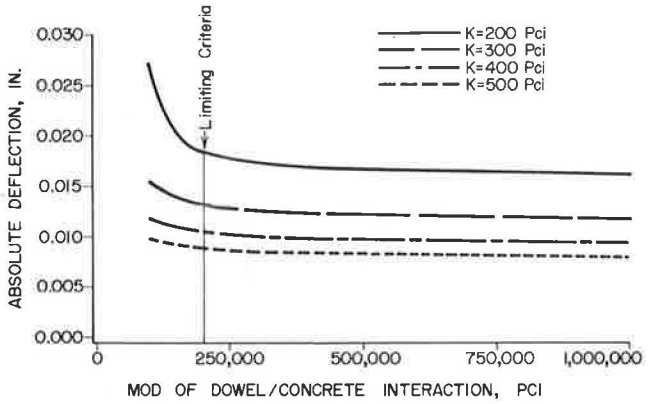

FIGURE 8 Variation of surface deflection at the joint 6 in. (15.24 cm) from the shoulder with the modulus of dowel-concrete interaction.

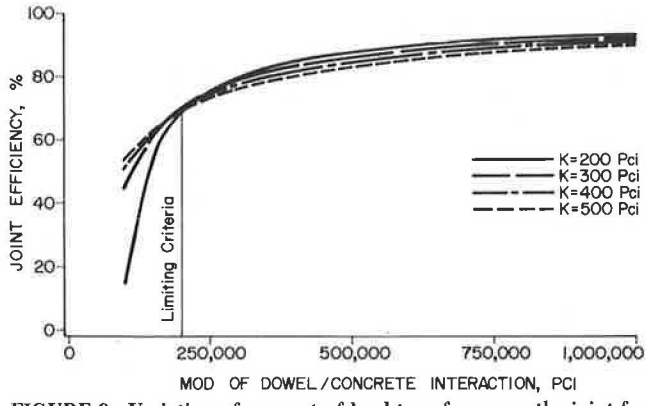

FIGURE 9 Variation of amount of load transfer across the joint for first dowel from the shoulder with modulus of dowel-concrete interaction.

EVALUATION PROCEDURE

From the sensitivity analysis it was concluded that a rigid pavement system can deteriorate if it loses its subgrade support (k < 200 pci) or if the dowel bar loses its interaction with the surrounding concrete. Therefore the condition of the joints in a rigid pavement can be established only if both the modulus of subgrade reaction and the modulus of dowel-concrete interaction are known. The ability to distinguish between the loss of subgrade support and the loss of dowel-concrete interaction is important in the selection of rehabilitation treatments. A loss of subgrade support can be repaired by subsealing, but a loss of dowel-concrete interaction requires the reestablishment of load transfer. The wrong repair scheme wastes money and will not extend the serviceability of the pavement.

Figures 10 and 11 were developed from the results of the sensitivity analysis for the purpose of determining these moduli and subsequently evaluating the condition of in-service joints. Although these figures can be combined, they have been separated for ease of explanation. For any given combination of joint efficiency and corner deflection there is a unique value of k and G. These values, computed with the JSLAB program, have been plotted in Figures 10 and 11 on isobars of k and G, respectively. Figure 10 shows the joint efficiency versus the surface deflection at Point A (shown in Figure 3) for seven different moduli of subgrade reaction (k): 100, 200, 300, 400, 500, 600, and 700 pci (27.20, 54.4, 81.60, 108.80, 135.5, 163.2, and 190.4 N/cm³).

Similarly, Figure 11 shows the joint efficiency versus the corner deflection of the same Point A for eight different moduli of dowel-concrete interaction (G): 0.1×10^6, 0.15×10^6, 0.175×10^6, 0.20×10^6, 0.25×10^6, 0.50×10^6, 0.75×10^6, and 1.00×10^6 pci (27.14, 40.7, 47.5, 54.2, 67.85, 135.70, 203.55, and 407.10 kN/cm³). This figure, which is based on the same data shown in Figure 10, can be used to determine whether the load transfer system (G) is adequate. Figures 10 and 11 can be used to estimate k and G, however, only if both the corner deflection and the efficiency of the joint have been measured. This evaluation technique differs from that used in most evaluation programs, in which only the relative deflection across the joint is measured. As a consequence, the two parameters, the modulus of subgrade reaction and the modulus of dowel-concrete interaction, can be estimated from these figures for a particular joint and then compared with the limiting values to determine whether the joint is structurally adequate.

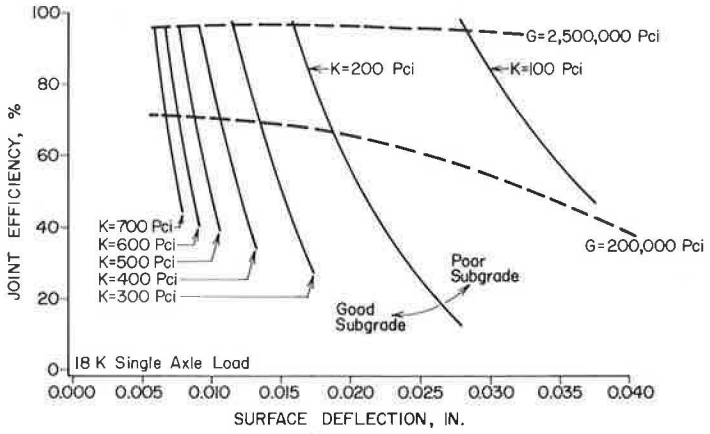

FIGURE 10 Joint efficiency versus surface deflection for various modulus values of subgrade reaction while modulus of dowel-concrete interaction is varied.

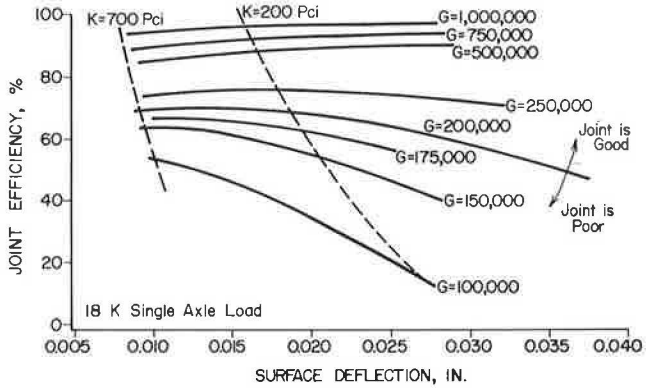

FIGURE 11 Joint efficiency versus surface deflection for various modulus values of dowel-concrete interaction while modulus of subgrade reaction is varied.

SUMMARY AND CONCLUSIONS

The methodology outlined here can be used to evaluate the condition of the subgrade support and the load transfer devices in a jointed concrete pavement. The methodology makes use of deflection measurements taken at the slab corners under an 18-kip (80-kN) single axle load. The absolute deflection and the relative deflection at the joint are required in order to predict the modulus of subgrade reaction (k) and the modulus of dowel-concrete interaction (G). A value of k less than 200 pci indicates a poor subgrade, and a value of G less than 200,000 pci indicates a poor joint system. Separating the evaluation of subgrade support and joint efficiency will help determine whether subsealing or joint replacement, or both, are required for the rehabilitation scheme.

The following conclusions have been drawn:

1. The JSLAB finite element program is a practical model of a jointed concrete pavement system. It can be used to calculate the stresses and deflections in a pavement system under realistic loading conditions. The model can be used to analyze joints that are doweled, keyed, or have an aggregate interlock.
2. The parametric study showed that the variations in the modulus of subgrade reaction and the modulus of dowel-concrete interaction have the most significant effect on changes in stresses and deflections in a jointed pavement system.
3. When the modulus of dowel-concrete interaction is 200,000 pci (54.3 kN/cm³) or less, the deflections of the pavement increase significantly and therefore the stresses in the pavement increase significantly.
4. The modulus of subgrade reaction and the modulus of dowel-concrete interaction can be predicted from deflection measurements at the corners of the pavement slab. Two measurements are required: the absolute deflection of the loaded slab and the relative deflection on either side of the joint.

ACKNOWLEDGMENT

This paper is based on "Fourth Cycle of Pavement Research at the Pennsylvania Transportation Research Facility," Research Project 82-11, sponsored by the Pennsylvania Department of Transportation in cooperation with the Federal Highway Administration.

REFERENCES

1. E.L. Wilson. Solid SAP, A Static Analysis Program for Three Dimensional Solid Structures. SESM 71-69. Structural Engineering Laboratory, University of California, Berkeley, 1969.
2. A.M. Tabatabaie and E.J. Barenberg. Finite-Element Analysis of Jointed or Cracked Concrete Pavements. In Transportation Research Record 671, TRB, National Research Council, Washington, D.C., 1978, pp. 11-17.
3. Y.H. Huang and S.T. Wang. Finite-Element Analysis of Concrete Slabs and Its Implication for Rigid Pavement Design. In Highway Research Record 466, HRB, National Research Council, Washington, D.C., 1973, pp. 55-69.
4. Y.H. Huang and S.T. Wang. Finite-Element Analysis of Rigid Pavements with Partial Subgrade Contact. In Highway Research Record 485, HRB, National Research Council, Washington, D.C., 1974, pp. 39-54.
5. A.S. Bhatia. Mathematical Modeling for Design of Pavements and Highway Systems. Ph.D. dissertation. Ohio State University, University Park, 1978.

6. R.D. Cook. Concepts and Applications of Finite Element Analysis. John Wiley and Sons, Inc., New York, 1981.
7. J.S. Przemieniecki. Theory of Matrix Structural Analysis. McGraw-Hill Book Company, New York, 1968.
8. H.M. Westergaard. Stresses in Concrete Pavements Computed by Theoretical Analysis. Public Roads, Vol. 7, No. 2, 1926.
9. Load Stresses at Pavement Edge: A Supplement to Thickness Design for Concrete Pavements. Report 1S030P. Portland Cement Association, Skokie, Ill., 1969.
10. M.I. Darter. Design of Zero-Maintenance Plain Jointed Concrete Pavement, Vol. 1: Development of Design Procedures. Report FHWA-RD-77-111. FHWA, U.S. Department of Transportation, 1977.

This study was sponsored by the Pennsylvania Department of Transportation and the Federal Highway Administration. The contents of this paper reflect the views of the authors, who are responsible for the facts and the accuracy of the data. The contents do not necessarily reflect the official views or policies of the sponsors.

Publication of this paper sponsored by Committee on Rigid Pavements.

Controlling Longitudinal Cracking in Concrete Pavements

CHHOTE L. SARAF and B. FRANK McCULLOUGH

ABSTRACT

The objective of the study reported in this paper was to investigate the development of longitudinal cracks in wide concrete pavements (two or more lanes in one direction) and to develop a model to estimate the depth of saw cut needed to control these cracks within the groove. The model developed uses the concepts of variability in the material properties of the concrete (tensile strength), pavement thickness (as constructed in the field), and depth of saw-cut groove. It was observed that estimates of longitudinal cracking have a reasonable match with field observations. It was observed that the longitudinal cracking of concrete pavements (two or more lanes in one direction) was dependent on the type of aggregate used in the concrete mix. Two types of aggregates were investigated. Uniformity of concrete mix strength (tensile) represented by standard deviation (tensile strength) affected the development of longitudinal cracks. A lower value of standard deviation obtained for concrete mix using lime rock aggregate in the mix was responsible for confining more cracks within the saw cut compared with the mix using river gravel aggregate. A sensitivity analysis of the model indicated that substantial reduction in saw-cut depth can be achieved if the variability of concrete strength during construction can be reduced.

Wide concrete pavements (two or more lanes in one direction) will develop longitudinal cracks due to shrinkage of concrete soon after it is poured. The repair of these cracks is difficult and expensive, especially when they are spalled. The presence of these cracks in pavement is unsightly. Therefore longitudinal joints at reasonable spacing (12 ft or one lane wide) are provided to encourage development of controlled cracks along these joints.

Longitudinal joints are generally formed by cutting a groove in the green concrete with a power saw. Adequate depth of saw cut must be provided to ensure that the longitudinal cracks will be confined within the groove. This provides an aesthetically acceptable regular longitudinal joint in the pavement at a low maintenance cost.

The performance of any saw-cut joint depends on its depth. An inadequate depth of saw cut may result in the development of longitudinal cracks away from the groove. These cracks eventually will spall and require expensive repair and maintenance.

The objective of this study was to investigate the development of longitudinal cracks in concrete pavements and to develop a model to estimate the depth of saw cut needed to control these cracks within the groove.

DEVELOPMENT OF LONGITUDINAL CRACKS ALONG THE SAW-CUT GROOVE

Let us assume that a wide concrete pavement is constructed with a saw cut, as shown in Figure 1. Fur-

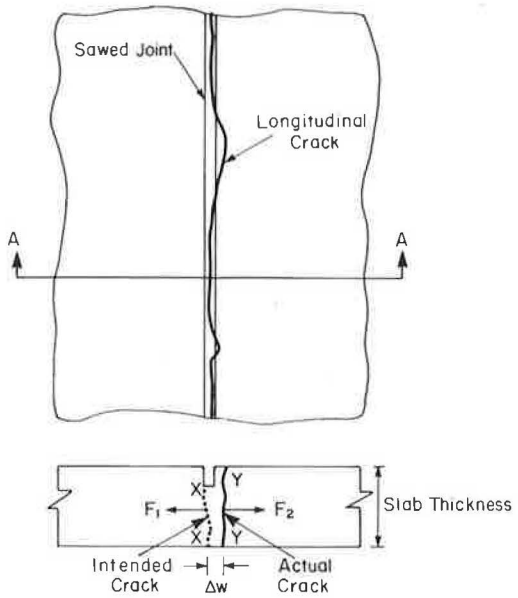

FIGURE 1 Concrete pavement with saw-cut joint and longitudinal crack.

ther, let us assume that, due to shrinkage of concrete, longitudinal cracks developed in the pavement as shown in Figure 1. This figure represents a typical longitudinal cracking pattern that was observed in a concrete pavement constructed in the Houston, Texas, area. The field observations of these cracks indicated that there were no cracks along the saw-cut joint where a longitudinal crack had occurred away from the saw cut (Figure 1).

Let us consider a cross section of this pavement along A-A (Figure 1). If the resultant tensile forces along x-x and y-y are, respectively, F_1 and F_2, then, just before cracking occurs along y-y,

$$F_1 \approx F_2 \qquad \text{if the distance } \Delta W \text{ is small} \tag{1}$$

The tensile forces F_1 and F_2 are resisted by the tensile strengths of the pavement sections along x-x and y-y. The tensile strength can be estimated by

$$T_1 = D_1 \cdot b \cdot t_1 \tag{2}$$

$$T_2 = D_2 \cdot b \cdot t_2 \tag{3}$$

where

T_1, T_2 = tensile strengths of pavement sections along x-x and y-y, respectively;
D_1, D_2 = depths of pavement sections along x-x and y-y, respectively;
b = assumed width of pavement sections; and
t_1, t_2 = unit tensile strength of concrete along sections x-x and y-y, respectively.

If the pavement section cracks along y-y, then $F_2 > T_2$ and $T_1 > F_1$ (because the section did not crack along x-x), but $F_1 \approx F_2$ (Equation 1). Therefore it is evident that if the section along y-y cracked, the tensile strength of concrete along x-x (T_1) should be greater than the tensile strength of concrete along y-y (T_2). Or $T_1 > T_2$ or $T_1/T_2 > 1.0$. Similarly, if cracking occurs along x-x, then $T_1/T_2 \leq 1.0$.

If the ratio T_1/T_2 is represented by R, then to develop a longitudinal crack along the saw cut (x-x), the following condition must exist:

$$R \leq 1.0 \tag{4}$$

Using this condition for cracking along x-x, it is now possible to estimate the probability of cracking along this section. This probability can be represented by

$$P[R \leq 1.0] \tag{5}$$

where P[R] represents the probability of the variable R.

An estimate of the probability represented by Equation 5 provides an assessment of the amount of cracking along x-x (saw cut).

STATISTICAL MODEL TO ESTIMATE THE PROBABILITY OF R FOR ($R \leq 1.0$)

The probability of the variable R, P[R] can be estimated if the distribution of R can be established. To determine the distribution of R, the following procedure is followed.

Because R is the ratio of T_1/T_2 as indicated earlier (Equation 4), the following expressions can be written:

$$R = T_1/T_2 \tag{6}$$

$$= (D_1 \cdot b \cdot t_1)/(D_2 \cdot b \cdot t_2) \qquad \text{(see Equations 2 and 3)}$$

$$= (D_1 \cdot t_1)/(D_2 \cdot t_2) \tag{7}$$

Taking the natural log (ln) of both sides of this equation gives

$$\ln R = \ln D_1 + \ln t_1 - \ln D_2 - \ln t_2 \tag{8}$$

Assume that D_1, D_2, t_1, and t_2 are independent random variables such that $\ln D_1$, $\ln D_2$, $\ln t_1$, and $\ln t_2$ are normally distributed. Then the variable ln R, which is a linear combination of four normally distributed variables (Equation 8), is also normally distributed with mean and standard deviations as indicated:

$$\text{Mean of } \ln R = \overline{RL} = \overline{DL1} + \overline{tL1} - \overline{DL2} - \overline{tL2} \tag{9}$$

$$\text{S.D. of } \ln R = \sigma_{RL} = (\sigma^2_{DL1} + \sigma^2_{tL1} + \sigma^2_{DL2} + \sigma^2_{tL2})^{1/2} \tag{10}$$

(assuming independence of $\ln D_1$, $\ln D_2$, $\ln t_1$, and $\ln t_2$)

where

$\overline{DL1}, \overline{DL2}, \overline{tL1}, \overline{tL2}$ = mean values of $\ln D_1$, $\ln D_2$, $\ln t_1$, and $\ln t_2$, respectively, and
$\sigma^2_{DL1}, \sigma^2_{DL2}, \sigma^2_{tL1}, \sigma^2_{tL2}$ = variances of $\ln D_1$, $\ln D_2$, $\ln t_1$, and $\ln t_2$, respectively.

Equations 9 and 10 fully describe the distribution parameters of ln R. Therefore the probability of R for ($R \leq 1.0$) can now be redefined as

$$P[R \leq 1.0] = P[\ln R \leq 0.0] \tag{11}$$

This probability can be estimated with the help of the standard parameter Z [Z is N(0,1)], where the parameter Z is defined as

$$Z = (\ln R - \overline{RL})/\sigma_{RL}$$

or

$$Z = (0 - \overline{RL})/\sigma_{RL} \quad \text{(if the probability for } \ln R \leq 0 \text{ is estimated)} \tag{12}$$

A standard table of normal distribution (1) can be used to estimate the desired probability.

VERIFICATION OF THE MODEL

Data from two projects were obtained to verify the crack prediction model described. The observed cracking along the saw-cut joint was estimated by measuring the total length of cracks in the saw-cut joint and expressing it as a percentage of total saw-cut joint length on the project. Figure 2 shows the locations of these projects. Brief descriptions of these projects follow.

Project 1

Project 1 is located near Houston, Texas, on TX-288 (inside the I-610 loop), as shown in Figure 2. About 2 mi of continuously reinforced concrete pavement (CRCP) were installed with a saw-cut joint at the center of a 24-ft-wide pavement. River gravel was used in the concrete mix for this project.

About 69 percent of the saw-cut joint developed longitudinal cracks. The remaining 31 percent of the cracks were observed to have developed away from the groove.

Project 2

This project is also located near Houston, Texas, on TX-288 (outside the I-610 loop), as shown in Figure 2. About 20 mi of CRCP were installed with a saw-cut joint at the 1/4 point of a 48-ft-wide pavement (a construction joint was at the center). Limestone aggregate was used in the concrete mix for this project.

About 99 percent of the saw-cut joint developed longitudinal cracks. The remaining 1 percent of the cracks was observed to have developed away from the groove.

Pavement cores 4 in. in diameter were obtained from both projects to measure the variations in thicknesses and tensile strengths along the saw-cut joint as well as away from but within about 2 ft of the joint. A summary of the test results is given in Table 1. Using these data, the probability of cracking along the saw-cut joint is calculated as follows:

Estimate of longitudinal cracks along saw-cut joint: Project 1

$$\overline{RL} = 1.969 + 6.369 - 2.236 - 6.269$$
$$= -0.167 \quad \text{(see Equation 9)}$$
$$\sigma_{RL} = (0.0195^2 + 0.237^2 + 0.0414^2 + 0.296^2)^{1/2}$$
$$= 0.382 \quad \text{(see Equation 10)}$$
$$Z = [0 - (-0.167)]/0.382$$
$$= 0.44 \quad \text{(see Equation 12)}$$

Using standard tables of normal distribution (1),

$$P[\ln R \leq 0] = 67 \text{ percent}$$

Therefore the estimated probability of cracking

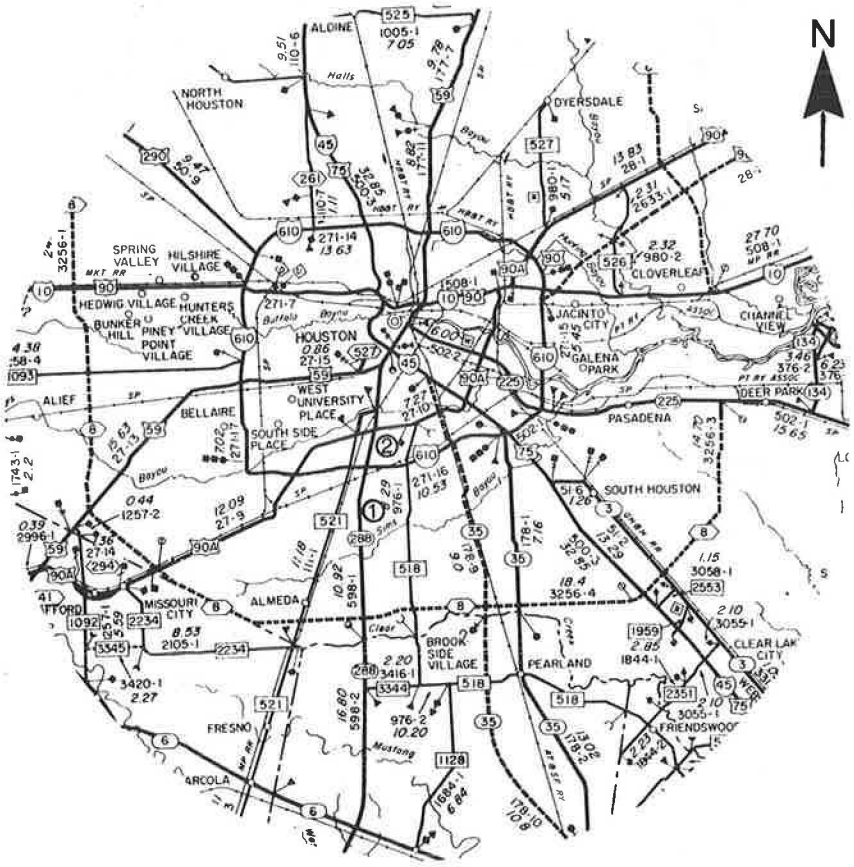

FIGURE 2 Locations of projects.

TABLE 1 Summary of Data Analysis

Project No.	Item	Original Measurements			Transformed Results Using $\log_e$	
		n	Mean	S.D.	Mean	S.D.
1	D_1	8	7.17	0.140	1.969	0.0195
	D_2	17	9.37	0.375	2.236	0.0414
	t_1	19	598	134	6.369	0.237
	t_2	34	549	147	6.269	0.296
2	D_1	6	6.39	0.195	1.854	0.0303
	D_2	13	9.19	0.200	2.218	0.0219
	t_1	12	495	90	6.188	0.188
	t_2	18	497	92	6.191	0.194

along a saw-cut joint is 67 percent. The observed cracking was 69 percent as described under Project 2. This indicates a reasonable match with the estimated value.

Project 2

$$\overline{RL} = 1.854 - 2.28 + 6.188 - 6.191$$
$$= -0.367$$
$$\sigma_{RL} = (0.0303^2 + 0.0219^2 + 0.188^2 + 0.194^2)^{1/2}$$
$$= 0.2727$$
$$Z = [0 - (-0.367)]/0.2727$$
$$= 1.346$$

Using standard tables of normal distribution, P [ln R $\leq$ 0] = 91 percent.

Therefore the estimated probability of cracking along the saw-cut joint is 91 percent. The observed cracking was 99 percent (see Project 2 description). This indicates a reasonable match with the estimated values.

IMPLEMENTATION OF THE MODEL

The model can be used to estimate the amount of longitudinal cracking that is expected to develop along the saw-cut groove, as illustrated earlier. For this purpose, the following information is obtained:

1. Mean and standard deviation of pavement thickness along the saw-cut joint and away from it and
2. Mean and standard deviation of tensile strength along the saw-cut groove and away from it.

Equations 9, 10, and 12 can be used to estimate the longitudinal cracking along the saw-cut groove, as illustrated earlier for Projects 1 and 2.

The model can also be used to determine the depth of saw-cut that would induce a specified amount of longitudinal cracking along the groove. To illustrate this, two curves were developed, as shown in Figure 3. The data obtained for two projects (described earlier) were used in these curves. These curves show the effect of depth ratio on longitudinal cracking along the saw-cut groove.

Suppose, for example, that it is desired to have at least 90 percent of the cracks confined within the saw-cut groove; then the saw-cut depths can be determined in each of the following cases:

1. Concrete mix with river gravel and
2. Concrete mix with limestone aggregate.

Using Figure 3, if 90 percent longitudinal cracks is selected, then D_1/D_2 = 56 percent (river gravel mix) and D_1/D_2 = 71 percent (limestone mix) because saw-cut depth = $D_1 - D_2 = D_2(1 - D_1/D_2)$. Therefore desired saw-cut depths are

1. River gravel mix = 0.44 D_2 and
2. Limestone aggregate mix = 0.39 D_2.

If it is assumed that D_2 = 10 in., the saw-cut depths are 4.4 and 3.9 in., respectively, for the given mixes.

DISCUSSION OF RESULTS

The results of this study are summarized in Equation 12, which makes possible the estimation of the prob-

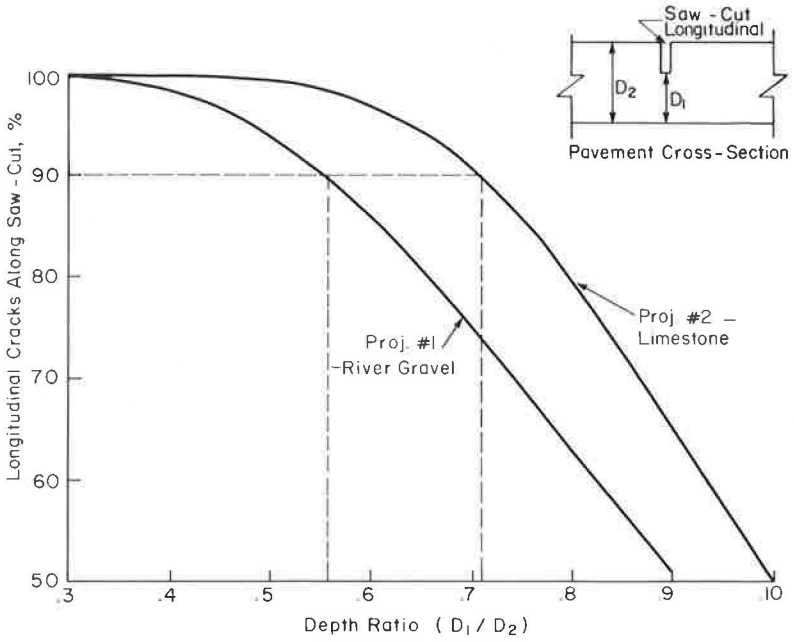

FIGURE 3 Effect of depth ratio on longitudinal cracking along saw cut.

ability of cracking along the saw-cut groove. As the value of Z increases, the probability of cracking increases (see standard table of normal distribution). Because Z is a ratio of $\overline{RL}$ and σ_{RL}, Equations 9 and 10 can be used to rewrite Equation 12 as follows:

$$Z = (\overline{DL2} + \overline{tL2} - \overline{DL1} - \overline{tL1})/[(\sigma^2_{DL1} + \sigma^2_{tL1} + \sigma^2_{DL2} + \sigma^2_{tL2})^{1/2}] \quad (13)$$

A study of Equation 13 indicates that the numerator will be largest when $\overline{DL1}$ and $\overline{tL1}$ are smallest. However, from a practical point of view, the tensile strength (tL1) alone cannot be reduced along the groove without changing tL2. Therefore the only parameter that can be controlled is $\overline{DL1}$. This means that the depth ratio (D_1/D_2) should be reduced or the saw-cut depth should be increased to increase the percentage of cracks along the groove. This is shown in Figure 3.

Alternatively, the denominator can be reduced to increase the value of Z. Because it is a combination of the variances of all four parameters (ln D_1, ln D_2, ln t_1, ln t_2), to reduce this quantity it will be necessary to obtain uniformity of thicknesses and concrete strengths (tensile) along the groove and away from the groove. If it is possible to achieve this, considerable reduction in saw-cut depth can be obtained, as shown in Figures 4 and 5. These figures were drawn for each project using the data given in Table 1 and assuming that the standard deviations are 1/2 and 1/4 of the values listed in the table.

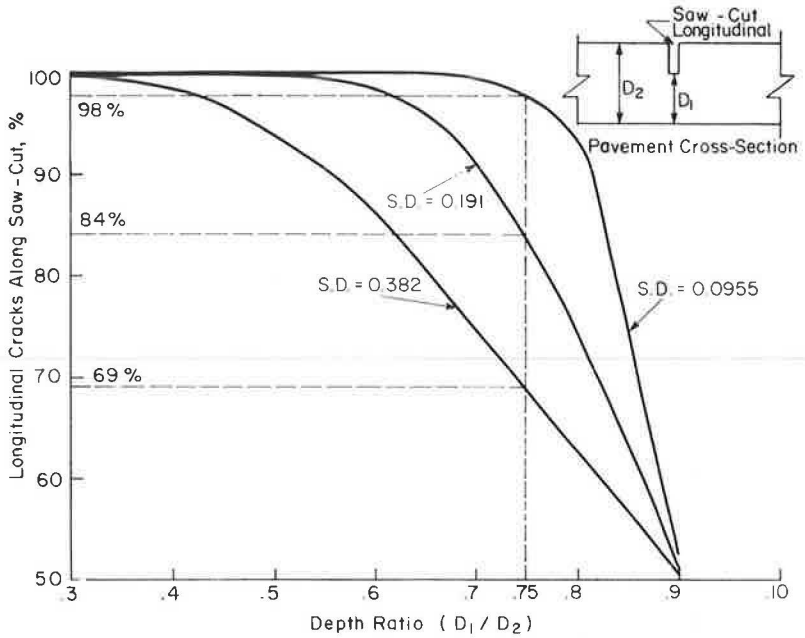

FIGURE 4 Effect of depth ratio on longitudinal cracking in river gravel mix (Project 1).

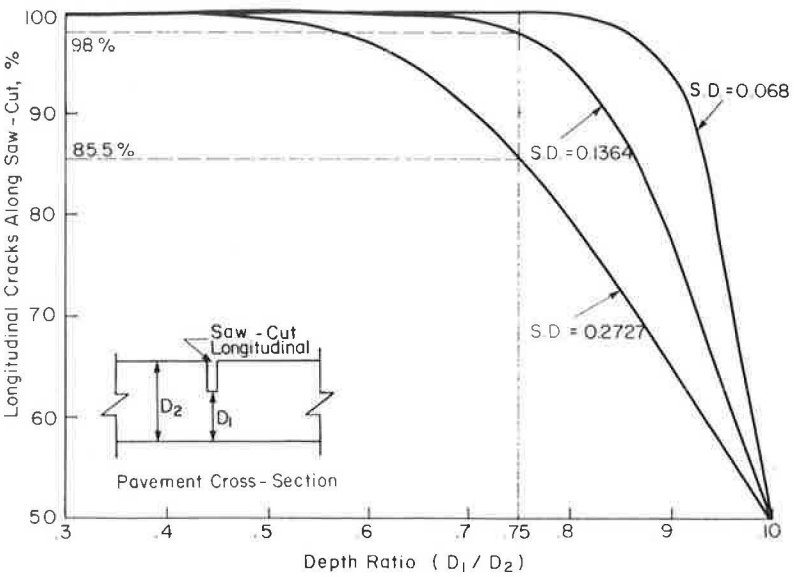

FIGURE 5 Effect of depth ratio on longitudinal cracking in limestone mix (Project 2).

It is clear from both of these figures that a substantial increase in longitudinal cracking can be obtained by reducing the standard deviation (see the examples in Figures 4 and 5 shown by a dotted line for a depth ratio = 0.75). This indicates that reasonable control of the quality of this construction material (concrete), pavement thickness, and saw-cut depth, all combined, can contribute to a reasonable saw-cut depth.

CONCLUSIONS

The results of this study can be summarized as follows:

1. The development of longitudinal cracks in a saw-cut groove can be explained by a model using the concepts of variability in concrete strength and thickness of pavement sections.
2. The model developed for this study is sensitive to the construction quality of pavement. An improvement in construction quality can result in reduction of saw-cut depths. The reliability of longitudinal cracks (being confined to saw-cut groove) is also improved. This can save construction costs as well as future maintenance and repair costs.
3. Figures 3-5 show that it is possible to induce any desired amount of longitudinal cracking along the saw-cut groove if an appropriate saw-cut depth is provided.
4. The aggregates used in concrete affect the development of longitudinal cracks along a saw-cut groove. This finding is based on a study of two aggregates (river gravel and limestone).

ACKNOWLEDGMENTS

The authors are pleased to acknowledge the combined efforts and support of the Center for Transportation Research at the University of Texas at Austin and the Texas State Department of Highways and Public Transportation, in cooperation with the FHWA, U.S. Department of Transportation.

REFERENCE

1. J.R. Benjamin and C.A. Cornell. Probability Statistics and Decision for Civil Engineers. McGraw-Hill Book Company, New York, 1970.

Publication of this paper sponsored by Committee on Rigid Pavements.

Westergaard Solutions Reconsidered

A. M. IOANNIDES, M. R. THOMPSON, and E. J. BARENBERG

ABSTRACT

The pioneering analytical work of Harold Malcom Westergaard (1888-1950) has been at the heart of slab-on-grade pavement design since the 1920s. Every code of practice published since then makes reference to the "Westergaard solutions." These solutions are only available for three particular loading conditions (interior, edge, and corner) and assume a slab of infinite or semi-infinite dimensions. Since their first appearance, beginning in the early 1920s, Westergaard equations have often been misquoted or misapplied in subsequent publications. To remedy this situation, a reexamination of these solutions using the finite element method is described in this paper. A number of interesting results are presented: (a) Several equations ascribed to Westergaard in the literature are erroneous, usually as a result of a series of typographical errors or misapplications, or both. The correct form of these equations and their limitations have now been conclusively established. (b) Westergaard's original equation for edge stress is incorrect. The long-ignored equation given in his 1948 paper should be used instead. (c) Improved expressions for maximum corner loading responses have been developed. (d) Slab size requirements for the development of Westergaard responses have also been established.

The pioneering analytical work of Harald Malcom Westergaard (1888-1950) has been at the heart of slab-on-grade pavement design since the 1920s. Every code of practice published since then makes reference to the "Westergaard solutions." These solutions are only available for three particular loading conditions (interior, edge, and corner) and assume a slab of infinite or semi-infinite dimensions. In practice, the slab size required for the development of Westergaard responses is determined empirically. Several investigators, however, have noted repeatedly that although the Westergaard solution agreed fairly well with their observations for the interior loading condition, it failed to give even a close estimate of the response in the cases of edge and corner loading. The time-honored Westergaard solutions deserve a thorough reexamination using the tool of finite element analysis now available.

The highlights of an effort to reevaluate the Westergaard solutions (1) are presented. The form, theoretical background, limitations, and applicability of these equations have been examined, and what are considered to be the most accurate formulas are presented herein. Several empirical adjustments to the Westergaard solutions are also considered, and slab size requirements for the development of Westergaard responses are established.

The basic tool for this study is the ILLI-SLAB finite element computer program developed and extensively used at the University of Illinois (2). The ILLI-SLAB model is based on classical medium-thick plate theory, and employs the 4-noded, 12-degree-of-freedom plate-bending element, known in finite element literature as ACM or RPBl2 (3). The Winkler-type subgrade assumed by Westergaard is modeled as a uniform, distributed subgrade through an equivalent mass formulation (4).

INTERIOR LOADING

As defined by Westergaard, this is the case of a wheel load at a "considerable distance from the edges," with pressure "assumed to be uniformly distributed over the area of a small circle with radius a" (5). After an extensive literature survey and comparisons with finite element results (6), the following interior loading equations are considered to be in their most general form.

Maximum bending stress, σ_i

Ordinary theory

$$BSIOT = \left\{[3P(1+\mu)]/2\pi h^2\right\}\ [\ell n\ (2\ell/a) + 0.5 - \gamma] + BSI2OT \quad (1a)$$

Special theory

$$BSIST = \left\{[3P(1+\mu)]/2\pi h^2\right\}\ [\ell n\ (2\ell/b) + 0.5 - \gamma] + BSI2ST \quad (1b)$$

For square

$$BSISQ = \left\{[3P(1+\mu)]/2\pi h^2\right\}\ [\ell n\ (2\ell/c') + 0.5 - \gamma] + BSI2SQ \quad (1c)$$

Supplementary, σ_2 (ordinary theory)

$$BSI2OT = \left\{[3P(1+\mu)]/64h^2\right\}\ [(a/\ell)^2] \quad (1d)$$

Supplementary, σ_2 (special theory)

$$BSI2ST = \left\{[3P(1+\mu)]/64h^2\right\}\ [(b/\ell)^2] \quad (1e)$$

Supplementary, σ_2 (for square)

$$BSI2SQ = \left\{[3P(1+\mu)]/64h^2\right\}\ [(c'/\ell)^2] \quad (1f)$$

Maximum deflection, δ_i

Circle

$$DEFIC = (P/8k\ell^2)\left\{1 + (1/2\pi)\ [\ell n\ (a/2\ell) + \gamma - 5/4]\ (a/\ell)^2\right\} \quad (1g)$$

where

P = total applied load;
E = slab Young's modulus;
μ = slab Poisson's ratio;
h = slab thickness;
k = modulus of subgrade reaction;
a = radius of circular load;
c = side length of square load;
ℓ = $\{Eh^3/[12(1-\mu^2)k]\}$ which is radius of relative stiffness;
b = $[(1.6a^2 + h^2)^{1/2}] - 0.675h$ if $a < 1.724h$
= a if $a > 1.724h$;
c' = $(e^{\pi/4-1}/2^{1/2})c$; and
γ = Euler's constant (= 0.577 215 664 90).

These equations have been incorporated into WESTER, a computerized compendium of closed-form solutions for slabs on grade, developed in the course of this research (1).

Equation 1a follows from Equation 50 given in 1939, with the term $[\ell n\ (2\ell/a) - \gamma]$ replacing the term $[\ell n\ (2\ell/\gamma a)]$ used by Westergaard (7). Note that the symbol γ as used in Equation 1a is the Euler constant, whereas Westergaard uses this symbol to denote the antilog of the Euler constant.

Equation 1a also includes supplementary stress, σ_2, first derived by Westergaard in 1939. This is calculated according to Equation 1d, which is the same as Equation 6 in "Stresses in Concrete Runways of Airports" (7). This additional term was introduced to account for the effect of the finite size of the loaded area and is "satisfactorily applicable when a does not exceed ℓ" (7). Its contribution is usually small, but it is included because of its rigorous analytical nature. The effect of the size of the loaded area will be discussed further hereafter.

Equation 1b employs Westergaard's "special theory," first proposed in 1926, in which radius b replaces the true radius, a, of the loaded area. This was introduced to account for the effect of shear stresses in the vicinity of the load, which is neglected in the "ordinary theory" of medium-thick plates. As Westergaard stated, "the effect of the thickness of the slab is equivalent to a rounding off of the peak in the diagrams of moments" (5). To determine the relation among h, a, and b, Westergaard (5) performed "numerical computations . . . in accordance with an analysis which is due to A. Nadai." Results were fitted with a hyperbola, the equation of which may be written in the form presented earlier, "which is suitable for numerical calculations" (5). The validity of Westergaard's semiempirical adjustment and of the resulting "special theory" has been debated by various investigators [see, for example, Scott (8)], but a full discussion of this issue would be beyond the scope of this paper. The authors recommend, however, using "ordinary theory" when comparisons with finite element results are made.

To obtain the interior stress in the case of a square loaded area, radius a is replaced in Equation 1-c by a constant, c', related to the length of the side of the square, c, as follows:

$$c' = (e^{\pi/4-1}/2^{1/2})\ c = 0.573804\ldots c$$

The resulting expression is not stated explicitly by Westergaard, but follows directly from his theory (9,10). Timoshenko and Woinowsky-Krieger (11) provide a theoretical justification for this substitution by showing that, loaded by the same total load P, a square side c and a circle radius a give the same maximum interior stress.

In 1948 Westergaard presented an equation for the stress under an elliptical loaded area [Equation 3 in "New Formulas for Stresses in Concrete Pavements of Airfields" (10)]. Setting both axes of the ellipse to a, this equation can be compromised with Equation 1a provided that the following assumption is made.

$$\ell n\, 2 + 1/2 - \gamma \approx 1/4\, \ell n\, 12(1 - \mu^2)$$

For $\mu = 0.15$, this assumption gives

$$0.6159316 \approx 0.6155374$$

This indicates that the term 0.6159 in Equation 9 in "Stresses in Concrete Pavements Computed by Theoretical Analysis" (5) is a truncated form of the term involving Euler's constant, not slab Poisson's ratio, μ. Equation 1a is, therefore, more general than the 1948 equation.

Equation 1g follows from Equation 51 in "Stresses in Concrete Runways of Airports" (7), described previously, with the introduction of Euler's constant. This form is more general than the one obtained from Equation 5 in "New Formulas for Stresses in Concrete Pavements of Airfields" (10), which makes the approximation noted in the previous paragraph.

Westergaard also presented an equation for supplementary stress, σ_3, to account for "the effects of a plausible redistribution" of subgrade reactions (12,7). This was a semiempirical adjustment to reduce calculated stresses so that they agreed better with the 1932 Arlington tests (13). Bergstrom et al. (14) note that "it appears advisable to neglect σ_3 in design," because it is difficult to evaluate and causes considerable reduction in stress. Further discussions of this term are presented by Bradbury (15) and Kelley (16).

Slab Size Requirements for the Development of Interior Loading Westergaard Responses

As mentioned earlier, the closed-form Westergaard solutions assume a slab of infinite dimensions, although in practice empirical guidelines have been developed for the least slab dimension, L, required to achieve the Westergaard "infinite slab" condition. In this section, analyses will be presented to establish similar guidelines using the finite element method. A slab with a radius of relative stiffness, ℓ, of 23.16 in. was used with a mesh fineness ratio (2a/h) of 1.8. An earlier study (6) indicated that this ratio of element size, 2a, divided by slab thickness, h, must be about 0.8 for 98 percent accuracy.

ILLI-SLAB results from this investigation are shown in Figure 1. Both maximum deflection and bending stress converge to large slab values. The convergence of deflection is from above, indicating that a smaller slab settles more than a bigger one in a "punch-like" fashion. Bending stress converges from below, as expected. The rate of convergence, defined as the slab size at which the solution is essentially that for an infinite slab, is different for deflection ($L/\ell = 8.0$) than for bending stress ($L/\ell = 3.5$). Surprisingly, deflection appears to be much more sensitive to slab size changes for (L/ℓ) values of less than 3, because of the previously mentioned punch-like effect. The limit value approached by maximum deflection is the Westergaard solution (Equation 1g). The value to which bending stress converges when slab size is expanded is slightly lower than Westergaard's (Equation 1a) due to the coarseness of the mesh used.

Effect of Size of Loaded Area

In his attempt to develop equations for a loaded area of finite size, Westergaard used an approach in which a solution for a point load is first derived. Then, the loaded area is split into a number of small subareas, and each subarea is replaced by a statically equivalent point load acting at its center. A summation is performed over these subareas. In the limit of refinement, this summation tends to an exact integration (17). Westergaard suggested that his equations were valid for any size of loaded

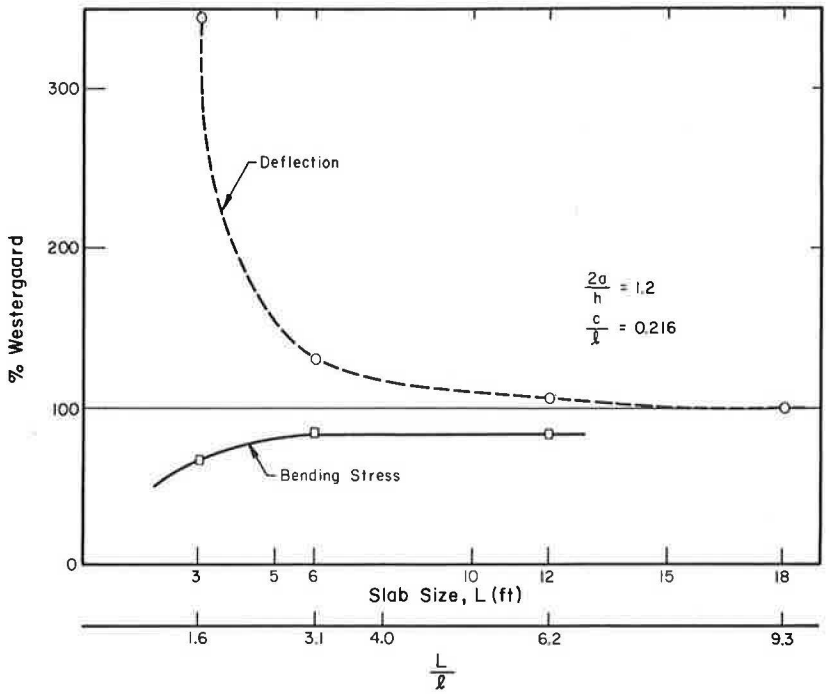

FIGURE 1 Effect of slab size on maximum interior loading responses.

area and that his "New Formulas" (10) assume that "the average width and length of the footprint of the tire is greater than the thickness of the slab in all significant cases."

Losberg (18) showed that the stress and deflection equations presented by Westergaard are only the first one or two terms of a rapidly converging infinite series. Westergaard's supplementary stress, σ_2, mentioned previously, for example, is an additional term of this series. The rate of convergence can be expected to vary depending on, among other things, the size of the loaded area.

Timoshenko and Woinowsky-Krieger (11) state that the equations apply only when the radius of the loaded area is "small in comparison with ℓ." Scott (8) attributes this restriction to the fact that "in the derivation of the equation a term of approximate value $0.1\,a^2/\ell^2$ was omitted." This cannot be the real cause of the restriction imposed by Timoshenko and Woinowsky-Krieger, because in most cases (even when the radius of the loaded area, a, is not "small in comparison with ℓ") this term is, indeed, negligible.

In this study the effect of the size of the loaded area was investigated using the finite element method. To eliminate slab size, mesh fineness, and element aspect ratio effects, a large (L/ℓ = 9.33) and fine ($2a/h$ = 0.6) mesh, which consisted of square elements (aspect ratio = 1.0), was used. The results are plotted in Figure 2.

It is observed that Westergaard stress values (Equation 1a) agree with finite element results for a loaded area whose side length, c (if square), is about 0.2 times the radius of relative stiffness, ℓ; if the load is circular, its radius, a, must be about 0.1ℓ. As (c/ℓ) or (a/ℓ) increase, finite element stresses become progressively higher than Westergaard's. Therefore the consequences of Westergaard's truncation, mentioned previously, must be borne in mind when attempting such comparisons. The results in Figure 2 also suggest an effect related to the internal finite element discretization of the applied load. This is discussed in more detail elsewhere (1).

EDGE LOADING

Westergaard defined edge loading as the case in which "the wheel load is at the edge, but at a considerable distance from any corner." The pressure is assumed to be "distributed uniformly over the area of a small semi-circle with the center at the edge" (5). Equations for a circular load at the edge were first presented in 1948 (10). The most general forms of the edge loading formulas follow.

Maximum bending stress, σ_e

Ordinary theory (semicircle)

$$BSEWOT = 0.529\,(1 + 0.54\mu)\,(P/h^2)\,[\log_{10}(Eh^3 \div ka_2^4) - 0.71] \quad (2a)$$

Special theory (semicircle)

$$BSEWST = 0.529\,(1 + 0.54\mu)\,(P/h^2)\,[\log_{10}(Eh^3 \div kb_2^4) - 0.71] \quad (2b)$$

"New" formula (circle)

$$BSEIC = [3(1+\mu)P/\pi(3+\mu)h^2]\left\{\ell n\,(Eh^3/100ka^4) + 1.84 - 4\mu/3 + [(1-\mu)/2] + 1.18\,(1+2\mu)\,(a/\ell)\right\} \quad (2c)$$

"New" formula (semicircle)

$$BSEIS = [3(1+\mu)P/\pi(3+\mu)h^2]\;[\ell n\,(Eh^3/100ka_2^4) + 3.84 - 4\mu/3 + 0.5\,(1+2\mu)\,(a_2/\ell)] \quad (2d)$$

Simplified "new" formula (semicircle)

$$BSELS = (-6P/h^2)\,(1+0.5\mu)\,[0.489\log_{10}(a_2/\ell) - 0.091 - 0.027\,(a_2/\ell)] \quad (2e)$$

Simplified "new" formula (circle)

$$BSELC = (-6P/h^2)\,(1+0.5\mu)\,[0.489\log_{10}(a/\ell) - 0.012 - 0.063\,(a/\ell)] \quad (2f)$$

Maximum deflection, δ_e

Original formula

$$DEFEW = (1/6^{1/2})\,(1+0.4\mu)\,(P/k\ell^2) \quad (2g)$$

"New" formula (circle)

$$DEFEIC = \left(\left\{P[(2+1.2\mu)^{1/2}]\right\}/[(Eh^3k)^{1/2}]\right)\,[1 - (0.76 + 0.4\mu)\,(a/\ell)] \quad (2h)$$

"New" formula (semicircle)

$$DEFEIS = \left(\left\{P[(2+1.2\mu)^{1/2}]\right\}/[(Eh^3k)^{1/2}]\right)\,[1 - (0.323 + 0.17\mu)\,(a_2/\ell)] \quad (2i)$$

Simplified "new" formula (semicircle)

$$DEFELS = (1/6^{1/2})\,(1+0.4\mu)\,(P/k\ell^2)\,[1 - 0.323\,(1+0.5\mu)\,(a_2/\ell)] \quad (2j)$$

Simplified "new" formula (circle)

$$DEFELC = (1/6^{1/2})\,(1+0.4\mu)\,(P/k\ell^2)\,[1 - 0.760\,(1+0.5\mu)\,(a/\ell)] \quad (2k)$$

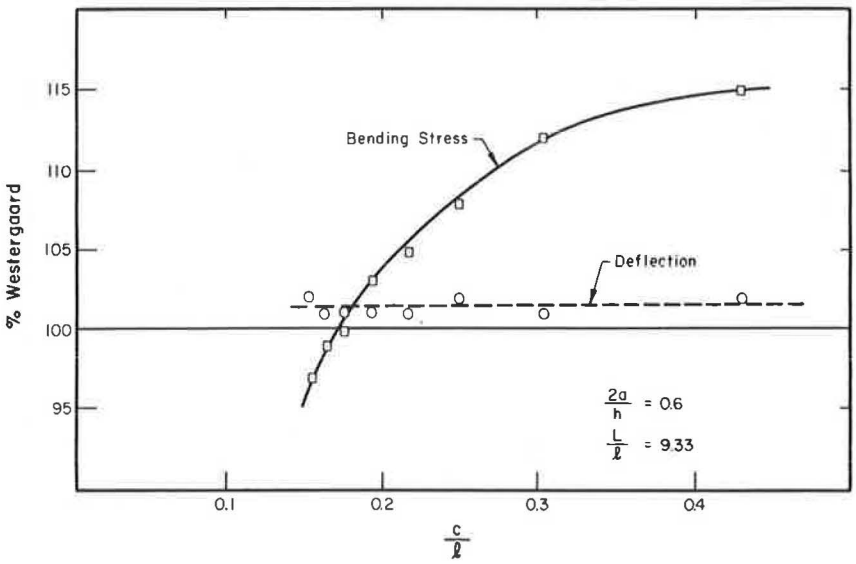

FIGURE 2 Effect of size of loaded area on maximum interior loading responses.

where

a_2 = radius of semicircle,
$b_2 = [(1.6a_2 + h^2)^{1/2}] - 0.675h$ if $a_2 < 1.724h$
$= a_2$ if $a_2 > 1.724h$, and
other symbols are as defined for Equations 1.

Equation 2a is identical to Equation 3 in "Analytical Tools for Judging Results of Structural Tests of Concrete Pavements" (12). Equation 2b employs the "special theory," which is also used for interior loading. In his 1948 paper, Westergaard (10) presented generalized solutions for maximum stress and deflection produced by elliptical and semielliptical loaded areas placed at a slab edge. Setting the lengths of both the major and minor semiaxes of the ellipse to a or a_2 leads to the corresponding solutions for a circle radius, a, or a semicircle radius, a_2, given by Equations 2c and 2d.

Losberg (18) presented simplified versions of these solutions by introducing "simplifications of the same type as Westergaard (19) himself introduced in his original formula for the case of edge loading" to eliminate the "complicated functional relationship" in which μ appears in these equations. Losberg (18) stated that his simplified equations "are well applicable, for the small μ-values here concerned." These are Equations 2e and 2f. Comparisons made during this study show that Losberg's simplified equations lead to results that are typically about 1 percent greater than those obtained by the general Equations 2c and 2d.

Equation 2g is Westergaard's original equation for edge deflection (5), and Equations 2h and 2i can be obtained from his 1948 paper (10), as indicated previously. The corresponding Losberg formulas (18) are given by Equations 2j and 2k. Setting the radius of the loaded area to zero, these formulas reduce to Equation 2g.

Alternative Westergaard Solutions

It was pointed out earlier, as well as by other investigators (14,18), that in the case of interior deflection and stress, as well as edge deflection, when the "new" formulas are specialized for a circular (or a semicircular) loaded area, they become identical to the corresponding original (5,12) equations. Results from this study show, however, that edge stresses calculated from the "new" formula are considerably different than those computed using the original formula. A number of alternative Westergaard solutions are considered in this section, in order to determine which one, if any, agrees best with finite element results.

In Table 1, five different Westergaard solutions are compared. In all of these, total applied load, P, and applied pressure, p, are matched in the Westergaard and finite element analyses. A previous study (6) confirmed that this is an appropriate representation of the square loaded area used in the finite element solution. The solutions given in Table 1 are code named WESI through WESV and were obtained using WESTER, which incorporates Equations 2.

The range of results in Table 1 is extremely wide. Therefore careful use of Westergaard's theory cannot be overemphasized. The most obvious effect is that the "new" formulas typically lead to stresses 55 percent higher and deflections 8 percent lower than the values obtained using the original formulas (compare WESIV with WESIII).

A comparison of WESIV and WESV indicates that the semicircular load is more severe than the circular load (i.e., leads to higher stresses and deflections), as expected. If both the circular and the semicircular loads are reduced to an equivalent point load acting at the respective center of gravity, this expectation is shown to be justified because the center of gravity of the circle is further toward the interior of the slab than is that of the semicircle.

This argument also leads to the conclusion that the difference in response from a circular and a semicircular load should be fairly small and proportional to the difference in the distance between the respective centers of gravity and the slab edge. The difference between WESIV and WESV stresses is about 1 percent, and deflection difference is about 5 percent. These differences are much more compatible with expected values than is the stress difference obtained using the original equation (compare WESI and WESIII).

Table 2 gives a comparison of WESV, ILLI-SLAB, and H-51 results. The latter is a computerized version of the Pickett and Ray (20) chart for edge loading (21). Stresses exhibit almost perfect agreement even at low (L/ℓ) values. Deflections are more sensitive to slab size effects, as shown in Figure 3. This graph shows that an (L/ℓ) value of about 5.0 is required for the development of Westergaard stresses and about 8.0 is required for Westergaard deflections. The trends shown in Figure 3 are similar to those observed for the interior condition. Note, however, that the requirement for the development of maximum edge stress ($L/\ell = 5.0$) is higher than for maximum interior stress ($L/\ell = 3.5$). The excellent agreement between ILLI-SLAB and H-51 results and the "new" formula confirms Losberg's observation that "the original formula for edge loading according to Westergaard (5) is, at least from a theoretical viewpoint, completely erroneous."

TABLE 1 Alternative Westergaard Solutions

Run No.	k (psi/in.)	h (in.)	Deflection, δ_e (mils)					Bending Stress, σ_e (psi)				
			WESI	WESII	WESIII	WESIV	WESV	WESI	WESII	WESIII	WESIV	WESV
1	50	12	112.7	Same as WESI		104.8	99.7	758	661	638	992	980
2	200	12	56.4			50.8	47.3	638	541	519	831	822
3	500	12	35.7			31.3	28.4	559	462	440	726	720
4	50	16	73.2			69.0	66.4	468	413	401	615	607
5	200	16	36.6			33.7	31.8	401	346	334	524	517
6	500	16	23.2			20.8	19.4	357	302	289	464	459
7	50	20	52.4			49.8	48.2	320	281	277	422	417
8	200	20	26.2			24.4	23.3	277	238	234	363	359
9	500	20	16.6			15.2	14.3	249	210	206	325	321

Note: WESI = Westergaard's original equations for circular "ordinary" theory, WESII = Westergaard's original equations for semicircular "special" theory, WESIII = Westergaard's original equations for semicircular "ordinary" theory, WESIV = "New" formulas for semicircular "ordinary" theory, and WESV = "New" formulas for circular "ordinary" theory. See Table 2 for other parameters used.

TABLE 2 Comparison with "New" Edge Loading Formulas

Run No.	k (psi/in.)	h (in.)	(L/ℓ)	Deflection, δ_e WESV (mils)	Deflection, δ_e ILLI-SLAB (mils)	Deflection, δ_e ILLI-SLAB WESV	Bending Stress, σ_e WESV (psi)	Bending Stress, σ_e ILLI-SLAB (psi)	Bending Stress, σ_e H-51 (psi)	Bending Stress, σ_e ILLI-SLAB WESV
1	50	12	4.84	99.7	109.7	1.10	980	974	951	0.99
2	200	12	6.85	47.3	49.2	1.04	822	813	808	0.99
3	500	12	8.61	28.4	29.3	1.03	720	705	711	0.98
4	50	16	3.90	66.4	78.5	1.18	607	593	591	0.98
5	200	16	5.52	31.8	34.1	1.07	517	515	504	1.00
6	500	16	6.94	19.4	20.2	1.04	459	454	452	0.99
7	50	20	3.30	48.2	63.3	1.31	417	395	396	0.95
8	200	20	4.67	23.3	25.8	1.11	359	356	348	0.99
9	500	20	5.87	14.3	15.1	1.06	321	319	317	0.99

Note: For the ILLI-SLAB solution: slab = 25 x 25 ft, (L/ℓ) = 3.30 to 8.61, E = 5 x 10^6 psi, μ = 0.15, P = 50,000 lb, p = 222.2 psi, and A = 15 x 15 in. (edge). For the Westergaard solution (WESV), "New" formulas, circular load, "ordinary" theory: p = 222.2 psi, E = 5 x 10^6 psi, and μ = 0.15. For the H-51 solution: 50 points are used to approximate tire print.

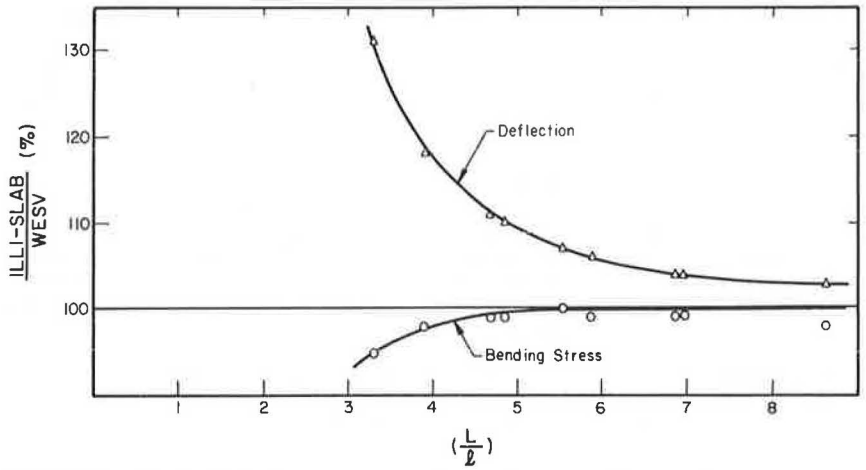

FIGURE 3 Effect of slab size on maximum edge loading responses.

The Pickett and Ray charts (20) for the edge loading condition on a dense liquid subgrade are based on a pair of integral equations identical to those presented by Westergaard (10). The results from these charts, therefore, agree with the "new" formulas, as indicated by H-51 results in Table 2. It is interesting to note that, although in several design codes reference is made to the original equation, the fact that multiple wheel loads are often considered implies that design charts in these codes have been obtained using the Pickett and Ray charts (i.e., the "new" formulas).

The question of the source of the discrepancy between Westergaard's original and new formulas for edge loading remains unanswered. It is too early to dismiss the original formulas as altogether false and useless. Bergstrom et al. (14) reported that values calculated using these equations are "in relatively close agreement with test results." They furthermore suggested that there are "no reasons to use the new formula for edge loading." On the other hand, Scott (8) suggests that "experimental indications are that the edge stresses experienced in practice are higher than the Westergaard (original) equation indicates." Laboratory model tests by Carlton and Behrmann (22) produced edge stresses 10 to 12 percent lower than the new formula predicts, reinforcing the expectation that in situ values probably lie between the two Westergaard equations.

The theoretical background for the original edge stress equation is also open to debate. The derivation of this equation is not presented in any of Westergaard's papers. Attempts by Losberg (18) to arrive at this formula through integration of the expressions for the concentrated load (19) did not produce agreement with Westergaard's result. If the probability of a gross theoretical blunder by such a meticulous investigator as Westergaard can be cast aside, for the time being, a possible explanation for this discrepancy is some assumption regarding subgrade support at the slab edge, which is implicit in the original formula but is never explicitly stated.

CORNER LOADING

Of the three fundamental cases of loading investigated by Westergaard, corner loading is undoubtedly the most obscure and debatable. The theoretical background for maximum corner deflection and stress equations is particularly weak. Their semiempirical and approximate nature has led to numerous revisions and modifications in the years since their original publication, in an attempt to reconcile observed slab behavior with theory. These are discussed by Kelley (16) and Pickett (23) and are summarized as follows:

Deflection

$$\delta_c = (P/k\ell^2)\,[1.1 - 0.88\,(a_1/\ell)] \qquad \text{Westergaard } (5) \qquad (3a)$$

Stress

$$\sigma_c = (3P/h^2) \qquad \text{Goldbeck } (25), \text{ Older } (26) \qquad (3b)$$

$$\sigma_c = (3P/h^2)\,[1 - (a_1/\ell)^{0.6}] \qquad \text{Westergaard } (5) \qquad (3c)$$

$$\sigma_c = (3P/h^2)\,[1 - (a/\ell)^{0.6}] \quad \text{Bradbury } (15) \tag{3d}$$

$$\sigma_c = (3P/h^2)\,[1 - (a_1/\ell)^{1.2}] \quad \text{Kelley } (16), \text{ Teller and Sutherland } (13) \tag{3e}$$

$$\sigma_c = (3.2P/h^2)\,[1 - (a_1/\ell)] \quad \text{Spangler } (28) \tag{3f}$$

$$\sigma_c = (4.2P/h^2)\left(1 - \left\{[(a/\ell)^{1/2}]/[0.925 + 0.22\,(a/\ell)]\right\}\right) \quad \text{Pickett } (23) \tag{3g}$$

Distance to point of maximum stress along corner angle bisector

$$X_1 = 2[(a_1\ell)^{1/2}] \quad \text{Westergaard } (5) \tag{3h}$$

where

a = radius of circular load tangent to both edges at corner and
a_1 = distance to point of action of resultant along corner angle bisector
= $(2^{1/2})a$. See Equations 1 for other symbols.

In the early 1920s a short and simple piece of analytical work was heralded as "the most important single step in the investigation of the mechanics of road slabs" (24). This was the first attempt to solve the problem of the "corner break" by two prominent engineers of the day working independently, A.T. Goldbeck of the Bureau of Public Roads and Clifford Older of the Illinois Highway Department. By assuming that in the corner region the slab acts as a cantilever of uniform strength (i.e., that in this region the subgrade reaction is negligible compared to the applied load), Equation 3b was proposed for the maximum stress, σ_c, due to a concentrated load, P, acting at the corner of a slab, of thickness h (25,26).

A few years later, Westergaard (5) took up the problem again, trying to account for the effect of a load distributed over some area, the resultant of which could be represented by a point load P acting at a small distance a_1 from the corner, along the bisector of the corner angle. Using a "simple approximate process" involving the use of the principle of minimum potential energy (27) he hoped to achieve an "improved approximation" of corner stress. Thus he first arrived at Equation 3a for corner deflection. He considered this equation "approximately applicable for plausible ranges of a_1 and ℓ" [presumably (a_1/ℓ) is not much greater than 0.1]. From this, he obtained bending moments by integration and concluded that the maximum stress "would be represented with satisfactory accuracy" by Equation 3c. Furthermore, the distance to the point of maximum stress along the corner angle bisector was found to be given "roughly" by Equation 3h.

Equations for the Corner Loading Condition Based on the Finite Element Method

In this section, ILLI-SLAB is used to establish a set of equations that would accurately predict the response of a slab, in full contact with a Winkler foundation, to a single load distributed over a small area at its corner. Equations 3, proposed by previous investigators, suggest that, from a theoretical viewpoint, the parameters involved in the determination of slab response can be lumped into three nondimensional ratios to be investigated, namely, $(\delta_c k\ell^2/P)$ $(\sigma_c h^2/P)$ and (a/ℓ) or (a_1/ℓ) for a circular, or (c/ℓ) for a square load.

The results obtained from several ILLI-SLAB analyses are plotted in a nondimensional fashion in Figures 4 and 5. Other available closed-form solutions are also shown in these figures for comparison. The latter were obtained using a circular load of the same area as the square one in ILLI-SLAB but are

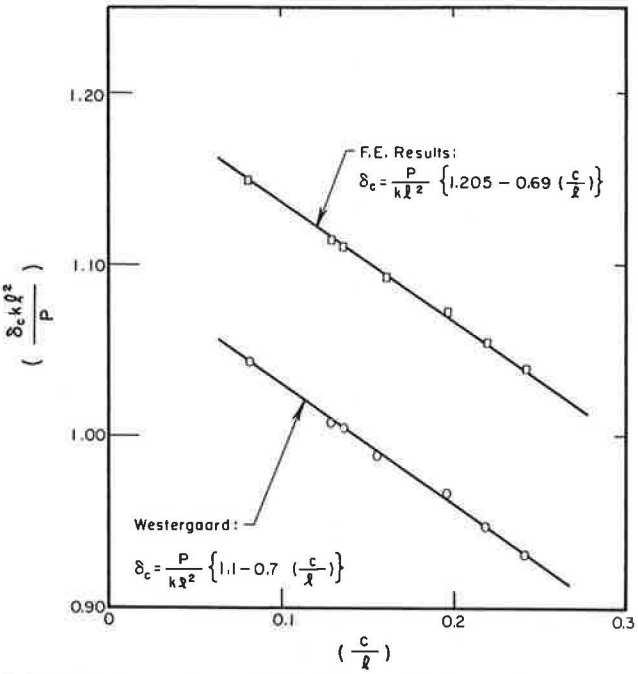

FIGURE 4 Comparison of ILLI-SLAB and Westergaard corner deflections.

plotted with the corresponding (c/ℓ) values along the ordinate. Though not mathematically rigorous, this facilitates direct comparison of the results. ILLI-SLAB stresses are values of the minor (tensile) principal stress occurring at the top fiber of the slab. The maximum normal stress obtained from finite element analysis (P. Frey, "Development of a Finite Element Based Expression to Predict Maximum Corner Loading Stresses in a Uniformly Supported Rigid Pavement on an Elastic Subgrade," University of Illinois, Urbana, 1983) significantly underestimates the critical stress.

Curves were fitted to ILLI-SLAB data with a special effort made to keep the general form of the equations the same as that of the Westergaard formulas. Thus a straight line may be used to describe corner deflections, δ_c, obtained using the finite element method (Figure 4). This line has the following equation:

$$\delta_c = (P/k\ell^2)\,[1.205 - 0.69\,(c/\ell)] \tag{4}$$

where c is the side length of square loaded area.

The similarity to Westergaard's equation indicates that Westergaard's approximation was fairly good. The finite element results obtained are typically about 10 percent higher than those predicted by Westergaard. A small part of this discrepancy is due to the lack of a theoretical solution for a square loaded area, as well as limitations of the finite element solution with respect to mesh fineness and slab size.

In the case of ILLI-SLAB maximum corner stresses, σ_c, curve fitting suggested the following equation:

$$\sigma_c = (3P/h^2)\,[1.0 - (c/\ell)^{0.72}] \tag{5}$$

The Goldbeck-Older equation is obviously a rough approximation of the theoretical solution, much more so at high values of (c/ℓ). This is expected, in view of the Goldbeck-Older assumption of a concentrated load acting on a cantilever. Assuming that finite element results give a fairly accurate pic-

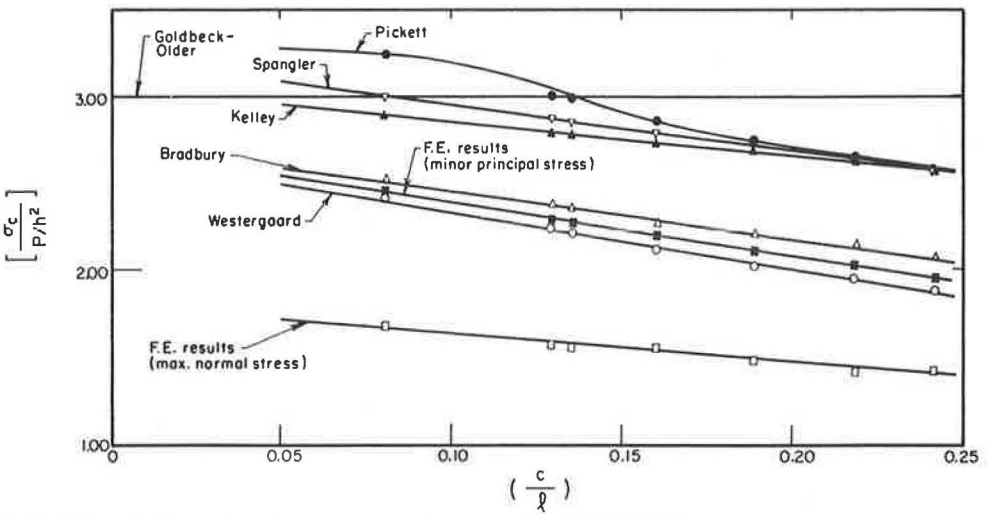

FIGURE 5 Nondimensional maximum bending stress for corner loading.

ture of the theoretical solution, the Westergaard equation represents a considerable improvement over the Goldbeck-Older one. The finite element method gives results that fall between those predicted by Westergaard (5) and those predicted by Bradbury (15). Note that the empirical modifications to the Westergaard formula proposed in the last 60 years--with the exception of Bradbury's--have tended to increase the discrepancy between calculated and theoretical stresses. These modified expressions are much closer to the Goldbeck-Older equation than to the theoretical solution. Scott (8) points out that "experimental indications are that the corner stresses experienced in practice are higher than the Westergaard equation indicates." Note, however, that, in the model tests mentioned previously, measured maximum corner stresses "were only 65 to 75 percent as great as those determined from the Westergaard equation" (22). The very significant limitations of the Winkler subgrade idealization for corner loading are reflected in Figure 5. As a result, discrepancies between measured responses and theory may be expected. In the absence of more conclusive field data, it is prudent to design for a higher corner stress than indicated by Westergaard's formula (Equation 3c).

Location of Maximum Stress

The results from a selected number of ILLI-SLAB runs are given in Table 3, where X_1 as obtained from Equation 3h is compared with the location of the minor (tensile) principal stress given by ILLI-SLAB. This shows that ILLI-SLAB usually gives a somewhat greater distance than Westergaard. On the other hand, model tests suggest values about 85 percent of Westergaard's (22). Curve fitting through the values of X_1 obtained by extrapolation from ILLI-SLAB, resulted in the following equation:

$$X_1 = 1.80\, c^{0.32}\, \ell^{0.59} \tag{6}$$

This best-fit equation indicates that the influence of the radius of relative stiffness, ℓ, is much greater than that of the size of the loaded area. Westergaard's equation suggests that these two parameters contribute equally to the determination of X_1.

Slab Size Requirements for Corner Loading Westergaard Responses

The pertinent results from this study are shown in Figure 6, in which ILLI-SLAB deflections and stresses are shown as percentages of the values given by the best-fit equations. The validity of any conclusions drawn from such a comparison is not considered to be greatly affected by the numerical accuracy of the proposed formulas. The patterns observed in Figure 6 are the same as those observed for the other loading conditions. Once again, stresses converge faster, requiring a minimum (L/ℓ) value of about

TABLE 3 Location of Maximum Corner Stress

Run No.	ℓ (in.)	c (in.)	Equivalent a (in.)	Location of σ_c, X_1 (in.)			
					ILLI-SLAB		
				Equation 3h	At Node	By Extrapolation	Proposed Equation
C001	31.07	2.5	1.41	15.74	18.03	18.50	18.33
C002	31.07	5.0	2.82	22.26	25.50	22.93	22.88
C003	31.07	7.5	4.23	27.27	30.41	26.00	26.05
C004	36.95	5.0	2.82	24.28	25.50	25.45	25.34
C005	26.13	5.0	2.82	20.42	20.62	20.67	20.66
C006	22.92	5.0	2.82	19.12	18.03	19.11	19.12
C007	38.56	5.0	2.82	24.80	25.50	26.10	25.99
C011	31.07	5.0	2.82	22.26	25.50	22.93	22.88
CT3	31.07	10.0	6.56	33.96	28.28	28.42	28.56

Note: Equivalent a = $(c/\pi^{1/2})$, Equation 3h: $X_1 = 2[(a_1\ell)^{1/2}]$, $a_1 = (2^{1/2})$ a, and proposed equation: $X_1 = 1.80\, c^{0.32}\, \ell^{0.59}$

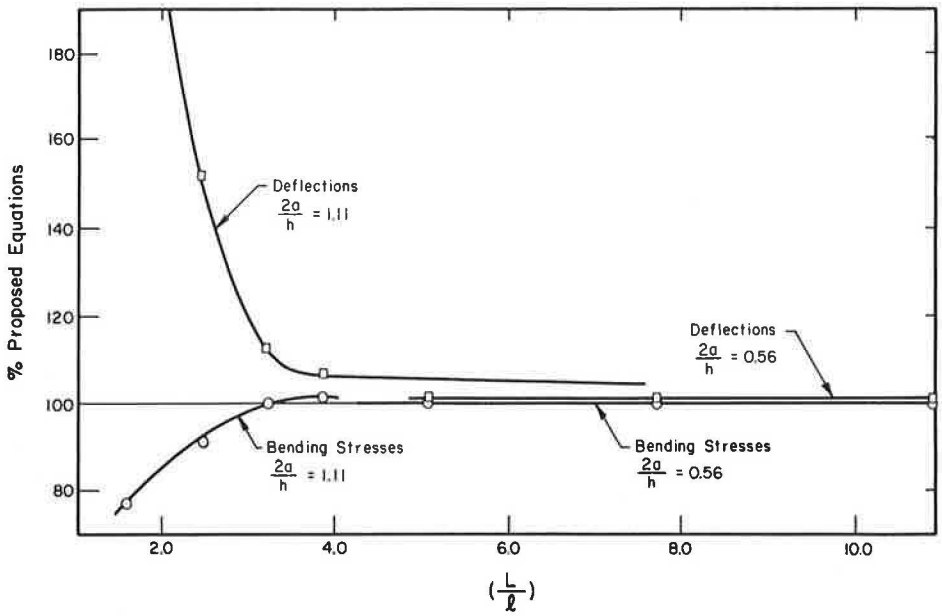

FIGURE 6 Effect of slab size on maximum corner loading responses.

4.0, and are less sensitive to changes in (L/ℓ) than are deflections. The latter are extremely sensitive even to small changes for (L/ℓ), smaller than about 3.0. Infinite slab deflection requires an (L/ℓ) ratio of at least 5.0. Slab size requirements established during this study are summarized in Table 4.

Effect of Size of Loaded Area

Figure 7 shows finite element corner loading responses as a function of (c/ℓ), where c is the side length of the applied square load. Responses are normalized with respect to the values obtained using proposed Equations 4 and 5.

TABLE 4 Slab Size Requirements for Westergaard Responses Based on the Finite Element Method

	(L/ℓ) Values for	
Load Placement	Maximum Deflection	Maximum Bending Stress
Interior	8.0	3.5
Edge	8.0	5.0
Corner	5.0	4.0

Note: L = least slab dimension and ℓ = radius of relative stiffness.

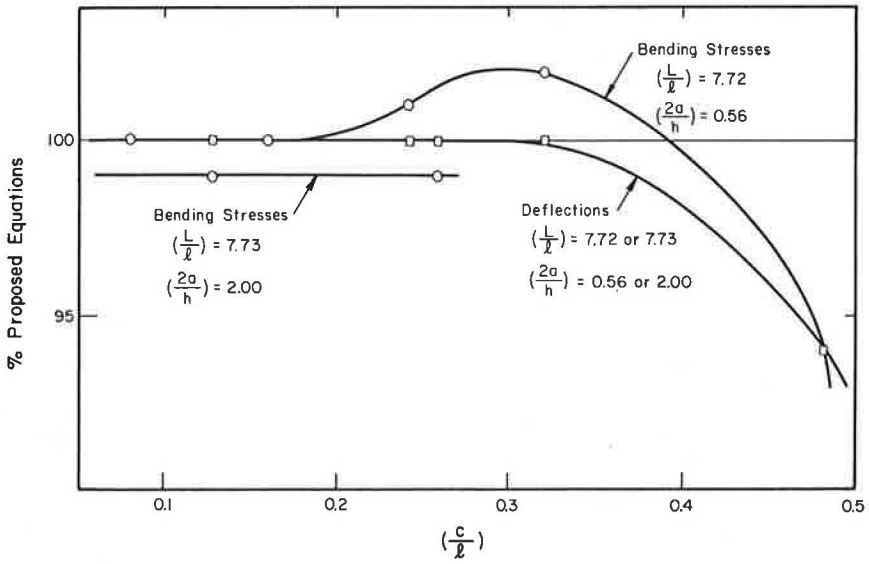

FIGURE 7 Effect of size of loaded area on maximum corner responses.

Deflections are not very sensitive to changes in (c/ℓ), but stresses diverge from the "theoretical" values as (c/ℓ) exceeds about 0.2. The trend exhibited by corner stresses is the reverse of that for interior loading. The effect of (c/ℓ) on corner stresses is less pronounced than on interior stresses. Comments made earlier with respect to this effect are also generally applicable to corner loading.

CONCLUSION

Since their first appearance, beginning in the early 1920s, Westergaard equations have often been misquoted or misapplied in subsequent publications. To remedy this situation, a reexamination of these solutions using the finite element method has been presented. This exercise yielded a number of interesting results:

1. Several equations ascribed to Westergaard in the literature are erroneous, usually as a result of a series of typographical errors or misapplications, or both. The correct form of these equations and their limitations have now been conclusively established (Equations 1-3).
2. Westergaard's original equation for edge stress (5) is incorrect. The long-ignored equation given in his 1948 paper (10) should be used instead.
3. Improved expressions for maximum corner loading responses have been developed (Equations 4-6).
4. Slab size requirements for the development of Westergaard responses have also been established (Table 4).

ACKNOWLEDGMENTS

The investigations for this paper were conducted under a research project (grant AFOSR-82-0143) sponsored by the Air Force Office of Scientific Research (AFOSR), Air Force Systems Command, Bolling Air Force Base, District of Columbia. Lt. Col. L.D. Hokanson was the Program Manager.

REFERENCES

1. A.M. Ioannides. Analysis of Slabs-on-Grade for a Variety of Loading and Support Conditions. Ph.D. dissertation. University of Illinois, Urbana, 1984.
2. A.M. Tabatabaie, E.J. Barenberg, and R.E. Smith. Longitudinal Joint Systems in Slip-Formed Rigid Pavements, Vol. II: Analysis of Load Transfer Systems for Concrete Pavements. Report FAA-RD-79-4, II. U.S. Department of Transportation, Nov. 1979.
3. O.C. Zienkiewicz. The Finite Element Method. 3rd ed. McGraw-Hill Book Company, New York, 1977.
4. D.J. Dawe. A Finite Element Approach to Plate Vibration Problems. Journal of Mechanical Engineering Science, Vol. 7, No. 1, 1965.
5. H.M. Westergaard. Stresses in Concrete Pavements Computed by Theoretical Analysis. Public Roads, Vol. 7, No. 2, April 1926. Also Proc., 5th Annual Meeting. HRB, National Research Council, Washington, D.C., 1926, as Computation of Stresses in Concrete Roads.
6. M.R. Thompson, E.J. Barenberg, A.M. Ioannides, and J.A. Fischer. Development of a Stress Dependent Finite Element Slab Model. Report TR-83-1061. U.S. Air Force Office of Scientific Research, Air Force Systems Command, Bolling Air Force Base, Washington, D.C., May 1983.
7. H.M. Westergaard. Stresses in Concrete Runways of Airports. Proc., 19th Annual Meeting, HRB, National Research Council, Washington, D.C., 1939. Also in Stresses in Concrete Runways of Airports. Portland Cement Association, Chicago, Ill., Dec. 1941.
8. R.F. Scott. Foundation Analysis. Prentice-Hall, Inc., Englewood Cliffs, N.J., 1981.
9. H.M. Westergaard. Stress Concentrations in Plates Loaded over Small Areas. ASCE Transactions, Vol. No. 108, 1943.
10. H.M. Westergaard. New Formulas for Stresses in Concrete Pavements of Airfields. ASCE Transactions, Vol. 113, 1948.
11. S. Timoshenko and S. Woinowsky-Krieger. Theory of Plates and Shells. 2nd ed., McGraw-Hill Book Company, New York, 1959.
12. H.M. Westergaard. Analytical Tools for Judging Results of Structural Tests of Concrete Pavements. Public Roads, Vol. 14, No. 10, Dec. 1933.
13. L.W. Teller and E.C. Sutherland. The Structural Design of Concrete Pavements, Part 5: An Experimental Study of the Westergaard Analysis of Stress Condition in Concrete Pavement Slabs of Uniform Thickness. Pubic Roads, Vol. 23, No. 8, April-June 1943.
14. S.G. Bergstrom, E. Fromen, and S. Linderholm. Investigation of Wheel Load Stresses in Concrete Pavements. Proceedings 13. Swedish Cement and Concrete Research Institute, Royal Institute of Technology, Stockholm, 1949.
15. R.D. Bradbury. Reinforced Concrete Pavements. Wire Reinforcement Institute, Washington, D.C., 1938.
16. E.F. Kelley. Application of the Results of Research to the Structural Design of Concrete Pavement. Public Roads, Vol. 20, No. 5, July 1935; Vol. 20, No. 6, Aug. 1939.
17. G. Pickett, M.E. Raville, W.C. Janes, and F.J. McCormick. Deflections, Moments and Reactive Pressures for Concrete Pavements. Bulletin 65. Engineering Experiment Station, Kansas State College, Pittsburg, Oct., 1951.
18. A. Losberg. Structurally Reinforced Concrete Pavements. Doktorsavhandlingar Vid Chalmers Tekniska Hogskola, Gotesborg, Sweden, 1960.
19. H.M. Westergaard. Om Beregning af Plader paa elastik Underlag med saerlight Henblik paa Sporgsmaalet om Spaendinger i Betonveje (On the Design of Slabs on Elastic Foundation with Special Reference to Stresses in Concrete Pavements). Ingenioren (Copenhagen), Vol. 32, 1923.
20. G. Pickett and G.K. Ray. Influence Charts for Concrete Pavements. ASCE Transactions, Vol. 116, 1951.
21. W.C. Kreger. Computerized Aircraft Ground Flotation Analysis--Edge Loaded Rigid Pavement. Research Report ERR-FW-572. General Dynamics Corp., Fort Worth, Tex., Jan. 1967.
22. P.F. Carlton and R.M. Behrmann. A Model Study of Rigid Pavement Behavior Under Corner and Edge Loadings. Proc., 35th Annual Meeting, HRB, National Research Council, Washington, D.C., 1956.
23. G. Pickett. Concrete Pavement Design, Appendix III: A Study of Stresses in the Corner Region of Concrete Pavement Slabs Under Large Corner Loads. Portland Cement Association, Skokie, Ill., 1946, reprint 1951.
24. H.M. Westergaard. Theory of Stresses in Road Slabs. Proc., 4th Annual Meeting, HRB, National Research Council, Washington, D.C., 1925.
25. A.T. Goldbeck. Thickness of Concrete Slabs. Public Roads, Vol. 1, No. 12, April 1919.
26. C. Older. Highway Research in Illinois. ASCE Transactions, Vol. 87, 1924.
27. H.M. Westergaard. What is Known of Stresses. Engineering News Record, Jan. 1937.

28. M.G. Spangler. Stresses in the Corner Region of Concrete Pavements. Bulletin 157. Engineering Experiment Station, Iowa State College, Ames, 1942.

The contents of this paper reflect the views of the authors who are responsible for the facts and the accuracy of the data presented herein. The contents do not necessarily reflect the official views or policies of the U.S. Air Force. This paper does not constitute a standard, specification, or regulation.

Publication of this paper sponsored by Committee on Rigid Pavements.

Establishing Load Transfer in Existing Jointed Concrete Pavements

WOUTER GULDEN and DANNY BROWN

ABSTRACT

In this paper are described the results of a research project that had the objective of developing construction procedures for restoring load transfer in existing jointed concrete pavements and of evaluating the effectiveness of the restoration methods. A total of 28 test sections with various load transfer devices were placed. The devices include split pipe, figure eight, vee, double vee, and dowel bars. Patching materials used on the project included three types of fast-setting grouts, three brands of polymer concrete, and plain portland cement concrete. The number and spacing of the devices and dowel bars were also variables in the project. Dowel bars and double vee devices were used on the major portion of the project. Performance evaluations were based on deflection tests conducted with a 20,000-lb axle load. Horizontal joint movement measurements and visual observations were also made. The short-term performance data indicate good results with the dowel bar installations regardless of patching materials. The sections with split pipe, figure eight, and vee devices failed in bond during the first winter cycle. The results with the double vee sections indicate the importance of the patching material to the success or failure of the load transfer system: some sections are performing well and other sections are performing poorly with double vee devices. Horizontal joint movement measurements indicate that neither the dowel bars nor the double vee devices are restricting joint movement.

Many miles of Interstate pavement have been constructed using plain jointed concrete pavements of various thicknesses and joint spacings. The presence of a joint is a discontinuity that causes higher stresses and deflections in the pavement especially in the outside corner area. Many designs of jointed concrete pavement relied on aggregate interlock to provide for the transfer of the load across the joint, thereby reducing stress concentration and deflections under load. Laboratory studies conducted by the Portland Cement Association (PCA) found that the effectiveness of load transfer from aggregate interlock depended on load magnitude, number of repetitions, slab thickness, joint opening, subgrade value, and aggregate angularity (1). It was also found that the effectiveness decreased with cumulative load applications.

The variability of the amount of load transfer available from aggregate interlock created by changes in joint openings points out the need to provide for a more positive means of load transfer. In Georgia, and in many other states, dowel bars are placed in newly constructed pavements. Many older concrete pavements do not have the dowel bars and this absence of a positive means of load transfer is a factor that contributes to the deterioration of these pavement sections. Faulting measurements made in Georgia in 1972 on projects that contained both doweled and nondoweled joints indicated that the presence of dowels reduced the rate of faulting (2).

The distress found in plain jointed concrete pavements in Georgia generally has been caused by the presence of an erodible base or subgrade, infiltration of surface water into the pavement system,

and excessive movement of the slab at the joints. These conditions have led to faulted joints and cracked slabs. A large program to rehabilitate these deteriorated pavements in Georgia has been under way since 1976. These efforts have consisted of reducing slab deflections by filling any voids under the pavement with grout, replacing broken slabs, resealing joints and grinding the surface to restore rideability and skid resistance, or overlaying with asphaltic concrete.

The problem of providing a positive load transfer across the joint was not addressed in the rehabilitation efforts mainly because of the lack of a viable cost-effective method of providing load transfer and reducing corner deflection in existing pavements. It is likely that the life of a large percentage of the rehabilitated pavements could be extended if load transfer across the joint could be established by positive means.

Research into this area has been started during the last several years in France and the United States. A report published by FHWA in 1977 contained conceptual proposals for two load transfer devices that could be placed in existing concrete pavement joints (3).

In 1980 the Georgia Department of Transportation received a contract from the Federal Highway Administration to place and evaluate the performance of load transfer devices on in-service concrete pavements. The objective of the research project was to develop construction procedures for restoring load transfer in existing concrete pavements and to evaluate the effectiveness of the restoration methods.

The objectives of the study were to be accomplished through installation of various load transfer devices and monitoring the performance of these devices under actual Interstate traffic conditions.

DESIGN AND PERFORMANCE OF TEST SITE

The location that was selected for the test site was on I-75 in the southbound lane approximately 40 mi south of Atlanta. The average daily traffic (ADT) on the test area is 15,000 to 17,000 vehicles per day with 19 percent heavy trucks.

The pavement in the test area is a 9-in. plain jointed concrete pavement with 30-ft joint spacing. The base course is a 3-in. bituminous stabilized soil aggregate on top of a 5-in. layer of granular subbase. The shoulder consists of a 6-in. cement-stabilized graded aggregate with a 1 1/2-in. asphaltic concrete topping. The pavement was opened to traffic about 1967.

This section was rehabilitated in 1976 by DOT maintenance forces because of the severe faulting and pumping that were taking place. The rehabilitation consisted of undersealing, spall repair, replacement of broken slabs, addition of edge drains, sealing of transverse joints, and grinding. Annual surveys conducted on this section have shown a significant increase in the faulting level in some areas since rehabilitation. There also has been an increase in the number of broken slabs and replaced slabs and visual signs of slab movement in the general area since the rehabilitation was completed in 1976.

EXPERIMENTAL LAYOUT

The test sections were designed to examine variables such as patching materials, types of load transfer devices, and number of devices or dowel bars per joint. The patching materials used in the sections were polymer concrete, rapid set materials, and high early strength portland cement concrete. The load transfer devices consisted of split pipe, figure eight, vee, and dowel bars. The interactions of these variables as used in the research project are given in Table 1. In addition, 10 control sections ranging from 3 to 17 joints in size were placed throughout the project. The deflection data obtained on the control joints were used as a guide to determine whether the load transfer devices were effectively minimizing the differential deflection across a joint and reducing the total deflections of a slab.

TABLE 1 Load Transfer Test Section Variables

Type of Device	Patching Material	Devices per Joint	No. of Joints	Test Section No.
Split pipe	Bonded with epoxy	4	6	1
Figure eight	Bonded with epoxy	4	20	2 and 3
Vee	Polymer concrete	4	10	4
Double vee	Polymer concrete	4	5	5
		4	35	5, 30, 31
		3	20	6
		2	20	7
		4 every other joint	39	22
	Set-45, Roadpatch, Horn 240	4	30	17,18 19
		4	98	20,27 29
	Portland cement concrete	3	45	25
		2	44	23
Double bars	Set-45, Roadpatch, Horn 240	8	30	8,9,10
	Polymer concrete	8	10	12
		8	20	11,14
		5	5	15
	Portland cement concrete	5	10	34
		4	5	16
		3	10	33

PATCHING MATERIALS AND LOAD TRANSFER DEVICES

A combination of five types of load transfer devices and seven patching materials was used in the test installations. All but two of the seven patching materials were used in short sections specifically placed to evaluate those materials.

The success or failure of a load transfer system depends on the performance of both the load transfer device and the patching materials. The following criteria must be met for a load transfer system to provide long-term performance:

1. The patching material and device must have sufficient strength to carry the required load;
2. Sufficient bond must be achieved between the device and the patching material to carry the required load;
3. Sufficient bond must be achieved between the patching material and the existing concrete to carry the required load;
4. The device must be able to accommodate movement caused by thermal movement of the concrete slabs;
5. The bond between the device and the patching material must be sufficient to withstand the forces due to thermal movement of the concrete slabs;
6. The patching materials must have little or no shrinkage during curing; shrinkage of the patching material can cause weakening or failure of the bond with the existing concrete; and

7. The patching material must develop strength rapidly so that traffic can be allowed on the slabs in a reasonable length of time (3 to 4 hr).

Patching Materials

Three types of patching materials were used to secure the load transfer devices: special quick-setting materials, polymer concretes, and high early strength portland cement concrete. The special quick-setting materials consisted of two brands of magnesium phosphate-based materials (Set 45 and Horn 240) and one fiberglass-reinforced portland cement-based material (Road Patch). The polymer concretes consisted of three brands of methyl methacrylate-based material (Concresive, Silikal, and Crylcon). The portland cement concrete used Type III cement, calcium chloride, and aluminum powder to improve setting times and reduce shrinkage.

A thorough laboratory evaluation or trial installation should be made of any patching material that is to be used in a load transfer system. Working time, bond strength, rapid early strength gain, and shrinkage are prime factors that must be evaluated before a patching material is chosen.

Load Transfer Devices

Georgia Split Pipe Device

This device was developed by the Georgia DOT Office of Materials and Research personnel and is shown in Figure 1. To install these devices the two sides of the "split pipe" are epoxied to either side of the 4-in.-diameter core hole and the epoxy is allowed to set. The top and bottom plates rest on the top and bottom edges of the two split pipe pieces. The four bolts are tightened and the load transfer between the slabs is carried by the four bolts and the epoxy bond between the split pipe pieces and the concrete core hole surfaces. Thermal expansion movement is accommodated by the slippage of the top and bottom plates on the end of the split pipe pieces.

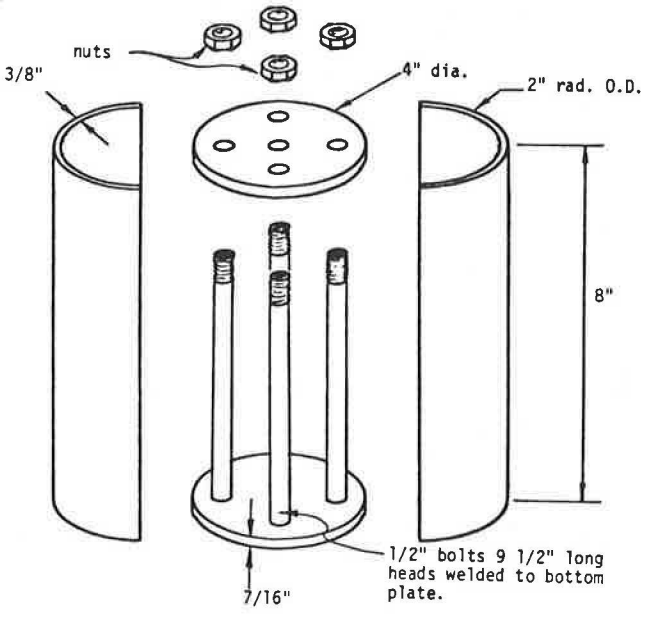

FIGURE 1 Georgia split pipe device.

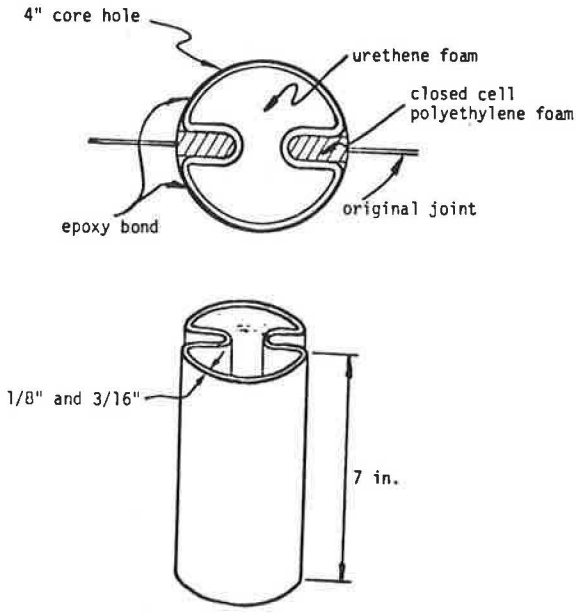

FIGURE 2 Figure eight device.

Figure Eight Device

This device is a single piece cylindrical metal shell formed in the shape of the numeral eight as shown in Figure 2. The device is installed in a 4-in.-diameter core hole and epoxy is used to bond the device to the walls of the core hole. The center of the device and the indentations on the side are filled with foam to keep out debris. The device has previously been used experimentally in France (4).

Vee Load Transfer Device

This type of load transfer device was first proposed in a report published by FHWA in 1977 (3) along with the figure eight device. The device consists of a 1/4-in.-thick steel plate bent into the shape of a V as shown in Figure 3. The device is not commercially available and was specially fabricated for this research project.

To be able to install the vee device, two 6-in.-diameter core holes have to be drilled and then filled with a patching material after installation. The vee portion was filled with urethane foam and a thin layer of polyethelyne foam was placed around the outside of the V to allow for expansion and contraction of the slab. An additional piece of foam was used to reestablish the joint.

Double Vee Load Transfer Device

This device is essentially two vee devices placed back to back and downsized to accommodate installation in a 6-in. core hole. The device was designed and initially tested at the University of Illinois (5) and is now commercially available under the trade name of LTD Plus. Some minor additional design changes to the device shown in Figure 4 have taken place since its use in this research project. The center section of the device is filled with foam to keep out debris and a thin foam pad is placed around the outside of the vee portion to allow for expansion and contraction. The devices used in this project are epoxy coated to prevent rusting and current devices are manufactured from stainless steel.

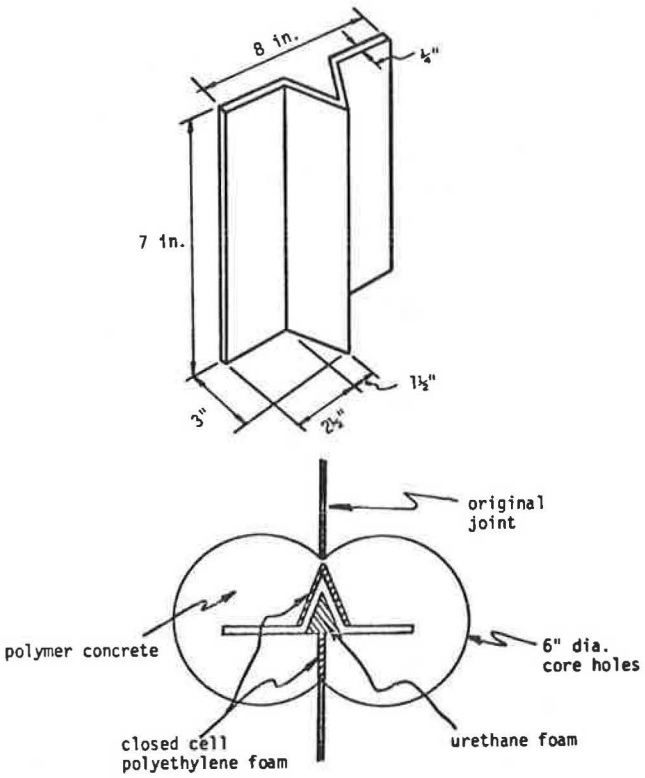

FIGURE 3 Vee device.

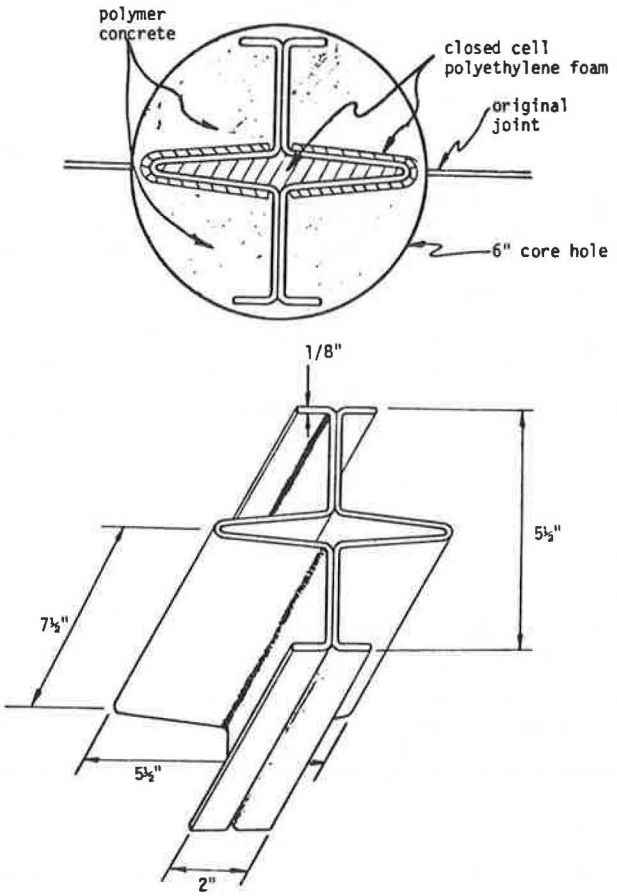

FIGURE 4 Double vee device.

Dowel Bars

Dowel bars are the most widely used load transfer device in new construction and were also used on this research project. The dowel bars were plastic-coated steel bars 18 in. long and 1 1/4 in. in diameter. The dowel bars were placed on chairs in the slots. Foam material was used to reestablish the joint over the bar when the patching material was placed.

CONSTRUCTION OF TEST SECTIONS

The first 22 test sections were constructed during the summer of 1981 and the remaining sections were placed during 1982. The 1982 test installation procedures were based on the most promising results from the 1981 installation.

The construction consisted of coring holes for all the devices or cutting slots for placement of the dowels. Four-in.-diameter holes were cut for the split pipe and figure eight devices. Six-in.-diameter holes were cut for the double vee devices, and two overlapping 6-in. holes were cut for the vee device. The slots were cut using a single bladed saw making four passes approximately 1 in. apart.

Placement of the devices and patching materials was done in accordance with the manufacturer's recommended procedures regarding cleaning the concrete, mixing time, use of primers, and so forth. The joint over each device was reestablished with a 1/2-in.-thick closed cell foam material during placement of the patching material.

Problems were encountered in 1981 with the placement of some of the polymer concrete. Some chemical components of the polymer concrete are sensitive to heat and had deteriorated. This chemical deterioration caused this polymer concrete to stay uncured. The low viscosity of the liquid component of the polymer concrete also posed a problem. This liquid component drained out of the polymer mix under the slab. This left a weak material near the top of the core hole. This problem became apparent after the 1981 installations when the material above the load transfer devices showed signs of raveling under traffic. This problem with the polymer concrete liquid component repeated itself in the Silikal test section in 1982. The liquid component "ran out" of the solid components, reducing to some degree the effectiveness of the material.

When the Crylcon test section was placed, precautions were taken to avoid the run out problem. Plaster was mixed and placed in the bottom of holes to seal any cracks and loose base material. When the Crylcon polymer concrete was placed in the holes run out did not occur and all material placed cured properly.

It was initially believed that a carbide-tipped cutting tool could be used successfully to cut slots for dowel bars in concrete at a reasonable rate of production.

A special mandrel was built by the CMI Corporation for a Rotomill PR-275-RT, which was owned by the Georgia Department of Transportation. The mandrel contained four rows of cutting teeth designed to cut slots 5 1/2 in. deep, 4 1/2 in. wide, and 15 in. apart center to center.

Before the Rotomill was placed on the Interstate test sections, a trial installation was attempted on US-41 near Macon, Georgia, in May 1981. One pass of four slots each was made in three joints before the trial was halted. Several problems were immediately apparent:

* The maximum depth of the slots that could be

cut was 3 1/2 to 4 in. due to physical restraints of the Rotomill.

- Excessive spalling occurred at the edges of the slots and at the joints themselves, which would make patching of the slots difficult.
- The machine endured excessive vibration during the cutting process, which could have damaged the equipment if cutting had been done on a long-term basis. The excessive vibration could possibly have been overcome by the use of a larger and heavier machine. The weight of the PR-275 was approximately 37,500 lb.
- An excessive amount of water and debris was left on the pavement. Cutting the slots with the Rotomill would make it necessary to place the dowels and patch the slots before opening the road to traffic because of the width of the slots. The threat of inclement weather would also hamper construction because workers would have to be sure that the slots could be patched before work was begun.

In light of these factors, it was concluded that cutting slots using carbide-tipped cutting equipment was not feasible.

Slots were cut in the concrete pavement on the actual test sections on I-75 using 30-in.-diameter diamond blade saws. The slots were cut 5 1/2 in. deep and approximately 3 1/2 in. wide, and were centered across the joints at the spacings indicated in Table 2. The length of the slots was such that the bottom of the slots was 20 to 24 in. long.

The slots were generally cut with a single blade saw. Four cuts were made per slot, leaving three "fins." After sawing, the slots are left open to traffic, with the fins in place, for several days while other slots are being sawed. These fins had a life expectancy of one week or less before they began to break out and the open slot became a hazard to traffic.

Both the sawing of the slots and the manual removal of the fins was a time-consuming process because no equipment was available to do this operation on a production basis.

DATA COLLECTION PROCEDURES

The performance of the test sections was monitored through deflection measurements and visual observa-

TABLE 2 Load Transfer Test Section Device Spacing

TYPE DEVICE	TEST SECTION NUMBER	SPACING OF DEVICES
Split Pipe	1	1' 3' 3' 3'
Figure Eight	2 and 3	1' 3' 3' 3'
Vee	4	1' 3' 3' 3'
Double Vee	5	1' 3' 3' 3'
	5, 30, 31	1' 2' 4.5' 2'
	6	1' 2' 5'
	7	1' 2'
	22	1' 2' 4.5' 2'
	17, 18, 19	1' 2' 4.5' 2'
	20, 27, 29	1' 2' 4.5' 2'
	25	1' 3' 5'
	23	1' 2'
Dowel Bars	8, 9, 10	9" 15" 15" 15" 15" 15" 15" 15"
	12	9" 15" 15" 15" 15" 15" 15" 15"
	11, 14	9" 15" 15" 15" 15" 15" 15" 15"
	15	17" 18" 18" 18" 18"
	34	9" 15" 15" 5' 15"
	16	12" 18" 18" 18"
	33	9" 15" 15"

OUTSIDE PAVEMENT EDGE

tions. Deflection measurements were made using a weight truck with a 20-kip load on a dual-tired single rear axle.

The procedure for measuring the slab movement was to position dial gauges on both corners at the joint and zero the gauges. The dial gauges were mounted on a frame that sat on the shoulder. A loaded truck was then slowly moved forward onto the slab until the rear wheels were positioned within 3 in. of the transverse joint and close to the shoulder joint. The deflection on the loaded side and on the unloaded side of the joint was then recorded. The truck then moved ahead slightly to position the rear wheels just past the joint and the deflection at both corners was once again recorded.

Horizontal joint movement was measured at 100 joints in the test area to determine if any of the load transfer devices were restraining contraction and expansion movements. This horizontal movement was measured using pins set in the concrete across the joints.

Close-up visual examinations were made of each load transfer installation during each evaluation period to determine bond failures and spalling, cracking, or subsidence of the patching material. The condition of the concrete pavement slabs in the entire experimental area was also noted on strip charts during each performance evaluation.

PERFORMANCE

Load Transfer Capabilities

The main criterion for evaluating the performance of the load transfer devices is of course their effectiveness in lessening the effects of the discontinuity in concrete pavement that is caused by the presence of a joint. A standard method for determining this effectiveness is to compare the deflection of the loaded side of a joint to the deflection of the unloaded side of the joint under a static or dynamic load.

The amount of load transfer can be calculated by a method first used by Teller and Sutherland (6):

$$LT\% = [(2\ Du)/(Dl + Du)] \times 100 \quad (1)$$

where

LT = load transfer as a percentage,
Du = deflection of unloaded slab, and
Dl = deflection of loaded slab.

Joint efficiency is also used to describe the amount of discontinuity caused by a joint and is defined as follows:

$$JE\% = (Du/Dl) \times 100 \quad (2)$$

Jointed concrete pavements in the field are constantly in vertical motion caused by changing temperature gradients in the concrete slab throughout a day. Slab corners are curled upward during morning hours and therefore lose contact with the subbase, and the reverse happens in the afternoon hours. The amount of load transfer that exists can change drastically throughout the day so that deflection measurements must be made several times during the day to determine load transfer values. If only one set of readings is to be obtained, the testing should be confined to the early morning hours when the highest deflections are likely to be encountered. Comparisons between test installations are only valid when the measurements are made at the time of maximum deflections and not when the slabs are curled down and in maximum contact with the subbase. This is especially true for pavements that have been under traffic for some time and have developed small voids under the slab corners.

The location of the load at the joint for which the load transfer is to be determined is important because the slab at the approach side of the joint usually does not contain as large a void as could be the case under the leave side of the joint. In general, the deflections measured on the approach side of the joint are less than the deflections obtained on the leave side.

The manner in which the load transfer and joint efficiency ratios are calculated causes the results to be highly dependent on the magnitude of the deflections as shown in the hypothetical example that follows.

Test Location	Deflection (mils) Loaded Side	Deflection (mils) Unloaded Side	Joint Efficiency (%)	Load Transfer (%)
1	6	1	17	29
2	10	5	50	87
3	35	30	86	92

The difference in deflections for all three joints in the preceding example is 5 mils, but the joint efficiency or load transfer becomes increasingly better with higher deflection levels.

From a performance standpoint, Test Location 1 in the example would be more desirable because it has low deflection levels yet fails to provide effective load transfer by the definitions given in Equations 1 and 2. The equations are meaningless for low deflection levels and a different approach must be used in analyzing the effectiveness of the various load transfer devices that were installed as part of this research project.

Because joint efficiency and load transfer percentages were not considered the best approach for analysis, another method was used. The deflection data obtained for this research project were analyzed in terms of maximum deflections and in terms of differential deflection between loaded and unloaded slab corners.

Deflections were obtained during three evaluation periods, January 1982, September 1982, and March 1983. Three sets of tests were made each time; one series was made early in the morning generally starting at 7:00 a.m., a second series of tests was run mid-morning starting at 10:00 a.m., and a third set was made in early afternoon starting at 1:00 p.m. The series of tests was done so as to be able to detect the changing deflection and load transfer conditions of the joints as they were affected by temperature changes and time of day.

The effects of seasonal changes on the load transfer conditions were evident from the three series of tests that were conducted at different times of the year and clearly showed that the higher deflections were obtained in September 1982 and always occurred in the early morning test series for all three evaluation periods. The deflections obtained with the load on the leave side of the joint also were generally larger than the deflection obtained on the approach side when loaded. The deflection data also show that the vertical movement measured in the early afternoon is generally negligible regardless of the magnitude of the movement measured in the early morning (Figure 5). Performance comparisons of the various load transfer systems were therefore based on deflections measured during the early morning hours when significant slab movements are likely to take place.

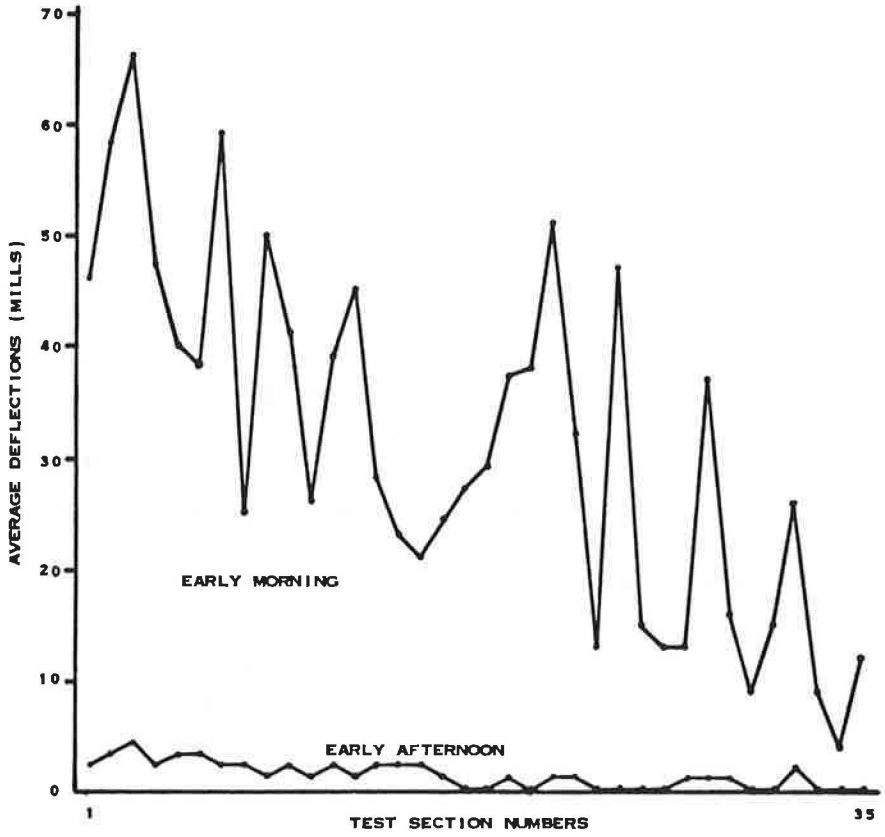

FIGURE 5 Deflection levels of leave slab corners, September 1982.

A low differential deflection value could indicate one of two conditions:

1. The loaded slab is in contact with the base and has a low total deflection value and transfer of load by means of a device is not necessary.
2. The load is being transferred across the joint to a large extent even though the maximum deflection of the slab may be large.

The field data also showed that, when there is a significant amount of interlock between adjoining slabs through mechanical or other means, the differential deflections are small and do not change much throughout the day regardless of the magnitude of the actual deflection.

The critical data for analysis are the deflections obtained during the early morning testing with the load placed on the leave side of the joint. The average differential deflection values for each test section are shown in Figure 6 for the March 1983 test period with the load placed on the leave slab. The bar charts in Figure 6 clearly show that all the sections with the dowel bars were performing well along with 10 of the 14 sections containing double vee devices. Section 4, containing the vee device, shows good performance on the bar chart; however, the data are suspect for this section for March 1983 because the deflection difference obtained in September 1982 was 35 mils. The March 1983 readings were generally much less than those obtained in September 1982 for sections showing poor performance. For the sections with good performance there generally was not much difference between the September 1982 and March 1983 differential deflection values. This is an indication of the seasonal influence on sections with little or no mechanical interlock. When adequate mechanical interlock is present, the seasonal influences are minimized in a manner similar to that noted previously for daily temperature cycle changes.

The discussion so far has been confined to average deflection values for each test section. An average value, however, can be artificially inflated by a few poor-performing joints within a test section when only a small number of joints make up the section. The percentage of joints with a differential deflection value of 10 mils or less for each test section is given in Table 3 for the case with the load on the leave slab and early morning test results. The values for September 1982 for Sections 23 and higher, excluding control sections, represent initial values because they were obtained soon after construction.

The sections containing dowel bars are all performing well compared to the control sections regardless of the number of dowels per joint. Little difference can be noted between the sections with the split pipe, figure eight, and vee device and the control sections, which are all performing poorly.

The performance of the sections with the double vee devices varies: half of the sections show good performance and half of the sections show marginal to poor performance.

Horizontal Joint Movement Restrictions

Horizontal joint movement measurements were made to determine if any of the load transfer devices would prevent the joint from functioning in a normal manner with respect to daily and seasonal temperature changes. Joint movement data are similar to deflection data in that they can vary from joint to joint and from day to day for a joint over the same temperature range.

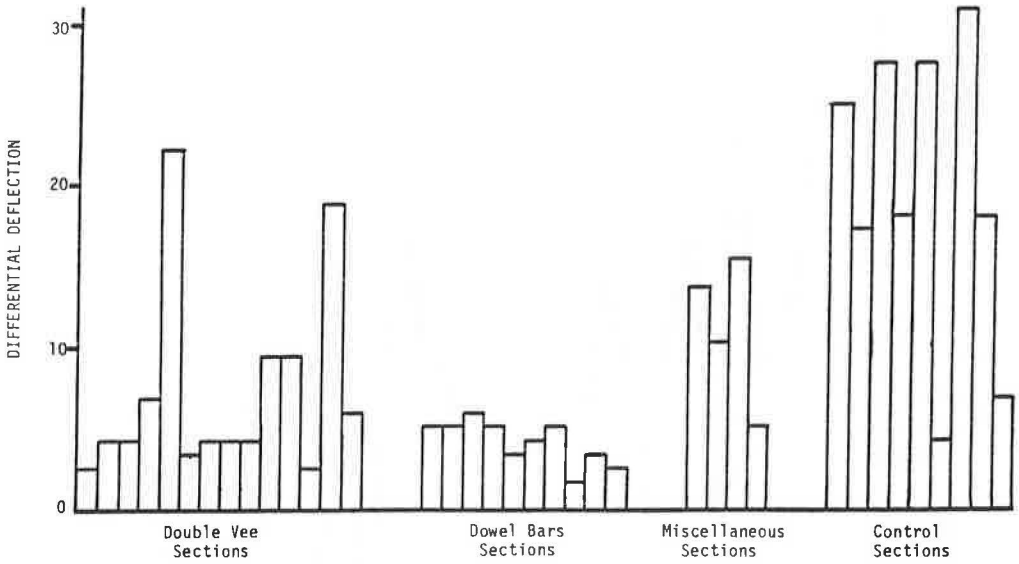

FIGURE 6 Differential deflection values in early morning on leave slab, March 1983.

TABLE 3 Percentage of Joints with Differential Deflections of 10 Mils or Less--Load on Leave Slab

Test Section	Dl-Du	
	September 1982	March 1983
Double vee		
5	85	95
6	70	65
7	20	30
17	70	70
18	50	40
19	90	100
20	90	90
22	71	76
23	95	75
25	98	98
27	95	93
29	100	91
30	90	90
31	90	90
Dowel bars		
8	90	100
9	60	90
10	80	90
11	100	90
12	80	100
14	100	100
15	100	100
16	80	100
33	90	100
34	100	90
Miscellaneous		
1	0	50
2	17	42
3	0	50
4	20	100
Control		
10A	33	33
13	0	20
18A	17	17
21	0	33
24	0	10
26	90	80
28	0	10
32	0	38
35	50	80

Note: Dl = deflection of loaded slab and Du = deflection of unloaded slab.

The resistance to opening or closing of a joint by the various load transfer devices is of concern because slab cracking can occur if the expansion and contraction movements cannot be accommodated at the joints. It is also important because excessive stress can cause a bond failure of the patching material thereby rendering the load transfer device useless.

The general indication from the joint movement data is that double vee devices and dowel bars do not excessively restrict horizontal joint movement. Bond failure had already taken place for the split pipe, figure eight, and vee devices when the first tests were made in January 1982. The bond failure could have been caused by excessive restraint of the joint movement, failure of the patching materials, installation problems, or other causes.

No detailed analysis of horizontal movement trends and variations will be made in this paper because the only reason for obtaining the data was to determine excessive restraint of horizontal joint movement imparted by the load transfer devices.

Visual Observations of Load Transfer Device Installations

Each of the load transfer installations was visually evaluated during each testing period. The items of concern are visible separations between the patching material and the devices or the pavement, loss of patching material, and cracking of the patching material.

Visual observations of the test sections have shown problems with disbonding between the patching material and the pavement on many of the double vee installations and on some of the dowel bar slots. The double vee installations with Horn 240 patching material have experienced cracking located over the fins of the device. Some transverse cracking at the end of the bars has been noted in the dowel installation with plain portland cement concrete as the patching material. To date, the best performing materials with the double vee are two polymers and plain portland cement concrete.

Reduction in Deflection Levels

One of the objectives of the research project was to determine if corner deflections of concrete slabs

would be reduced by placing load transfer devices in the joint.

Determination of the amount of reduction that can be expected when load transfer systems are installed was a difficult proposition because the magnitude of joint deflection changes from day to day and from location to location even within short distances.

An estimate was made by comparing the deflection levels of "failing" joints to "good" joints within a section and by comparing the average deflection levels of joints that were performing well to control sections in the immediate vicinity. For comparison purposes a joint was considered to have failed to provide adequate load transfer when the differential deflection was more than 10 mils. The analysis was based on deflections obtained during the early morning testing conducted in March 1983 and only those joints where the load transfer systems are performing well were included in the analysis.

The short-term performance data indicate that a definite reduction in deflection levels can be obtained using mechanical load transfer. A reduction ranging from 50 to 75 percent was obtained in the dowel sections, and similar reductions were measured in the double vee sections, which were still performing well. To enhance the long-term performance of the joint, it is advisable to stabilize excessively moving slabs through undersealing before load transfer devices or dowel bars are installed. In Georgia a deflection value of more than 0.030 in. is considered excessive on the basis of past experience with undersealing of concrete pavements.

Overall Performance

A rating of the performance of the various installations is given in Table 4. These ratings are based on the authors' interpretation of the percentage of joints having differential deflection values of 10 mils or less, the average differential deflection values, and the visual appearance of the installation obtained during the last comprehensive evaluation conducted in March 1983. The split pipe, figure eight, and vee devices all failed within the first winter and their performance rating is not included in Table 4.

A visual condition survey conducted in June 1984 indicated additional bond failures in the various test sections. The visual ratings indicate overall performance of the test sections and do not mean that each individual joint has failed in a "marginal" or "poor" performing section.

The ratings do indicate that the dowel sections are generally performing better than the sections with other load transfer devices. All the ratings are based on only 3 years of traffic, and long-term performance of any of the installations now rated as "good" is still in question.

CONCLUSIONS

1. The success or failure of a load transfer system depends on both the device and the patching material. The patching material must develop sufficient strength and bond to allow the device to open and close and to withstand the vertical stresses imparted by the loads. The load transfer device must be able to accommodate horizontal joint movements without disbonding the patching material.
2. Commonly used formulas for calculating load transfer and joint efficiency are inadequate for conveying the true effect of a load transfer system. These formulas cause the load transfer value to be highly dependent on the magnitude of the deflection levels. The difference in deflection between the loaded and unloaded slab is a better indicator of the performance of the joint.
3. Analysis of the effectiveness of any load transfer at a joint should be based only on the deflection levels that are present during the early morning hours when significant slab movements are likely to take place.
4. The sections with the split pipe device, the vee device, and the figure eight device and some of the sections with the double vee have failed to provide adequate load transfer by the criteria used in this study.
5. The sections with the dowel bars, regardless of the number of bars per joint, are performing better than the other sections after 2 and 3 years of traffic although some failures are occurring. Horizontal joint movement measurements indicate that

TABLE 4 Performance Ratings of Test Sections

Patching Material	Type of Device	Test Section No.	Devices per Joint	March 1983 Performance Rating	June 1984 Visual Rating
Set 45	Double vee	17	4	Marginal	Marginal
	Dowels	8	8	Good	Good
Road Patch	Double vee	18	4	Poor	Poor
	Dowels	9	8	Good	Good
Horn 240	Double vee	19	4	Good	Poor
	Dowels	10	8	Good	Marginal
Concresive	Double vee	5	4	Good	Poor
		6	3	Marginal	Poor
		7	2	Poor	Poor
		22	4	Marginal	Poor
	Dowels	12	8	Good	Good
Crylcon	Double vee	30	4	Good	Good
Silikal	Double vee	31	4	Good	Marginal
Portland cement	Double vee	20	4	Good	Good
		23	2	Marginal	Marginal
		25	3	Good	Marginal
		27	4	Good	Marginal
		29	4	Good	Marginal
	Dowels	11	8	Good	Marginal
		14	8	Good	Good
		15	5	Good	Good
		16	4	Good	Good
		33	3	Good	Marginal
		34	5	Good	Good

the dowel bars and the double vee devices do not excessively restrict horizontal joint movement. Bond failures had already taken place for the split pipe, figure eight, and vee devices when the first horizontal movement measurements were made during the first winter cycle.

6. The short-term performance data indicate that a definite reduction in deflection levels can be obtained using dowel bars or double vee devices. The amount of reduction on the research sections ranged from 50 to 75 percent when the deflection levels of the good performing test sections were compared to control sections in the immediate vicinity. These data are based on short-term performance only.

RECOMMENDATIONS

1. The type of patching material to be used with a load transfer device must be given careful consideration and laboratory tests should be conducted on new materials to determine ultimate bond strength, rate of strength gain, working time, and other factors before any material is used on a construction project.

2. It is recommended that the core hole walls or slot walls be grooved or a rough wall be provided in load transfer installations to reduce the dependency on the bond between the patching material and the existing concrete to carry the load.

3. The core hole or slot must be thoroughly sealed on the bottom and along the side when polymer concrete is used as the patching material to prevent drainage of the liquid component in the polymer concrete mix.

4. Retrofitted load transfer installations should not be installed to reduce excessive deflections in slabs but should be placed to prevent high deflections from reccurring when slabs have been stabilized.

It is desirable that vertical slab movement in excess of 0.030 in. measured during early morning hours be reduced through undersealing before the installation of any load transfer devices.

5. It is recommended that for dowel installations three dowels be placed in the outside wheelpath and two dowels be placed in the inside wheelpath with a dowel spacing similar to Test Section 34. When long-term performance data have been obtained it may be possible to eliminate the load transfer devices in the inside wheelpath. Four double vee devices per joint should be used on future installations.

6. Any future installations should be placed on an experimental basis until long-term performance data can be obtained on the current test sections. New installations are encouraged to provide additional performance data under a variety of traffic, weather, and design conditions.

ACKNOWLEDGMENTS

The data and information presented in this paper are the result of a research study funded by the Federal Highway Administration.

REFERENCES

1. B.E. Colley and H.A. Humphrey. Aggregate Interlock at Joints in Concrete Pavements. In Highway Research Record 189, HRB, National Research Council, Washington, D.C., 1967, pp. 1-18.
2. W. Gulden. Pavement Faulting Study. Research Project 7104, Final Report. Georgia Department of Transportation, Atlanta, 1975.
3. W.B. Ledbetter et al. Techniques for Rehabilitating Pavements Without Overlays--A System Analysis. FHWA-RD-78-108. FHWA, U.S. Department of Transportation, Vol. 1, Sept. 1977.
4. F. Verhée. Structural Maintenance of Cement Concrete Pavements, Assessment of Present Ideas--Results of French Experiments. Proc., 2nd International Conference on Concrete Pavement Design, Purdue University, West Lafayette, Ind., 1981.
5. L. Korbus and E.J. Barenberg. Longitudinal Joint Systems in Slip-Formed Rigid Pavements. FAA-RD-79-4, IV Interim Report. FAA, U.S. Department of Transportation, Vol. 4, Nov. 1981.
6. L.W. Teller and E.J. Sutherland. A Study of Structural Action of Several Types of Transverse and Longitudinal Joint Design. Public Roads, Vol. 17, No. 7, Sept. 1936.

Publication of this paper sponsored by Committee on Rigid Pavements.

Lateral Placement of Truck Wheels Within Highway Lanes

P.R. SHANKAR and CLYDE E. LEE

ABSTRACT

In recognition of the need for representative statistical data on the lateral placement of truck wheels within highway lanes, a video camera was used in a following vehicle to record rear-view images of trucks operating on multilane highways in Texas. Analysis of the data set that resulted from evaluating these images produced four frequency distributions of lateral wheel positions that are definitive for two different truck types and for two roadway alignment conditions. A single frequency distribution could not be used to describe the observed placement patterns with acceptable accuracy. To illustrate the effects of laterally distributed traffic loading on the design thickness of rigid pavements, computations were made for 1, 10, and 20 million repetitions of loads concentrated at the pavement edge and for the same number of loads distributed laterally in accordance with a representative frequency distribution. A thickness reduction of about 15 percent could be realized if the lateral distribution of loads were incorporated into the design process.

Increasing numbers of trucks on the highways coupled with the tendency to move heavier loads on each truck indicate a need for improved traffic data and for more refined pavement design procedures that take into account the magnitude of critical wheel loads that will be applied to pavement structures, their frequency of occurrence, and their lateral distribution among and within the lanes of multilane highways. Most pavement design procedures currently in use employ estimates of the directional and the lanewise distribution of mixed traffic loading, but none of the procedures accounts directly for the effects of varying lateral placement of wheel loads within the lane.

To illustrate the relative importance of lateral load placement in rigid pavement design, it is worthwhile to recall Westergaard's analysis of stresses in the pavement slab. In his work, Westergaard (1) considered three cases of load application: (a) corner, (b) edge, and (c) interior location. For typical highway pavements, his equations indicate that the maximum tensile stress in the slab due to edge loading will be approximately 1.5 times that for interior loading and that maximum deflections will be about three times as great for the respective loading positions. Pickett and Ray, cited in Yoder and Witczak (2), extended Westergaard's original theoretical work and developed influence charts for solving the general equations. Their work also shows that wheel loads applied at the pavement edge cause considerably higher stresses in the slab than do the same loads positioned laterally further away from the edge.

A pavement design procedure should recognize the stochastic nature of lateral wheel load placement within the lane, generally between these extreme locations, and account for the cumulative effects of different levels of stress and different numbers of repetitions of the various stresses that result. None of the popular pavement design procedures evaluates the effects of lateral wheel placement directly. The AASHTO Interim Guide (3), which is widely used for design purposes, estimates the overall effects of various amounts of mixed traffic through an empirical correlation of the observed pavement performance at the AASHO Road Test with the known amount of controlled truck traffic that was applied to pavement test sections there. The actual lateral distribution of truck traffic at the road test was not incorporated as a variable into the definitive cause and effect equations that were developed.

Few statistical data are available on the lateral placement of truck wheels within the traffic lane. Most research studies that have produced quantitative information about wheel placement have been directed toward identifying driver behavior patterns and determining the relationship between vehicle width and the effective width of the highway lane (4-6). An extensive series of studies on lateral placement of vehicles in highway lanes was conducted by the Bureau of Public Roads in the 1950s using a segmented switch on the road surface (7). This gave incremental measurements of wheel location only at a single point along the roadway. Photographic techniques have been used to record the varying lateral position of vehicles moving along the roadway (8-10), but none of these studies has concentrated on characterizing the patterns of truck wheel placement within the lane on multilane highways. This information is needed for pavement design and performance evaluation.

With the overall objective of defining a representative frequency distribution for the lateral placement of truck wheels with respect to the pavement edge on multilane highways in Texas, video photography was chosen as the most appropriate means for obtaining an adequate data set under actual traffic operating conditions. A sampling plan was devised, and a practicable data reduction procedure was developed. Analysis of the video-taped data showed that a single frequency distribution could not be used to represent the various patterns of lateral placement of truck wheels within the lane with acceptable accuracy; therefore, four different frequency distributions were defined. Each distribution describes the observed pattern of lateral wheel placement for a particular set of traffic and road-

way alignment circumstances that can be easily identified when designing or evaluating sections of pavement. To demonstrate the applicability of this type of traffic loading information in design, a series of computations was made. Results of these computations are given later in this paper. Significant reduction in the design thickness of rigid pavement slabs was indicated when stress calculations were based on the observed lateral distributions of wheel loads rather than on the assumption that all loads would occur at the pavement edge.

DATA COLLECTION AND REDUCTION

Because a continuous record of wheel placement for individual trucks as they traveled along the roadway was desired, a video camera mounted in a following van was used to record the rear-view image of trucks on two selected multilane (in each direction) highways. The sampled sections included a 26-mi segment of I-35 near Austin and a 16-mi segment of US-59 north of Houston. About 6 hr of video recordings of the movements of some 50 different trucks on carefully chosen sections of these highways with various alignments, cross sections, and pavement types were obtained during daylight hours. The time during which each individual truck was followed varied from about 2 to 20 min. An attempt was made to include various types of trucks in the sample, roughly in proportion to the percentages registered in Texas. Measurement of the lateral distance between the right edge of the truck tire image and the left side of the pavement edge line was made from the replayed images on a video monitor with the aid of a grid placed on the curved screen. The known width of the lane between the marked edge lines and lane lines was used to scale the measurements. A detailed description of the construction of the grid, which was used to correct for the inherent distortion in the video image, and the measuring technique that was used for data reduction is given elsewhere (11). It was also possible to note from the video images other factors such as traffic, pavement condition, and ramps or shoulders that might have influenced the driver's choice of lateral position at any given time.

ANALYSIS OF DATA

The objective of the analysis was to use the available data to define a representative frequency distribution, or a set of frequency distributions, of lateral placement of truck wheels on sections of multilane highways in Texas. The resulting frequency distributions were to be presented in a form that could be used in pavement design with relative ease.

In addition to the video image of the rear view of trucks that were followed, a visual image of the date and time (in 1-sec increments) was recorded. Thus the wheel placement pattern of each truck could be enumerated at exact 1-sec intervals throughout the time that the truck was followed. To reduce all the recorded data at each 1-sec interval was prohibitive and unnecessary; therefore, a systematic data sampling procedure was devised. The sampling rates were 5- to 10-sec intervals on roadway sections with straight horizontal alignment and 2- to 5-sec intervals on sections with horizontal curvature. A uniform small-interval sampling rate was not always feasible because the broken lane line markings sometimes did not appear in the video image at the selected time for sampling. An evaluation of the selected sampling rates, as described in detail elsewhere (11), showed that the rates were entirely adequate to place the observed wheel position properly in the appropriate 1-ft interval that would subsequently be recommended for inclusion in a pavement design procedure.

Table 1 gives all the individual trucks that were observed, the truck type, the time during which each was followed, and the number of measurements of wheel placement that were made from the video recordings. Table 2 gives a summary of the overall characteristics of lateral wheel placement in terms of mean position away from lane edge and observed variance. To determine whether the duration of the selected observation time on every truck was adequate, each data set was tested for stability. Statistics of interest concerning a time-varying phenomenon such as lateral wheel placement are said to be stable in a statistical sense if they are not affected significantly when the time origin of the data set is shifted. All the selected observation times and the duration of time that each truck was followed proved to be adequate for estimating mean values and variance of the lateral placement of truck wheels within the highway lane because the stability tests did not reveal significant differences.

A number of factors can possibly cause the lateral placement of truck wheels to vary at any given location and time. The factors that were evaluated in this study are given in Table 3 along with the chosen levels of each factor. An analysis of variance (ANOVA) procedure was used to identify which of the factors and which levels contributed signifi-

TABLE 1 Observations of Truck Wheel Placement

Truck Identification No.	Type	Total Time Followed (sec)	No. of Observations
1	3-S2	417	44
2	2-axle	501	61
3	3-S2	241	19
4	3-S2	560	68
5	2-axle	326	35
6	3-axle	242	29
7	3-S2	664	86
8	3-S2	382	51
9	3-S2	751	88
10	3-axle	435	42
11	2-axle	622	89
12	2-axle	255	39
13	2-axle	425	42
14	3-S2	641	33
15	3-S2	1,027	89
16	3-S2	925	95
17	3-S2	583	62
18	2-axle	223	23
19	3-axle	396	39
20	3-S2	370	38
21	3-S2	110	29
22	3-axle	105	19
23	3-S2	120	14
24	3-axle	180	15
25	3-S2	460	44
26	3-S2	311	26
27	3-S2	349	33
28	3-S2	601	83
29	3-S2	282	35
30	3-S2	421	39
31	3-S2	109	17
32	3-S2	372	36
33	3-S2	943	159
34	3-S2	652	73
35	3-S2	611	75
36	3-S2	482	54
37	3-S2	461	57
38	3-S2	574	63
39	3-S2	423	33
40	3-S2	867	95

TABLE 2 Overall Characteristics of Lateral Wheel Placement for Trucks Observed

Truck Identification No.	Mean Placement (ft)	Variance (ft^2)
Truck Type: 3-S2		
1	1.09	0.76
3	1.26	1.02
4	0.96	0.65
7	1.71	0.73
8	1.19	0.74
9	1.40	0.77
14	0.72	1.05
15	1.27	0.75
16	1.92	1.17
17	1.38	0.97
20	1.87	1.10
21	0.76	0.89
23	2.7	0.9
25	1.61	0.9
26	1.52	1.06
27	0.81	0.77
28	1.03	0.73
29	1.38	0.94
30	1.46	0.68
31	0.96	0.65
32	1.62	0.88
33	1.62	0.67
34	1.15	0.76
35	1.80	0.66
36	1.81	0.66
37	1.34	0.68
38	1.97	0.88
Truck Type: 3-Axle and 2-Axle		
2	1.6	0.76
5	2.09	1.0
6	1.5	0.89
10	0.61	0.79
11	2.28	0.53
12	1.98	0.69
13	1.97	1.15
18	1.23	0.62

TABLE 3 Factors and Levels Included in Sample

Factors	Levels
Truck type	Single unit
	2-axle
	3-axle
	Tractor and semitrailer
	3-S2
	2-S1
Geometry	Straight
	Downgrade
	Upgrade
	Left curve, level
	Right curve, level
	Left curve, downgrade
	Right curve, downgrade
	Left curve, upgrade
	Right curve, downgrade
Pavement surface	Rigid pavement (concrete)
	Flexible pavement (asphalt)
Lanes	Inside lane
	Center lane
	Outside lane

cantly to explaining the observed variability in lateral wheel placement. Truck type and section geometry were found to be significant influencing factors, but pavement surface type and lane location were not. Two types of trucks--single unit and tractor and semitrailer--were found to have significantly different frequency distributions of lateral wheel placement. Also, two categories of roadway geometry--straight sections and sections with horizontal curvature (regardless of vertical alignment)--exhibited different patterns of lateral wheel placement. The details of the statistical analysis are again given elsewhere (11).

It was necessary to establish four representative frequency distributions for lateral truck wheel placement within the highway lane. Table 4 gives the percentages of truck wheel placements that were observed to fall within the indicated 1-ft intervals with respect to the right pavement edge for each condition. Because no significant difference was found between the placement patterns in the Austin and in the Houston areas, it may be assumed that the tabulated values are representative of general conditions throughout the state. An expanded data set would be needed to substantiate this assumption, however.

TABLE 4 Frequency Distribution of Lateral Wheel Placements for Different Truck Types and Roadway Alignments

Wheel Placement[a] (midpoints of interval) in ft	Tractor and Semitrailer on Straight Sections	Tractor and Semitrailer on Curved Sections	Single-Unit Trucks on Straight Sections	Single-Unit Trucks on Curved Sections
−1.0	1[b]	0.5	3	2
0.0	12	14	16	20
1.0	38	35	20	25
2.0	38	34	41	36
3.0	10	16	19	16
4.0	1	0.5	1	1

[a]Wheel placement is measured between the right-hand edge of the rear tire and the inside edge of the lane or edge line.
[b]Numbers in the table denote the percentage of observation within each class interval.

EFFECTS OF LATERAL WHEEL PLACEMENT ON DESIGN THICKNESS OF RIGID PAVEMENTS

Design procedures for highway pavements have been developed on the assumption that wheel loads are applied at some standard or average lateral location within the lane. The general AASHO Road Test equation (3), for example, characterizes traffic loading only in terms of the number of single or tandem axle loads and their respective magnitudes. The actual lateral positions of the test truck wheels that occurred during the road test were not incorporated into the equation as a variable. In extending this general empirical equation to handle conditions other than those that existed at the road test, a relationship was developed only between the observed number of axle load applications of various types, which produced a given terminal serviceability index at the road test, and the ratio of the modulus of rupture to the maximum tensile stress in the concrete slab as calculated by Spangler's equation for corner loading. Thus the AASHO design equations and nomographs do not allow for direct evaluation of the effects of varying lateral distribution of traffic wheel positions within the lane.

The lateral distribution of truck wheel loads of different magnitudes and number of repetitions across the pavement surface produces various levels of stress, and therefore damaging effects, at any selected point in the pavement slab. To illustrate the relative effect of such lateral distribution of load, design thicknesses for two loading conditions have been determined--one for the edge loading condition and another for the laterally distributed loading condition.

A finite element program (12) was used to calculate the stresses, due to loads positioned at various points on the surface of the slab, at different points in a concrete pavement slab. By running the program several times, with an 18-kip single axle load positioned at a different place each time, the various stress levels that would result at any selected point in the slab from each load position were identified. Then the cumulative damaging effect of repeated applications of these various stress levels at a critical point in the slab was assessed. A pavement thickness that could accommodate a laterally distributed loading frequency pattern without exceeding selected strength-to-stress ratios was finally determined by successive approximation. For comparison, the thickness required for repeated applications of an 18-kip single axle load, all in the conventional edge loading position, was determined using the same procedure.

Slab Model

A 12-ft by 12-ft slab was considered for evaluation purposes. The slab was divided into 144 square elements so that each node was 1 ft away from the adjacent node. The loads were imposed at the nodes, and each node had associated with it a certain slab stiffness and a subgrade stiffness. Figure 1 shows a schematic of the arrangement of nodes and the position of the wheel loads. The edge and corner conditions of the slab were simulated by reducing the stiffness of the slab and the spring support to one-half or one-quarter of the original stiffness, respectively, at the appropriate nodes. A computation was then carried out by the program to determine the stresses (both tensile and compressive) at all the nodal points for each selected loading condition.

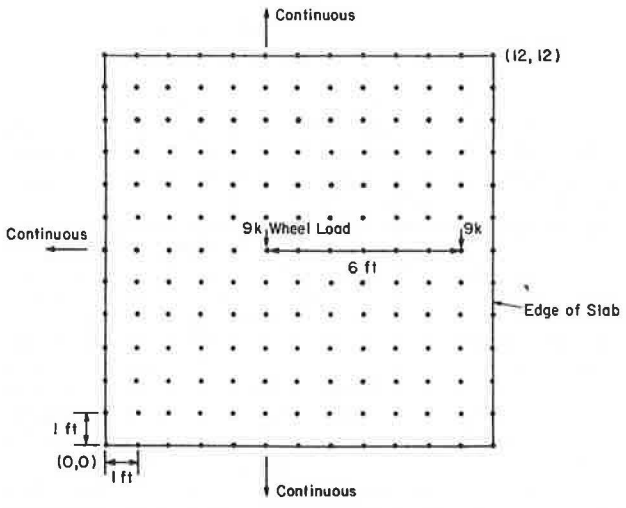

FIGURE 1 Finite element modeling of a slab subjected to an 18-kip axle load.

Use of Vesic's Fatigue Model

Vesic and Saxena (13) used the AASHO Road Test data to develop a fatigue model that incorporated several different loading configurations on rigid pavements of various thicknesses. A concrete slab 30 ft long and 12 ft wide with a transverse joint in the center was modeled in their analysis. Single axle and tandem axle loads were positioned laterally as shown in Figure 2 (inset) and were shifted in nodal increments toward the joint. The resulting maximum tensile stresses were then plotted against the distance of the load from the joint. Figure 2 shows a sample curve. Similar curves were developed for various magnitudes of loads and pavement thicknesses. The lateral placement of the outer wheel was always assumed to be 2.5 ft away from the pavement edge (average wheel path) because AASHO Road Test data were reported only for this condition.

The maximum tensile stress that occurred for different load magnitudes and for different pavement thicknesses was then plotted against the number of repetitions accommodated before the pavement reached a present serviceability index of 2.5 (data available from AASHO Road Test). Vesic and Saxena found that a unique relationship could be described as follows:

$$N_t = 225{,}000\,(f_c/\sigma)^4$$

where

N_t = number of replications of an equivalent 18-kip single axle load needed to reduce the present serviceability index to a value (t),
f_c = modulus of rupture (strength) of the concrete, and
σ = maximum tensile stress in the concrete due to axle loading.

This fatigue model has been used to approximate the effect of distributing wheel load repetitions laterally across the pavement and to calculate the cumulative damage. The slab model used for this purpose was 12 ft by 12 ft, and no joints were present. The basic load position case--that of applying all the repetitions near the edge of the slab--to a certain extent is similar to the critical loading condition of Vesic and Saxena with the axle near the joint. The lateral shift case (i.e., shifting the load repetitions laterally inward from the edge of the slab) compares with Vesic's and Saxena's shifting of the loading configuration longitudinally, away from the transverse joint. Thus a stress distribution curve for the several loading configurations in this analysis might resemble Vesic's and Saxena's stress distribution curves shown in Figure 2. No empirical data concerning the fatigue effects of loads positioned at various lateral positions in the lane are known to exist. Thus an effort was made in this evaluation to adhere as closely as possible to Vesic's and Saxena's loading configuration so that their fatigue model could be used to compare the cumulative damage that might occur to the pavement for laterally distributed loads. The actual loading configurations and the modeling procedure are described in further detail next.

Thickness Required for Repeated Application in the Edge Loading Position (Case 1)

Vesic's and Saxena's fatigue model (13), as shown previously, was used to relate the number of replications to the allowable stress ratio. The terminal serviceability index (t) was set at 2.5. The following assumptions were made in applying this model:

- That the stress ratio is an adequate indicator of the effect of the number of load repetitions on reducing the present serviceability index and
- That the model is valid regardless of where the loads are positioned and where the maximum tensile stresses occur.

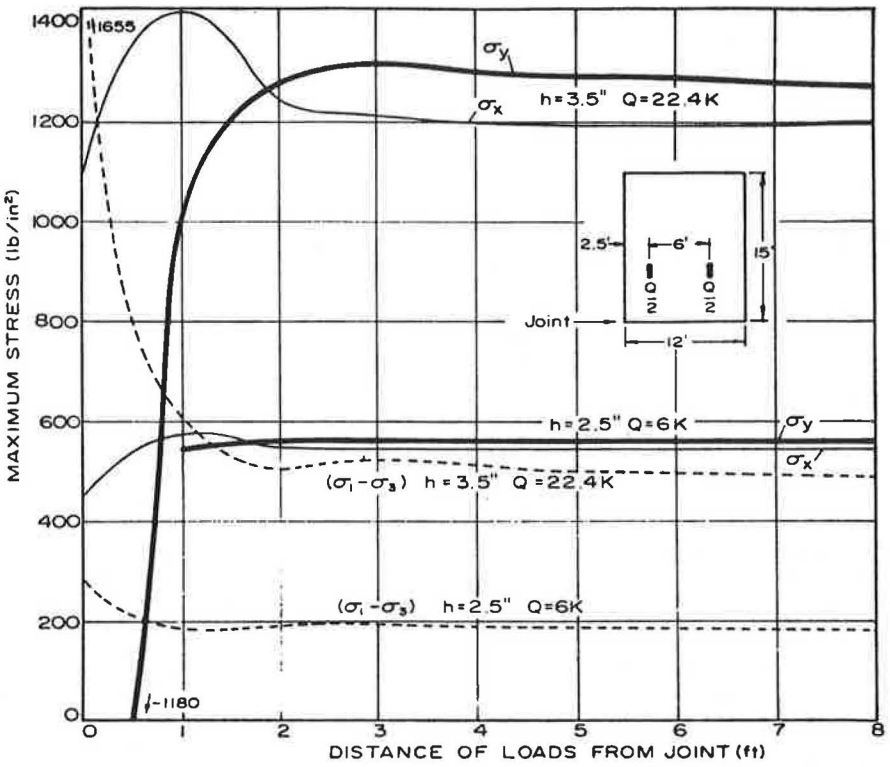

FIGURE 2 Maximum tensile stress as a function of load position for Vesic's model *(13)*.

With these assumptions, the following procedure was carried out:

- Taking the number of replications of the standard 18-kip single axle load that would occur at the edge loading position before failure, the allowable stress ratio was calculated from the fatigue model.
- A modulus of rupture (strength) of concrete was taken as 650 psi, and the maximum allowable tensile stress was calculated from the stress ratio.

The same finite element model (12) that was employed by Vesic and Saxena (13) was then used to calculate the maximum tensile stress in a slab of some trial thickness caused by an 18-kip single axle load being placed at the center of the slab longitudinally with the center of the outside wheel 1.0 ft from the edge of the slab. This maximum tensile stress (under the outside wheel) was compared with the maximum allowable tensile stress from the fatigue model; then another trial thickness was chosen so as to make the calculated stress more nearly equal to the allowable stress for fatigue loading. By making successive adjustments in slab thickness, these stresses were made approximately equal. The resulting thickness was that which would be needed to sustain the chosen number of applications of an 18-kip single axle load in the edge loading position (Case 1) while reducing the present serviceability index to a value of 2.5.

Thickness Required for a Laterally Distributed Application of Loads (Case 2)

The percentages given in Table 4 represent the frequency of application of heavy axle loads in the right lane of multilane highways at the designated transverse locations in 1-ft intervals. Because the distances indicated in the table were measured to the outer wheel edge and the load is considered to be applied at the center of the dual wheels, the modeled loading position is 1 ft to the left of the wheel position placement that is shown in the table.

The lateral loading pattern used for comparison with edge loading is similar to that for tractor and semitrailer trucks on straight alignment and is distributed as follows:

- Right wheel 1 ft from the edge line: 10 percent of total applications (edge loading); loading coordinates were (5,6) and (11,6) each wheel carrying 9 kips.
- Right wheel 2 ft from the edge line: 40 percent of applications; loading coordinates were (4,6) and (10,6).
- Right wheel 3 ft from the edge line: 40 percent of applications; loading coordinates were (3,6) and (9,6).
- Right wheel 4 ft from the edge line: 10 percent of applications; loading coordinates were (2,6) and (8,6).

The first step was to determine the magnitudes and the locations of stresses in the slab caused by the different loading positions. The stresses under nodes (11,6), (10,6), (9,6), and (8,6) were tabulated. The following values for pavement material characteristics were used in the computer program:

$E = 5 \times 10^6$ psi = modulus of elasticity for concrete,
$k = 100$ psi/in. = modulus of subgrade reaction, and
$\mu = 0.15$ = Poisson's ratio for concrete.

An example of stresses for an 8-in. slab thickness is given in the following table.

Loading Position		Tensile Stress Under Node (psi) for Position			
Left Wheel	Right Wheel	(11,6)	(10,6)	(9,6)	(8,6)
(5,6)	(11,6)	-330.6	-215.9	-155.9	-133.4
(4,6)	(10,6)	-208.4	-281.9	-189.8	-141.7
(3,6)	(9,6)	-135.8	-180.2	-265.2	-180.0
(2,6)	(8,6)	-93.8	-118.8	-169.4	-258.6

To account for the accumulated damage due to these several loadings, the following procedure incorporating Minor's hypothesis was used.

Assuming that maximum cumulative damage for 10 million load applications occurs under node (10,6), where 40 percent of the load repetitions occur, the possible number of replications for the different stress levels were calculated as follows:

1. Stress at (10,6) due to loading at nodes (10,6) and (4,6) = -281.9 psi.
2. Additional stress at (10,6) due to loading at nodes (11,6) and (5,6) = -215.9 psi.
3. Additional stress at (10,6) due to loading at nodes (9,6) and (3,6) = -180.2 psi.
4. Additional stress at (10,6) due to loading at nodes (8,6) and (2,6) = -118.8 psi.

Each of these stresses has associated with it a certain number of possible applications of load, which can be calculated from the Vesic fatigue model. The possible replications and the corresponding actual replications are

	Possible	Actual
1 =	6,350,000	4,000,000
2 =	18,500,000	1,000,000
3 =	38,100,000	4,000,000
4 =	Very large	1,000,000
Total		10,000,000

The cumulative linear damage hypothesis (Minor's hypothesis) states that the sum of the ratio of actual to theoretical (or possible) application for each type of load must be equal to unity before failure occurs. Assuming that failure refers to the pavement reaching a present serviceability index of 2.5, the cumulative damage is as follows:

$$(4{,}000{,}000/6{,}350{,}000) + (1{,}000{,}000/18{,}500{,}000) + (4{,}000{,}000/38{,}100{,}000) + \text{negligible} = 0.63$$

$$+ 0.05 + 0.10 + \text{negligible} \simeq 0.80$$

Note that the cumulative damage index for an 8-in. slab thickness was arrived at after trying several other thicknesses. The actual procedure calls for evaluating the cumulative damage for different thicknesses until the sum of the ratios is close to unity. In this case further iteration is possible until the cumulative damage equals exactly 1, but only minor change in the thickness would be required.

This procedure has been used to determine thicknesses needed to accommodate 1, 10, and 20 million replications of the standard 18-kip single axle load both for the edge loading case and for the laterally distributed loading case using the material properties stated previously. For comparison, design thicknesses have also been determined from the AASHTO Interim Guide (3) nomographs. These values are given in Table 5.

TABLE 5 Design Thicknesses in Inches for Different Lateral Loading Positions and Design Procedures

Condition	Total No. of 18-Kip Axles (millions) 1	10	20
All loads edge location, Vesic fatigue model	7.0	9.1	10.0
Laterally distributed loads, Texas study of tractor and semitrailer trucks, straight alignment, Vesic fatigue model (see Table 4)	6.0	7.8	8.5
AASHTO Interim Guide *(3)*	5.9	8.8	9.9

SUMMARY

Theoretical considerations have shown that there is a considerable difference in the stresses calculated for the edge loading case and for the interior loading case in the design of rigid highway pavements. In practice, wheel loads are distributed laterally across the lane in accordance with a frequency distribution pattern. Field studies, using a video recorder in a following vehicle, produced a data set of representative truck wheel placements on multilane highways in Texas. Analysis of these data resulted in frequency distributions of wheel placement for two truck types and for two horizontal alignment conditions. To illustrate the possible application of these distributions in pavement design, a procedure was devised for evaluating the cumulative critical stress replications in a pavement slab. For one case, all load replications were applied in the edge loading position and a finite element program was used to calculate the resulting stresses. For another case, the finite element program was used to determine the various maximum tensile stresses at different points in the pavement slab and a fatigue model by Vesic and Saxena (13) was used to relate the stresses to allowable load repetitions. Using Minor's linear damage hypothesis, a comparison of the thicknesses required for 1, 10, and 20 million load replications showed that reduction in the design pavement thickness of between 14 and 16 percent could be realized when loads were distributed laterally according to a representative frequency distribution. These results indicate that the lateral distribution of load repetitions has significant effects on the stress conditions in rigid pavements and that design procedures should incorporate means for recognizing the variability in lateral wheel position within the lane. A computer program can be easily devised to perform the calculations needed for determining design thickness in accordance with the procedures described.

REFERENCES

1. H.M. Westergaard. Computations of Stresses in Concrete Roads. Proc., HRB, National Research Council, Washington, D.C., Vol. 5, Part 1, 1925, pp. 90-112.
2. E.J. Yoder and M.W. Witczak. Principles of Pavement Design. 2nd ed. John Wiley and Sons, Inc., New York, 1975.
3. AASHTO Interim Guide for Design of Pavement Structures. American Association of State Highway and Transportation Officials, Washington, D.C., 1974.
4. W.P. Walker. Influence of Bridge Width on Transverse Positions of Vehicles. Proc., HRB, National Research Council, Washington, D.C., Vol. 21, 1941, pp. 361-365.
5. A. Taragin. Transverse Placement of Vehicles as Related to Cross Section Design. Proc., HRB, National Research Council, Washington, D.C., Vol. 23, 1943, pp. 342-350.

6. A. Taragin. Effect of Roadway Width on Traffic Operations--Two Lane Concrete Roads. Proc., HRB, National Research Council, Washington, D.C., Vol. 24, 1944, pp. 292-318.
7. Vehicle Speed and Placement Survey on Two Lane Rural Highways. Road Design Division, Texas Highway Department, Austin, March 1957.
8. D.H. Weir and C.S. Sihilling. Measures of Lateral Placement of Passenger Cars and Other Vehicles in Proximity to Inner City Buses on Two Lane and Multi-Lane Highways. Final Report. Environmental Design and Control Division, FHWA, U.S. Department of Transportation, Oct. 1972.
9. E.J. Miller and G.N. Stuart. Vehicle Lateral Placement on Urban Roads. Journal of the Transportation Engineering Division, ASCE, Vol. 108, Sept. 1982.
10. E. Ellard. Vehicle Size-Lane Width Interaction: A Pilot Project. M.S. thesis. University of Toronto, Toronto, Canada, 1975.
11. P.R. Shankar. Lateral Placement of Truck Traffic in Highway Lanes. Ph.D. dissertation. University of Texas at Austin, 1984.
12. J.J. Panak and H. Matlock. A Discrete-Element Method of Analysis for Orthogonal Slab and Girder Bridge Floor Systems. Research Report 26-25. Center for Highway Research, University of Texas at Austin, May 1972.
13. A.S. Vesic and S.K. Saxena. Analysis of Structural Behavior of AASHO Road Test Rigid Pavements. NCHRP Report 97. HRB, National Resarch Council, Washington, D.C., 1970.

Publication of this paper sponsored by Committee on Rigid Pavements.

ILLI-PAVE Mechanistic Analysis of AASHO Road Test Flexible Pavements

ROBERT P. ELLIOTT and MARSHALL R. THOMPSON

ABSTRACT

The stress-dependent, finite element pavement model known as ILLI-PAVE was used to study the performance of AASHO Road Test flexible pavement sections. Analyses were conducted to identify significant relationships between the appearance of fatigue cracking in the asphalt concrete (AC) surface and the AC strain and subgrade deviator stress predicted by ILLI-PAVE. Deflection and temperature data from the road test were used with ILLI-PAVE to "back calculate" seasonal variations in subgrade support and load-induced pavement stresses and strains. The structural response-performance relationships identified explain the observed behavior of the AASHO Road Test pavement sections in a realistic fashion. Seasonal damage factors and weighting factors based on these relationships provide a mechanistic explanation of the seasonal effects that is consistent with experience. These results demonstrate that ILLI-PAVE is a powerful tool for pavement design and analysis. It provides an adequate and valid representation of the structural behavior of conventional flexible pavements and can be used to effectively evaluate nondestructive test (NDT) data and determine the structural characteristics of existing pavement systems. ILLI-PAVE, therefore, will serve as a sound basis for the development of mechanistic procedures for the design of new flexible pavements and for the selection of rehabilitation strategies for existing flexible pavements.

In a preliminary effort to select transfer functions for a mechanistic flexible pavement design procedure, the performance of the flexible pavement sections of Lane 1, Loop 4 of the AASHO Road Test was studied. The mechanistic design procedure is to be based on the structural response predictions (stresses, strains, and deflections) of the stress-dependent, finite element pavement model known as ILLI-PAVE. This model was selected on the basis of previous studies by Figueroa (1) and Hoffman and Thompson (2) that showed that ILLI-PAVE provided reliable and realistic predictions of the structural behavior of pavement. Simplified equations, referred to as ILLI-PAVE structural response algorithms, were

developed (3) that predict the "critical" response parameters for the standard 18-kip single axle load. The AASHO Loop 4 pavement sections selected for study had been subjected to 18-kip single axle loads and thus were compatible with the stresses and strains predicted by the ILLI-PAVE algorithms.

In mechanistic pavement design, the pavement system is analyzed on the basis of the predicted structural response (stresses, strains, and deflections) of the system to moving vehicle loads. Pavement layer thicknesses (surface, base, and subbase) are selected to resist the detrimental effects of these predicted response parameters for some desired number of load repetitions. The relationships used for thickness selection are collectively referred to as transfer functions. Transfer functions relate structural response to pavement performance. However, because the predicted stresses, strains, and deformations for a given pavement are not the same for all structural models, the transfer functions are "model dependent" and must be developed for the model used in the design procedure.

The AASHO Road Test pavements were studied to identify significant relationships between the appearance of fatigue cracking in the AC surface and the AC strain and subgrade deviator stress predicted by the ILLI-PAVE structural response algorithms. Flexible pavement cracking at the road test was divided into three classes. The first to appear were fine, disconnected hairline cracks called Class 1. As these lengthened, widened, and connected to form an alligator crack pattern, they were classified as Class 2 cracks. The cracking was called Class 3 when the crack edges became spalled and the individual pieces loosened and moved under traffic. The analyses discussed here were based on the appearance of Class 1 cracks.

MATERIAL CHARACTERIZATION

ILLI-PAVE includes stress-strain material characterization models that realistically represent the nonlinear, stress-dependent resilient behavior of granular materials and fine-grained soils. Included in the model is a shear strength-based "stress adjustment" feature that compensates for predicted stresses that exceed the actual strength of the granular base and subgrade materials (e.g., tensile stresses in the granular base). This feature has been described by Raad and Figueroa (4).

The basic relationship used to model the behavior of granular base material is

$$Er = K\theta^n \tag{1}$$

where

Er = resilient modulus of the material;
K,n = constants determined from laboratory testing; and
θ = the sum of the three principal stresses, $\sigma_1 + \sigma_2 + \sigma_3$ (in triaxial testing $\theta = \sigma_1 + 2\sigma_3$).

The ILLI-PAVE algorithms were developed (3) using K and n values for the AASHO Road Test granular materials reported by Traylor (5).

The behavior of fine-grained subgrade soil is represented by two intersecting, arithmetic, straight line relationships as shown in Figure 1. The mathematical expression for the model is

$$Er = Eri + K1 \cdot (Sd - Sdi) \quad \text{for } Sd < Sdi \tag{2}$$

and

$$Er = Eri + K2 \cdot (Sd - Sdi) \quad \text{for } Sd > Sdi \tag{3}$$

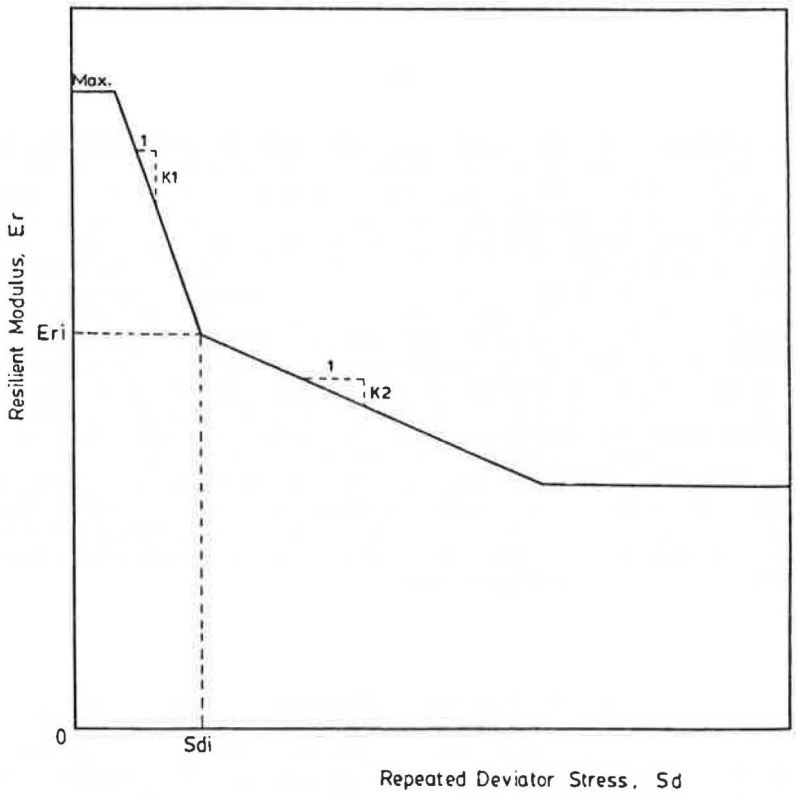

FIGURE 1 Typical representation of the resilient modulus-repeated deviator stress relationship for fine-grained soils.

where

Er = resilient modulus,
Eri = resilient modulus at the "breakpoint" between the two Er versus Sd slopes,
K1,K2 = slopes of the Er versus Sd relationship,
Sd = deviator stress, and
Sdi = deviator stress at the breakpoint between the ER versus Sd slopes.

The K1, K2, and Sdi values used in developing the ILLI-PAVE algorithms were based on the results of an extensive study of Illinois soils (including the AASHO subgrade) by Thompson and Robnett (6).

Asphalt concrete (AC) is modeled in ILLI-PAVE as a linear elastic solid. For this study, the AC modulus (Eac) was calculated using the equation developed by the Asphalt Institute (7) with mix data reported from the road test (8). Figure 2 shows a plot of the temperature-Eac relationship used in the analyses. For comparison, laboratory test results on AC samples taken from the road test pavements and reported by Austin Research Engineers (9) are shown.

ANALYSIS OF SUBGRADE VARIATION

Two types of algorithms were used in the study, design response algorithms and pavement analysis algorithms. The design response algorithms predict the critical stress and strain in the pavement system due to an 18-kip single axle load. The prediction is made on the basis of the AC thickness, the granular base thickness, the AC modulus, and the subgrade Eri. The design response algorithms will serve as the basis of the mechanistic design procedure.

The pavement analysis algorithms are for use in analyzing the structural response of existing pavements using nondestructive testing (NDT) data. The NDT data are used to "back calculate" subgrade Eri and to estimate the load-induced stresses and strains.

For this study, the pavement analysis algorithms were used to determine the apparent seasonal variation in the subgrade Eri during the road test. The Benkelman beam deflection data from the road test were converted to equivalent moving wheel load deflections by multiplying the deflection measurements by 0.62. This conversion was based on speed-deflection studies conducted during the road test (8). AC modulus variation was estimated using the average AC temperature reported at the time of deflection testing (Figure 3). These Eac values and the deflections of each pavement section were used in the analysis algorithms to estimate subgrade Eri's at the time of testing. Only sections that had not yet cracked at the time of testing were included in the analyses of each period. The average Eri for all sections analyzed was selected as the Eri for each deflection test date. Figure 4 shows a plot of seasonal vari-

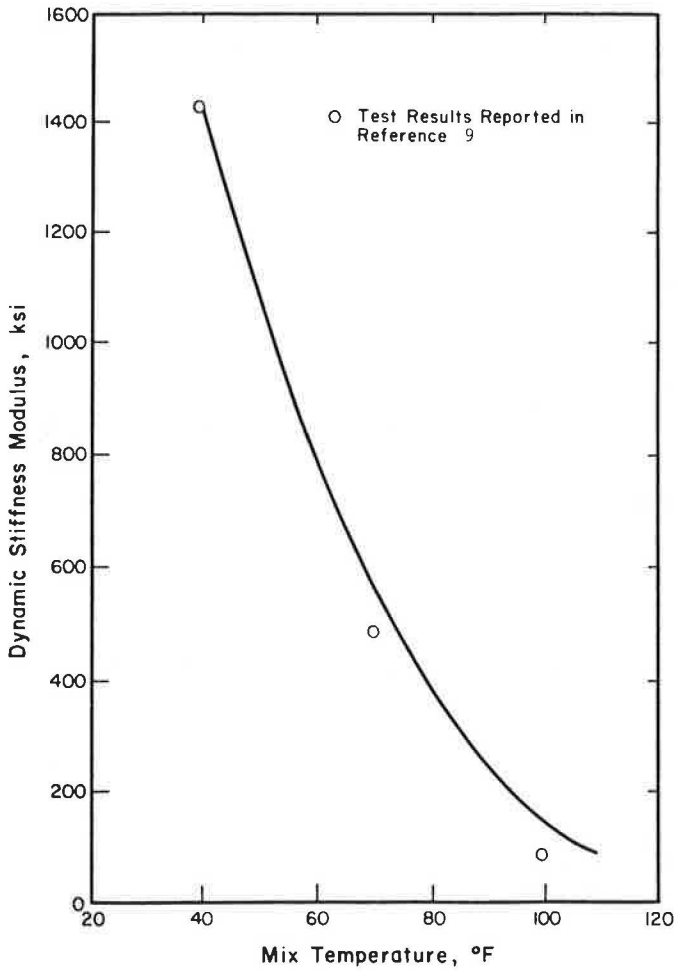

FIGURE 2 AC mix temperature-modulus relationship used in analysis of AASHO Road Test sections.

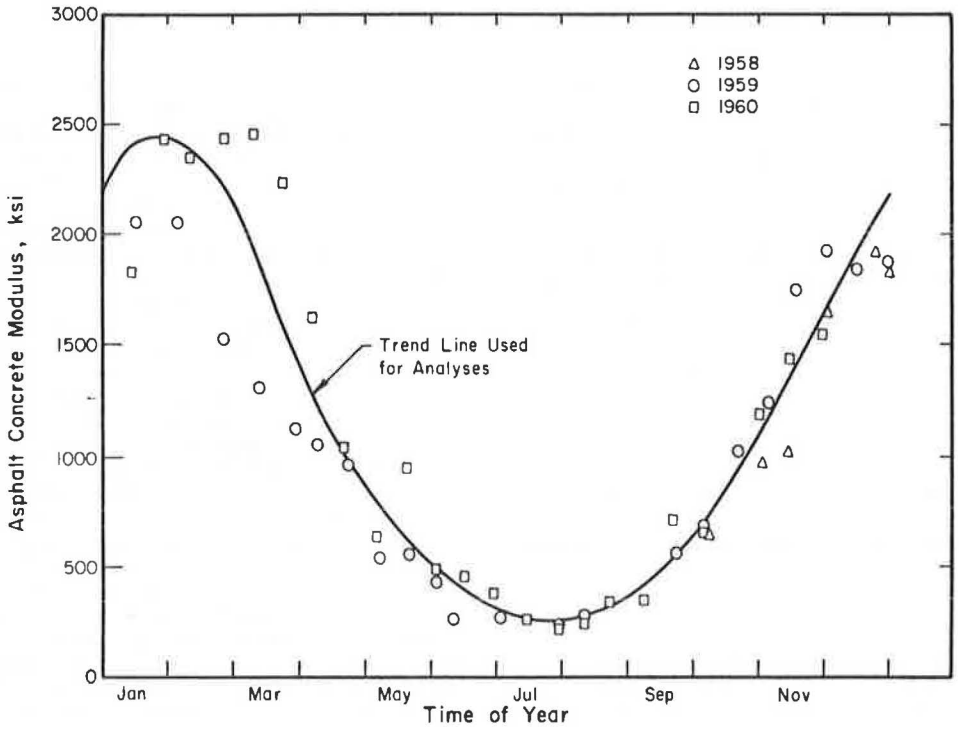

FIGURE 3 Trend of AC modulus during AASHO Road Test.

ation in subgrade Eri. The Eac and Eri trends shown in Figures 3 and 4 were subsequently used with the design response algorithms for the structural response-performance analyses.

EFFECT OF GRANULAR TYPE ON STRUCTURAL RESPONSE

ILLI-PAVE model analyses based on K and n values typical of crushed stone and gravel base courses showed that the type of granular material has only a limited effect on the structural response (stresses, strains, and deflections) of the pavement system (3). For design purposes, the response differences were not deemed sufficient to warrant including granular type as a variable in the ILLI-PAVE algorithms. Therefore only base thickness, with no differentiation for material type, was included.

Deflection data from the AASHO Road Test were analyzed to determine the validity of this decision. Both gravel and crushed stone were used in the road test flexible pavements. The crushed stone was referred to as the base course and the gravel was called the subbase. In Loop 4, base course thicknesses were 0, 3, and 6 in. Subbase thicknesses were 4, 8, and 12 in. Each possible combination of these thicknesses was used with AC thicknesses of 3, 4, and 5 in. Deflection data gathered during the early phases of the test (before significant damage was done to any of the pavements) were analyzed to determine the relative effect of each type of granular material on structural response. For the 3-in. AC sections, data from the first two measurement periods were used. Data from the first three periods were used for the 4- and 5-in. thicknesses.

Correlation and regression analyses were conducted using the measured deflections as the dependent variable and the thickness of granular material as the independent variable. Two types of analyses were made, one using the total, combined granular thickness (crushed stone plus gravel) as a single independent variable and the other using the two thicknesses as separate independent variables. The data for each AC thickness were analyzed individually to eliminate any thickness interaction effect.

Comparison of the correlation coefficients and standard errors of estimate for the two types of analysis were used as an indication of the relative significance of separating or combining the thicknesses in terms of structural response. Table 1 gives the results of the analyses. In general, the correlation coefficients were slightly higher when the separate thicknesses were used; however, standard errors of estimate were nearly the same for both cases with an equal split between the separate and combined thickness analyses in the number that produced the lower standard error of estimate (four each). These results demonstrate that the type of granular material has little effect on structural response of pavement.

This should not be interpreted to imply that the type and quality of granular material do not influence pavement performance. The structural re-

TABLE 1 Analysis of Early AASHO Road Test Data for the Relative Effects of Granular Base and Subbase

Section Asphalt Thickness (in.)	Testing Index Day	Correlation Coefficient		Standard Error of Estimate	
		Separate[a]	Combined[b]	Separate[a]	Combined[b]
3	827	0.84	0.81	14.5	14.4
3	871	0.80	0.79	16.6	16.0
4	827	0.91	0.83	6.3	8.0
4	871	0.89	0.71	4.1	6.0
4	997	0.87	0.64	11.3	16.6
5	827	0.78	0.78	7.9	7.4
5	871	0.79	0.72	5.9	6.2
5	997	0.83	0.83	6.1	5.7

[a]The thickness of base and subbase were treated as two independent variables.
[b]Base and subbase thicknesses were added and treated as a single independent variable.

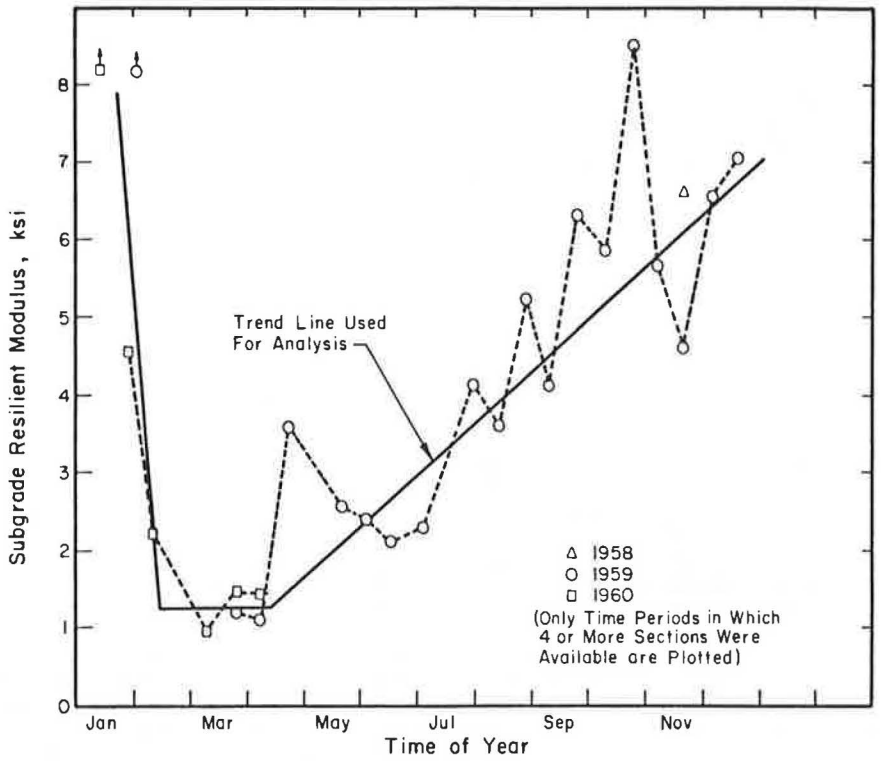

FIGURE 4 Trend of subgrade Eri during AASHO Road Test.

sponse may be similar but the relationships between response and performance will differ. Differing design criteria related to performance (or differing transfer functions) must be established for various types and qualities of base.

ASPHALT STRAIN VERSUS CRACKING

Fatigue Relationships for Asphalt Concrete

Except for temperature cracks and long-term weathering cracks, AC surface cracking in conventional flexible pavements is normally considered to be associated with fatigue. Thus there should be some relationship between the radial strain at the bottom of the AC layer and the number of load repetitions to crack appearance. Laboratory testing indicates that the relationship can be expressed in the form:

$$N = K \cdot eac^a \quad (4)$$

where

N = number of load repetitions to cracking,
K = multiplication constant determined by testing,
eac = magnitude of load-induced strain, and
a = power constant determined by testing.

Laboratory testing is conducted under controlled conditions in which the temperature of the mix does not vary and either the applied stress or the induced strain is held constant. In actual pavements each of these items changes continuously over the life of the pavement, complicating the behavioral relationships. For the AASHO pavements, this is somewhat simplified because the loading was constant. However, with the seasonal variations in subgrade support conditions and the changes in AC modulus due to temperature fluctuations, the AC strain variations over the life of the pavements are quite large and complicated.

Research reported by Bonnaure et al. (10) and by Finn et al. (11) indicate that the fatigue effect of the load-induced strain is a function not only of the strain magnitude but also of the modulus of the AC. This has been expressed as fatigue equations having the general form:

$$N = K \cdot eac^a \cdot Eac^b \quad (5)$$

where Eac is the AC dynamic stiffness modulus and b is a power constant determined by testing.

Equation 5 quantifies some of the AC temperature variation effects but does not address the problems associated with variations in the strain value itself. To account for the strain variations, Miner's hypothesis of damage accumulation has been used with reasonable success with numerous materials including AC (12). This hypothesis together with the general fatigue equation shown previously was employed in analyzing the road test pavements.

Miner's hypothesis can be expressed mathematically in terms of relative damage factors. Cracking is expected to occur when the sum of the damage factors equals one. The equation for the damage factors is

$$Di = ni/Ni \quad (6)$$

where

Di = relative damage during some period i,
ni = number of load applications during the period, and
Ni = total number of load applications the pavement could carry for the strain induced under the conditions prevailing during the period.

In Equation 6 Ni is determined by a fatigue equation of the form shown previously and is a function of the load-induced strain (eac) and AC modulus. The object of the analyses was to select appropriate values for the fatigue equation constants K, a, and b. The approach taken in the analyses was to (a) select reasonable estimates of the appropriate values for a and b, (b) use these values with the road test data and the design algorithm for AC strain to calculate average Ks for each combination of a and b for all sections, and (c) select the K, a, and b combination that provides the best prediction of the actual data.

Selection of a and b Values for Fatigue Analysis

Three tentative values were selected for b. These were -0.854, -1.4, and -1.8. The first value was selected on the basis of Finn's analysis (12) of the fatigue behavior of the road test pavements. The other two values were taken from the fatigue equations reported by Bonnaure et al. (10).

Preliminary estimates of the a constant were made using the deflection-based performance equations from the AASHO Road Test (8) with the deflection algorithm developed in another study (3). Two performance-deflection equations were available from the road test. One was for the number of load applications to a present serviceability index of 2.5 (the point at which most major highways are rehabilitated); the other was to a present serviceability index of 1.5 (the point at which the road test pavements were removed from test). The equations are

$$\log N2.5 = 9.40 + 1.32 \cdot \log L - 3.25 \cdot \log dsn \quad (7)$$

and

$$\log N1.5 = 10.18 + 1.36 \cdot \log L - 3.64 \cdot \log dsn \quad (8)$$

where

N2.5 and N1.5 = number of axle load applications to a present serviceability index of 2.5 and 1.5, respectively;
L = axle load in kips; and
dsn = spring normal Benkelman beam deflection.

As discussed previously, Benkelman beam deflections from the road test were converted for purposes of analysis to equivalent dynamic deflections by multiplying by 0.62. Substituting this conversion and the standard 18,000-lb (18-kip) axle load value into Equations 7 and 8 yields

$$\log N2.5 = 10.3822 - 3.25 \cdot \log Do \quad (9)$$

and

$$\log N1.5 = 11.1315 - 3.64 \cdot \log Do \quad (10)$$

where Do is the dynamic surface deflection in mils.

One algorithm has been developed (3) to estimate AC strain (eac) based on surface deflection. This algorithm is

$$\log eac = -5.0898 + 1.1126 \cdot \log Do \qquad SEE = 0.115 \qquad R^2 = 0.79 \quad (11)$$

where eac is tensile strain in the bottom of the AC, in inches per inch. Solving for log Do and substituting this into Equations 9 and 10, performance equations in the form of AC fatigue equations are obtained. These equations are

$$\log N2.5 = -4.4856 - 2.92 \cdot \log eac \quad (12)$$

and

$$\log N1.5 = -5.5204 - 3.27 \cdot \log eac \quad (13)$$

The constants 2.92 and 3.27 are analogous to the a constant of the fatigue equation. These values were taken as an approximation of the value for a that would best represent the fatigue properties of the AASHO Road Test mixes.

Two values for a in this general range were subsequently selected for use in the analyses. These were 3.16 and 3.29. The 3.16 value was taken from work reported by Thompson (13), and the 3.29 value came from the fatigue equation developed by the Asphalt Institute (7) in their analysis of the AASHO Road Test.

Determination of K Coefficient

A computer analysis program was developed for determining fatigue equation K coefficients. The program analyzed each AASHO pavement section from Lane 1 Loop 4 using all combinations of the a and b values selected. The program was based on Miner's hypothesis of accumulated damage and used the AC strain design algorithm. Algorithm inputs were the material thicknesses of each section and AC modulus and subgrade Eri's for each analysis period.

For purposes of analysis, the total time of the road test was divided into as many discrete periods as possible. The number of periods and their length were dictated by the time between deflection testing during the road test. In general, 2-week periods were used. The controlling factor was the date on which surface deflections were measured and reported because these data were used to estimate the subgrade Eri. Each analysis period then was the time between successive dates of deflection measurement.

AC modulus values for each analysis period were determined using the Asphalt Institute equation and the average measured AC temperature during the period. Eri values were selected on the basis of the work discussed under "Analysis of Subgrade Variation." For analysis periods from the start of the road test until late in the second spring, the average of the section Eri values was selected as the best estimate of the day of test Eri; and the average of two consecutive days of test Eri's was selected as the subgrade Eri for the analysis period. By late in the second spring, only four analysis sections remained that had not developed cracking. This number was not considered sufficient to provide a good Eri estimate. For the remainder of the analysis periods, Eri values were selected on the basis of the seasonal trend of values established from the earlier periods.

Table 2 gives the end dates of the analysis periods, the modulus values used for each period, and the total number of 18-kip single axle loads applied to the road test pavements to the end of the period.

The analysis program calculated damage factors (Di) for each pavement section during each analysis period using the number of axle applications during the period (ni) and the fatigue equation (Ni) with the K coefficient set equal to 1.0. For those periods in which the Eri is listed as "frozen," the damage factor was set equal to zero. Each section's damage factors were accumulated until the total number of axle applications equaled that reported for the occurrence of cracking.

With the K coefficient set equal to 1.0, each section's damage factor sum provided an estimate of

TABLE 2 Material and Load Application Data Used in Analysis of AASHO Road Test Pavement Sections

Period End Date	Total Axle Loads	Eac (ksi)	Eri (ksi)	Period End Date	Total Axle Loads	Eac (ksi)	Eri (ksi)
10/7/58	400	622	5.0	12/16/59	375,440	1,818	6.8
11/3/58	1,280	964	5.4	12/30/59	385,800	1,860	7.0
11/14/58	3,760	1,000	5.9	12/30/59	385,800	1,860	7.0
12/3/58	11,620	1,607	6.3	1/13/60	407,960	1,818	Frozen
12/24/58	25,460	1,900	6.7	1/27/60	445,200	2,423	Frozen
12/31/58	28,920	1,800	7.0	2/10/60	480,940	2,348	3.4
1/14/59	35,660	2,059	Frozen	2/24/60	507,280	2,423	1.9
2/4/59	52,300	2,060	Frozen	3/9/60	542,380	2,459	1.3
2/25/59	69,920	1,508	Frozen	3/23/60	572,360	2,230	1.2
3/11/59	75,780	1,300	1.2	4/6/60	603,460	1,610	1.3
3/27/59	79,600	1,116	1.2	4/20/60	636,040	1,037	1.3
4/8/59	86,120	1,054	1.1	5/4/60	671,200	624	1.6
4/22/59	97,580	964	2.3	5/18/60	707,180	938	1.9
5/6/59	106,620	535	3.3	6/1/60	735,100	488	2.2
5/20/59	119,360	556	2.8	6/15/60	774,440	448	2.5
6/3/59	136,220	420	2.5	6/29/60	809,760	392	2.8
6/10/59	143,660	250	2.3	7/13/60	836,320	257	3.1
7/1/59	169,140	262	2.3	7/27/60	871,400	211	3.5
7/29/59	201,120	225	3.2	8/10/60	905,780	222	3.8
8/12/59	219,040	275	3.9	8/24/60	932,040	327	4.1
9/9/59	251,920	312	4.3	9/7/60	953,860	327	4.4
9/23/59	273,900	553	5.2	9/21/60	988,480	701	4.7
10/5/59	292,480	675	6.1	10/5/60	1,213,360	649	5.0
10/21/59	306,042	1,004	7.2	11/2/60	1,085,900	1,179	5.4
11/4/59	324,720	1,216	7.1	11/16/60	1,103,840	1,408	5.9
11/18/59	338,160	1,734	5.2	11/30/60	1,113,760	1,528	6.3
12/2/59	354,400	1,901	5.6				

the K coefficient appropriate to that section and combination of a and b coefficients. That is, if that value were used for K, the sum of the damage factors for the section would be 1.0. The average of the damage factor sums for all sections for each a and b combination was selected as the best overall estimate of the K coefficient.

Damage factor sums for each a and b combination were subsequently determined for all sections using these K coefficients. The means and standard deviations of the damage factor sums were then calculated. The means, of course, were all 1.0 because of the method used to select K. The variation in the standard deviations was relatively small, ranging from 1.05 to 1.09. The a and b combination producing the lowest standard deviation was selected. The resulting equation is

$$\log N = 2.2340 - 3.16 \cdot \log eac - 1.4 \cdot \log Eac$$

$$SEE = 0.40 \qquad R^2 = 0.53 \qquad (14)$$

where

N = predicted number of 18,000-lb axle load applications to crack appearance;
eac = predicted AC strain, in inches per inch; and
Eac = dynamic stiffness modulus of the AC, in psi.

A plot of the actual versus predicted numbers of load applications using this equation is shown in Figure 5.

SUBGRADE DEVIATOR STRESS VERSUS LOAD APPLICATIONS

It is generally recognized, and the Road Test results confirm, that spring is the most critical time of year in terms of distress development in conventional flexible pavements. In recognition of this, the relationship between crack development and subgrade deviator stress was studied in terms of the predicted stress for typical spring conditions at the road test.

A subgrade deviator stress for each pavement section was predicted for typical spring conditions. The modulus values used to represent spring conditions (Eac = 1,340 ksi and Eri = 1.4 ksi) were selected on the basis of an analysis of seasonal load damage effects (3).

The predicted stresses were then related to the number of 18-kip single axle loads applied to each section before Class 1 cracking was observed. This produced the following equation:

$$\log N = 7.2558 - 0.6378 \cdot sd \qquad SEE = 0.23 \qquad R^2 = 0.82 \qquad (15)$$

where

N = number of 18-kip single axle applications and
sd = predicted subgrade deviator stress.

The correlation coefficient for this equation is 0.908; and the standard error of estimate is 0.233. In terms of typical pavement life predictive equations, these two statistical parameters show the equation and relationship to be quite good. Figure 6 shows a plot of the predicted versus actual number of load applications for the analysis sections using this equation.

MODIFIED FATIGUE RELATIONSHIP

For comparison purposes, the 18-kip single axle applications to Class 1 AC cracking were predicted using the subgrade deviator stress relationship (Equation 15) and the AC strain relationship (Equation 14). These two predictions were then compared to the actual numbers of applications. The deviator stress-based prediction was closer to the actual number more frequently than was the AC strain-based prediction. This was particularly true for the thinner pavement sections for which the strain-based prediction was always high. For all sections less than 15 in. in total thickness, the subgrade deviator stress provided the closer prediction.

On the basis of this observation, it was concluded that fatigue was probably not the major cause of cracking in pavements having a total thickness (AC plus granular) of less than 15 in. Cracking in

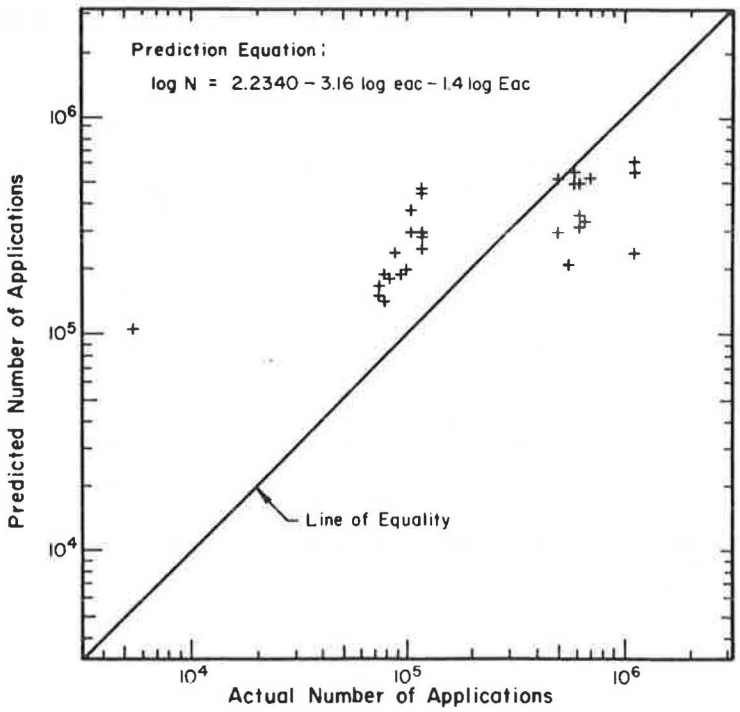

FIGURE 5 Comparison of actual versus predicted 18,000-lb axle applications to Class 1 cracking based on asphalt strain.

these pavements probably was controlled by excess permanent deformation and strain due to overstressing the granular materials and subgrade. Indeed, all of the sections developed significant surface rutting before cracking became apparent, suggesting that permanent deformation and strain (as opposed to the resilient AC radial strain predicted by the algorithms) played a major role in the behavior of all the sections.

To provide a better predictor of fatigue-type crack development, another analysis was conducted using only those sections having a total (AC plus granular) thickness of 15 in. or more. This analysis was conducted in a manner identical to that de-

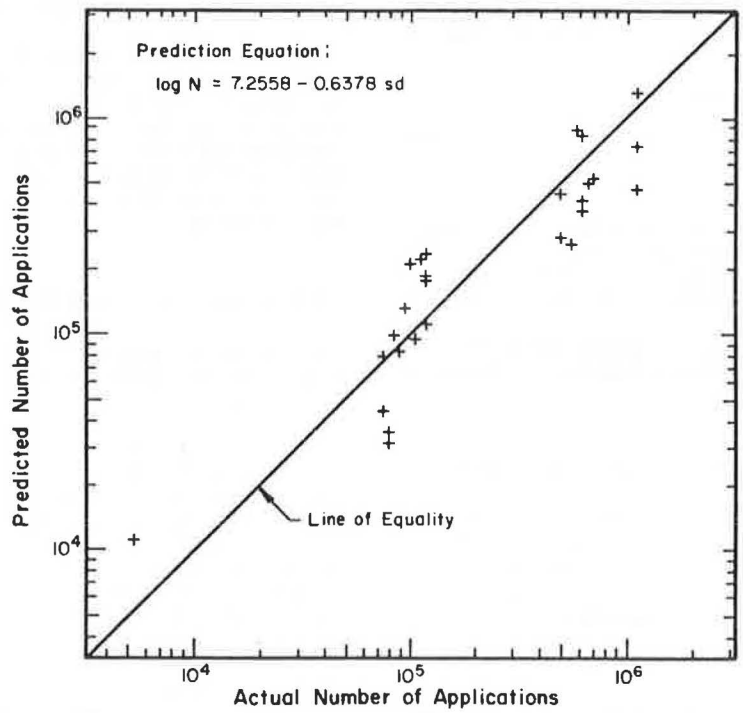

FIGURE 6 Comparison of actual versus predicted 18,000-lb axle applications to Class 1 cracking based on subgrade deviator stress.

scribed under "Determination of K Coefficient." The same a (3.16) and b (1.4) constants were used in the analysis to solve for the K coefficient. The equation produced is

$$\log N = 2.4136 - 3.16 \cdot \log eac - 1.4 \cdot \log Eac$$

$$SEE = 0.30 \qquad R^2 = 0.25 \tag{16}$$

Figure 7 shows a plot of the actual versus predicted number of load applications for the analysis sections using this equation. The modified equation provides a better prediction for the sections that withstood a greater number of load applications before Class 1 cracking was observed.

SEASONAL LOAD-DAMAGE EFFECTS

Equation 16 was used to evaluate the seasonal load-damage effects on the Loop 4 AASHO Road Test flexible pavements. For this analysis, relative damage factors (Di) were determined for each pavement design on a weekly basis using a constant traffic volume. Weekly Eri and AC modulus values were selected from examination of the seasonal trends identified for the road test (Figures 3 and 4). On the basis of frost penetration data from the road test, a 7-week period was selected to represent frozen subgrade conditions. During this time, a 0.0 relative damage factor was assigned. Table 3 gives the weekly AC modulus and Eri values used in the analysis.

The seasonal damage factors are the sum of the weekly factors for each season. In this analysis, the seasons were defined as periods of 13 consecutive weeks with the first week of spring being the first week following the 7 weeks of frozen subgrade. The seasonal periods are given in Table 3.

Results are given in Table 4. Although all AC and base thickness combinations from Loop 4 pavements were examined, only the AC thickness had an effect on the relative seasonal damage factors. Although the total number of load applications (N) increased with thickness of granular material, the relative seasonal effect was the same for any single AC thickness.

Additional analyses were performed for AC thicknesses of from 2 to 6 in. using the weighting factor concept established by Gomez-Achecar and Thompson (14). Under this concept, a weighting factor (WFi) for any time period is determined by the equation

$$WFi = Nf/Nai \tag{17}$$

where

Nf = total number of load repetitions to failure over the pavement's normal life and
Nai = number of load repetitions to failure if the conditions (stiffness moduli) during the period prevailed throughout the life of the pavement.

Weekly weighting factors determined for AC pavement surfacing thicknesses of 2 to 6 in. are shown in Figure 8. The trends displayed in this figure are consistent with the seasonal relationships normally accepted on the basis of pavement performance observation.

For conventional flexible pavements (AC surface on a granular base), spring is generally recognized as the critical time of year in terms of load-induced damage. At the AASHO Road Test, the first observation of cracking was normally reported in the spring and most of the sections taken out of test failed during the spring. The second most severe season is normally considered to be fall, followed by summer. Winter, at least in the northern states, is normally the least severe due to frozen conditions. It is also generally recognized that the relative seasonal severity shifts as the AC thickness increases. Summer is the most critical for full-depth (AC for the entire thickness) pavements. Ac-

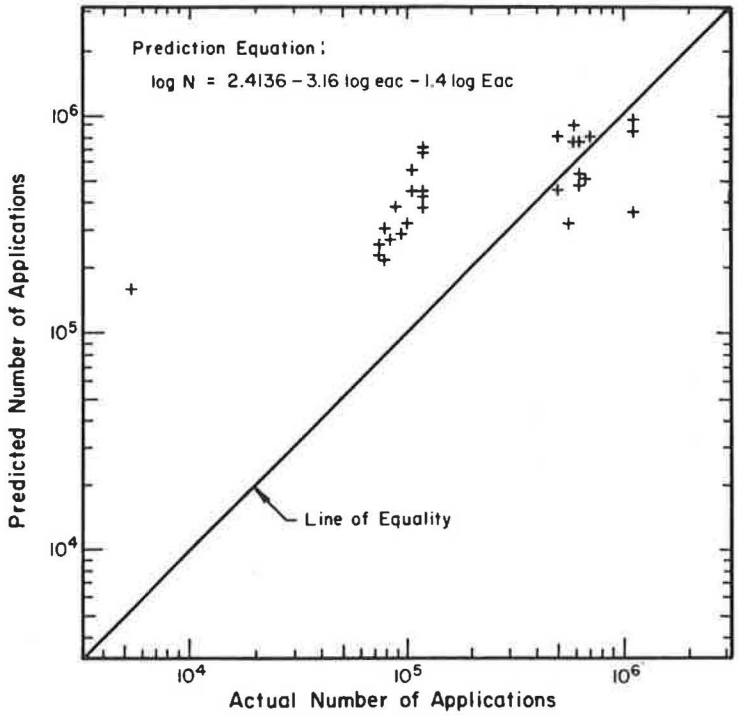

FIGURE 7 Comparison of actual versus predicted 18,000-lb axle applications to Class 1 cracking based on modified AC strain equation.

TABLE 3 Weekly AC Modulus and Subgrade Eri Values Used in Relative Seasonal Effect Analysis

Midweek Date	Asphalt Eac (ksi)	Subgrade Eri (ksi)	Season	Midweek Date	Asphalt Eac (ksi)	Subgrade Eri (ksi)	Season
1/3	2,250	Frozen	Winter	7/4	290	3.1	Summer
1/10	2,380	Frozen	Winter	7/11	260	3.2	Summer
1/17	2,420	Frozen	Winter	7/18	250	3.4	Summer
1/24	2,450	Frozen	Winter	7/25	240	3.6	Summer
1/31	2,430	Frozen	Winter	8/1	250	3.7	Summer
2/7	2,400	Frozen	Winter	8/8	270	3.9	Summer
2/14	2,350	Frozen	Winter	8/15	290	4.0	Summer
2/21	2,280	1.2	Spring	8/22	310	4.2	Fall
2/28	2,240	1.2	Spring	8/29	350	4.3	Fall
3/7	1,950	1.2	Spring	9/5	390	4.5	Fall
3/14	1,770	1.2	Spring	9/12	430	4.6	Fall
3/21	1,600	1.2	Spring	9/19	500	4.8	Fall
3/28	1,440	1.2	Spring	9/26	580	5.0	Fall
4/4	1,300	1.2	Spring	10/3	660	5.1	Fall
4/11	1,150	1.2	Spring	10/10	750	5.3	Fall
4/18	1,040	1.4	Spring	10/17	850	5.4	Fall
4/25	910	1.5	Spring	10/24	970	5.6	Fall
5/2	810	1.7	Spring	10/31	1,080	5.7	Fall
5/9	730	1.8	Spring	11/7	1,180	5.9	Fall
5/16	650	2.0	Spring	11/14	1,310	6.1	Fall
5/23	580	2.1	Summer	11/21	1,430	6.2	Winter
5/30	500	2.3	Summer	11/28	1,560	6.4	Winter
6/6	450	2.5	Summer	12/5	1,700	6.5	Winter
6/13	400	2.6	Summer	12/12	1,820	6.7	Winter
6/20	360	2.8	Summer	12/19	1,950	6.8	Winter
6/27	310	2.9	Summer	12/26	2,100	7.0	Winter

TABLE 4 Relative Damage Factors by Season of the Year Based on Fatigue Analysis

Thickness (in.)		Seasonal Relative Damage Factors				Thickness (in.)		Seasonal Relative Damage Factors			
Asphalt	Base	Spring	Summer	Fall	Winter	Asphalt	Base	Spring	Summer	Fall	Winter
3	4	.42	.16	.23	.19	4	12	.38	.21	.25	.16
3	7	.42	.16	.23	.19	4	14	.38	.21	.25	.16
3	8	.42	.16	.23	.19	4	15	.38	.21	.25	.16
3	10	.42	.16	.23	.19	4	18	.38	.21	.25	.16
3	11	.42	.16	.23	.19	5	4	.34	.26	.27	.13
3	12	.42	.16	.23	.19	5	7	.34	.26	.27	.13
3	14	.42	.16	.23	.19	5	8	.34	.26	.27	.13
3	15	.42	.16	.23	.19	5	10	.34	.26	.27	.13
3	18	.42	.16	.23	.19	5	11	.34	.26	.27	.13
4	4	.38	.21	.25	.16	5	12	.34	.26	.27	.13
4	7	.38	.21	.25	.16	5	14	.34	.26	.27	.13
4	8	.38	.21	.25	.16	5	15	.34	.26	.27	.13
4	10	.38	.21	.25	.16	5	18	.34	.26	.27	.13
4	11	.38	.21	.25	.16						

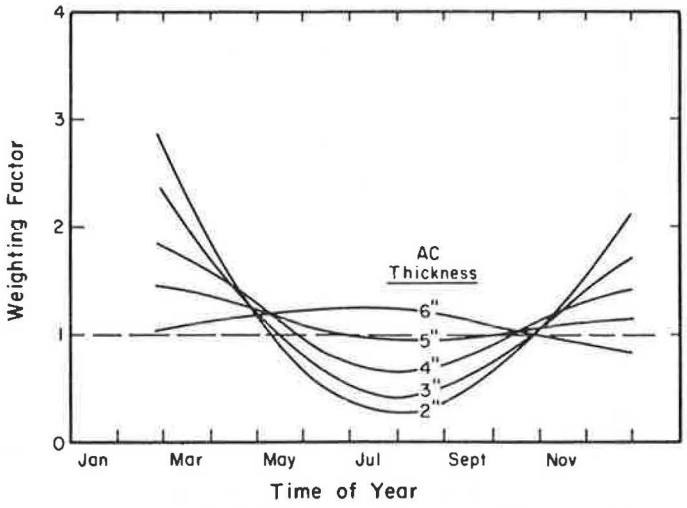

FIGURE 8 Seasonal weighting factors for various thicknesses of AC surfacing.

cording to Figure 8, the shift in critical seasons from spring to summer occurs at about 6 in. of AC.

The damage factor analysis results given in Table 4 also directly correspond to these general seasonal relationships. For each AC thickness (3, 4, and 5 in.), the spring season produced the highest relative damage factor and winter the lowest. The fall damage factor is the second highest for the 3- and 4-in. surfaces. As expected, with increased thickness the spring damage factor decreases and the summer factor increases.

CONCLUSIONS

The analyses reported in this paper demonstrate that the ILLI-PAVE structural model and algorithms provide an adequate and valid representation of the structural behavior of conventional flexible pavements. The structural response-performance relationships explain the observed behavior of the AASHO Road Test pavement sections in a realistic fashion. Seasonal damage factors and weighting factors based on these relationships provide a mechanistic explanation of seasonal effects that is consistent with experience.

The analyses also demonstrate that the ILLI-PAVE analysis algorithms can be used to effectively evaluate NDT data and determine the structural characteristics of existing pavement systems. ILLI-PAVE, therefore, is a powerful tool for pavement design and analysis. It will serve as a sound basis for the development of mechanistic procedures for the design of new flexible pavements and for the selection of rehabilitation strategies for existing flexible pavements.

ACKNOWLEDGMENTS

This paper is based on the results of Project IHR-510, Mechanistic Evaluation of Illinois Flexible Pavement Design Procedures. IHR-510 was sponsored by the Illinois Department of Transportation (Division of Highways) and the U.S. Department of Transportation (Federal Highway Administration).

REFERENCES

1. J.L. Figueroa. Resilient Based Flexible Pavement Design Procedure for Secondary Roads. Ph.D. dissertation. University of Illinois at Urbana-Champaign, 1979.
2. M.S. Hoffman and M.R. Thompson. Mechanistic Interpretation of Nondestructive Pavement Testing Deflections. Civil Engineering Studies, Transportation Engineering Series, No. 32, University of Illinois at Urbana-Champaign, 1981.
3. R.P. Elliott and M.R. Thompson. Mechanistic Design Concepts for Conventional Flexible Pavements. Civil Engineering Studies, Transportation Engineering Series, No. 42, University of Illinois at Urbana-Champaign, 1985.
4. L. Raad and J.L. Figueroa. Load Response of Transportation Support Systems. Journal of the Transportation Engineering Division, ASCE, Vol. 106, No. TE1, Jan. 1980.
5. M.L. Traylor, Jr. Nondestructive Testing of Flexible Pavements. Ph.D. dissertation. University of Illinois at Urbana-Champaign, 1979.
6. M.R. Thompson and Q.L. Robnett. Final Report--Resilient Properties of Subgrade Soils. Civil Engineering Studies, Transportation Engineering Series, No. 14, University of Illinois at Urbana-Champaign, 1976.
7. Research and Development of the Asphalt Institute's Thickness Design Manual (MS-1). 9th ed. Research Report 82-2. The Asphalt Institute, College Park, Md., 1982.
8. The AASHO Road Test, Report 5--Pavement Research. Special Report 61E. HRB, National Research Council, Washington, D.C., 1962.
9. Austin Research Engineers, Inc. Asphalt Concrete Overlays of Flexible Pavements, Vol. 1: Development of New Design Criteria. Report FHWA-RD-75-75. FHWA, U.S. Department of Transportation, 1975.
10. F. Bonnaure, A. Gravois, and J. Udron. A new Method for Predicting the Fatigue Life of Bituminous Mixes. Proc., Association of Asphalt Paving Technologists, 1980.
11. F. Finn, C.L. Saraf, R. Kulkarni, K. Nair, W. Smith, and A. Abdullah. Development of Pavement Structural Subsystems. NCHRP Final Report, Vol. 1, Project 1-10B. TRB, National Research Council, Washington, D.C., 1977.
12. F. Finn, C. Saraf, R. Kulkarni, K. Nair, W. Smith, and A. Abdullah. The Use of Distress Prediction Subsystems for the Design of Pavement Structures. Proc., Fourth International Conference on Structural Design of Asphalt Pavements, University of Michigan, Ann Arbor, 1977.
13. M.R. Thompson. Concepts for Developing a Nondestructive Testing Based Asphalt Concrete Overlay Thickness Design Procedure. Civil Engineering Studies, Transportation Engineering Series, No. 34, University of Illinois at Urbana-Champaign, 1982.
14. M. Gomez-Achecar and M.R. Thompson. Mechanistic Design Concepts for Full-Depth Asphalt Concrete Pavements. Civil Engineering Studies, Transportation Engineering Series, No. 41, University of Illinois at Urbana-Champaign, 1984.

Publication of this paper sponsored by Committee on Flexible Pavements.

ILLI-PAVE-Based Response Algorithms for Design of Conventional Flexible Pavements

MARSHALL R. THOMPSON and ROBERT P. ELLIOTT

ABSTRACT

In a mechanistic design procedure a structural model is used to predict pavement responses (stresses, strains, displacements). The ILLI-PAVE structural model considers nonlinear, stress-dependent resilient modulus material models and failure criteria for granular materials and fine-grained soils. The computational techniques of the ILLI-PAVE computer program are too costly, complex, and cumbersome to be used for routine design. To incorporate ILLI-PAVE structural model concepts into a mechanistic design concept, simplified analysis algorithms that reliably predict ILLI-PAVE response solutions for typical flexible pavements are needed. ILLI-PAVE-based design algorithms for conventional flexible pavements [asphalt concrete (AC) surface plus granular base and subbase] are presented for AC radial strain, surface deflection, subgrade deviator stress, subgrade deviator stress ratio, subgrade vertical strain, and subgrade deflection. Pertinent design algorithm inputs are AC thickness, AC modulus, granular layer thickness, and subgrade resilient modulus (E_{Ri}). Additional algorithms relating AC radial strain and subgrade deviator stress ratio and surface deflection are also presented. The algorithms are sufficiently accurate for inclusion in mechanistic design procedures.

The various components of a mechanistic design procedure for conventional [asphalt concrete (AC) granular base and subbase] flexible pavements are shown in Figure 1. In this paper emphasis is placed on materials characterization, the structural model, and pavement response components. Concepts for a mechanistic design procedure based on the ILLI-PAVE structural model (1) and design algorithms developed from a comprehensive ILLI-PAVE data base (2) are presented. Development of a design procedure based on these concepts should include consideration of climatic effects and the establishment of appropriate transfer functions.

Climatic effects (temperature, moisture, freeze-thaw) can be considered by quantifying their effects on material characteristics (resilient moduli and shear strength). Such considerations should be based on an extensive study of local climatic and soil conditions.

Transfer functions relating pavement response and pavement performance are not proposed. Typical transfer functions consider pavement responses related to subgrade permanent strain (subgrade resilient strain, subgrade stress, subgrade stress ratio) and AC fatigue (AC strain). Transfer functions should be developed on the basis of consideration of the paving materials, soils, climate, and so forth relevant to local conditions. Laboratory testing information and field performance data are essential inputs to calibrating a transfer function.

Transfer functions are an important part of a total mechanistic design procedure. Transfer functions appropriate for use with the ILLI-PAVE procedure are not necessarily compatible with linear elastic (or other) analysis procedures.

The analyses and algorithms presented in this paper are only for 18,000-lb single axle load conditions. Mixed traffic should be converted to equiva-

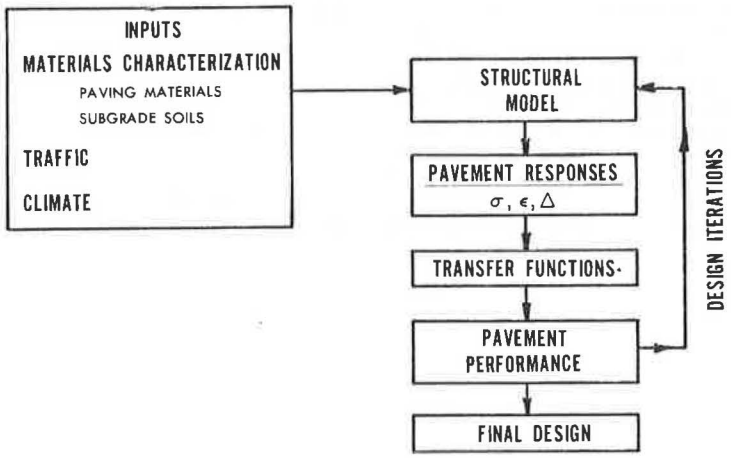

FIGURE 1 Components of a mechanistic design procedure.

lent 18,000-lb single axle loads when the ILLI-PAVE procedure is incorporated into a comprehensive design procedure.

ILLI-PAVE

In ILLI-PAVE (1) the pavement is considered an axisymmetric solid of revolution. Nonlinear, stress-dependent resilient modulus material models and failure criteria for granular materials and fine-grained soils (1-3) are incorporated into ILLI-PAVE. The principal stresses in the granular and subgrade layers are modified at the end of each iteration so that they do not exceed the strength of the materials as defined by the Mohr-Coulomb theory of failure.

Studies comparing measured and ILLI-PAVE-predicted load deformation responses reported by Raad and Figueroa (1), Suddath and Thompson (4), Traylor (5), Hoffman and Thompson (6), Gomez and Thompson (7), and Elliott and Thompson (8) yielded favorable results. The ILLI-PAVE approach has been successfully used in developing a highway flexible pavement overlay design procedure based on nondestructive testing data analyses (9), as well as mechanistic thickness design procedures for secondary road flexible pavements (10) and soil-lime layers (11). Gomez and Thompson (7) and Elliott and Thompson (8) successfully used ILLI-PAVE procedures to analyze the pavement responses and predict the performance of the AC plus bituminous treated granular base sections (the "Base Type Studies") and the Loop 4 flexible pavement sections of the AASHO Road Test.

Although the computational techniques of the ILLI-PAVE computer program are too costly, complex, and cumbersome to be used for routine design, simplified analysis algorithms that reliably predict ILLI-PAVE response solutions for typical flexible pavements have been developed (8) to incorporate ILLI-PAVE structural model concepts into a mechanistic design concept. The algorithms can be easily programmed for inexpensive calculator or computer applications.

SOILS AND MATERIAL CHARACTERIZATION

General

The resilient behavior of a soil or material is an important property for pavement analysis and design. A commonly used measure of resilient response is the resilient modulus defined by

$$E_R = \sigma_D/\epsilon_r$$

where

E_R = resilient modulus,
σ_D = repeated deviator stress, and
ϵ_r = recoverable axial strain.

Repeated unconfined compression or triaxial testing procedures are often used to evaluate the resilient moduli of fine-grained soils and granular materials. Resilient moduli are stress dependent: fine-grained soils experience resilient modulus decreases with increasing stress, whereas granular materials stiffen with increasing stress level.

Granular Materials

Granular materials stiffen as the stress level increases. Repeated load triaxial testing is used to characterize the resilient behavior of granular materials. Resilient modulus is a function of the applied stress state:

$$E_R = K\theta^n$$

where

E_R = resilient modulus,
K, n = experimentally derived factors, and
θ = first stress invariant = $\sigma_1 + \sigma_2 + \sigma_3$.

Note that $\theta = \sigma_1 + 2\sigma_3$ in a standard triaxial compression test.

Figure 2 shows an E_R-θ relation for a sandy gravel. Rada and Witczak (12) have summarized and statistically analyzed extensive published resilient modulus data for a broad range of granular materials. The average values and ranges for K and n are given in Table 1 and shown in Figure 3 for several granular materials and coarse-grained soils. The relation between K and n developed by Rada and Witczak is shown in Figure 4.

The granular material model used in this study is $E_R = 9{,}000\ \theta^{0.33}$ (θ and E_R in psi). The values are typical for dense-graded crushed stone base materials and the AASHO crushed stone base (5). Other pertinent data for the crushed stone are given in Table 2.

Fine-Grained Soils

Two stress-dependent behavior models have been proposed for describing the stress softening behavior of fine-grained soils. The arithmetic model is shown in Figures 5 and 6, and the semilog model is shown in Figure 7. Extensive resilient laboratory testing, nondestructive pavement testing, and pavement analysis and design studies at the University of Illinois have indicated that the arithmetic model (Figure 5) is adequate for flexible pavement analysis and design activities.

In the arithmetic model, the value of the resilient modulus at the breakpoint in the bilinear curve, E_{Ri} (Figure 5), is a good indicator of a soil's resilient behavior. The slope values, K_1 and K_2, display less variability and influence pavement structural response to a smaller degree than E_{Ri}. Thompson and Robnett (13) developed simplified procedures for estimating the resilient behavior of fine-grained soils based on soil classification, soil properties, and moisture content.

Four fine-grained subgrade types (very soft, soft, medium, and stiff) are included in this study. Pertinent subgrade properties and characteristics are given in Table 2. Resilient moduli-repeated deviator stress level relations used in the ILLI-PAVE model are shown in Figure 8.

Asphalt Concrete

A constant linear resilient modulus is used to represent the AC layer. AC modulus-temperature relations must be considered in selecting modulus values. Procedures for establishing AC modulus-pavement temperature relations are presented by the Asphalt Institute (14) and Shell (15) design procedures. The AC modulus values selected for this study are consistent with the range of AC moduli and temperatures expected to be encountered in Illinois. The modulus values and other properties used in the analyses are given in Table 2.

DESIGN ALGORITHM DEVELOPMENT

Elliott and Thompson (8) have demonstrated that type of aggregate base material (crushed stone or gravel)

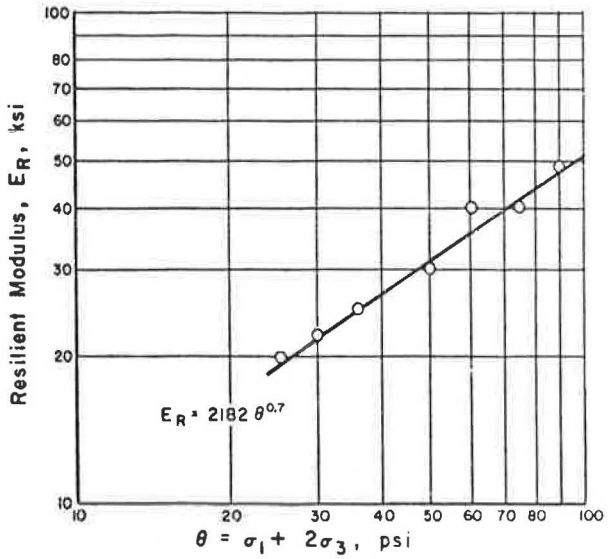

FIGURE 2 Resilient modulus-θ relation for a sandy gravel [AASHTO A-1-b(0)].

TABLE 1 Typical Resilient Property Data *(12)*

Granular Material Type	No. of Data Points	K (psi) Mean	K (psi) Standard Deviation	n Mean	n Standard Deviation
Silty sands	8	1,620	780	0.62	0.13
Sand-gravel	37	4,480	4,300	0.53	0.17
Sand-aggregate blends	78	4,350	2,630	0.59	0.13
Crushed stone	115	7,210	7,490	0.45	0 23

Note: $E_R = K\theta^n$ where E_R = resilient modulus (psi) and K, n = experimentally derived factors from repeated triaxial testing data.

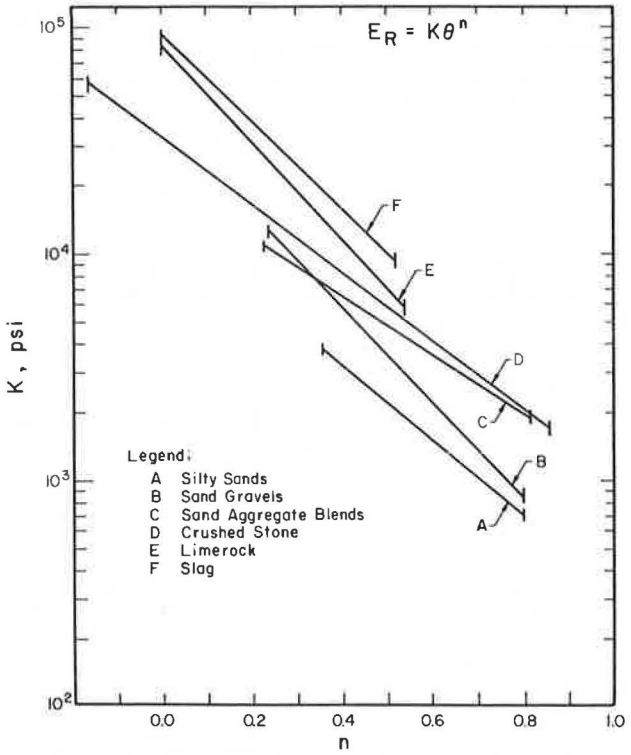

FIGURE 3 K and n relationships for various types of granular materials identified by Rada and Witczak *(12)*.

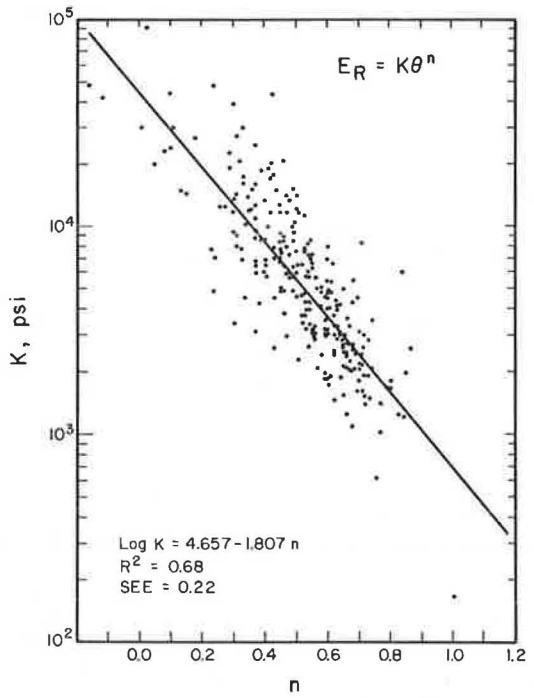

FIGURE 4 Relationship between K and n values for granular materials identified by Rada and Witczak *(12)*.

has a limited effect (10± percent) on ILLI-PAVE-calculated structural response (AC strain, surface deflection, subgrade deflection, subgrade strain, and subgrade deviator stress). Thus ILLI-PAVE structural response algorithms were developed only for the crushed stone base model. All ILLI-PAVE analyses were based on a 9,000-lb circular load (80 psi pressure) as a representation of one dual wheel of the standard 18-kip (18,000-lb) single axle load.

Design response algorithms were developed as the basis of a mechanistic design procedure. Algorithms for predicting the following pavement responses were established:

1. AC radial strain at the bottom of the AC surface layer,

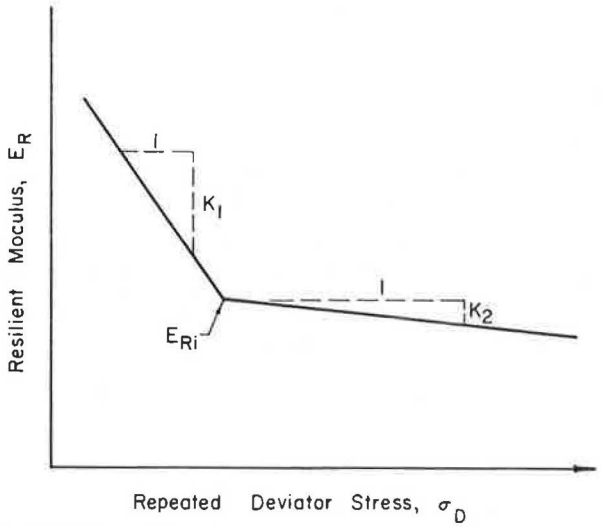

FIGURE 5 Arithmetic model for stress-dependent resilient behavior of fine-grained soils.

TABLE 2 Summary of Material Properties for ILLI-PAVE Solutions

	Asphalt Concrete			Crushed	Subgrade			
	40°F	70°F	100°F	Stone	Stiff	Medium	Soft	Very Soft
Unit weight (pcf)	145.00	145.00	145.00	135.00	125.00	120.00	115.00	110.00
Lateral pressure								
Coefficient at rest	0.37	0.67	0.85	0.60	0.82	0.82	0.82	0.82
Poisson's ratio	0.27	0.40	0.46	0.38	0.45	0.45	0.45	0.45
Unconfined compression strength (psi)					32.80	22.85	12.90	6.21
Deviator stress (psi)								
Upper limit					32.80	22.85	12.90	6.21
Lower limit					2.00	2.00	2.00	2.00
K1 (ksi/psi)					-1.11	-1.11	-1.11	-1.11
K2 (ksi/psi)					-.178	-.178	-.178	-.178
Deviator stress at break-point (psi)					6.20	6.20	6.20	6.20
Eri (ksi)					12.34	7.68	3.02	1.00
E failure (ksi)				4.00	7.605	4.716	1.827	1.00
E constant modulus (ksi)	1,400.00	500.00	100.00					
Er model (psi)				$9{,}000\theta^{0.33}$				
Friction angle (degrees)				40.00	0.0	0.0	0.0	0.0
Cohesion (psi)				0.00	16.4	11.425	6.45	3.105

2. Subgrade deviator stress,
3. Subgrade stress ratio (subgrade deviator stress to unconfined compressive strength),
4. Subgrade vertical strain,
5. Surface deflection, and
6. Subgrade deflection.

These responses are those generally used in various transfer functions (see Figure 1) relating pavement response to pavement performance. Additional algorithms relating AC radial strain and subgrade stress ratio to surface deflection (all response parameters) were also developed.

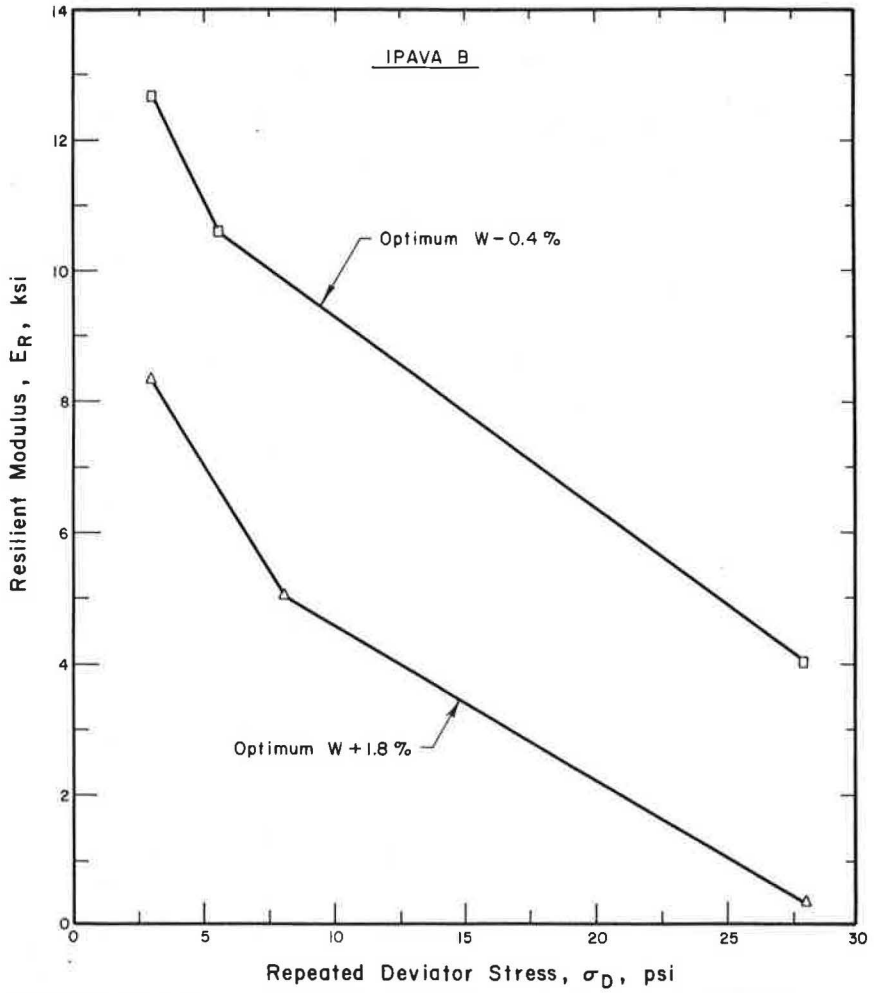

FIGURE 6 Typical stress-dependent resilient behavior of a fine-grained soil [AASHTO A-7-6(36)].

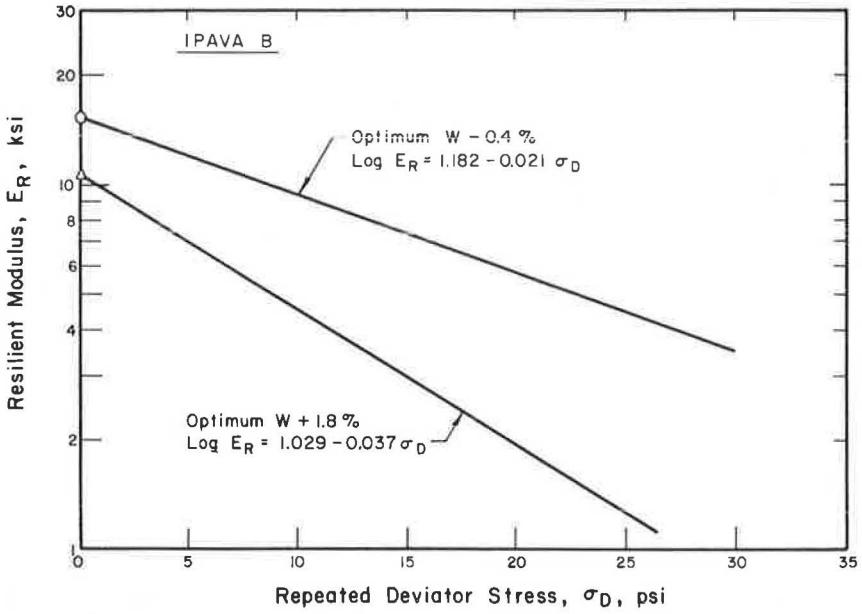

FIGURE 7 Semilog model for stress-dependent resilient behavior of a fine-grained soil [AASHTO A-7-6(36)].

Algorithms relating to AC and granular base and subbase rutting were not developed. It is intended that rut development within the AC portion of the pavement system be controlled by the proper selection of materials, mix design, and construction control. Similarly, rutting in the granular layer or layers is controlled by AC minimum thickness requirements and appropriate specifications to govern quality of, and placement procedures for, granular material.

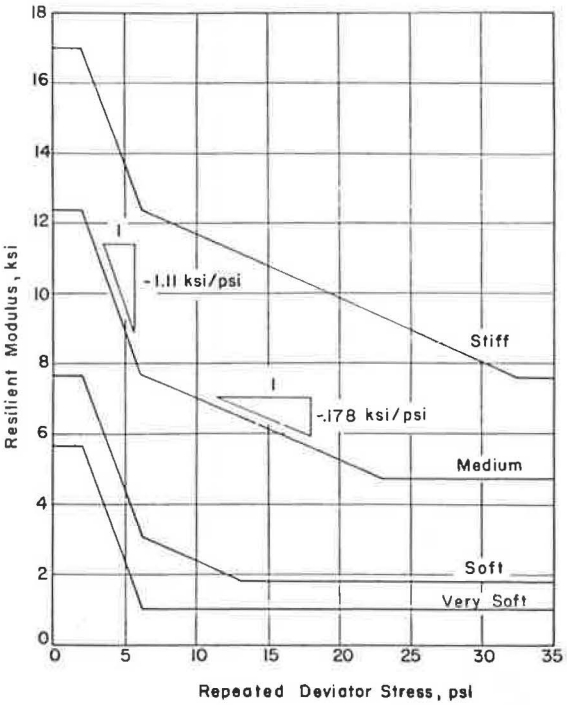

FIGURE 8 Resilient modulus-deviator stress relations for ILLI-PAVE subgrades.

Design Algorithms

The design algorithms were developed using the SPSS stepwise regression program (16). The regression equation is developed in a series of steps by entering the independent (prediction parameters) variables one at a time. At each step, the variable entered is the one that makes the greatest improvement in the prediction of the dependent variable (pavement response parameter). The pavement factors included in the analyses as independent variables were (a) thickness of AC, (b) thickness of granular base course, (c) AC modulus, and (d) subgrade E_{Ri}.

The ILLI-PAVE data base included information for 168 pavement configurations. These included AC thicknesses of 1.5, 3, 5, and 8 in. Granular base thicknesses were 4, 6, 9, and 12 in. for AC thicknesses of 1.5 and 3 in. For the 5- and 8-in. AC thicknesses, granular base thicknesses were 18 and 24 in. These thicknesses are representative of a broad range of typical flexible pavement designs. Four levels of subgrade moduli and strength (stiff, medium, soft, and very soft) and three levels of AC modulus (1,400, 500, and 100 ksi) were evaluated for each combination of AC and granular base thickness. The ILLI-PAVE response data are presented elsewhere (8).

Even though AC thicknesses of 2 to 3 in. are not uncommon on low-volume roads, the 1.5-in. data were not used in developing the algorithms for AC surfaced roadways. Examination of the 1.5-in. data in comparison with the 3- to 8-in. data revealed that the relative effect of AC thickness on some of the response parameters changes in the 1.5- to 3-in. thickness range.

For example, the strain in the bottom of the AC layer generally decreases with an increase in thickness. However, in most cases the strain in the 1.5-in. thickness was less than in the 3-in. thickness. It was concluded that inclusion of the 1.5-in. data would cause the algorithms to predict unconservative (low) strain values in some cases. Conversely, it was reasoned that exclusion of these data would permit the developed algorithms to more accurately fit the usual design thicknesses (3 to 5 in.) whereas

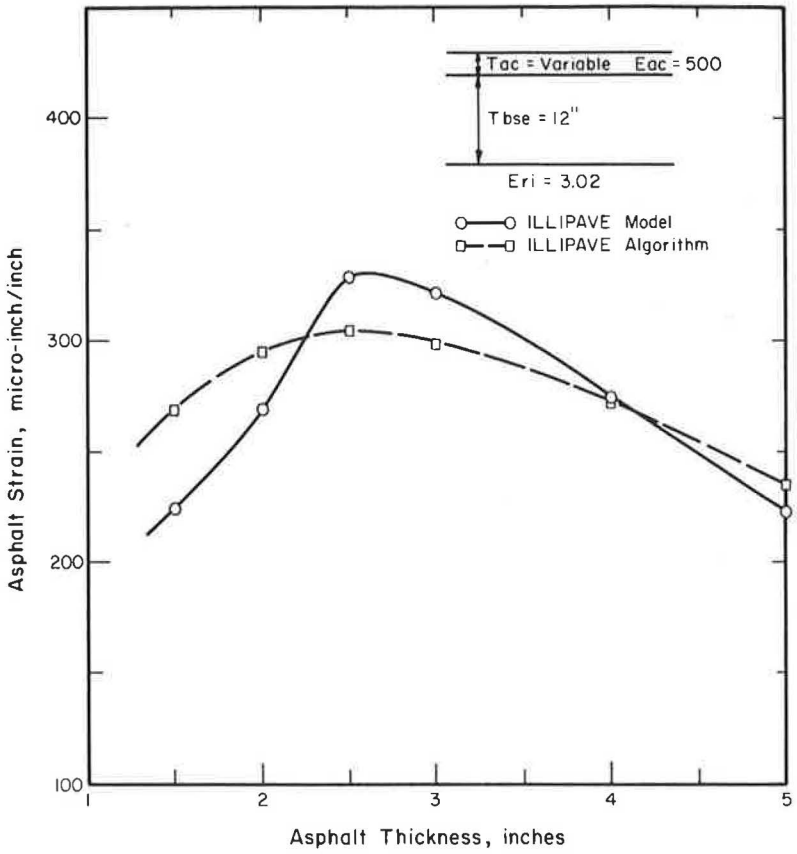

FIGURE 9 Comparison of ILLI-PAVE model and algorithm predictions of AC strain versus thickness for one design condition.

their extrapolation to lesser thicknesses would be somewhat conservative.

To demonstrate this effect, ILLI-PAVE predictions of AC strain for one design condition and AC thicknesses of 1.5 to 5 in. are shown in Figure 9. This plot shows a transition in the strain-thickness relationship at about 2.5 in. The cause of this transition has not been explored. A plausible explanation is that above approximately 2.5 in. the AC layer provides an "elastic structural layer" action, while a thinner AC layer exhibits a "membrane type" behavior.

For purposes of comparison, Figure 9 also includes a plot of the AC strains predicted by the developed algorithm. The algorithm predictions compare quite well with the model predictions and exhibit a similar, but less pronounced, transition.

The algorithms are shown in Figure 10. Included in the figure are the related statistical parameters that indicate the accuracy and reliability of the equations and the significance of the variables.

The various statistical parameters show that the algorithms are excellent. The standard errors of estimate and standard deviations of error are generally within the accuracy of the ILLI-PAVE model itself as determined by comparing the results of ILLI-PAVE analyses made using differing element mesh configurations.

The algorithms should not be used to solve for any of the independent variables. It might be tempt-

ASPHALT STRAIN ALGORITHM

log eac =
2.9496+.1289Tac-.5195(log Tbse)/Tac-.0807(log Eac)Tac-.0408(log Eri)

Std.Er.					
Coef.	.0318	.0048	.0828	.0015	.0089
Norm.					
Coef		1.065	-.1378	-1.917	-.0688

R = .990 Std. Dev. of Error = 26.9 Std. Err. of Est. = .03623 (1.087)

SUBGRADE DEVIATOR STRESS

log sd =
1.7694-.0735Tac-.0222Tbse-.2539(log Eac)+.0223Eri

Std.Er.					
Coef.	.0383	.0048	.0013	.0130	.0014
Norm.					
Coef		-.4458	-.4786	-.3548	.2900

R = .985 Std. Dev. of Error = .901 Std. Err. of Est. = .06007 (1.148)

FIGURE 10 Algorithms.

SUBGRADE DEVIATOR STRESS RATIO

log Sr =
.3056+.0560Tac-.0222Tbse-.0495(log Eac)Tac-.4242(log Eri)

Std.Er.					
Coef.	.0182	.0082	.0014	.0025	.0149
Norm.					
Coef.		.3105	-.4380	-.7897	-.4800

R = .987 Std. Dev. of Error = .0615 Std. Err. of Est. = .06074 (1.150)

SUBGRADE VERTICAL STRAIN

log ez =
4.5040-.0738Tac-.0334Tbse-.3267(log Eac)-.0231Eri

Std.Er.					
Coef.	.0392	.0049	.0014	.0133	.0014
Norm.					
Coef		-.3591	-.5789	-.3664	-.2404

R = .990 Std. Dev. of Error = 144 Std. Err. of Est. = .0615 (1.152)

SURFACE DEFLECTION

log DO =
1.9692+.0465Tac-.5637(log Tbse)/Tac-.0464(log Eac)Tac-.2079(log Eri)

Std.Er.					
Coef.	.0403	.0060	.1048	.0019	.0112
Norm.					
Coef		.4796	-.1872	-1.383	-.4383

R = .974 Std. Dev. of Error = 3.47 Std. Err. of Est. = .04586 (1.111)

SUBGRADE DEFLECTION

log Ds =
2.0169+.0375Tac-1.095(log Tbse)/Tac-.0405(log Eac)Tac-.2426(log Eri)

Std. Er.					
Coef.	.0549	.0082	.1430	.0026	.0153
Norm.					
Coef.		.4182	-.3920	-1.297	-.5515

R = .943 Std. Dev. of Error = 3.56 Std. Err. of Est. = .06258 (1.155)

ASPHALT STRAIN - DEFLECTION ALGORITHM

log eac =
.9102+1.1126(log DO)

Std. Er.		
Coef.	.0803	.0591
Norm.		
Coef.		.8889

R = .889 Std. Dev. of Error = 78.3 Std. Err. of Est. = .1147 (1.302)

SUBGRADE DEVIATOR STRESS RATIO - DEFLECTION ALGORITHM

log Sr =
-2.876+1.671(log DO)

R = 0.928 Std. Err. of Est. = 0.135 (1.36)

where:

eac = tensile strain in the bottom of the AC layer, in micro-in/in
ez = vertical strain at the top of the subgrade, in micro-in/in
sd = deviator stress at the top of the subgrade, in psi
Sr = deviator stress/unconfined compressive strength ratio
DO = surface deflection at the point of loading, in mils
Ds = subgrade deflection under the point of loading, in mils
Tac = thickness of the AC layer, in inches
Tbse = thickness of aggregate base course, in inches
Eac = resilient modulus of the AC layer, in ksi
Eri = "breakpoint" resilient modulus of the subgrade, in ksi

FIGURE 10 continued.

ing to use the surface deflection design algorithm as a pavement analysis tool to solve for or back calculate the subgrade resilient modulus. The general practice of using regression equations in this manner is not correct and can lead to unnecessary errors. The appropriate approach is to develop separate regression equations using each desired unknown parameter as the dependent variable. Analysis algorithms developed in this manner are reported elsewhere (8).

SUMMARY

ILLI-PAVE-based design algorithms for conventional flexible pavements (AC surface plus granular base and subbase) are presented. The algorithms are sufficiently accurate for inclusion in mechanistic design procedures. Pertinent design algorithm inputs are AC thickness, AC modulus, granular layer thickness, and subgrade E_{Ri}. The algorithms should not be extrapolated beyond the range of variables considered in the ILLI-PAVE data base unless check runs are conducted with ILLI-PAVE to determine the validity of the algorithms in the area of extrapolation.

Factors relating to climate, traffic, and transfer functions for local conditions must be appropriately evaluated and included in the development of a complete mechanistic design procedure.

ACKNOWLEDGMENTS

This paper is based on the results of Project IHR-510, Mechanistic Evaluation of Illinois Flexible Pavement Design Procedures. IHR-510 was sponsored by the Illinois Department of Transportation (Division of Highways) and the U.S. Department of Transportation (Federal Highway Administration).

REFERENCES

1. L. Raad and J.L. Figueroa. Load Response of Transportation Support Systems. Journal of the Transportation Engineering Division, ASCE, Vol. 106, No. TE1, Jan. 1980.
2. J.L. Figueroa. Resilient Based Flexible Pavement Design Procedure for Secondary Roads. Ph.D. dissertation. University of Illinois, Urbana, 1979.
3. M.S. Hoffman and M.R. Thompson. Mechanistic Interpretation of Nondestructive Pavement Testing Deflections. Civil Engineering Studies, Transportation Engineering Series, No. 32, University of Illinois at Urbana-Champaign, June 1981.
4. L.P. Suddath and M.R. Thompson. Load-Deflection Behavior of Lime-Stabilized Layers. Technical Report M-118. U.S. Army Construction Engineering Research Laboratory, Champaign, Ill., 1975.
5. M.R. Traylor. Nondestructive Testing of Flexible Pavements. Ph.D. dissertation. University of Illinois, Urbana, 1979.
6. M.S. Hoffman and M.R. Thompson. Nondestructive Testing of Flexible Pavements--Field Testing Program Summary. Civil Engineering Studies, Transportation Engineering Series, No. 31, University of Illinois at Urbana-Champaign, June 1981.
7. M. Gomez and M.R. Thompson. Mechanistic Design Concepts for Full-Depth Asphalt Concrete Pavements. Civil Engineering Studies, Transportation Engineering Series, No. 41, University of Illinois at Urbana-Champaign, Aug. 1984.
8. R.P. Elliott and M.R. Thompson. Mechanistic Design Concepts for Conventional Flexible Pavements. Civil Engineering Studies, Transportation Engineering Series, No. 42, University of Illinois at Urbana-Champaign, 1985.
9. M.R. Thompson. Concepts for Developing a Nondestructive Based Asphalt Concrete Overlay Thickness Design Procedure. Civil Engineering Studies, Transportation Engineering Series, No. 34, University of Illinois at Urbana-Champaign, June 1982.
10. J.L. Figueroa and M.R. Thompson. Simplified Structural Analyses of Flexible Pavement for Secondary Roads Based on ILLI-PAVE. In Transportation Research Record 766, TRB, National Research Council, Washington, D.C., 1980, pp. 5-10.
11. M.R. Thompson and J.L. Figueroa. Mechanistic Thickness-Design Procedure for Soil-Lime Layers. In Transportation Research Record 754, TRB, National Research Council, Washington, D.C., 1980, pp. 32-36.
12. G. Rada and M.W. Witczak. Comprehensive Evaluation of Laboratory Resilient Moduli Results for Granular Material. In Transportation Research Record 810, TRB, National Research Council, Washington, D.C., 1981, pp. 23-33.
13. M.R. Thompson and Q.L. Robnett. Resilient Properties of Subgrade Soils. Journal of the Transportation Engineering Division, ASCE, Vol. 105, No. TE1, Jan. 1979.
14. Research and Development of the Asphalt Institute's Thickness Design Manual (MS-1). 9th ed. Research Report No. 82-2. The Asphalt Institute, College, Park, Md., 1982.
15. Shell Pavement Design Manual. Shell International Petroleum Company Limited, London, England, 1978.
16. Statistical Package for Social Sciences (SPSS). 2nd ed. McGraw-Hill Book Company, New York, 1975.

Publication of this paper sponsored by Committee on Flexible Pavements.

Investigation of Seasonal Load Restrictions in Washington State

JOE P. MAHONEY, JO A. LARY, JAY SHARMA, and NEWTON JACKSON

ABSTRACT

Presented in the paper are the results of monitoring seasonal changes in surface deflections, temperatures, moisture contents, and calculated layer moduli for six test sites in the state of Washington. The goal of the data collection and analysis was to evaluate the Washington State Department of Transportation (WSDOT) load restriction tables used on some state routes during the spring thaw. Further, a criterion was developed to estimate when seasonal load restrictions need to be applied to those pavement sections that require them. Extensive use was made in the study of the WSDOT falling weight deflectometer to obtain pavement surface deflection basins and of multilayered elastic computer programs to analyze the data.

Pavement engineers throughout much of the United States are faced with the recurring problem of weakened pavement structures during the spring thaw. To reduce the pavement deterioration that can occur during this period, load restrictions for truck traffic are often applied. A survey reported in NCHRP Synthesis Report 26 (1,p.77) revealed that slightly less than one-half of the states use seasonal load restrictions. When such restrictions are used, several questions arise and can include the following:

1. Which pavement sections require load restrictions?
2. When should restrictions be applied and removed?
3. For Washington State, are the present load restrictions (developed in 1952) adequate, and how do they affect groups such as freight and timber hauling companies and school buses?

The current load restriction tables used in Washington State are summarized in Table 1 and can be applied at two levels:

1. Emergency load restrictions and
2. Severe load restrictions.

TABLE 1 Current WSDOT Load Restriction Tables[a]

Conventional Tires			Tubeless Tires		
	Allowable Gross Load (lb)			Allowable Gross Load (lb)	
Tire Width (in.)	Emergency	Severe Emergency	Tire Width (in.)	Emergency	Severe Emergency
7.00	1,800	1,800	8-22.5	2,250	1,800
7.50	2,250	1,800	9-22.5	2,800	1,900
8.25	2,800	1,900	10-22.5	3,400	2,250
9.00	3,400	2,250	11-22.5	4,000	2,750
10.00	4,000	2,750	11-24.5	4,000	2,750
11.00[b]	4,500	3,000	12-22.5[b]	4,500	3,000
12.00[c]	4,500		12-24.5[c]	4,500	

[a]Last revised October 1957.
[b]Or more—severe emergency condition.
[c]Or more—emergency condition.

To date, the Washington State Department of Transportation (WSDOT) has applied such load restrictions primarily on the basis of experience and occasionally on the basis of either Benkelman beam or falling weight deflectometer (FWD) pavement surface deflections. Most load restrictions are applied to low-traffic-volume routes such as the Federal Aid secondary system. Further, most counties use identical load restrictions and application periods.

The overall objective of the reported research was to evaluate the effect of freeze-thaw in pavement layers on pavement structural capacity. More specifically the objectives were to

1. Measure the variation of base and subgrade moisture content, frost depth and location, and pavement deflection (surface and in situ);
2. Develop procedures for using easily obtained data or otherwise provide for predicting when load restrictions should be applied on a given pavement structure; and
3. Determine an appropriate load restriction criterion.

To accomplish these objectives it was necessary to

1. Collect data at several test sites, including measurement of
   - Frost depth using frost tubes,
   - Moisture contents using soil cells,
   - Soil temperature using soil cells,
   - Dynamic deflection basins using the FWD,
   - Static deflections using a Benkelman beam, and
   - Dynamic and static deflections using an extensometer permanently buried in the pavement structure.
2. Collect weather data. These data, obtained from National Oceanic and Atmospheric Administration climatic reports or the WSDOT maintenance offices, were used to calculate freezing indices and to estimate depth of freeze using the modified Berggren equation.
3. Obtain pavement samples. Samples of the base and subgrade materials and cores of the asphalt concrete were obtained for laboratory resilient modulus determination. At the time of sampling, the in situ

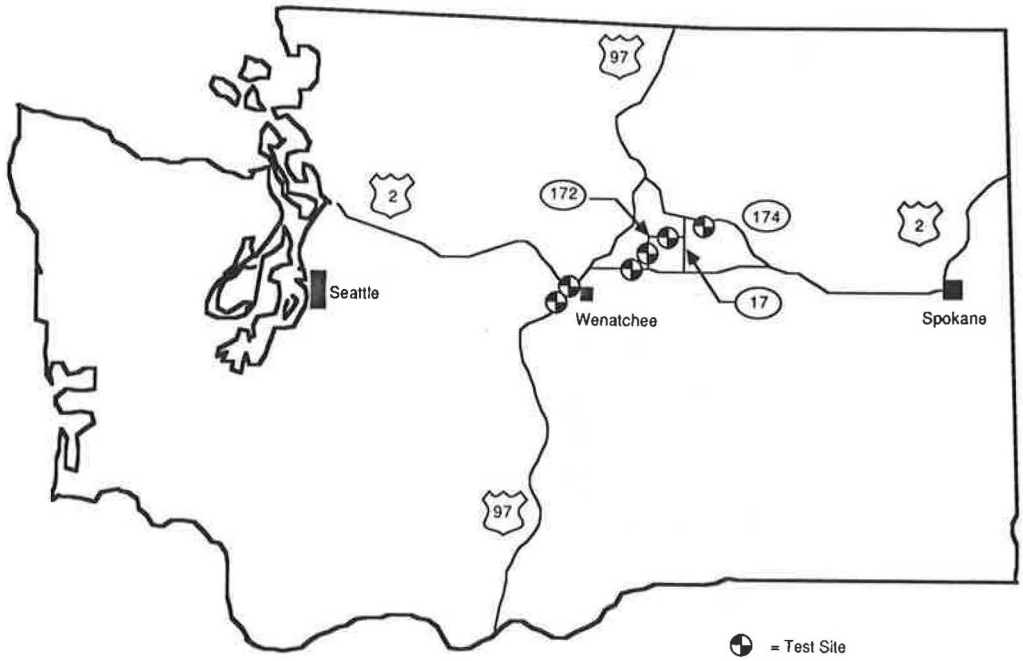

FIGURE 1 Location of field test sites.

density and moisture content of the base and subgrade were determined.

FIELD STUDY

Site Selection

Test sites on existing WSDOT routes were chosen in the central part of Washington (WSDOT District 2). In this part of the state the design freezing index is about 1,000 degree-days (Fahrenheit). Several criteria were used as a basis for selecting the test sites and include

1. The pavement must be located in an area of potential deep frost and be plowed in the winter to keep it free of snow;
2. Each test site should have a reasonable amount of heavy truck traffic (weight but not necessarily volume); and
3. The site locations should encompass a variety of subgrade soil and drainage conditions.

Using these criteria as a partial basis, six 500-ft-long test sites were selected (locations shown in Figure 1) for deflection testing, and four of the sites were instrumented. An overview of the significant test site features is given in Table 2.

Data Collected

Field data were collected at the six test sites during a 15-month period beginning in January 1982, with special emphasis on the spring thaw period. The following data were collected:

1. Pavement surface deflection using the FWD or Benkelman beam, or both;
2. Extensometer readings;

TABLE 2 Principal Test Site Features

State Route and Mile Post	Instrumentation	Pavement Structure[a]	Subgrade		Traffic, 1982 *(2)*	
			Class	Percentage Passing 200 Sieve	ADT	Percentage Trucks
SR 97, MP 184	2 frost tubes 1 moisture tube[b]	4-in. ACP 4-in. CSTC 6-in. ballast	A-1-a(0)	9	3,500	11
SR 2, MP 117	2 frost tubes 2 moisture tubes 1 extensometer	6-in. ACP 17-in. gravel base	A-1-b(0)	16 to 19	11,500	10
SR 2, MP 160	2 frost tubes 1 moisture tube	2-in. ACP 9-in. CSTC	A-1-a(0)	9 to 12	1,000	
SR 172, MP 2	FWD testing	2.6-in. BST 6-in. gravel base			180	6
SR 172, MP 21	FWD testing	2-in. BST 9-in. gravel base			530	6
SR 174, MP 2	2 frost tubes 1 moisture tube 1 extensometer	0.5-in. BST 2-in. ACP 10-in. gravel base	A-1-b(0)	18 to 22	820	16

[a]Nomenclature: ACP = asphalt concrete pavement, CSTC = crushed surfacing top course, and BST = bituminous surface treatment.
[b]Each moisture tube consisted of four moisture cells.

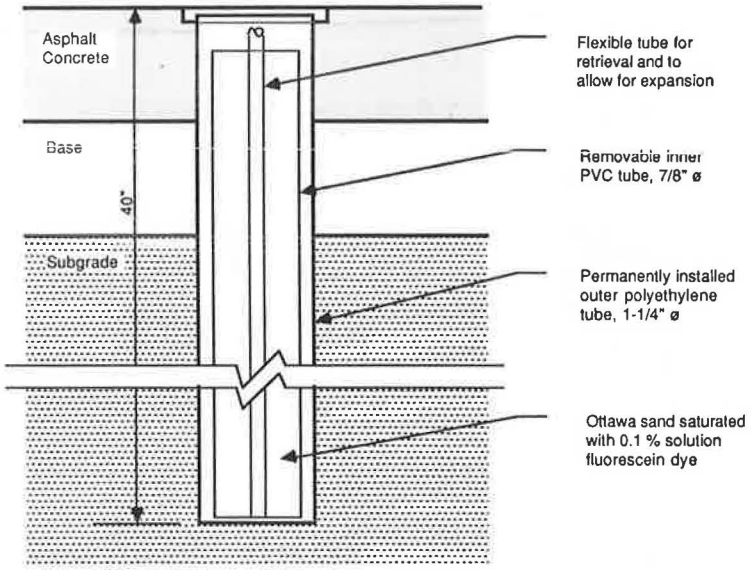

FIGURE 2 Schematic of in situ frost tube.

3. Pavement surface temperature;
4. Base and subgrade temperature;
5. Soil cell resistivity (for moisture content determination); and
6. Depth of frost penetration (using frost tubes).

Instrumentation

A primary objective of the study was to measure changes in pavement strength over the project duration. To this end, four of the six test sites were instrumented (as indicated in Table 2) with frost tubes to measure depth of freezing and soil cells (Soiltest MC 310A) to measure subgrade and base course moisture contents and temperatures. Extensometers were installed at two sites to measure pavement surface deflections. Paint marks were placed on the pavement surface to facilitate repeating deflection testing at the same locations. Sketches of typical frost tube and extensometer construction and soil cell layout are shown as Figures 2-4.

Deflection Measurements

With the advent of computer programs that provide for using pavement deflections to estimate in situ pavement layer moduli, the usefulness of devices that provide such measurements continues to increase. Three approaches were used in the study to measure pavement deflections:

1. Benkelman beam,
2. FWD, and
3. Extensometer.

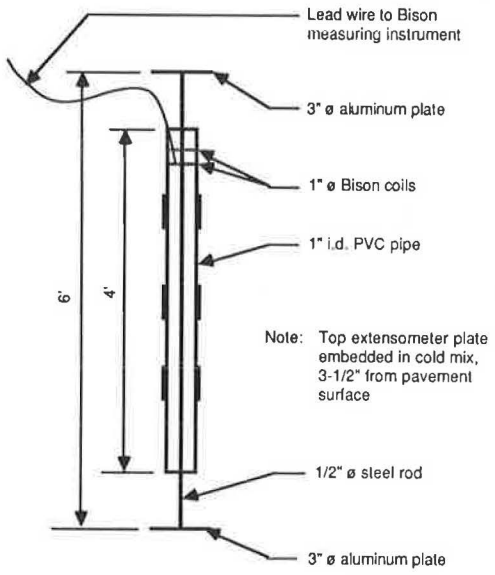

FIGURE 3 Schematic drawing of extensometer.

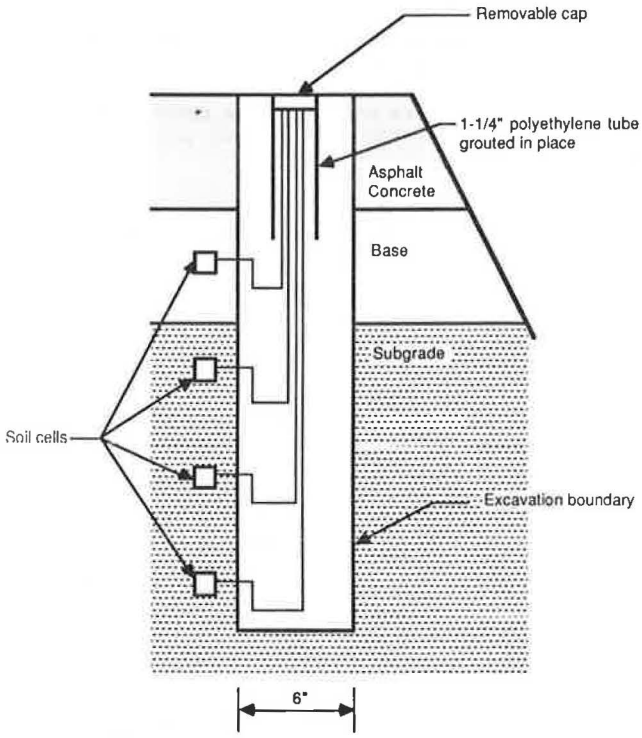

FIGURE 4 Typical soil cell layout.

The Benkelman beam was used to measure single-point rebound deflections along with a single axle, dual tire 18,000-lb axle load (quasi-static loading). The FWD was used to measure deflection basins (with seven sensors). The FWD can apply a dynamic load ranging from 3,000 to 24,000 lb and simulates a vehicle moving at speeds greater than 30 mph. Finally, the extensometer was used to measure deflections under various axle and tire loadings. The Benkelman beam and FWD measurements were taken at 50-ft intervals at each test site.

Typical Results

The type and range of the data collected from the test sites will be illustrated by use of two of the six test sites [SR 2, milepost (MP) 160 and SR 172, MP 2].

FWD Deflections

For the two selected test sites, the maximum pavement deflection (first sensor) averaged over each test site and normalized to a 9,000-lb load is plotted versus time in Figures 5 (SR 2, MP 160) and 6 (SR 172, MP 2). According to these data, spring was the period of highest deflection, as expected (similar trends were observed for the four other test sites). In general, maximum deflections were reached in late February or early March. During the January 1984 site visits, the measured deflections ranged from 9 to 20 percent of the previous summer values, which illustrates the increased stiffness of frozen pavement layers.

Figures 5 and 6 were developed on the basis of several site visits and corresponding data. These trends (as plotted) mask the actual variations that occurred at other times for which data are not available.

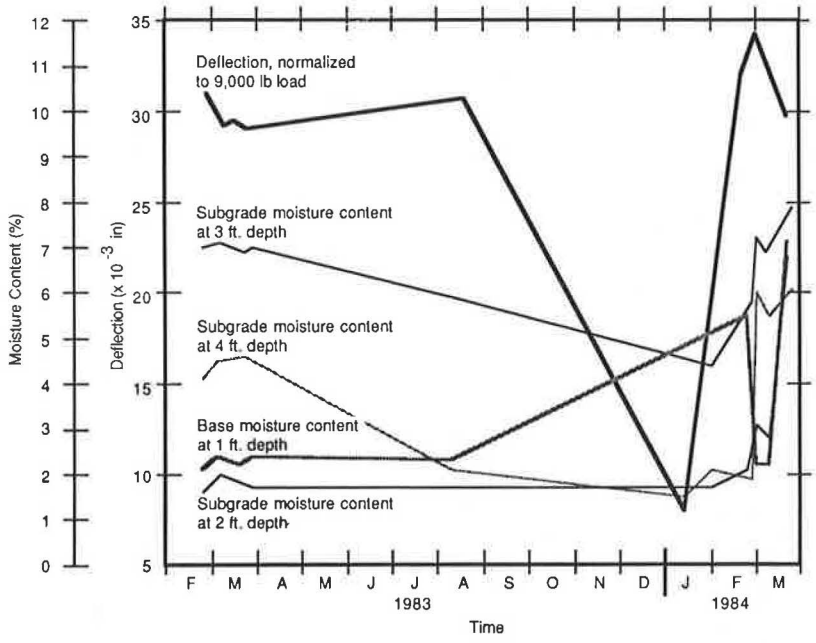

FIGURE 5 SR 2, MP 160—plot of FWD first sensor deflection and base and subgrade moisture contents versus time.

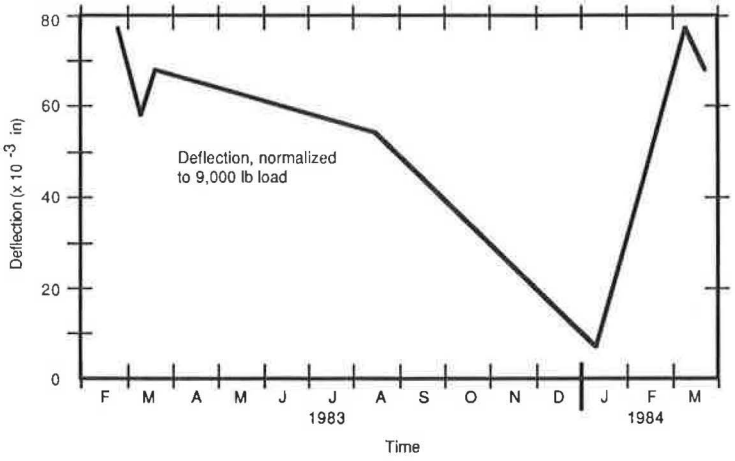

FIGURE 6 SR 172, MP 2—plot of FWD first sensor deflection versus time.

Base and Subgrade Moisture Contents

It is generally accepted that soils (and asphalt concrete) exhibit a decrease in strength with increasing moisture content. To this end, soil resistivity was measured and later converted to soil moisture content when the appropriate laboratory calibrations were completed. An example of the annual change in soil moisture content is shown in Figure 5. Moisture content tends to increase with depth (as expected) and is most variable during the thawing period (winter-spring 1984). Of significance is the high moisture content of the base course, which was essentially as high as the moisture content in the subgrade located 2 ft below the measurement point in the base. This will be further discussed later.

Temperature

As previously discussed, a variety of measurements was made to relate air and pavement temperatures. Soil cells were used to measure in situ soil temperatures as well as soil resistivity for moisture determination. Frost tubes were used in an attempt to measure locations of frost up to a depth of 4 ft; however, numerous problems arose with these and the resulting data were of little use.

On the basis of air temperature data from the nearest WSDOT maintenance facility, freezing indices were calculated and are given in Table 3. These data show the differences in just two winters (1982-1983 and 1983-1984). The design freezing indices (the average of the three coldest winters out of the last 30 years of record) range between 900 and 1,100 degree-days through the part of Washington State where the test sites are located (the mean freezing index for a 30-year record is about 500 degree-days). Thus the winter of 1982-1983 was slightly less severe than average and the winter of 1983-1984 was above average.

By use of the modified Berggren equation (3), various estimates of the depth of ground freezing were made. Assuming the pavement structure and the upper portion of the subgrade can be characterized as a homogeneous granular material (γ_d = 130 pcf, w = 5 percent) for thermal purposes, depths of freeze were calculated for the appropriate freezing indices at each test site and are given in Table 3. Also given in this table are the measured depths of frost (soil cells). The calculated and measured values are at least within the same range (recall that the soil cells were placed at 1-ft intervals of depth, making such comparisons quite approximate). Overall, the temperature data and associated calculations suggest that typical depths of freeze beneath the test sites are about 3 to 4 ft with maximum frost penetration occurring in late January through mid-February. As will be shown in the next section, relatively few thawing degree days are required to place these pavement structures in a "critical period."

DATA ANALYSIS

The method for determining pavement material properties and their variation with time for the six test sites is described in this section. Further, development of a temperature-based criterion for establishing when to apply load restrictions is presented along with the procedure for determining the magnitude of restrictions.

Material Properties

The BISDEF computer program (4) was used along with FWD data to estimate the moduli (or resilient moduli, M_R) and the associated stress sensitivity relations for the pavement layers. This program is based on layered elastic theory and was developed at the U.S. Army Corps of Engineers Waterways Experiment Station. It uses the concept of minimizing the difference between the program-calculated and the measured deflection basins. The program varies the layer modulus until a match is made between the input basin and the BISDEF-predicted basin within a specific margin of error.

The modulus for each pavement layer was estimated for each site visit and test site. The program was also used to calculate bulk stress at the middle of the base course and bulk or deviator stress at the top of the subgrade. Because a minimum of three stress levels (or FWD load magnitudes) was used during each site visit, it was possible to develop the stress-sensitivity relationships ($M_R - \theta$ or $M_R - \sigma_d$) for the base and subgrade layers. These relationships were necessary for additional modeling, which will be discussed later.

The required inputs for the BISDEF program were

1. Measured deflections (mils) and associated distances from the center of the load (inches).
2. Range of modulus values for each layer (psi),
3. Initial estimate of the modulus value for each layer (psi),
4. Thickness of each layer (inches),
5. Poisson's ratio for each layer,
6. Load stress (psi) and load radius (inches), and
7. Points in the pavement structure where stresses are desired.

TABLE 3 Freezing Indices and Calculated Depth of Frost Penetration for the Six Test Sites

Test Site	Winter	Freezing Index (degree-days Fahrenheit)	Calculated Depth of Frost (ft)	Minimum Measured Depth of Frost (ft)	Probable Date of Maximum Depth of Frost[a]
SR 97, MP 184	1982-1983	475	3.3		Feb. 9, 1983
	1983-1984	685	4.0	5	Jan. 23, 1984
SR 2, MP 117	1982-1983				
	1983-1984	510	3.4	3+	Jan. 23, 1984
SR 2, MP 160	1982-1983	400	3.1		Feb. 11, 1983
	1983-1984	730	4.1	3+	Jan. 23, 1984
SR 172, MP 2	1982-1983	475	3.3		Feb. 15, 1983
	1983-1984	745	4.2		Jan. 23, 1984
SR 172, MP 21	1982-1983	475	3.3		Feb. 15, 1983
	1983-1984	745	4.2		Jan. 23, 1984
SR 174, MP 2	1982-1983	170	2.0		Jan. 5, 1983
	1983-1984	470	3.3	2+	Jan. 24, 1984

[a]Based on recorded temperature data.

The measured deflections input to the program were the average deflection basins over each test section for each site visit. The input deflections were selected from four of the FWD sensors and were located at spacings of 0, 11.8, 25.6, and 47.2 in. from the center of loading. An initial estimate of each layer modulus was based on judgment and other previously completed work. The load radius was that of the FWD loading plate (5.9 in.) and the load stresses were the actual stresses applied to the pavement structure by the FWD.

The results of the BISDEF analysis are given in Tables 4 and 5 for the two test sites used in this paper to illustrate the study findings (SR 2, MP 160 in Table 4 and SR 172, MP 2 in Table 5). The stress relationships presented are of the form $M_R = k_1\theta^{k_2}$ for layers that behaved as coarse-grained materials and $M_R = k_1\sigma_d^{-k_2}$ for layers that behaved as fine-grained materials (M_R decreasing with increasing stress.) The SR 172, MP 2 test site was run as a two-layer system with the bituminous surface treatment and base course combined into one layer. This was done because the computer program would not close when the site was run as a three-layer system.

In general, for all test sites as well as the two sites shown, the base and subgrade moduli were higher for the August 1983 site visit than at other times of the year (as might be expected). Further, the pavement layer moduli were substantially higher when frozen. An interesting trend for SR 2, MP 160 was that the base modulus decreased 41 percent from August 1983 to March 1984, but the subgrade modulus on both dates was about the same. For SR 172, MP 2, the base modulus decreased about 27 percent and the subgrade modulus 44 percent for the same time interval (this test site had the largest decrease in subgrade modulus of the six). The maximum observed decrease in modulus for the base was 78 percent (August 1983 and March 1984 testing dates). For all test sites (except SR 2, MP 117, which exhibited extensive fatigue cracking and was actually weaker during the summer months), the base course modulus was reduced by an average of about 52 percent and the subgrade modulus by about 23 percent.

Magnitude of Load Restrictions

The PSAD2A computer program (5) was used to calculate deflections and strains under a given wheel load for the summer (strongest condition) and the spring (weakest condition) for each of the test sites. This was done to determine the change in strains and deflections between the two cases so that a spring load could be found that induced the same strains and deflections, and hence potential pavement damage, as occurred in the summer under maximum loading.

Several input values were required for the PSAD2A program and included for each layer

1. Poisson's ratio,
2. Dry density,
3. Thickness,
4. Stress-modulus relationship (from BISDEF analysis), and
5. Initial estimate of modulus for each layer.

Because the vast majority of trucks uses tubeless tires and the maximum wheel load is in part a func-

TABLE 4 SR 2, MP 160—Results of BISDEF Analysis for Determination of Resilient Moduli, Stresses, and Stress Relationships for each Site Visit

Date	Temperature (°F)	Applied Stress (psi)	AC M_R (psi)	Base M_R (psi)	Subgrade M_R (psi)	Base θ (psi)	Subgrade σ_d (psi)	Base Stress Relationship	Subgrade Stress Relationship
02/24/83	50	57.86	1,200,000	14,800	13,900	21.86	11.67	$1,266\theta^{0.814}$	$29,862\ \sigma_d^{-0.307}$
		88.17	1,500,000	20,800	13,100	28.42	15.85	$r^2 = 0.962$	$r^2 = 0.944$
		123.01	1,200,000	29,400	11,700	49.18	20.29		
03/03/83	45	56.72	1,200,000	21,600	13,100	18.94	10.51	$6,706\theta^{0.396}$	$17,462\ \sigma_d^{-0.118}$
		83.06	1,200,000	24,400	13,000	26.53	14.96	$r^2 = 0.997$	$r^2 = 0.791$
		121.37	1,268,000	27,500	12,100	34.75	20.38		
03/09/83	47	55.80	1,000,000	25,300	13,500	18.98	10.51	$9,508\theta^{0.327}$	$25,782\ \sigma_d^{-0.268}$
		82.44	1,222,000	26,400	13,000	25.71	14.62	$r^2 = 0.836$	$r^2 = 0.864$
		116.70	1,300,000	30,000	11,500	31.02	18.74		
03/13/83	60	42.70	1,100,000	15,200	10,000	13.90	7.27	$2,787\theta^{0.658}$	$21,904\ \sigma_d^{-0.199}$
		83.96	1,029,000	26,800	12,700	26.90	15.10	$r^2 = 0.953$	$r^2 = 0.926$
		121.83	1,267,000	28,000	12,200	35.08	20.53		
		152.87	1,318,000	30,500	11,500	40.01	24.33		
03/24/83	40	58.52	2,155,000	16,800	13,000	17.84	9.90	$4,245\theta^{0.474}$	$21,088\ \sigma_d^{-0.201}$
		88.36	2,460,000	18,800	12,800	25.05	14.20	$r^2 = 0.669$	$r^2 = 0.632$
		125.46	1,600,000	26,300	12,200	34.44	20.41		
		150.67	2,400,000	20,800	10,600	36.41	22.05		
08/17/83	72	80.08	931,000	28,800	11,100	23.08	13.50	$282\theta^{1.473}$	$6,152\ \sigma_d^{0.227}$
		125.98	1,000,000	43,300	12,000	30.44	19.04		
01/10/84	34	76.63							
		108.83							
		144.39							
02/21/84	42	71.0	1,096,000	20,800	12,900	24.54	13.50	$6,277\theta^{0.376}$	$21,492\ \sigma_d^{-0.197}$
		95.7	1,140,000	23,000	12,200	30.73	17.30	$r^2 = 0.988$	$r^2 = 0.994$
		129.2	1,258,000	24,600	11,700	38.35	22.16		
03/01/84	48	71.3	1,184,000	16,500	12,500	25.30	13.75	$4,628\theta^{0.398}$	$26,576\ \sigma_d^{-0.287}$
		95.9	1,327,000	18,800	11,800	31.05	17.31	$r^2 = 0.886$	$r^2 = 0.994$
		125.8	1,462,000	19,300	11,000	37.60	21.46		
03/09/84	60	66.6	972,000	24,700	12,800	22.26	12.39	$4,461\theta^{0.554}$	$26,189\ \sigma_d^{-0.282}$
		91.0	552,000	30,400	12,000	30.80	16.83	$r^2 = 0.984$	$r^2 = 0.968$
		121.8	579,000	32,700	11,000	37.29	21.03		
03/21/84	49	66.0	658,000	30,300	12,900	22.53	12.36	$18,504\theta^{0.151}$	$17,637\ \sigma_d^{-0.122}$
		93.3	819,000	29,600	12,600	30.00	16.86	$r^2 = 0.536$	$r^2 = 0.947$
		127.1	700,000	33,000	12,000	39.20	22.19		

TABLE 5 SR 172, MP 2—Results of BISDEF Analysis for Determination of Resilient Moduli, Stresses, and Stress Relationships for each Site Visit

Date	Temperature (°F)	Applied Stress (psi)	1st Layer M_R (psi)	Subgrade M_R (psi)	1st Layer θ (psi)	Subgrade σ_d (psi)	1st Layer Stress Relationship	Subgrade Stress Relationship
02/24/83	50	47.46	13,400	5,000	47.58	15.91	$613\theta^{0.781}$	$2{,}593\ \sigma_d^{0.239}$
		72.69	14,800	5,700	73.09	24.62		
		103.32	24,300	5,700	97.88	28.70	$r^2 = 0.788$	$r^2 = 0.937$
03/03/83	38	49.54	25,900	5,800	46.72	13.55	$12{,}272\theta^{0.195}$	$5{,}457\ \sigma_d^{0.024}$
		71.65	28,000	5,900	67.02	19.03		
		105.24	29,900	5,900	97.54	27.07	$r^2 = 0.996$	$r^2 = 0.741$
03/09/83	47	47.95	28,800	6,800	45.45	13.34	$12{,}978\theta^{0.209}$	$7{,}634\ \sigma_d^{-0.045}$
		68.40	31,000	6,700	64.20	18.40		
		101.05	33,500	6,600	93.67	26.01	$r^2 = 0.999$	
03/17/83	39	49.22	21,200	6,600	48.25	15.34	$14{,}995\theta^{0.096}$	$6{,}205\ \sigma_d^{0.021}$
		70.68	23,700	6,600	68.36	21.06		
		102.86	22,800	6,700	100.23	31.43	$r^2 = 0.386$	$r^2 = 0.806$
08/17/83	75	74.70	26,000	8,600	73.76	23.85	$6{,}393\theta^{0.326}$	$8{,}600\ \sigma_d^{0.0}$
		105.82	29,000	8,600	103.09	32.32		
01/10/84	34	72.84	371,100	59,900	65.82	17.08		
		104.21	348,300	59,300	94.82	25.06		
		143.49	326,800	50,500	128.97	32.96		
03/01/84	46	56.8	23,700	4,500	52.39	14.36	$952\theta^{0.817}$	$2{,}268\ \sigma_d^{0.258}$
		78.5	32,000	4,800	70.38	17.86		
		110.0	39,200	5,100	96.80	23.27	$r^2 = 0.982$	$r^2 = 0.994$
03/07/84	60	55.2	19,900	5,300	53.14	16.19	$2{,}355\theta^{0.520}$	$3{,}352\ \sigma_d^{0.163}$
		74.9	19,000	5,500	72.79	22.69		
		103.9	27,400	5,800	97.13	27.56	$r^2 = 0.619$	$r^2 = 0.935$
03/21/84	50	57.1	28,400	6,000	53.42	15.20	$13{,}761\theta^{0.173}$	$7{,}719\ \sigma_d^{-0.093}$
		77.6	27,000	5,800	72.80	20.82		
		107.0	31,600	5,700	98.14	26.49	$r^2 = 0.432$	$r^2 = 0.988$

tion of tire width, it was decided that the following tire sizes would be used in the subsequent analysis: 8-22.5, 9-22.5, 10-22.5, 11-22.5, 12-24.5, 14-17.5, and 16-22.5. Only single tires on single axles were evaluated because these were considered to be the most critical.

For the summer load cases, the maximum allowable load per time would be input. This maximum was determined by use of the Revised Code of Washington (RCW) 46.44.042, which allows 550 lb per inch width of tire up to a tire width of 12 in. and 660 lb per inch width for tires 12 in. wide or wider. For example, an 11-in.-wide tire can legally carry 6,050 lb and a 12-in.-wide tire 7,920 lb. Corresponding tire pressures were based on tire inflation pressures recommended by the Tire and Rim Association, Inc.

TABLE 6 Tire Loads and Tire Pressures for the Spring Condition

Percentage of Maximum Load	Tire Size	Tire Pressure (psi)	Load/Tire (lb)
100	8-22.5	105	4,400
	9-22.5	115	4,950
	10-22.5	105	5,500
	11-22.5	100	6,050
	12-24.5	115	7,920
	14-17.5	100	9,240
	16-22.5	90	10,000
75	8-22.5	80	3,300
	9-22.5	75	3,712
	10-22.5	70	4,125
	11-22.5	65	4,538
	12-24.5	80	5,940
	14-17.5	100	6,930
	16-22.5	75	7,500
50	8-22.5	55	2,200
	9-22.5	55	2,475
	10-22.5	55	2,750
	11-22.5	65	3,025
	12-24.5	65	3,960
	14-17.5	65	4,620
	16-22.5	55	5,000

These pressures were found to be reasonable for modeling purposes on the basis of a previous study performed for WSDOT (6). The tire loads and pressures for the summer condition (maximum condition) are given in Table 6 (100 percent of maximum load).

For the spring condition, the following cases were developed:

1. The maximum load and tire pressure as used for the summer condition,
2. Seventy-five percent of the maximum load and corresponding tire pressure as recommended by the Tire and Rim Association, and
3. Fifty percent of the maximum load and the recommended tire pressure.

The resulting tire loads and pressures are given in Table 6.

The output parameters from PSAD2A, which were evaluated for both the summer and spring analyses, were

1. Surface deflection (δ),
2. Horizontal strain at the bottom of the bituminous bound layer (ε_t),
3. Vertical strain at the top of the base course (ε_{VB}), and
4. Vertical strain at the top of the subgrade (ε_{VS})

When these deflections and strains had been calculated, the spring load that caused the same damage as the maximum allowable load during the summer was computed. This was done by use of plots developed from the previously listed program outputs for each test site and tire size and is shown for SR 2, MP 160 and tire size 11-22.5 in Figure 7. This figure was constructed as follows:

1. Surface deflection versus load was plotted for the three loads used in the spring analysis and a curve was fitted through the points and

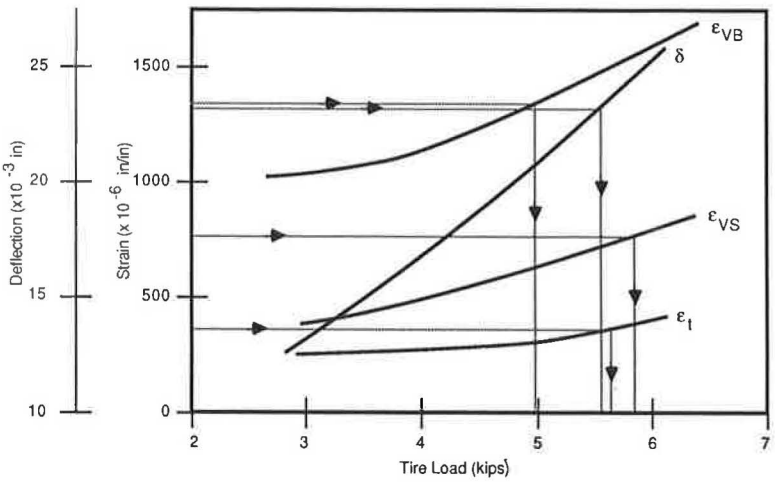

FIGURE 7 SR 2, MP 160—tire size 11-22.5.

2. ϵ_t, ϵ_{VB}, and ϵ_{VS} versus load were plotted for the same three loads and the corresponding curves were drawn.

The next step was to determine the spring load that would result in the same deflections and strains as did the summer case. This was done by entering the plot (such as Figure 7) on the vertical axis with δ, ϵ_t, ϵ_{VB}, or ϵ_{VS}. A horizontal line was then drawn to intersect the appropriate curve and then drawn vertically down to the tire load axis.

The allowable spring wheel loads so determined are given in Tables 7 and 8 for the two featured test sites. For SR 2 and tires up to 12 in. wide, the reduction in allowable load is no more than about 20 percent (from summer to spring conditions). This reduction increases for 14- and 16-in. tires. For SR 172, the reduction in allowable load for the critical criterion (surface deflection) is about 60 percent. A comparison of the percentage reduction between just these two pavement structures illustrates a basic difference between SR 2, which was originally designed to mitigate the effects of frost action, and SR 172, which was not.

Finally, Table 9 gives the allowable spring load and critical criterion for each tire size and test site. The low-volume routes such as SR 172 and SR 174 clearly have the largest reduction in allowable loads, as would be expected. On the basis of this type of analysis, actual load restrictions could be varied for each site; however, from a practical standpoint, this is not enforceable. If load restrictions are needed for a specific pavement structure, then only one or two levels of restrictions should be considered. From the analysis a spring allowable load of about 40 percent of the summer allowable appears reasonable (a 60 percent reduction). Interestingly, the corresponding allowable spring

TABLE 7 SR 2, MP 160—Spring Allowable Loads and Corresponding Percentage of the Maximum Legal Load

Tire Size	Maximum Legal Tire Load (lb)	Spring Allowable Load for δ (lb)	Percentage of Maximum Legal Load	Spring Allowable Load for ϵ_t (lb)	Percentage of Maximum Legal Load	Spring Allowable Load for ϵ_{VB} (lb)	Percentage of Maximum Legal Load	Spring Allowable Load for ϵ_{VS} (lb)	Percentage of Maximum Legal Load
8-22.5	4,400	4,020	91	4,080	93	3,670	83	4,400	100
9-22.5	4,950	4,600	93	4,600	93	4,190	85	4,920	99
10-22.5	5,500	5,050	92	5,020	91	4,600	84	5,390	98
11-22.5	6,050	5,570	92	5,830	96	4,990	82	5,900	98
12-24.5	7,920	7,170	90	7,120	90	6,180	78	7,600	96
14-17.5	9,240	8,115	88	6,640	72	6,020	65	8,790	95
16-22.5	10,000	8,900	89	7,820	78	6,760	68	9,560	96

Note: δ = surface deflection, ϵ_t = horizontal strain at the bottom of the asphalt concrete, ϵ_{VB} = vertical strain at the top of the base, and ϵ_{VS} = vertical strain at the top of the subgrade.

TABLE 8 SR 172, MP 2—Spring Allowable Loads and Corresponding Percentage of the Maximum Legal Load

Tire Size	Maximum Legal Tire Load (lb)	Spring Allowable load for δ (lb)	Percentage of Maximum Legal Load	Spring Allowable Load for ϵ_{VS} (lb)	Percentage of Maximum Legal Load
8-22.5	4,400	1,820	41	2,330	53
9-22.5	4,950	2,180	44	2,720	55
10-22.5	5,500	2,400	44	2,980	54
11-22.5	6,050	2,450	40	3,200	53
12-24.5	7,920	3,800	48	4,400	56
14-17.5	9,240	4,400	48	4,920	53
16-22.5	10,000	4,680	47	5,300	53

Note: δ = surface deflection and ϵ_{VS} = vertical strain at the top of the subgrade.

TABLE 9 Summary of the Critical Criteria and Corresponding Spring Allowable Load for Each Tire Size Modeled

Tire Size	Site	Critical Criterion for Each Site	Spring Allowable Load (lb)	Percentage of Maximum Legal Load
8-22.5	SR 97, MP 183.48	δ	3,775	86
	SR 2, MP 117.38	ϵ_t	5,200	118
	SR 2, MP 159.6	ϵ_{VB}	3,670	83
	SR 172, MP 2.0	δ	1,820	41 (critical)
	SR 172, MP 21.4	ϵ_{VB}	2,400	54
	SR 174, MP 2.0	ϵ_{VB}	3,130	71
9-22.5	SR 97, MP 183.48	δ	4,325	87
	SR 2, MP 117.38	δ	5,460	110
	SR 2, MP 159.6	ϵ_{VB}	4,190	85
	SR 172, MP 2.0	δ	2,180	44 (critical)
	SR 172, MP 21.4	ϵ_{VB}	2,730	55
	SR 174, MP 2.0	ϵ_{VB}	3,490	70
10-22.5	SR 97, MP 183.48	δ	4,900	80
	SR 2, MP 117.38	δ	6,230	113
	SR 2, MP 159.6	ϵ_{VB}	4,600	84
	SR 172, MP 2.0	δ	2,400	44 (critical)
	SR 172, MP 21.4	ϵ_{VB}	2,750	50
	SR 174, MP 2.0	ϵ_{VB}	3,700	67
11-22.5	SR 97, MP 183.48	δ	4,875	80
	SR 2, MP 117.38	δ	6,770	112
	SR 2, MP 159.6	ϵ_{VB}	4,990	82
	SR 172, MP 2.0	δ	2,450	40
	SR 172, MP 21.4	ϵ_{VB}	2,290	38 (critical)
	SR 174, MP 2.0	ϵ_{VB}	3,850	64
12-24.5	SR 97, MP 183.48	δ	6,300	80
	SR 2, MP 117.38	δ	8,550	108
	SR 2, MP 159.6	ϵ_{VB}	6,180	78
	SR 172, MP 2.0	δ	3,800	48
	SR 172, MP 21.4	ϵ_{VB}	3,600	45 (critical)
	SR 174, MP 2.0	ϵ_{VB}	4,780	60
14-17.5	SR 97, MP 183.48	ϵ_t	6,020	65
	SR 2, MP 117.38	δ	9,380	102
	SR 2, MP 159.6	ϵ_{VB}	6,020	65
	SR 172, MP 2.0	δ	4,400	48
	SR 172, MP 21.4	ϵ_{VB}	3,460	37 (critical)
	SR 174, MP 2.0	ϵ_{VB}	4,670	50
16-22.5	SR 97, MP 183.48	ϵ_t	5,990	60
	SR 2, MP 117.38	δ	11,100	111
	SR 2, MP 159.6	ϵ_{VB}	6,760	68
	SR 172, MP 2.0	δ	4,680	47
	SR 172, MP 21.4	ϵ_{VB}	3,320	33 (critical)
	SR 174, MP 2.0	ϵ_{VB}	4,780	48

loads from this analysis fall within the range of the current WSDOT load restrictions (Table 1).

Criterion for When to Apply Load Restrictions

A basic issue addressed in the study was when to establish load restrictions on a specific highway (assuming that load restrictions are necessary). A criterion based on deflection measurements provides certainty as to the need for load restrictions. At least for the near future, it is impossible for WSDOT equipment and personnel to be at all the necessary locations during the potentially critical months of January, February, and March. An alternative approach is to use temperature data to estimate the depth of thaw in a pavement and thus whether it is near or in the critical period.

Figure 8 was prepared by calculating the depth of thaw for various thaw indices using the modified Berggren equation (3):

$$x = \lambda \left[(48\ k_{avg}\ n\ TI/L)^{1/2}\right]$$

where

x = depth of thaw (ft),
λ = dimensionless coefficient that corrects formula for neglected effects of volumetric heat,
k_{avg} = average thermal conductivity of the soil (Btu/hr·ft·°F),
n = factor for converting air thawing index to surface thawing index,
TI = air thawing index (degree-days, Fahrenheit), and
L = soil latent heat (Btu/ft^3).

The pavement structure was assumed to be homogeneous and composed of either a coarse-grained or a fine-grained soil (with corresponding dry densities of 130 and 100 pcf, respectively). An $n = 1.5$ was assumed (dark bituminous surface) along with $\lambda = 0.7$ for the fine-grained soil and $\lambda = 0.6$ for the coarse-grained soil. The pavement surface thickness was assumed to have a negligible effect on the depth of thaw (other than color). As shown in Figure 8 the depth of thaw for equal thawing indices is clearly greater for coarse-grained soils than for fine-grained soils. Further, it is reasonable to expect that the upper portions of all WSDOT pavement structures will behave as coarse-grained soil. Thus at an air TI = 30 the depth of thaw will be about 12 in. and at an air TI = 50 about 15 in. For most pavement structures this would result in the surface and base courses but not necessarily all of the subgrade being thawed.

The temperature data from the test sites and the BISDEF analysis of FWD data reinforce the modified Berggren calculations that the test sites reached their critical condition after receiving about 50 degree-days of thawing temperature. Thus it was

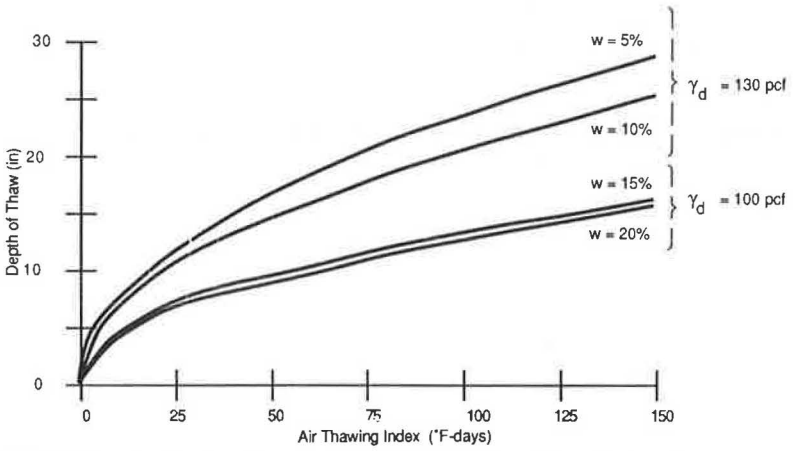

FIGURE 8 Air thawing index versus depth of thaw for thin asphalt surfaced pavements.

recommended that WSDOT tentatively adopt a TI ≈ 30 degree-days to indicate pavement structures approaching a critical condition and a TI ≈ 50 degree-days to indicate pavement structures in a critical condition. Clearly, pavement structure, subgrade soil, and winter temperature history will influence such criteria; however, WSDOT district maintenance personnel in the numerous maintenance offices record high and low daily temperatures for other purposes each winter. Now this same, available information can be used as a rule-of-thumb to assess the need for load restrictions.

CONCLUSIONS

The following conclusions are warranted:

1. The falling weight deflectometer is an excellent device for collecting the information required to evaluate the structural capacity of pavements. Further, Benkelman beam and FWD maximum deflections correlated well; however, the deflection basins obtainable with the FWD provide a significantly improved ability to analyze pavement structure.
2. For the field test sites that normally require seasonal load restrictions, the base course moduli vary more than the subgrade moduli. The subgrade moduli are relatively stable throughout the year (except when frozen). The base course weakness is due to excessive moisture available during the thawing period. The excessive moisture in the base course is exacerbated by either a still frozen subgrade or a low permeability subgrade soil (i.e., a water drainage path is temporarily reduced or eliminated), or both.
3. A multilayered elastic analysis computer program (BISDEF) was used along with FWD data to characterize the materials in the pavement layers for each test site with time. Criteria were developed that essentially reduce the allowable loads for a summer condition to equivalent loads during the critical period (spring thaw). On the basis of this analysis for the more critical test sites, a reduction in legal loads of about 60 percent is required. Further, the analysis tends to reinforce the current WSDOT load restriction tables.
4. A criterion was developed that can be used to determine when load restrictions should be initiated on a pavement structure requiring such limitations (the criterion does not identify which pavements require load restrictions). The criterion is based on thawing degree-days and can be readily used by the WSDOT maintenance offices that record daily high and low temperatures. Both field data and an analytical procedure suggest that pavements susceptible to weakening during the critical period will approach this condition after a thawing index of 30 degree-days has occurred and will be in the critical period after accumulating 50 degree-days (one thawing degree-day is equal to an average daily temperature of 1°F above freezing). Clearly, site-specific deflection data are the single best criterion to use in assessing the need for load restrictions, but deflection data can be expensive to obtain and difficult to get at the needed time. A temperature-based criterion is the next best alternative (and the least expensive).

REFERENCES

1. T.C. Johnson, R.L. Berg, K.L. Carey, and C.W. Kaplar. Roadway Design in Seasonal Frost Areas. NCHRP Synthesis of Highway Practice 26. TRB, National Research Council, Washington, D.C., 1974.
2. 1982 Annual Traffic Report. Washington State Department of Transportation, Olympia, 1982.
3. Calculation Methods for Determination of Depths of Freeze and Thaw in Soils--Emergency Construction. Technical Manual 5-892-6. Department of the Army, Sept. 1966.
4. A.J. Bush III. Nondestructive Testing for Light Aircraft Pavements. Report FAA-RD-80-9-II. U.S. Army Corps of Engineers, Nov. 1980.
5. R.G. Hicks, J.D. Swait, Jr., and E.O. Chastain. Use of Layered Theory in the Design and Evaluation of Pavement Systems. 3rd ed. Department of Civil Engineering, Oregon State University, Corvallis, Jan. 1978.
6. J. Sharma, J. Hallin, and J.P. Mahoney. Evaluation of Present Legislation and Regulations on Tire Sizes, Configurations, and Load Limits. Report WA-RD-59.1. Washington State Department of Transportation, Olympia, July 1983.

Publication of this paper sponsored by Committee on Flexible Pavements.

Effects of Higher Tire Pressures on Strain in Thin AC Pavements

FREDDY L. ROBERTS and BARRY T. ROSSON

ABSTRACT

Since the oil embargo of 1973 and the attendant increase in fuel prices, pressures to increase truck sizes and weights have intensified. A second factor, which has also been on the increase but which has been given little attention, is tire inflation pressures. Inflation pressures have increased from in the vicinity of 80 psi to a typical value of 120 psi found in Texas tire pressure surveys in 1984. The objective of this paper is to evaluate the effect of this increase in tire pressures on tensile strains in thin asphalt concrete pavements. To determine the stress distribution between the tire and the road surface, the researchers used a finite element computer program developed at Texas Transportation Institute to study the effect of tire parameters on road surface friction forces. This computer program was used to develop the vertical pressure distribution and the horizontal surface shear forces for a free-rolling truck tire inflated to both 75 and 125 psi. A series of computer runs was made using ILLI-PAVE to determine the horizontal tensile strains for asphalt concrete surfaces 1, 1.5, 2, and 4 in. thick over an 8-in. granular base with three different moduli and a subgrade soil that is stress sensitive with an initial modulus of 10 ksi. This series of runs showed that increased truck tire pressures increase tensile strain and attendant fatigue cracking dramatically, that some thin pavement structures cannot provide adequate service, and that design procedures must be upgraded to consider pavement materials that can resist these high tensile strains. In general, to provide adequate service, materials should be either thin and flexible or thick and stiff.

During the last few years, pressure on legislatures has concentrated on either increasing gross vehicle weights from current levels to more than 100,000 lb or increasing the size of trailers, or both. Concern over the effects of these increases on pavement deterioration has been so great that highway engineers have largely ignored in their analyses another factor that has also been on the increase: tire inflation pressures. With the increased cost for fuel and the desire to reduce rolling resistance and increase fuel economies, tire manufacturers have responded by designing and marketing both bias and radial tires that operate at higher inflation pressures. This means that pavements that were designed for 70,000- to 80,000-lb gross vehicle weight (GVW) vehicles carrying loads on tires inflated to 75 to 80 psi are now carrying heavier loads at significantly increased tire pressures. To determine the current levels of tire pressures and their effects on Texas highways the Texas State Department of Highways and Public Transportation (SDHPT) contracted with the Texas Transportation Institute (TTI) to perform two research projects. The first project is to determine typical tire inflation pressures, their contact pressure distributions, and their effects on highway pavements. The second project includes evaluation and design of thin asphalt concrete (AC) pavements including evaluation of suitable materials with which to build these thin pavements. This paper includes portions of both of these studies.

TIRE MODELS IN PAVEMENT ANALYSIS

Initial analyses of the states of stress in solid bodies involved the use of point load on uniform elastic materials of semi-infinite extent; later analysis techniques included strip loads of finite width and infinite length. As analysis of pavement systems became more sophisticated, Westergaard and Burmister extended the analysis to include more than one layer and also began to model the tire as a circle of uniform vertical pressure with no surface shear forces. This tire model continued to be used in the highway design community until the last few years. More recently highway engineers have begun to use finite element models developed by tire carcass designers to define the stress conditions that occur at the tire-pavement interface.

Tielking Tire Model

The finite element tire model used in this study was originally developed during an analytical and experimental investigation of tire-pavement interaction (1) to provide the capability for calculating the distributions of sliding velocity and normal pressure in the tire-pavement contact interface. A relatively general, nonlinear finite element shell-of-revolution computer program (2,3) was chosen as the foundation for the finite element tire model. A Fourier transform procedure for solving the shell contact problems of the foundation program was developed (4) and incorporated into the finite element program, giving this tire model the unique capability of calculating contact boundary and interface pressure distribution for a specified tire deflection.

The shell elements used in the tire model are orthotropic. A material property subroutine was developed to generate orthotropic moduli from cord and rubber property data and geometric data describing the ply structure of the tire carcass. Although the shell elements are homogeneous and orthotropic,

they are sensitive to details of carcass design including tire materials and geometry.

The tire is modeled by an assemblage of axisymmetric curved shell elements. The elements are connected to form a meridian of arbitrary curvature and are located at the carcass midsurface. Figure 1 shows the assembly of 21 elements along the midsurface of a G78-14 tire. A cylindrical coordinate system is used, with r, w, and z indicating radial, circumferential, and axial directions, respectively. Each element forms a complete ring that is initially axisymmetric with respect to z. The elements are connected at nodal circles (numbered in Figure 1) hereafter referred to as nodes.

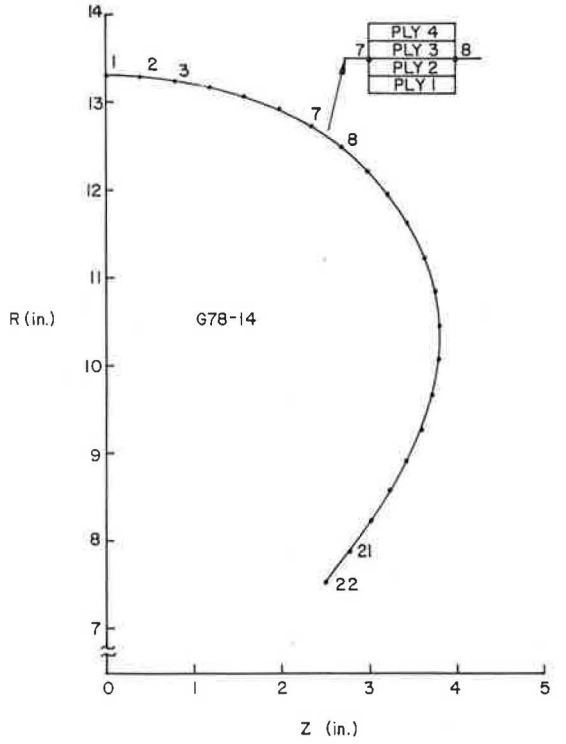

FIGURE 1 Finite elements positioned on the tire carcass midsurface.

The finite elements are homogeneous and orthotropic with a set of moduli specified for each individual element. The orthotropic moduli for each element are determined by the ply structure surrounding the element.

The finite element model is clamped at the edges (Node 22 in Figure 1), pressurized, and rotated to induce centrifugal force loading. It is then brought into contact with a rigid, frictionless surface perpendicular to the plane of symmetry (the r-θ plane). The contact surface (the pavement) is at the specified loaded radius (Rℓ) measured from the z-axis. The internal pressure, the angular velocity, and the loaded radius are the only operating variables specified before contact deformation and pressure in the contact region are calculated. Tielking and Schapery (4) describe the mathematical procedures used to calculate the contact pressure distribution and deformation of the tire deflected against the pavement.

The deflected shape of a nylon tire meridian passing through the center of the contact region is plotted in Figure 2 for tire deflection $\delta = 0.9$ in. Figure 2 also shows both the inflated, undeflected meridian and the calculated contact pressure distribution along the meridian. The calculated tire load is 850 lb (for $\delta = 0.9$ in.).

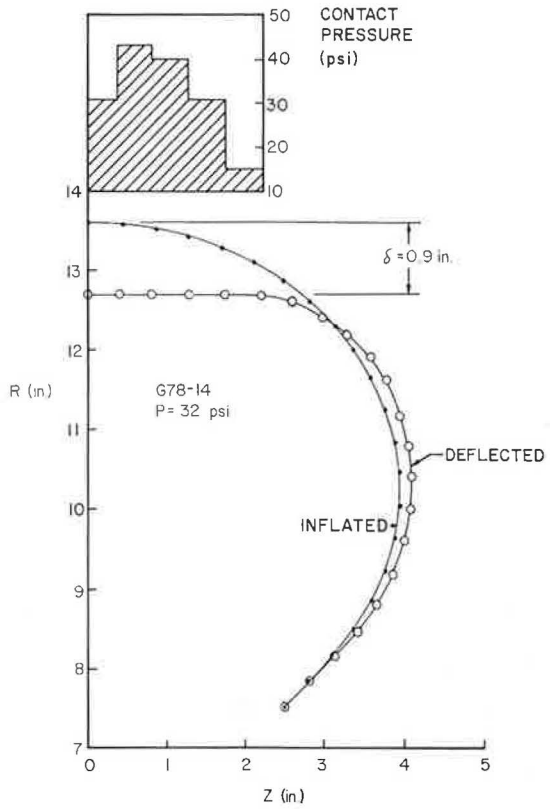

FIGURE 2 Deflected shape and tire contact pressure distribution results from finite element tire model.

This finite element tire model is believed to be the first to have the capability of calculating the contact pressure distribution in the footprint of a deflected tire. This capability is important because contact pressure has a profound influence on all aspects of tire performance. The finite element tire model enables analytical investigations to be made of how tire design variables influence contact pressure distribution.

The rolling-tire results are calculated by superimposing the angular velocity of the rolling tire on the solution for static contact against a frictionless surface. The sliding velocities of points in the contact region are calculated as outlined elsewhere (5). The sliding velocity and the normal contact pressure determine the friction coefficient at each point in the footprint. The resultant braking and driving and steering shear forces respond to tire operating variables such as inflation pressure, tire load, and slip angle through the influence of these operating variables on the distribution of sliding velocity in the footprint. Tire side force is similarly obtained by summing the lateral shear forces in the contact region.

Tire Selected for Study

For the study reported in this paper, a typical 10.00-20 bias-ply truck tire carcass was obtained; the input data were developed by performing measurements on a section of the tire; and the tire pressure distributions were calculated. Figure 3 shows the

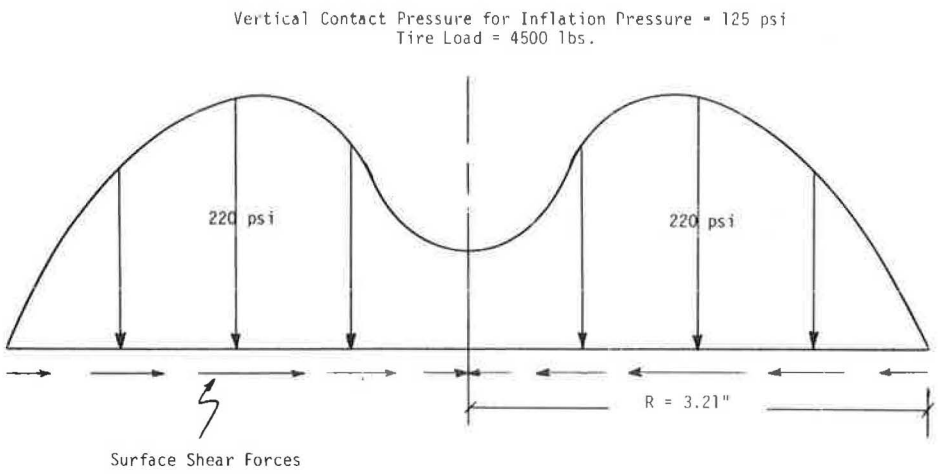

FIGURE 3 Nonlinear vertical tire pressure distribution with lateral surface shear forces as developed using finite element model by Tielking.

vertical and horizontal contact pressure distributions for this tire inflated to 125 psi.

Two tire pressures were selected for this analysis, 75 and 125 psi. These two values were selected because the first value represents a typical historical value used for design and analysis of highway pavement structures, and the second value represents current inflation pressure on Texas highways as shown by a field study conducted by TTI during the spring and summer of 1984. Although the second value may appear high to some readers, representatives from tire manufacturers indicate that within the next 5 years inflation pressures will continue to rise to nearly 150 psi. The impetus for these higher values is reduced rolling resistance, which produces reduced vehicle operating costs.

PAVEMENT MODEL SELECTED FOR ANALYSIS

The computer program used for this analysis is a modified version of ILLI-PAVE (6). This program was chosen over two other programs, PLANE and CRANLAY, because the modified version of ILLI-PAVE had more flexible material property inputs and because tire pressure distribution could be input in a variety of ways.

The computer programs PLANE and CRANLAY were written by Harrison, Wardle, and Gerrard in Australia in 1972 (7). PLANE is an elastic layer theory program that only considers a single layer of infinite depth with material property inputs defined elastically in two directions as orthorombic, cross-anisotropic, or isotropic. The tire load is represented as a strip of specified width and magnitude but infinite in extent. There are, however, 12 different load cases that can occur in pairs: uniform and linear vertical stress, uniform and linear lateral shear stress, and displacement-defined loads.

CRANLAY is also an elastic layer theory program with the capability of accepting up to five horizontal layers with material properties defined as either cross-anisotropic or isotropic. Tire load is input as a circular load of specified radius and magnitude. CRANLAY has only two different load cases, which must be run separately: uniform vertical pressure and linear radial shear stress. Both programs output the stresses, strains, and displacements in the layer or layers of the system.

The third pavement program examined was ILLI-PAVE. It is a version of a program written by Wilson (8-10) that was modified and made user friendly by the research staff of the Construction Engineering Laboratory at Champaign, Illinois, in 1982. It is a finite element program that models a pavement three dimensionally by using a two-dimensional half space of a finite solid of revolution. This rectangular half space is divided into a set of rectangular elements connected at their nodal points. ILLI-PAVE loading is of the "flexible plate" type (i.e., a uniform circular contact pressure). The material modular properties of ILLI-PAVE can be input as a function of the minor principal stress, the deviator stress, the first stress invariant, or simply as a constant elastic modulus.

This program was selected because it had the material property inputs that were needed and the tire load input capabilities could be changed to allow nonuniform vertical pressure and lateral shear pressures. This was accomplished by externally calculating the UZ and UR load values and reading them directly into the program as input. The uniform contact pressure of the original ILLI-PAVE was set to approximately zero, and the UZ and UR values were read in as the load input. UZ is the variable used to define the vertical force or displacement at a node on the surface, and UR is the variable used to define the horizontal force or displacement at a node. Because the UZ and UR values are generated externally, any desired distribution of load in the vertical or horizontal direction can be input. The UZ and UR values were calculated using the pressure distribution output from the Tielking tire model.

The ILLI-PAVE output gives the displacements of nodes and stresses at the midpoint of the element. Strains in the surface were calculated externally using Hooke's law.

STUDY PARAMETERS

The basic objective of this paper is to evaluate the effects of increased tire pressure on thin asphalt concrete pavements that are typically used on the Texas farm-to-market system. Therefore the following series of material combinations and layer thicknesses was used to determine the stress and strain state for two different tire inflation pressures and a 4,500-lb single wheel load:

- Surface
  Thickness: 1, 1.5, 2, and 4 in. and

Elastic moduli: 50, 100, 200, 400, and 800 ksi.

- Base
  Thickness: 8 in. and
  Elastic moduli: stress-sensitive.

Equation	Typical Base Modulus (psi)
$4886\theta^{0.239}$	20,000
$7000\theta^{0.325}$	40,000
$8787\theta^{0.365}$	60,000

where θ = bulk stress

- Subgrade
  Thickness: infinite and
  Elastic moduli: as defined in Figure 4.
  Note: Only one subgrade soil was included in this analysis.

The tire pressure distributions for most computer runs were based on results from the model developed by Tielking; however, several runs were made using the uniform vertical pressure case. The primary differences that occurred as a result of using these two models are that the inflation pressure and contact pressure are equal for the uniform vertical case and that, when the Tielking model is used, the contact pressure distribution is nonuniform and not equal to the tire inflation pressure. Therefore the tire contact radius for these two pressure cases is different; the uniform pressure case is larger.

STUDY RESULTS

Several types of comparisons will be made using results from the ILLI-PAVE computer runs. These comparisons will include plots to show the effects of tire pressure on horizontal tensile strain at the bottom of the surface, the effects of base modulus on tensile strain, and the effects of both surface thickness and modulus on strains. An additional analysis is included to evaluate the effect of tensile strains on predicted fatigue damage through the use of a fatigue damage factor. Each analysis will be presented separately in the following sections.

Tire Pressure Effects

The series of computer runs used in this analysis is the same set described in the Study Parameters section. All runs for this analysis included a 4,500-lb load with nonuniform vertical pressure and with lateral surface shear forces. To describe the effects of tire pressure on tensile strain, Figures 5 and 6 have been prepared. Figure 5 shows the change in tensile strain for a surface of varying thickness and with a modulus of 400 ksi, and Figure 6 shows the same information for a surface with a modulus of 50 ksi.

The increase in tire pressures produces increases in the strain ranging from 20 to 30 percent for the 1-in. surface data in Figure 5 with the 30 percent increase occurring for the stiffest base layer. Notice that the effect of increased tire pressure decreases with increasing surface thickness and that the relative increase for a 4-in. surface is less than 10 percent.

Figure 6 shows that at 75-psi inflation pressure a surface 1 in. thick is in compression for the moderate and strong bases and that the tensile strain is low for the weak base. However, when the tire pressure increases to 125 psi, the 1-in. surface still remains in compression for the moderate and strong bases but the tensile strain increases dramatically for the weak base condition. For the low

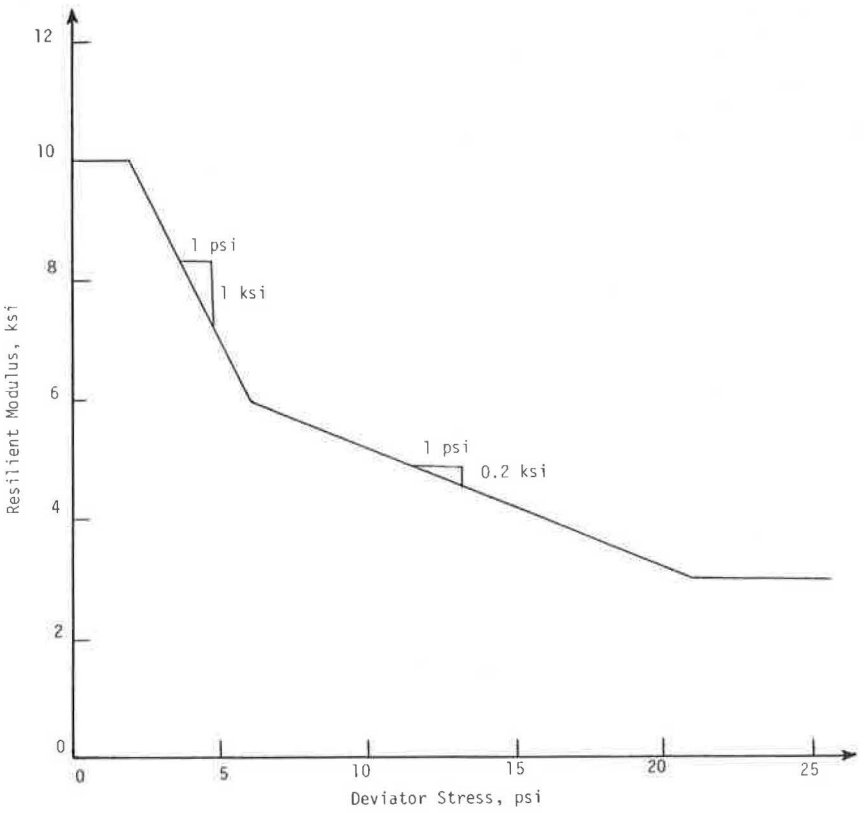

FIGURE 4 Resilient modulus-deviator stress relationship for subgrade soil.

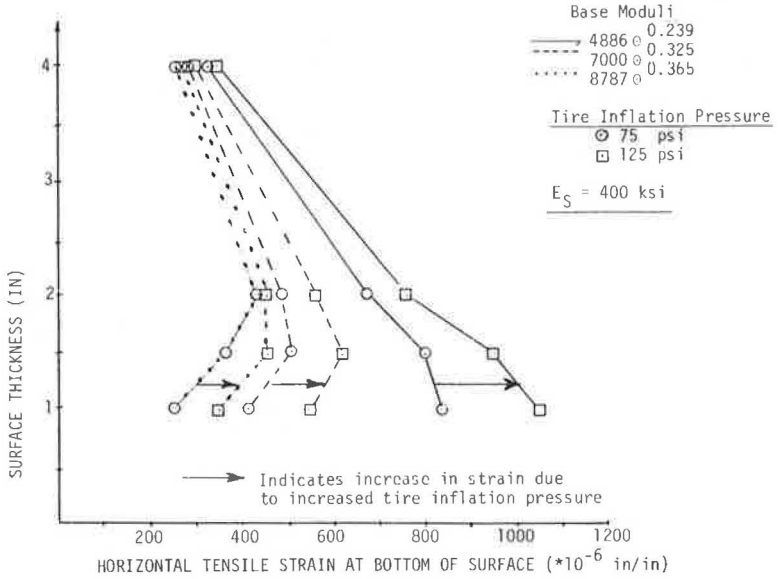

FIGURE 5 Effects of increased tire pressure on tensile strain for a surface modulus of 400 ksi.

modulus base all the thicknesses experience strains near or in excess of 0.001 in. per inch, which Monismith says is the upper limit of linear behavior of these materials: "For strains exceeding 0.001 in./in., asphalt concrete mixtures are nonlinear, rate dependent materials with different properties in tension and compression" (11).

The increases in strain for the 2-in. surface range from about 30 to 55 percent for the weak to strong bases, indicating the significance of the effect of increasing tire pressures on surfaces with low moduli. Therefore it is important to recognize that the general advice often given, to make thin pavements flexible, must be conditioned by adding that the surface thickness should be limited to less than 1.5 in. for moderate and strong bases. Extremely flexible asphalt concrete materials should probably not be used in combination with weak granular bases, especially because tire pressures have increased substantially during the last few years.

For thick flexible surfaces, the increase in tire pressure produces a smaller increase in tensile strain than for thinner surfaces, but the increase in strain for the more flexible surfaces, shown in Figure 6, is much larger than that experienced by the stiffer surfaces shown in Figure 5. In general, as the surface thickness increases, the surface modulus is more important in determining the strain level than the base modulus; however, as the surface thickness decreases, the effect of the base modulus becomes more significant.

Base Modulus Effects

The effects of base modulus are shown more clearly in Figures 7 and 8, which contain plots of strain

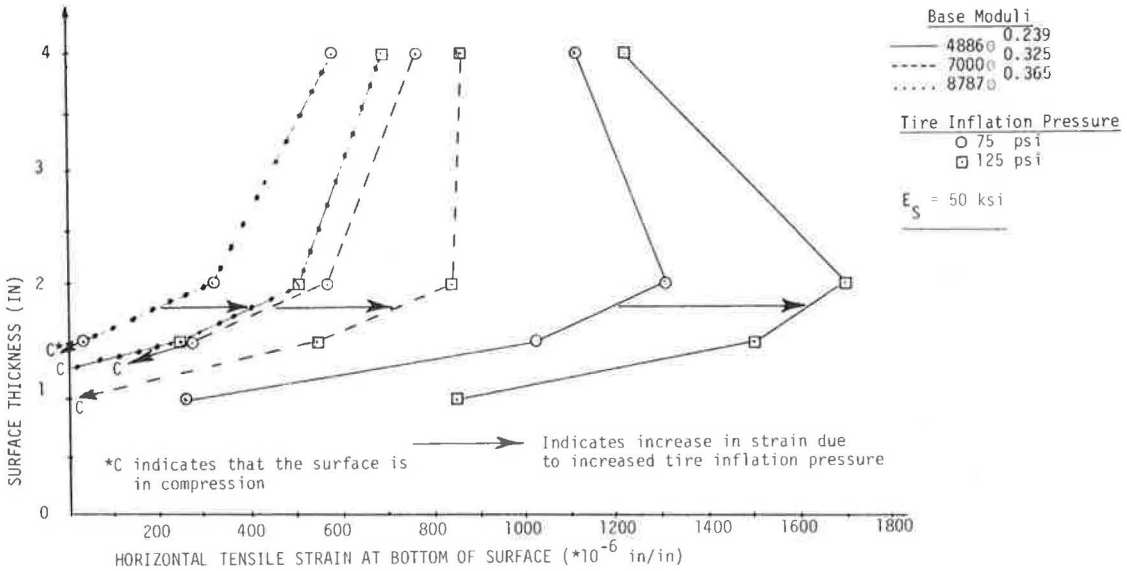

FIGURE 6 Effects of increased tire pressure on tensile strain for a surface modulus of 50 ksi.

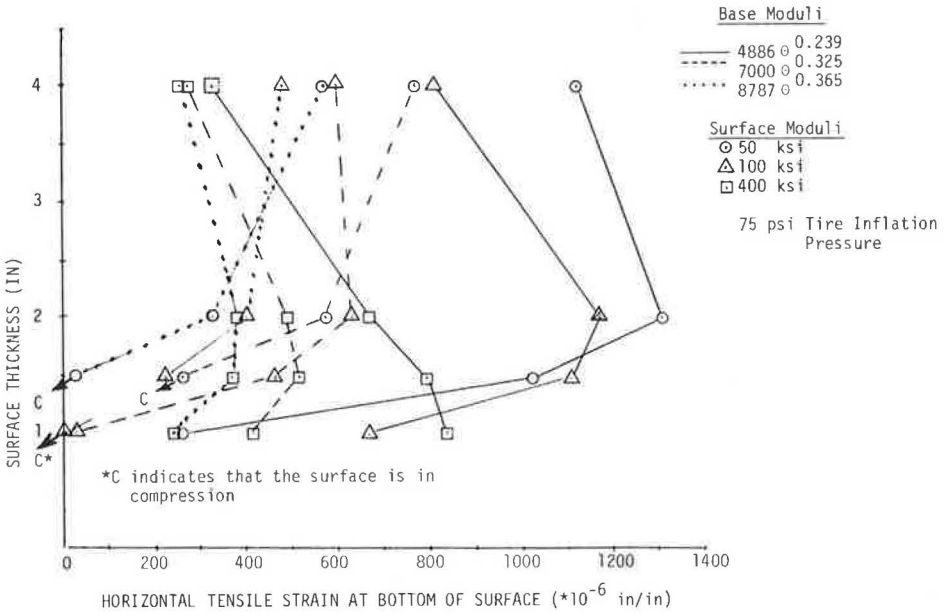

FIGURE 7 Effects of surface and base moduli on tensile strain at the bottom of the surface layer for surface moduli of 50, 100, and 400 ksi and a tire pressure of 75 psi.

for four different surface moduli for each of three different base moduli included in the study. In reviewing the plots of Figures 7 and 8, it is evident that for the stiff and moderate base moduli the 1-in.-thick 50- and 100-ksi modulus surfaces are either in compression or have tensile strains of less than 50 microinches per inch. At these strain levels those material combinations should perform quite adequately in the field. Even for the low base modulus and 50-ksi surface modulus the tensile strain in the 1-in. surface is low enough for quite satisfactory field service. It should be noted that as the tensile strain increases to levels of about 300 microinches per inch, the fatigue life can be expected to be reduced quite significantly.

The plots in Figure 8 show the interaction among base modulus, surface modulus, and surface thickness. For the 4-in. surface the strain is affected more by surface modulus than by base modulus: for the 400- and 800-ksi surfaces the strain values for the three base conditions are clustered together, but for the 50-ksi surface the strains for the different base moduli vary significantly but are still widely separated from the other two sets of surface modulus data. Note that at the 2-in. thickness the data for the three surface moduli began to overlap with the 50-ksi surface modulus covering almost the whole range of the 2-in. data whereas for the other surface moduli the different base stiffnesses begin to cause the strain levels to spread out and to overlap.

At the 1-in. thickness the effect of surface

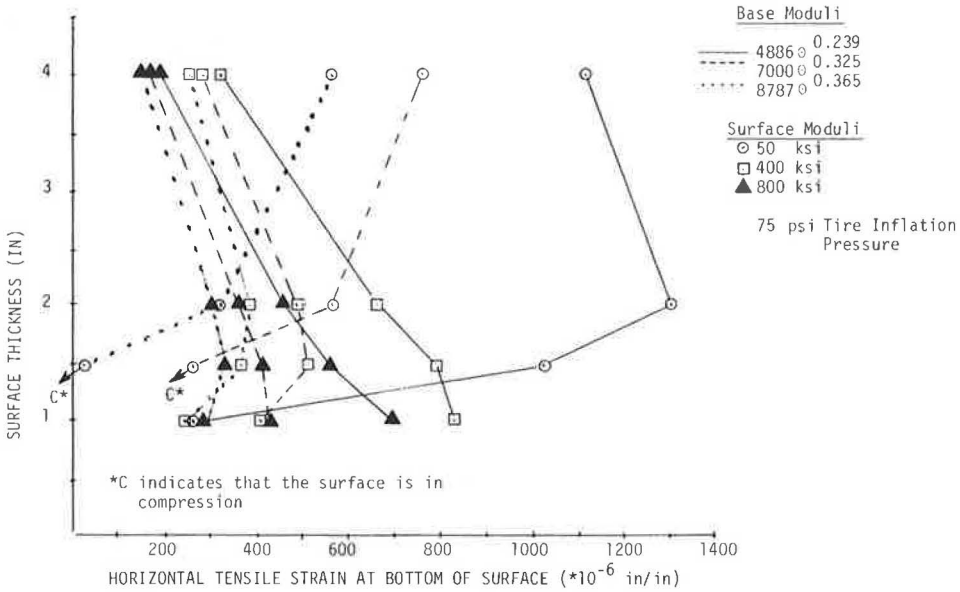

FIGURE 8 Effects of surface and base moduli on tensile strain at the bottom of the surface layer for 50, 400, and 800 ksi surface moduli and a tire pressure of 75 psi.

modulus is slight compared to the effect of the base modulus. Notice that in Figure 8 the points for the 400- and 800-ksi surfaces for each of the base moduli are nearly on top of each other for the high and moderate base moduli are quite close to each other for the low base moduli. At the 1-in. surface thickness the 50-ksi surface is either in compression or the strain level is at a quite acceptable level for adequate performance for low-volume roadways.

The data for 50-ksi and 100-ksi surface moduli in Figures 7 and 8 show that the base modulus effect is greatest for the 2-in. surface thickness. For the 400- and 800-ksi surface moduli the base modulus effect is greatest for the 1-in. surface thickness. For the range of surface thicknesses between 1 and 2 in., there is considerable overlap of the strain at the various combinations of surface and base moduli, and these data indicate the sensitivity of tensile strain to different combinations of thickness, surface modulus, and base modulus.

Surface Modulus and Thickness Effects

To evaluate the effects of surface modulus on strains for different base moduli and tire pressures, Figures 9-11 have been prepared. Each figure contains plots of tensile strain (microinches per inch) at the bottom of the surface for each combination of surface thickness and surface modulus. The plot on the top of each figure is the strain for a 75-psi inflation pressure, and on the bottom is strain for a 125-psi inflation pressure. The contour lines on each figure represent lines of equal strain.

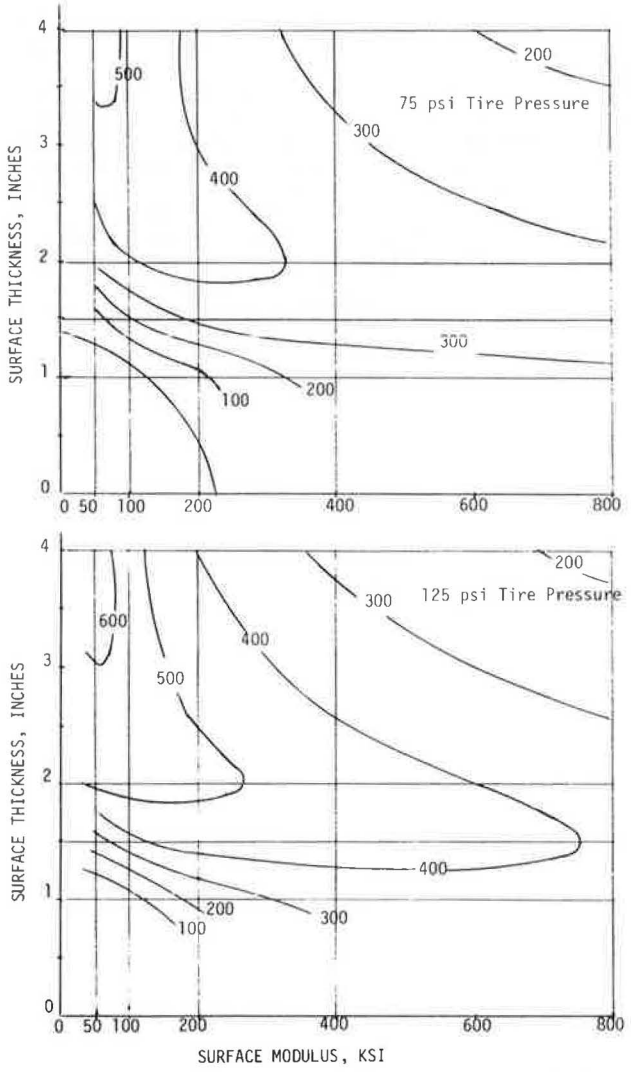

FIGURE 9 Tensile strain contours for $87870^{0.365}$ base modulus.

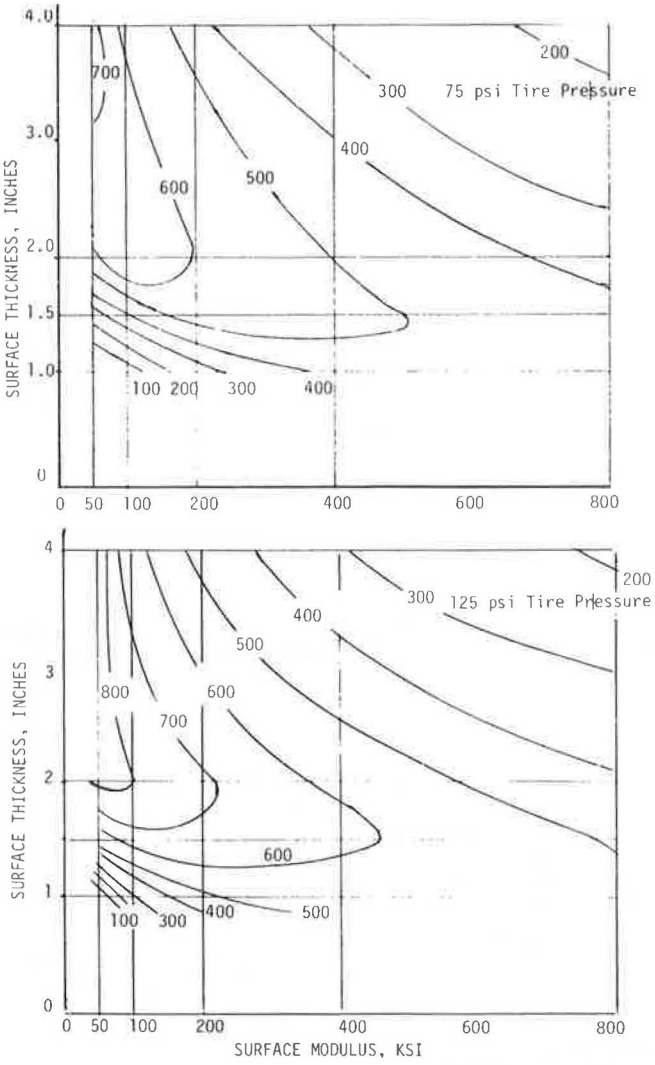

FIGURE 10 Tensile strain contours for $70000^{0.325}$ base modulus.

To resist fatigue damage, the tensile strains in the pavement structure must be kept fairly low, the exact level depending on the total traffic to be carried on the roadway and the characteristics of the surfacing layer. Because low strains are desirable, the first analysis of the plots in Figures 9-11 involved identifying the low strain areas. For purposes of discussion the authors have selected a strain level of 300 microinches per inch as a level below which reasonably adequate performance can be achieved and above which performance begins to be significantly impaired.

Strain levels below 300 occur in both the upper right and the lower left corners in Figures 9 and 10, but only in the upper right corner in Figure 11. Notice also that increasing tire pressure from 75 to 125 psi results in higher strain levels being wedged between the areas of low strain level thereby compressing and driving these low strain levels more toward opposite corners. Increased tire pressure for the weak base condition (Figure 11) resulted in there

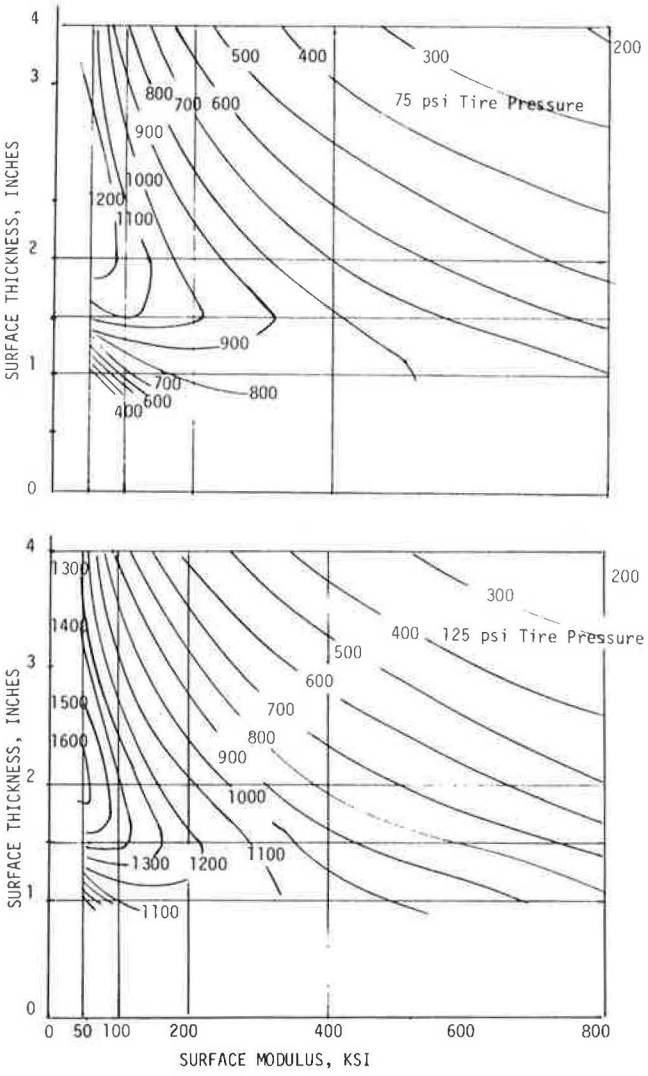

FIGURE 11 Tensile strain contours for $4886\theta^{0.239}$ base modulus.

being no strain level below 300 for the low-modulus surface combinations in the bottom left corner.

Review of the isostrain lines in Figures 9-11 led the authors to conclude that for thin asphalt concrete surfaces the surface moduli should be low and the base moduli for the flexible bases should be high. Only with this combination of materials can tensile strains be reduced to levels that will provide adequate fatigue resistance.

The strain levels for surface thickness of 1.5 to 2 in. are quite high except for the high base modulus combined with surface moduli of more than 300 ksi. At these strain levels reduced service life will occur but pavements with several years of life should result, depending on the traffic levels. For the moderate and weak bases, these high tire pressures produce strains too high to provide even marginal lengths of service life.

To provide a more definite indication of the effects of the interaction between tire pressure and surface thickness and moduli on fatigue cracking, an analysis was conducted to estimate the additional fatigue damage produced by the increase in tire pressure from 75 to 125 psi. To perform this analysis, a fatigue equation developed from AASHO Road Test results was selected (12). The equation was developed by using the observed number of weighted 18-kip equivalent single axle loads (ESALs) required to produce Class 2 fatigue cracking, and the calculated tensile strain at the bottom of the surface layer was developed using ELSYM5. A regression analysis produced the following equation (12):

$$W_{18} = 9.7255 \times 10^{-15} \ (1/\varepsilon)^{5.16267}$$

where

W_{18} = number of weighted 18-kip axle loads before Class 2 cracking and
ε = transverse strain calculated using ELSYM5 for 27 AASHO test sections;
R^2 = 0.9294.

To evaluate the additional damage produced by the increase in tire pressure from 75 to 125 psi, a fatigue damage factor was calculated. The fatigue damage factor is a ratio of the number of 18-kip ESALs that the pavement could sustain at the lower tire pressure divided by the number that could be carried at the higher tire pressure; that is,

$$FDF = (\varepsilon_{p2}/\varepsilon_{p1})^{5.16267}$$

where

FDF = fatigue damage factor,
ε_{p1} = strain at bottom of surface at tire pressure p1 = 75 psi, and
ε_{p2} = strain at bottom of surface at tire pressure p2 = 125 psi.

These fatigue damage factors have been plotted for each combination of surface modulus and thickness and for each base modulus in Figures 12-14. In studying these plots it must be remembered that these factors are relative and not absolute. For example, the fatigue damage factors for surface moduli of 400 and 800 psi in all three figures are quite similar. It could be erroneously concluded that to minimize the effect of increased tire pressure, stiffer pavement structures should be built. That this conclusion is erroneous can be confirmed by looking at Figures 10 and 11 that show that for 1- and 1.5-in.-thick surfaces, the tensile strains are greater than 500 microinches per inch, which is too high for adequate fatigue life.

These plots indicate the significance of the interaction between surface modulus and thickness and its effect on fatigue damage and indicate again that thinner pavements should be as flexible as possible in order to be in compression and thereby bypass the problem of fatigue cracking. Notice that the 1-in.-thick surface with 50- and 100-ksi moduli in Figure 12 is in compression. The data point out the relative sensitivity of thin, lower modulus surface materials to the effects of increased tire pressure and the relative insensitivity of thick, higher modulus materials to increased tire pressure.

CONCLUSIONS

On the basis of the limited results included in this paper, the following tentative conclusions can be drawn:

1. The granular base modulus significantly affects the tensile strains experienced by thin asphalt concrete pavements with the greatest effect at low thicknesses.
2. The surface modulus significantly affects the

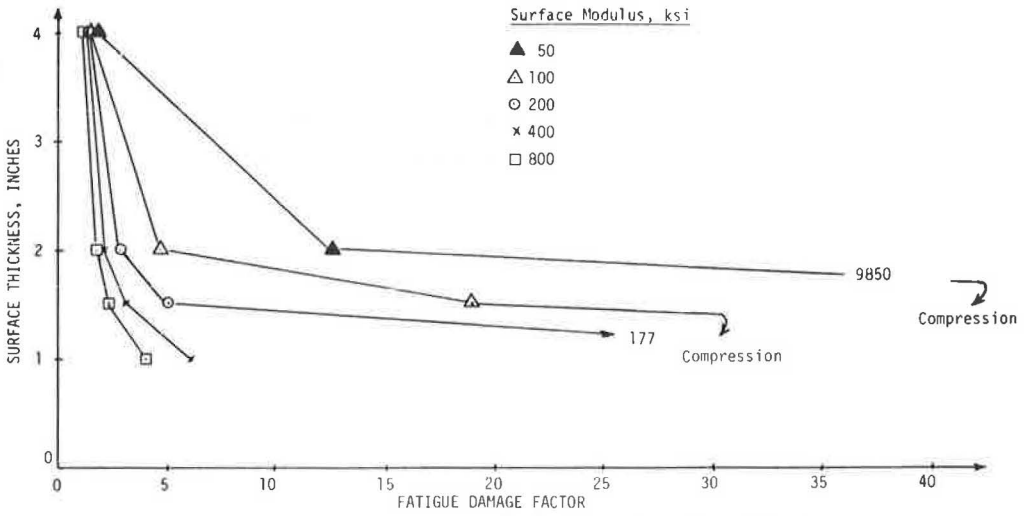

FIGURE 12 Fatigue damage factor due to increasing tire pressure from 75 to 125 psi $8787\theta^{0.365}$ base modulus.

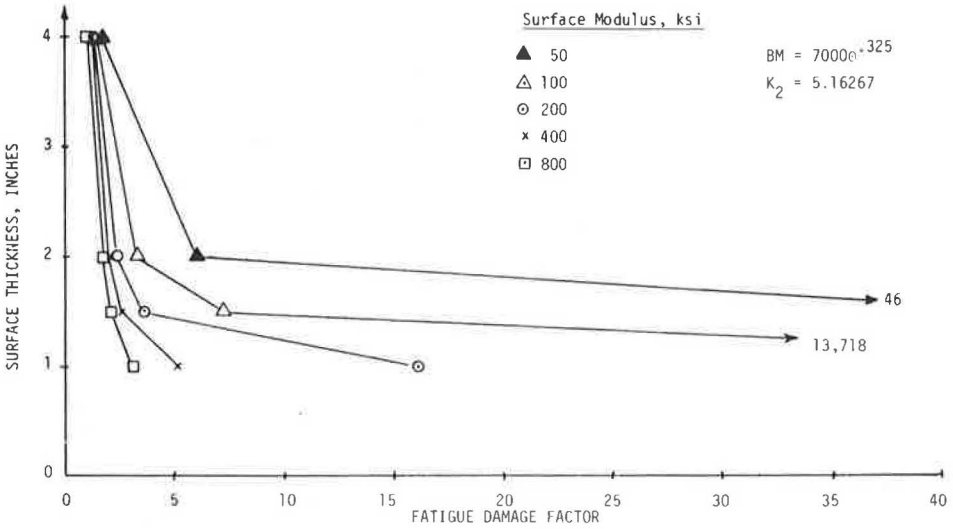

FIGURE 13 Fatigue damage factor due to increasing tire pressure from 75 to 125 psi for $7000\theta^{0.325}$ base modulus.

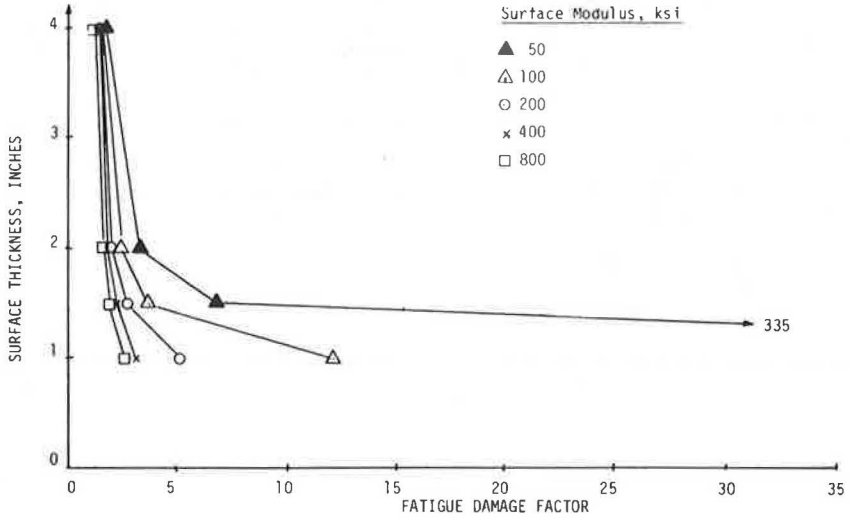

FIGURE 14 Fatigue damage factor due to increasing tire pressure from 75 to 125 psi for $4886\theta^{0.239}$ base modulus.

tensile strain at the bottom of the surface for thin asphalt layers. A low surface modulus over strong and moderate bases produced compression in the surface, but as the surface modulus increased so did tensile strains.

3. The effect of increased tire pressure on strain was so great for the weak base modulus that normal hot-mixed materials appear to be unsuitable. Only thick layers of extremely stiff surfacing produced low enough strains for satisfactory fatigue lives. The fatigue damage factors, calculated to show the relative effect of increasing tire pressure from 75 to 125 psi, show that the greatest relative effect occurs for low-modulus, thin surfaces.

4. The design of thin pavement structures must include careful consideration of the interactions of base modulus, surface thickness, and surface modulus and their effect on tensile strains. This is especially true if the predominant failure mode for these pavements is fatigue cracking.

ACKNOWLEDGMENTS

The research described in this paper was carried out at the Texas Transportation Institute at Texas A&M University. The authors are grateful for the support of the Texas State Department of Highways and Public Transportation and that of the Federal Highway Administration, U.S. Department of Transportation.

REFERENCES

1. R.A. Schapery and J.T. Tielking. Investigation of Tire-Pavement Interaction During Maneuvering: Theory and Results. Report FHWA-RD-78-72. FHWA, U.S. Department of Transportation, June 1977.
2. J.R. Tillerson and W.E. Haisler. SAMMSOR II--A Finite Element Program to Determine Stiffness and Mass Matrices of Shells of Revolution. TEES-RPT-70-18. Texas A&M University, College Station, Oct. 1970.
3. W.E. Haisler and J.A. Stricklin. SNASOR II--A Finite Element Program for the Static Nonlinear Analysis of Shells of Revolution. TEES-RPT-70-20. Texas A&M University, College Station, Oct. 1970.
4. J.T. Tielking and R.A. Schapery. A Method for Shell Contact Analysis. Computer Methods in Applied Mechanics and Engineering, Vol. 26, No. 2, May 1981, pp. 181-195.
5. J.T. Tielking and R.A. Schapery. Calculation of Tire-Pavement Shear Forces. ASME Symposium Proc., ASME Symposium on The General Problem of Rolling Contact, Vol. 40, 1980, pp. 19-39.
6. ILLI-PAVE--A Finite Element Program for the Analysis of Pavements. Construction Engineering Laboratory and the Transportation Facilities Group, Department of Civil Engineering, University of Illinois at Urbana, May 1982.
7. W.J. Harrison, L.J. Wardle, and C.M. Gerrard. CRANLAY and PLANE--Computer Programs for Circle and Strip Loads on Layered Anisotropic Media. Commonwealth Scientific and Industrial Research Organization, Canberra, Australia 1972.
8. E.L. Wilson. A Digital Computer Program for the Finite Element Analysis of Solids with Non-Linear Material Properties. University of California, Berkeley, 1965.
9. E.L. Wilson. A Digital Computer Program--A Finite Element Analysis of Axisymmetric Solids with Orthotropic, Nonlinear Material Properties. University of California, Berkeley, July 1967.
10. J.M. Duncan, C.L. Monismith, and E.L. Wilson. Finite Element Analysis of Pavements. In Highway Research Record 228, HRB, National Research Council, Washington, D.C., 1968, pp. 18-33.
11. C.L. Monismith. Fatigue Characteristics of Asphalt Paving Mixtures and Their Use in Pavement Design. Symposium on Fatigue in Asphalt Pavements, Albuquerque, University of New Mexico, Jan. 7, 1981.
12. Asphalt Concrete Overlays of Flexible Pavements, Vol. 1: Development of New Design Criteria. Report FHWA-RD-75-75. FHWA, U.S. Department of Transportation, June 1975.

Publication of this paper sponsored by Committee on Flexible Pavements.

Viscoelastoplastic Model for Predicting Performance of Asphaltic Mixtures

JACOB UZAN, ARIEH SIDES, and MORDECHAI PERL

ABSTRACT

A mechanistic model for predicting performance of asphalt mixtures in terms of crack propagation rate, fatigue life assessment, and permanent deformation characteristics is presented. The model is based on stress evaluation by the finite element method and on a comprehensive viscoelastoplastic material law. A critical octahedral shear strain is assumed to be the failure criterion. A computer simulation of the resilient and residual deflections of uncracked beams as well as a fatigue crack growth simulation of an initially cracked beam are performed. These results are then compared with laboratory tests performed at various load levels with varying periods of loading and unloading. The agreement between the predicted and the measured performance of the sand-asphalt mixture in terms of residual and resilient deflection, crack length versus number of load applications, and rest period effect on fatigue life is found to be quite good. The simulation is then applied to predict rutting parameters, fatigue life curves, and crack propagation rate versus stress intensity factor for the sand-asphalt mixture.

The rational structural design of flexible pavements is well established and has already reached the stage of calibration and verification. In the calibration phase it has been found that some aspects related to material characterization, such as the effects of the crack growth process and of the rest period on the fatigue life of bituminous mixtures, have been ignored. These effects are presently being accounted for during the design procedure by the use of correction factors that vary from 1 (where no correction is needed) to 700 (1-4). It appears that these correction factors are dependent on material and load as well as on environmental conditions and should therefore be determined specifically at each particular site.

Extensive laboratory and field studies of bituminous mixture fatigue performance clearly indicate that

- An increase of the rest period ratio prolongs fatigue life by a factor of up to 25 (5-8);
- The main part of fatigue life consists of the crack growth stage, which is considerably longer than the crack initiation phase (2-3);
- The crack grows according to Paris' law (9-12); and
- The testing program required for a complete fatigue performance characterization is prohibitively large and impractical.

From these results it is evident that a rational and more accurate prediction model for fatigue life of bituminous mixtures is required.

It is the purpose of this paper to present an improved mechanistic model for fatigue crack growth prediction incorporating the rest period effect. The model is based on a comprehensive material law accounting for the elastic, plastic, viscoelastic, and viscoplastic strain components (13-14). Because there are a limited number of different bituminous mixtures, this model can also be used statewide to optimize mix design.

Following the material characterization testing program and the results, the proposed mechanistic model for fatigue crack growth prediction is presented. Then numerical results and experimental verification for fatigue crack growth in sand-asphalt are given including an analysis of the rest period ratio effect.

MATERIAL CHARACTERIZATION

In the present study it is crucial to decompose the material's response to loading into time-dependent and time-independent strain components as well as into recoverable and irrecoverable ones. The repetitive creep test is found to be most appropriate to comply with this required resolution. Uniaxial compressive and tensile repetitive creep tests are therefore to be conducted at 25°C, using a sand-asphalt mixture. Details of the mixture properties, the experimental procedure, and the results of the compression tests are presented elsewhere (13). Recently these experiments were supplemented by a series of tension tests to account for the different responses of the mixture to tensile and compressive loading. These results are published elsewhere (14).

The total strain (ϵ_t) is thus resolved into its four components (Figure 1):

$$\epsilon_t = \epsilon_e + \epsilon_p + \epsilon_{ve} + \epsilon_{vp} \quad (1)$$

where

- ϵ_e = elastic strain--recoverable and time independent,
- ϵ_p = plastic strain--irrecoverable and time independent,
- ϵ_{ve} = viscoelastic strain--recoverable and time dependent, and
- ϵ_{vp} = viscoplastic strain--irrecoverable and time dependent.

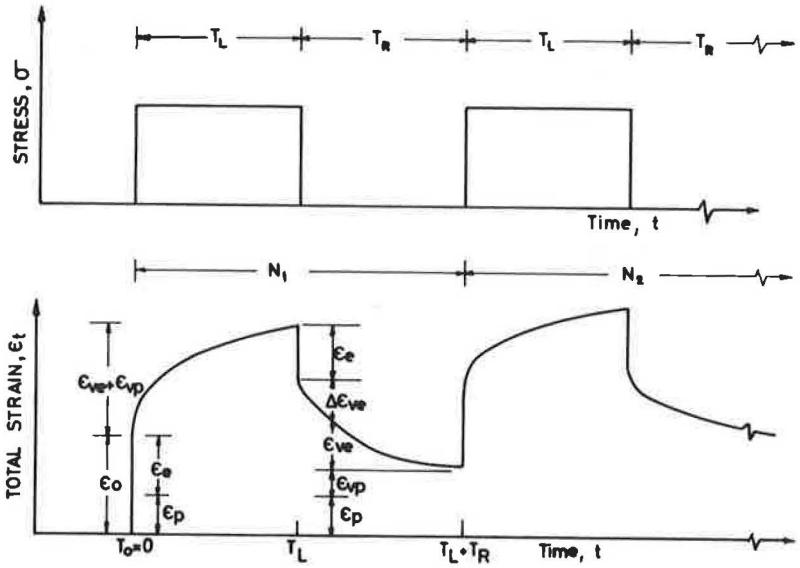

FIGURE 1 Schematic representation of the various strain components.

Each strain component is expressed as a function of the stress level, loading time, and number of repetitions as follows:

$$\epsilon_e = \sigma/E \tag{2}$$

$$\epsilon_p = (\sigma/H)\, N^a \tag{3}$$

$$\epsilon_{ve} = (a_1 \sigma + a_2 \sigma^2) t^{\alpha} \tag{4}$$

$$\epsilon_{vp} = (b_1 \sigma + b_2 \sigma^2) T_L{}^{\beta} N^b \tag{5}$$

where

σ = applied stress (MPa);
E = elastic modulus (MPa);
H = plastic modulus (MPa);
N = number of load repetitions;
t = time elapsing from the beginning of the test (sec);
T_L = loading time during each cycle (sec); and
$a, a_1, a_2, \alpha, b, b_1, b_2, \beta$ = material constants.

The experimentally evaluated values for the various parameters in Equations 2-5 are given in Table 1.

In the uniaxial creep repetitive tensile tests it was found that the total strain at failure is in the range of 0.8 to 2.2 percent for a stress level of 0.05 to 0.1 MPa. Similar results, 0.4 to 0.8 and 1.0 to 2.5 percent, are reported by Monismith et al. (15) and Tons and Krokosky (16) for constant strain rate and creep tests of asphalt concrete at 25°C (77°F). For the case of high asphalt content and low strain rate corresponding to the present testing conditions, it appears that the uniaxial tensile strain of failure is 0.8 to 2.5 percent. Because it is intended to apply these values to multiaxial loading, the failure strain is replaced by the critical octahedral shear strain corresponding values of which are 1.1 to 3.3 percent (for a Poisson's ratio of 0.4). To overcome the range of critical strain experimentally measured, a parametric study of sensitivity will be conducted.

TABLE 1 Material Constants of the Strain Components

	Unit	Compression	Tension
E	MPa	613	590
H	MPa	278.5	∞
a		0.35	
a_1	MPa^{-1}	8.9×10^{-4}	9.4×10^{-4}
a_2	MPa^{-2}	-5.0×10^{-4}	0
α	0	0.29	0.58
b		0.19	0.62
b_1	MPa^{-1}	1.9×10^{-3}	5.9×10^{-4}
b_2	MPa^{-2}	-8.4×10^{-4}	0
β		0.22	0.27

FATIGUE CREEP CRACK GROWTH SIMULATION

A mechanistic model is developed for the simulation of fatigue creep crack growth. Further on the simulation is applied to the three-point bend specimen (i.e., a simple supported beam loaded by a time-varying uniformly distributed load applied at its midspan). By superposing loading and unloading periods of different durations, the repetitive character of the cyclic loading is reproduced and various rest period ratios are possible.

To make the simulation feasible the model was simplified on the basis of the following assumptions:

1. The stress distribution in the specimen is evaluated for a homogeneous, isotropic, linear elastic material by the finite element method.
2. Equivalent loading and unloading moduli of deformation are evaluated using the constitutive law determined for the uniaxial compressive and tensile repetitive creep test and on a strain energy consideration.
3. Strains are evaluated using stresses and the equivalent loading or unloading moduli of deformation.
4. The crack is assumed to grow upward when the octahedral shear strain in the vicinity of the crack tip reaches its critical value.
5. The crack is extended by applying the unzipping procedure, with an increment that equals one mesh size of the finite element grid.

6. As the crack grows, the stress field ahead of the crack tip changes.

The equivalent number of cycles corresponding to the new state of stress field is evaluated using a time-hardening scheme (17).

It should be noted that assumptions 1 to 3 do not strictly comply with the compatibility conditions of continuum and thus neglect the stress redistribution occurring in the beam. Experimental verification of the adequacy of these assumptions and approximations will be presented in the next section. The failure criterion is discussed separately.

The fatigue creep crack growth simulation is incrementally performed. Each step is associated with a specific crack size. Initially the beam is assumed to have a small crack on its centerline, emanating from its lower side, which is in tension. Furthermore, the beam is stress and strain free. During subsequent steps, as the crack extends, the accumulated strains and the number of cycles of each step serve as initial conditions for the next one.

The simulation pursues the following algorithm for the first step: for a given initial crack length the stress distribution in the three-point bend specimen is determined via the NONSAP finite element code (18). (For details on the geometry of the specimen and the finite element breakdown see Figure 2). The stress along the centerline of the beam ahead of the crack tip is evaluated at the nodal points and is then averaged for each two adjacent elements to provide a unique distribution of stress on the crack line. Equivalent loading and unloading moduli of deformation representing the beam are computed using the following equation, which is based on equal strain energy considerations:

$$1/\bar{E} = \left\{ \sum_{i=1}^{n} (1/E_i) \left[\sigma_{xx}^{(i)2} + \sigma_{yy}^{(i)2} - 2\mu\sigma_{xx}^{(i)} \sigma_{yy}^{(i)} \right] \right\} \div \left\{ \sum_{i=1}^{n} \left[\sigma_{xx}^{(i)2} + \sigma_{yy}^{(i)2} - 2\mu\sigma_{xx}^{(i)} \sigma_{yy}^{(i)} \right] \right\} \quad (6)$$

where

$\bar{E}$ = equivalent loading or unloading modulus of deformation,
$\sigma_{xx}^{(i)}$, $\sigma_{yy}^{(i)}$ = stress components (i denotes nodal point number), and
E_i = modulus of deformation at ith nodal point evaluated by Equations 1-5.

Using the equivalent modulus and stress field the incremental octahedral shear strain caused during the nth loading cycle is evaluated at all nodal points and is added to the previously accumulated octahedral shear strain. The total octahedral shear strain near the crack tip is compared with its assumed critical value. If the critical value is not reached, unloading is performed and the incremental resilient octahedral shear strain is determined and subtracted from the previously accumulated strain. Cyclic loading and unloading are repeated for the same crack length and stress distribution until the total octahedral shear strain ahead of the tip reaches its critical value. When this occurs the crack is extended by one mesh size (one element length) and stresses are reevaluated for the new geometric configuration. The accumulated number of load repetitions at all nodal points ahead of the crack tip is replaced by an equivalent initial number of repetitions that corresponds to the accumulated octahedral shear strain, the new state of stress, and the new crack length. This updating procedure is based on a time-hardening scheme and is independently performed for the plastic and viscoplastic strain components. The crack extension procedure described herein is then repeated until unstable crack length occurs.

For each crack length, the mode I stress intensity factor (K_I) is evaluated from the finite element solution via the vertical displacement of the quarter point of the singular isoparametric element (19,20, see Figure 2). The stress intensity factor is used in the analysis.

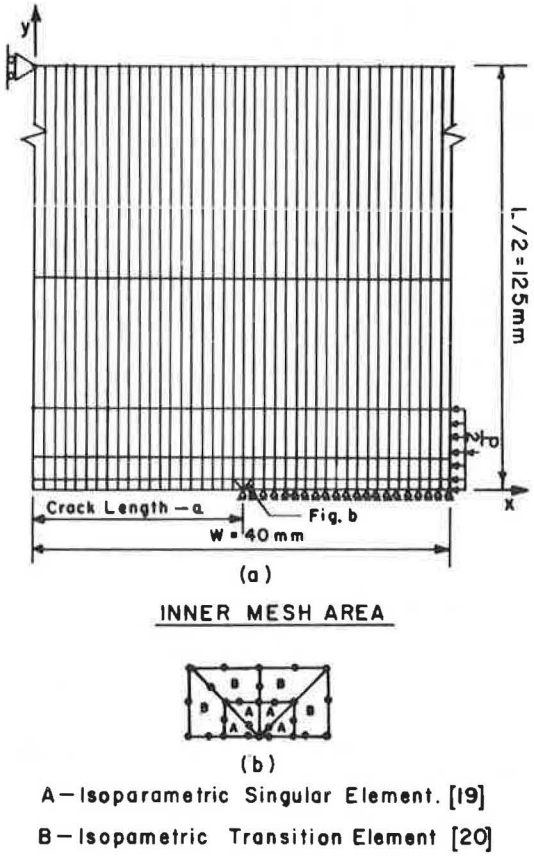

FIGURE 2 Geometry of the specimen and finite element breakdown.

Crack Growth Criterion

In the unzipping procedure, the crack is advanced by one mesh size increments. It is obvious that the results of the analysis are dependent on the mesh size and the distance from the crack tip at which the strain is calculated.

Sensitivity analyses show that when the strain is calculated at one-eighth of the mesh size ahead of the crack tip, the numerical results of load repetition are almost independent of the mesh size. Therefore, as a numerical stability consideration, the point located one-eighth mesh size from the crack tip is adopted in the simulation process.

The crack is extended as the mean octahedral shear strain within the element ahead of the crack tip reaches its critical value. Because the analysis is performed employing the one-eighth point, the fracture can be expressed as

$$\gamma_{oct}^{1/8} \geq 2^{1/2} \cdot \gamma_{oct}^{cr} \quad (7)$$

where

$\gamma_{oct}^{1/8}$ = octahedral shear strain at the one-eighth point and
γ_{oct}^{cr} = octahedral shear strain at failure.

EXPERIMENTAL VERIFICATION

A testing program was designed to provide verification of the various assumptions and approximations made throughout the simulation process. It includes repetitive creep tests in bending of uncracked beams and fatigue tests on initially cracked ones. The

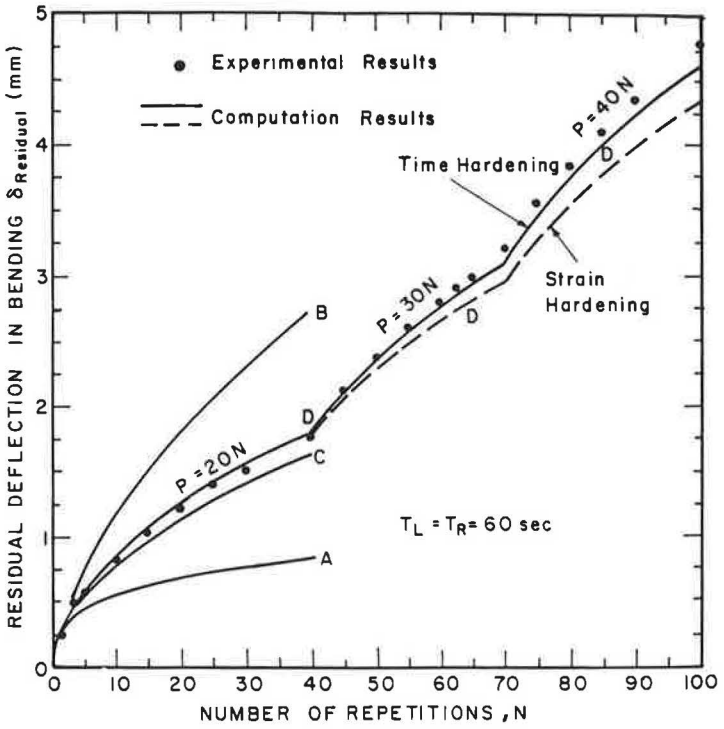

FIGURE 3 Experimental and computed residual deflection at varying cyclic loading ($T_L = T_R = 60$ sec).

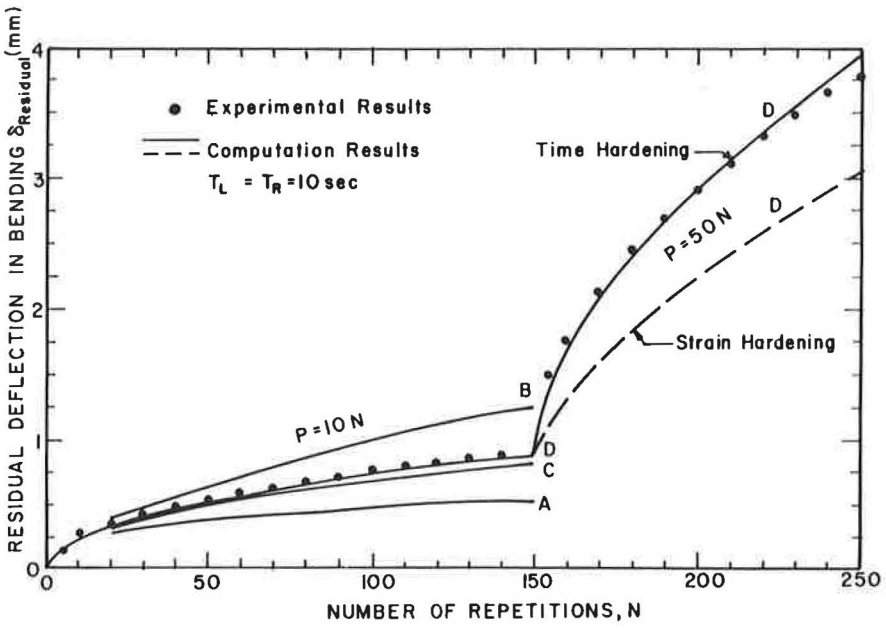

FIGURE 4 Experimental and computed residual deflection at varying cyclic loading ($T_L = T_R = 10$ sec).

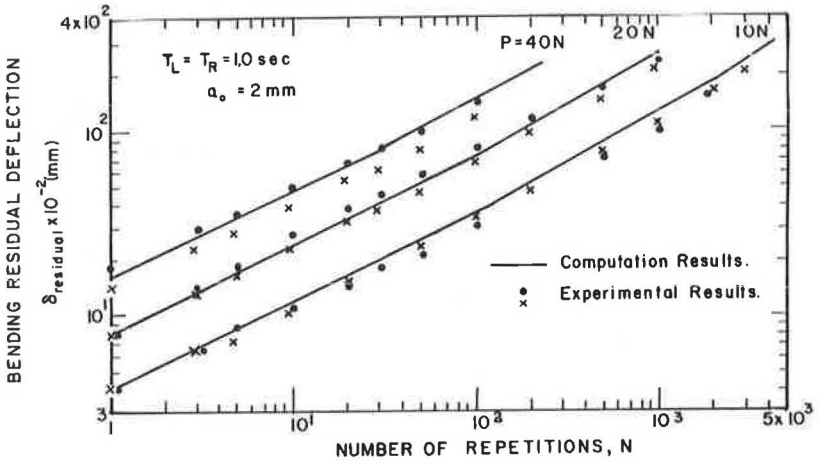

FIGURE 5 Experimental and computed residual deflection for initially cracked beam ($T_L = T_R = 1.0$ sec).

residual and the resilient deflections as well as crack lengths for various load levels, loading and unloading durations (T_L and T_R, respectively), and initial crack lengths were recorded as a function of load cycle number. Some results are presented hereafter.

Residual Deflection of Uncracked Beams

The residual deflection of uncracked beams subjected to a varying cyclic loading is shown in Figures 3 and 4. The results obtained when applying the first load level serve to develop a procedure for determining the equivalent loading and unloading moduli.

The residual deflection at the beam midspan after N loading cycles $[\delta^{(N)}_{residual}]$ is computed using the following equation (21):

$$\delta^{(N)}_{residual} = \sum_{i=1}^{N} \Delta\delta_i = \sum_{i=1}^{N} \delta_o \left[(E_o/\bar{E}^{(N)}_{\ell o}) - (E_o/\bar{E}^{(N)}_{un\ell o})\right] \quad (8)$$

where

δ_o = deflection corresponding to the finite element analysis;
E_o = modulus of deformation corresponding to finite element solution; and
$\bar{E}^{(N)}_{\ell o}$, $\bar{E}^{(N)}_{un\ell o}$ = equivalent loading and unloading moduli of deformation, respectively.

The loading and unloading moduli necessary for the numerical evaluation of the residual deflection are calculated by four different methods: (a) compressive material constants (Curve A); (b) tensile material constants (Curve B); (c) bilinear material equation (22, Curve C):

$$\bar{E} = (4 \cdot E_{com} \cdot E_{ten})/(E_{com}^{1/2} + E_{ten}^{1/2})^2 \quad (9)$$

where E_{com} and E_{ten} are the compression and tension moduli of deformation, respectively, for loading or unloading; and (d) from strain energy considerations (Curve D) as expressed in Equation 6. The method of equal strain energy is found to be adequate and is therefore adopted in the simulation process.

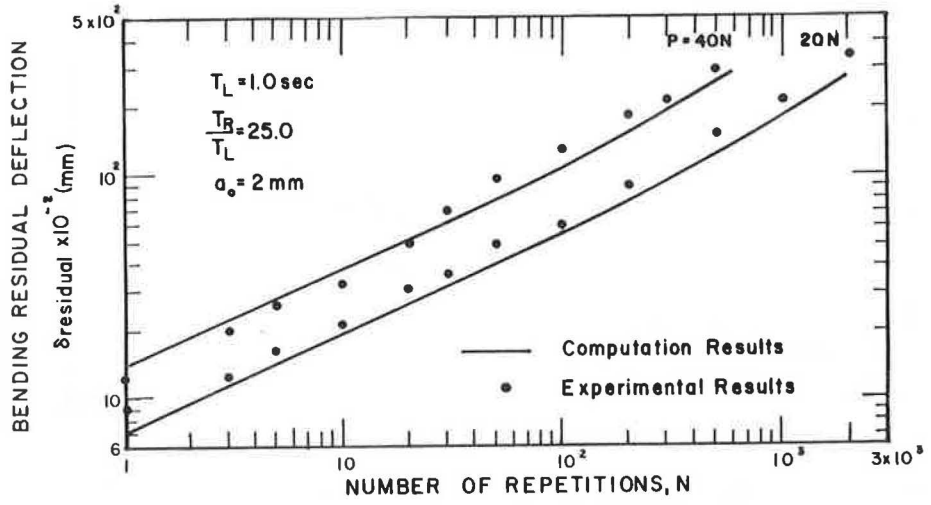

FIGURE 6 Experimental and computed residual deflection for initially cracked beam ($T_R/T_L = 25.0$).

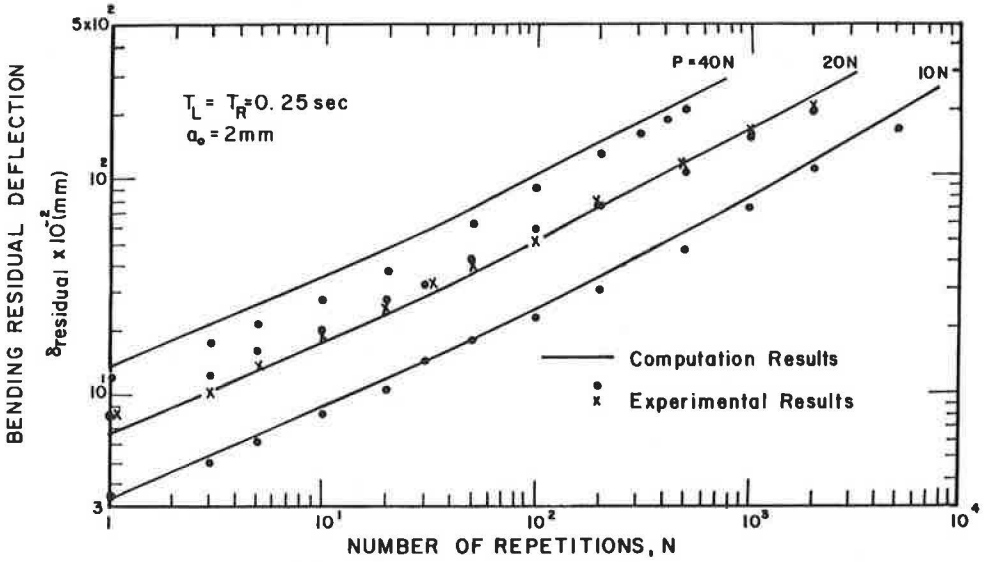

FIGURE 7 Experimental and computed residual deflection for initially cracked beam ($T_L = T_R = 0.25$ sec).

The subsequent load levels are used to determine which superposition method should be used in the case of increasing load. In Figures 3 and 4 the residual deflection evaluated by both time- and strain-hardening procedures is presented with the experimental results. It can be seen that time hardening is more adequate and fits the experimental results quite well. It should be mentioned that similar results were reported by Monismith (17).

Residual Deflection of Cracked Beams

Fatigue test results for cracked beams in bending are shown in Figures 5-7. These results correspond to an initially cracked beam subjected to different load levels with various loading and unloading periods. The residual deflections were computed using Equations 6 and 8. It can be seen that the simulation prediction is good and is thus applicable to the loading-to-unloading ratio effect on the pavement.

Crack Length Versus Number of Cycles

Crack length versus the number of load repetitions for various initial crack lengths, load levels, and T_R and T_L are shown in Figures 8-13. For each particular case three predicted curves are shown corre-

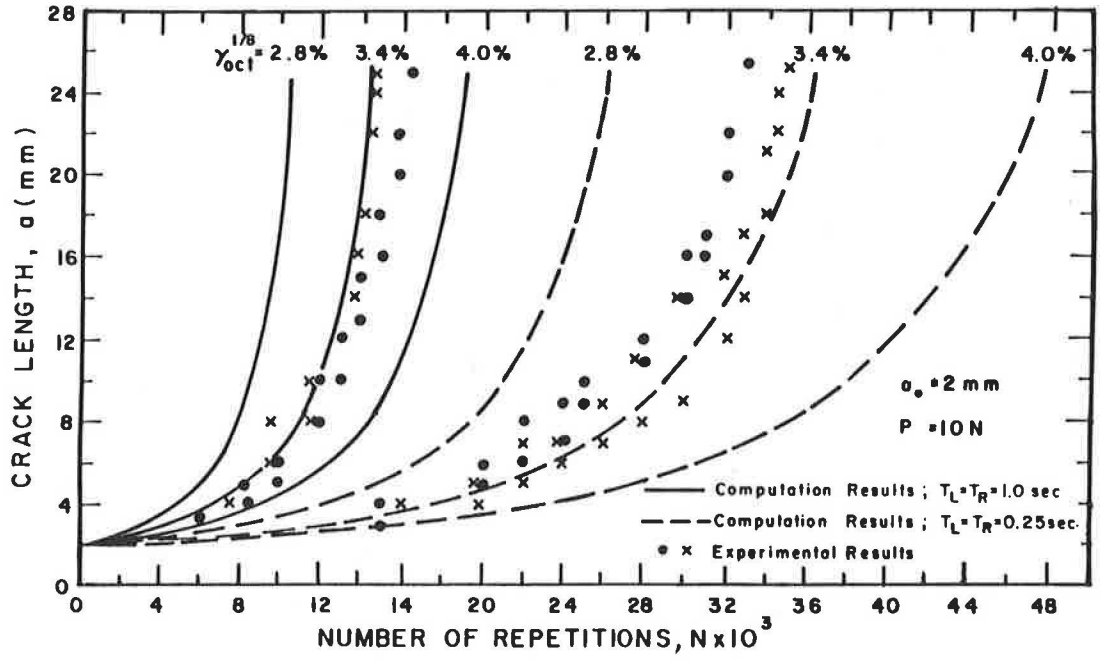

FIGURE 8 Experimental and predicted a–N curve for P = 10 N.

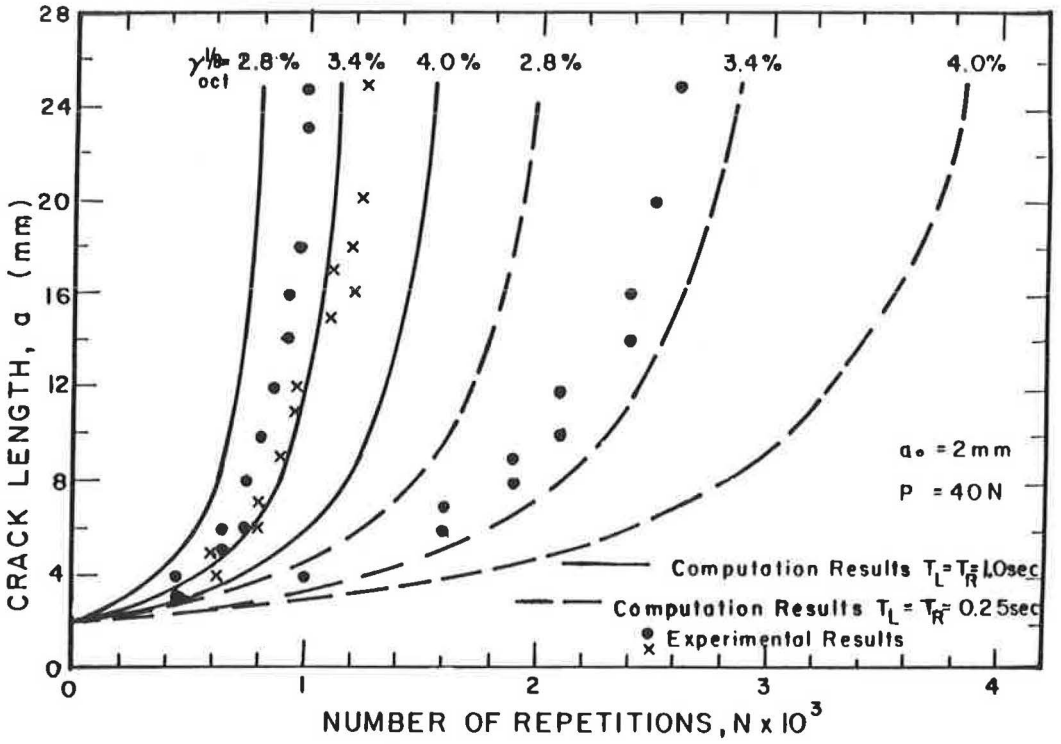

FIGURE 9 Experimental and predicted a–N curve for P = 40 N.

sponding to $\gamma_{oct}^{1/8}$ = 2.8, 3.4, and 4.0 percent critical octahedral shear strain. It appears that the predicted results are in better agreement with the experimental data for a critical octahedral shear strain of 3.4 percent. It is worth mentioning that this value corresponds to the upper limit of the uniaxial tension test results reported previously.

Table 2 gives the predicted and experimental fatigue life (N_T and N_p, respectively) and their ratio. The ratio N_p/N_T is found to be in the range of 0.81 to 1.20 for all cases.

These results, although not yet fully verified, support the validity of this simulation procedure, which therefore might be used for permanent deforma-

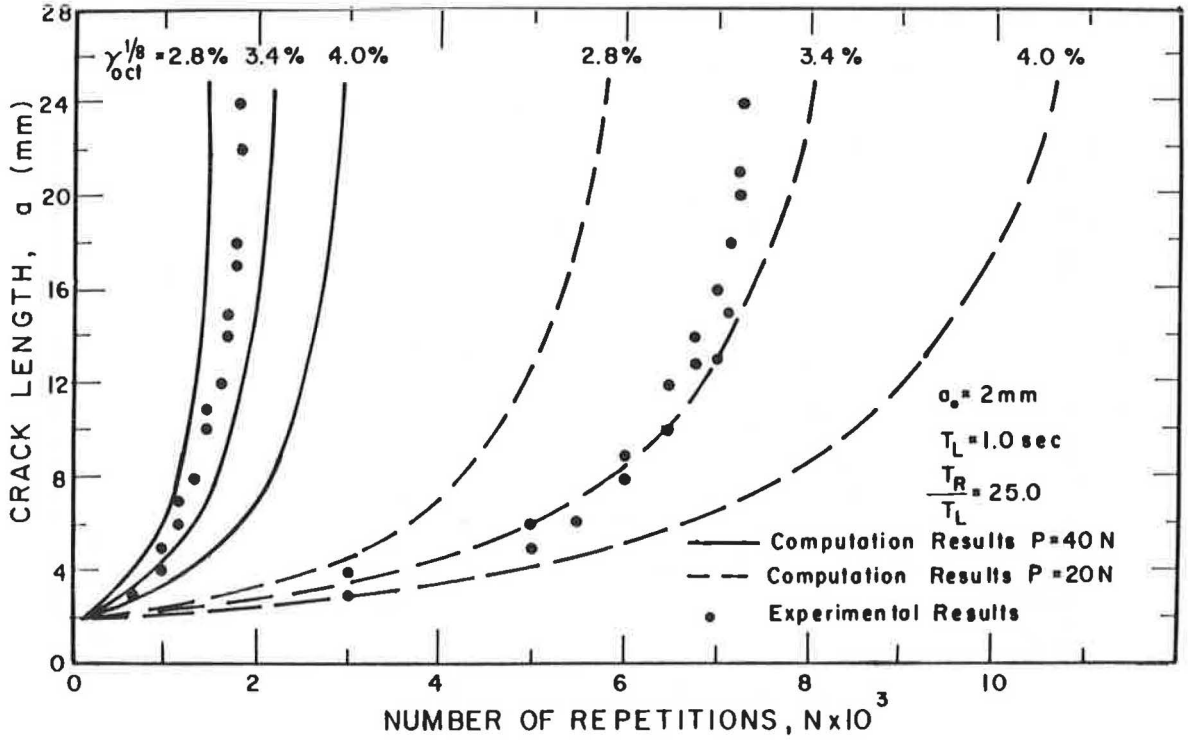

FIGURE 10 Experimental and predicted a–N curve for T_R/T_L = 25.0.

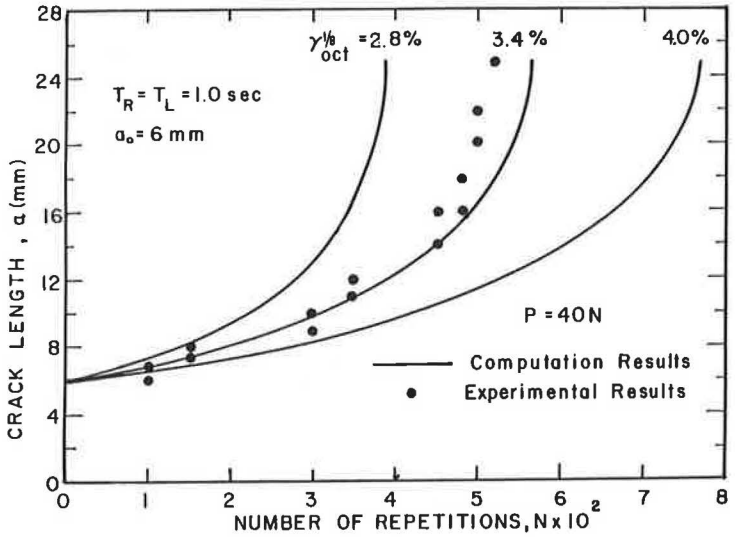

FIGURE 11 Experimental and predicted a–N curve for a_o = 6 mm.

tion characterization and for fatigue life assessment of the sand-asphalt mixture.

PERMANENT DEFORMATION OF SAND-ASPHALT MIXTURES

In permanent deformation analyses of pavements the relevant parameters commonly used are α and μ that describe the residual strain versus the number of load repetitions (23–26). The test results (see Figure 3) as well as the ones predicted (by Equations 1-6) given in Table 3 indicate that the value of these parameters depends on the loading mode: compression, tension, or bending. The values for the bending mode case are as expected; they are situated between those obtained in compression and those obtained in tension. This conclusion points out that the compressive creep test may be inadequate for describing the permanent deformation characteristics of asphaltic materials.

FATIGUE LIFE PREDICTION

In the previous section it was shown that the model predicts fatigue creep crack growth quite well (Figures 8-13 and Table 2). In this section the fatigue life prediction will be expressed in engineering terms: bending tensile strain versus number of load repetitions to failure, the effect of the rest period, and Paris' law.

ε-N Curve

Two predicted ε-N curves simulated for two different loading periods together with experimental results from Monismith et al. (27) and Pell and Cooper (28) are shown in Figure 14. The predicted values are in good agreement with those of Monismith et al. for similar mixture stiffness.

Pell's and Cooper's results are well below the predicted ones. However, Pell's and Cooper's results were found by Witczak (29) to be on the conservative side compared to most results reported in the literature. Thus it may be concluded that the prediction is quite good.

Effect of Rest Period

The beneficial effect of the rest period between consecutive loading phases is well established

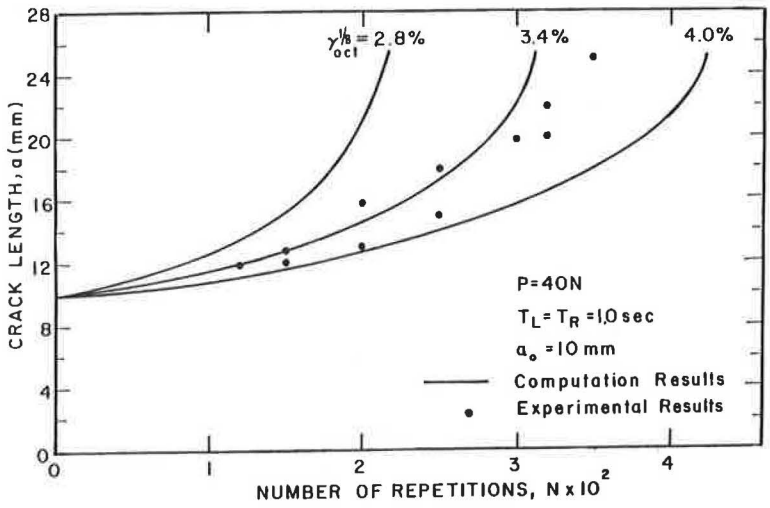

FIGURE 12 Experimental and predicted a–N curve for a_o = 10 mm.

TABLE 2 Predicted and Experimental Crack Growth Repetitions

Loading Period T_L (sec)	T_R/T_L	Initial Crack Length a_o (mm)	Load Level P (N)	Predicted Fatigue Life N_p	Experimental Fatigue Life N_T	N_p/N_T
			10	14,654	14,522-16,493	0.89-1.01
1.0	1.0	2.0	20	4,240	4,482-5,170	0.82-0.95
			40	1,154	1,007-1,260	0.92-1.15
1.0	5.0	2.0	20	5,894	5,550	1.07
			40	1,590	1,329	1.20
			20	8,067	7,400	1.09
1.0	25.0	2.0	40	2,168	1,847	1.17
			10	36,397	33,080-35,211	1.03-1.10
0.25	1.0	2.0	20	10,533	9,879-11,166	0.94-1.07
			40	2,863	2,601	1.10
			20	14,544	14,629	0.99
0.25	8.0	2.0	40	3,945	4,895	0.81
		6.0		574	511	1.12
1.0	1.0	10.0	40	315	351	0.90
		14.0		166	138	1.20

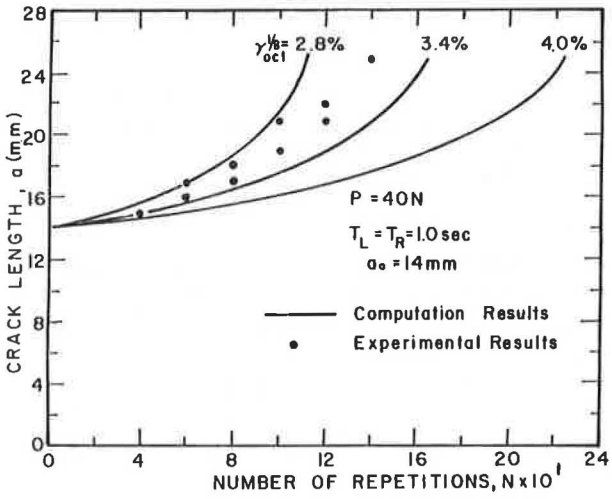

FIGURE 13 Experimental and predicted a-N curve for a_o = 14 mm.

(5-8). From Figures 9 and 10 and Table 2 it can be found that for a rest period ratio of 25 (T_R/T_L = 25) and a load of 40 N, fatigue life is increased by a factor of 1.47 to 1.83 with respect to the experimental results and by a factor of 1.9 with respect to the predicted one. Furthermore, the results in Table 2 indicate that the effect of the rest period depends on the loading duration.

TABLE 3 Test and Computed Results of the α and μ Parameters

	Compression	Tension	Bending
Test Results, $T_L = T_R$ = 60 sec			
α	0.67	0.38	0.49
μ	0.72	0.43	0.60
Computed Results, $T_L = T_R$ = 0.1 sec			
α	0.67	0.38	0.59
μ	0.63	0.15	0.45

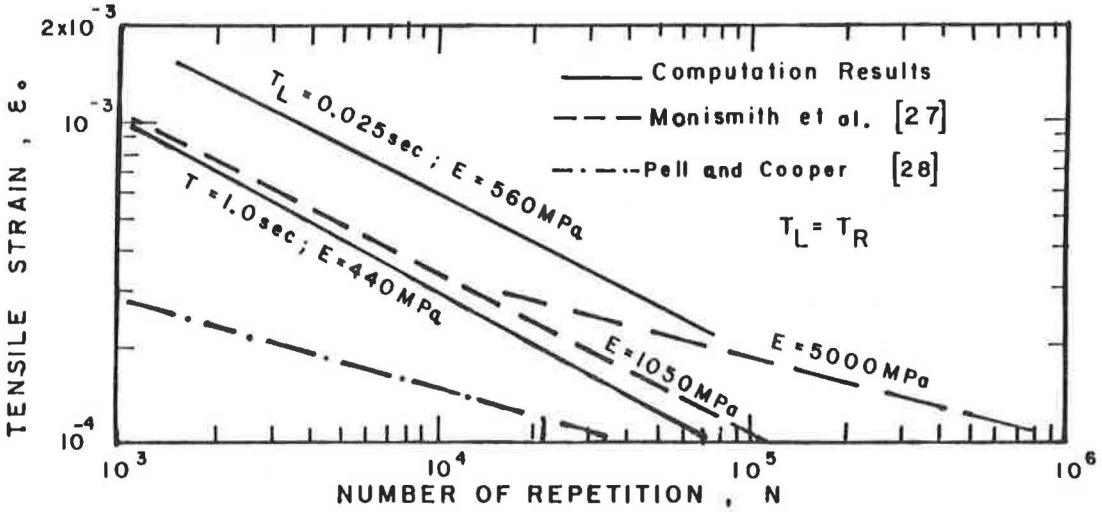

FIGURE 14 Predicted tensile strain versus number of load repetitions.

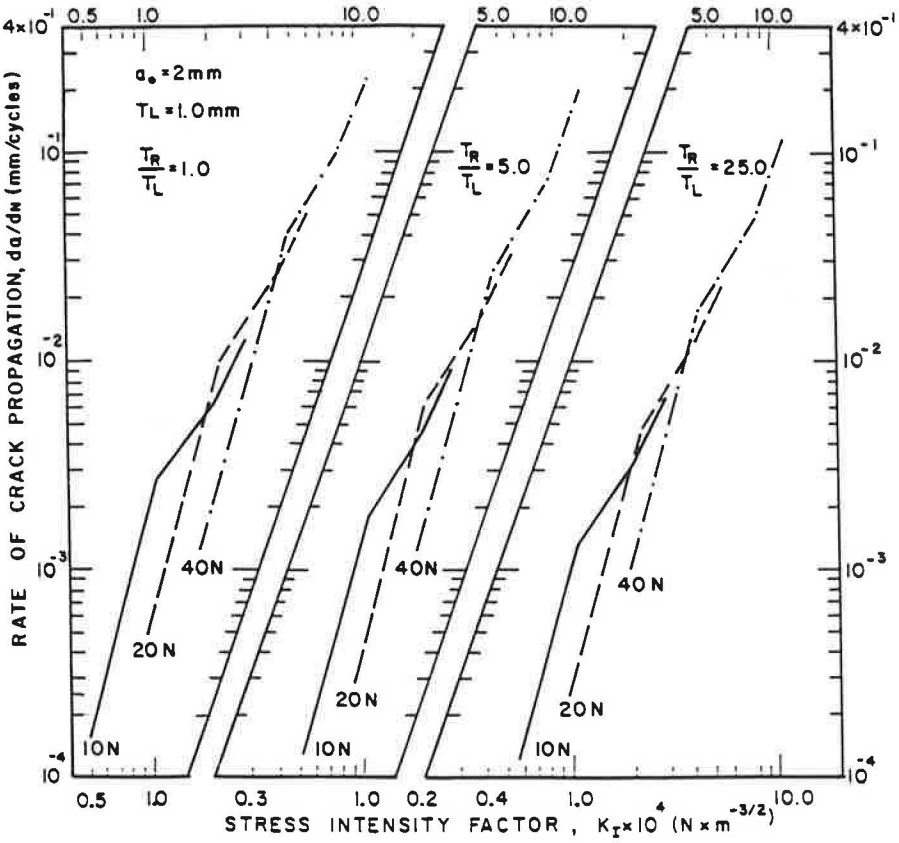

FIGURE 15 Predicted da/dN versus K_I for various T_R/T_L.

Paris' Law

Fatigue life prediction as well as crack repetition in asphaltic material have recently been dealt with using the fracture mechanics theory approach and in particular Paris' law (9-12), that is,

$$da/dN = A K_I^n \quad (10)$$

where

a = crack length,
N = number of load applications,
K_I = mode I stress intensity factor, and
A,n = material constants.

The stress intensity factor as previously mentioned is evaluated from the finite element analysis. The crack propagation rate (da/dN) can be calculated both from the experimental results and from the simulated a-N curve. Predicted relations between the crack propagation rate and the stress intensity factor are shown in Figures 15 and 16. From these figures it can be seen that

1. The relation between da/dN and K_I is load dependent to a certain extent. A similar dependence is noted in the test results of Majidzadeh et al. (9,12).
2. The curve consists of three distinguishable segments for a small initial crack case, which tend to become one line as initial crack length increases.
3. The crack growth rate depends on the initial crack length (see Figure 16).

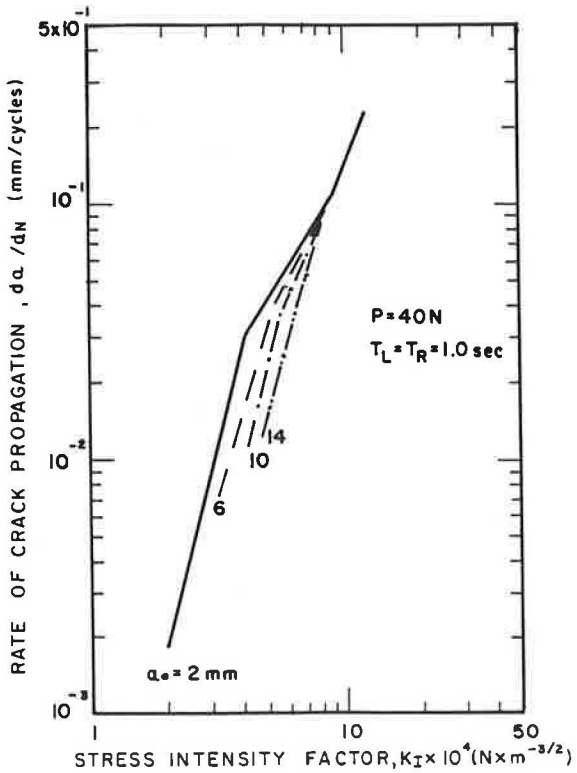

FIGURE 16 Predicted da/dN versus K_I for various initial crack lengths.

An effort to include the loading level, the loading and unloading durations, and the initial crack length in one Paris-like law is presently being made.

SUMMARY

A mechanistic model for predicting performance of sand-asphalt mixtures is presented and verified by laboratory tests. The model is found to give good results for a broad range of variables: load levels, loading and unloading durations, and initial crack lengths. It is shown that the model is adequate for predicting permanent deformation characteristics and the fatigue life of the sand-asphalt mixture used in the present research. It can therefore be applied confidently to the parametric study of the performance of asphalt material with a limited test program.

ACKNOWLEDGMENT

This research was supported by the Technion Vice-President for Research Funds through the L. Edelstein Research Fund.

REFERENCES

1. S.F. Brown and P.S. Pell. A Fundamental Structural Design Procedure for Flexible Pavements. Proc., 3rd International Conference on the Structural Design of Asphalt Pavements, London, England, Vol. 1, Sept. 1972, pp. 326-342.
2. W. Van Dijk. Practical Fatigue Characterization of Bituminous Mixes. Proc., Association of Asphalt Paving Technologists, Vol. 44, 1975, pp. 38-74.
3. S.F. Brown, J.M. Brunton, and P.S. Pell. The Development and Implementation of Analytical Pavement Design for British Conditions. Proc., 5th International Conference on the Structural Design of Asphalt Pavements, Delft, The Netherlands, Vol. 1, Aug. 1982, pp. 3-16.
4. N.W. Lister, W.D. Powell, and R.T.N. Goddard. A Design for Pavement to Carry Very Heavy Traffic. Proc., 5th International Conference on the Structural Design of Asphalt Pavements, Delft, The Netherlands, Vol. 1, Aug. 1982, pp. 84-91.
5. K.D. Raithby and A.D. Sterling. Some Effects of Loading History on the Fatigue Performance of Rolled Asphalts. TRRL Report LR 496. Transport and Road Research Laboratory, Department of the Environment, Crowthorne, Berkshire, England, 1972.
6. L. Francken. Fatigue Performance of a Bituminous Road Mix Under Realistic Test Conditions. In Transportation Research Record 712, TRB, National Research Council, Washington, D.C., 1979, pp. 30-37.
7. W. Van Dijk and W. Vinner. The Energy Approach to Fatigue for Pavement Design. Proc., Association of Asphalt Paving Technologists, Vol. 46, 1977, pp. 1-40.
8. F.D. Bonnaure, A.H.J.J. Huibers, and A. Boonders. A Laboratory Investigation of the Influence of Rest Periods on the Fatigue Characteristics of Bituminous Mixes. Proc., Association of Asphalt Paving Technologists, Vol. 52, 1982, pp. 104-128.
9. K. Majidzadeh, D.V. Ramsamooj, and A.T. Chan. Analysis of Fatigue and Fracture of Bituminous Paving Mixtures. Project RF-2845, Phase I. Ohio State University Research Foundation, Columbus, 1970.
10. D.V. Ramsamooj. Fatique Cracking of Asphalt Pavements. In Transportation Research Record 756, TRB, National Research Council, Washington, D.C., 1981, pp. 43-48.
11. K. Majidzadeh, E.M. Kauffman, and C.L. Saraf. Analysis of Fatigue of Paving Mixtures from the Fracture Mechanics Viewpoint. STP 508. ASTM, 1972, pp. 67-83.
12. K. Majidzadeh, C. Buranarom, and M. Karakomzian. Application of Fracture Mechanics for Improved Design of Bituminous Concrete. Report FHWA-RD-76-92. FHWA, U.S. Department of Transportation, Vol. 2, 1976.
13. M. Perl, J. Uzan, and A. Sides. Visco-Elasto-Plastic Constitutive Law for a Bituminous Mixture Under Repeated Loading. In Transportation Research Record 911, TRB, National Research Council, Washington, D.C., 1983, pp. 20-27.
14. A. Sides, J. Uzan, and M. Perl. A Comprehensive Visco-Elasto-Plastic Characterization of Sand-Asphalt under Compression and Tension Cyclic Loading. ASTM, Journal of Testing and Evaluation, Vol. 13, No. 1, 1985, pp. 49-59.
15. C.L. Monismith, G.A. Secor, and K.E. Secor. Temperature Induced Stresses and Deformation in Asphalt Concrete. Proc., Association of Asphalt Paving Technologists, Vol. 34, 1965, pp. 248-285.
16. E. Tons and E.M. Krokosky. Tensile Properties of Dense Graded Bituminous Concrete. Proc., Association of Asphalt Paving Technologists, Vol. 32, 1963, pp. 497-529.
17. C.L. Monismith. Rutting Prediction in Asphalt Concrete. In Transportation Research Record 616, TRB, National Research Council, Washington, D.C., 1976, pp. 2-8.
18. K.J. Bathe, E.L. Wilson, and R.H. Iding. NONSAP--A Structural Analysis Program for Static and Dynamic Response of Nonlinear Systems. Report 74-3. Structural Engineering Laboratory, University of California, Berkeley, Feb. 1974.
19. R.S. Barsoum. On the Use of Isoparametric Finite Element in Linear Fracture Mechanics. International Journal for Numerical Methods in Engineering, Vol. 10, 1976, pp. 15-37.
20. P.P. Lynn and A.R. Ingraffea. Transition Elements to be Used with Quadratic Point Crack Tip Elements. International Journal of Numerical Methods in Engineering, Vol. 12, 1978, pp. 1031-1038.
21. J. Uzan. Permanent Deformation in Pavement Design and Evaluation. International Symposium on Bearing Capacity of Roads and Airfields, Trondheim, Norway, Vol. 2, 1982, pp. 658-669.
22. S. Timoshenko and J.N. Goodier. Theory of Elasticity. 2nd ed. McGraw-Hill Book Co., New York, 1951, 506 pp.
23. R.L. Lytton, D. Saylak, and D.E. Pickett. Prediction of Sulphur-Asphalt Pavement Performance with VESIS IIM. Proc., 4th International Conference on the Structural Design of Asphalt Pavements, University of Michigan, Ann Arbor, Vol. 1, Aug. 1977, pp. 855-861.
24. C.L. Monismith, K. Inkabi, C.F. Freeme, and D.B. McLean. A Subsystem to Predict Rutting in Asphalt Concrete Pavement Structures. 4th International Conference on the Structural Design of Asphalt Pavements, University of Michigan, Ann Arbor, Vol. 1, Aug. 1977, pp. 529-539.
25. J.B. Rauhut, R.C.G. Haas, and T.W. Kennedy. Comparison of VESYS IIM Predictions to Brampton/AASHO Performance Measurements. Proc., 4th International Conference on the Structural Design of Asphalt Pavements, University of Michigan, Ann Arbor, Vol. 1, Aug. 1977, pp. 131-138.

26. J. Verstaten, J.E. Romain, and V. Veverka. The Belgian Road Research Centre's Overall Approach to Asphalt Pavement Structural Design. Proc., 4th International Conference on the Structural Design of Asphalt Pavements, University of Michigan, Ann Arbor, Vol. 1, Aug. 1977, pp. 298-324.
27. C.L. Monismith, K.E. Secor, and E.W. Blackmer. Asphalt Mixture Behaviour in Repeated Flexure. Proc., Association of Asphalt Paving Technologists, Vol. 30, 1961, pp. 188-222.
28. P.S. Pell and K.E. Cooper. The Effect of Testing and Mix Variables on the Fatigue Performance of Bituminous Materials. Proc., Association of Asphalt Paving Technologists, Vol. 44, 1975, pp. 1-37.
29. M.W. Witczak. Pavement Performance Models Repeated Load Fracture of Pavement Systems. Report 5-76-15, FAA DOT-FA 73WAI-377. FHWA, U.S. Department of Transportation, Vol. 1, 1977, 193 pp.

Publication of this paper sponsored by Committee on Flexible Pavements.

Load Rating of Light Pavement Structures

KOON MENG CHUA and ROBERT L. LYTTON

ABSTRACT

A new approach to determining the damage that overweight vehicles can do to light pavement structures is described. This procedure uses deflections measured with either the Dynaflect or the falling weight deflectometer to determine the number of passes of a specific load that will cause a critical level of rut depth in a light pavement structure. This method was based on field observations and ILLI-PAVE, a finite element pavement analysis program. In the study, a hyperbolic curve is used to describe both the stress-softening and the stress-hardening form of load deflection characteristics observed on light pavements. A method of determining the nonlinear elastic material properties for the base course and the subgrade using the falling weight deflectometer or the Dynaflect was developed. From the data collected with the pavement dynamic cone penetrometer, it appears that the stiffness of the granular base course depends, not surprisingly, on the degree of compaction of the material. The model adopted for accumulated permanent deformation due to repetitive loading and reloading follows a hyperbolic-shaped load deflection curve with a linear unloading path. Thick pavements, which are usually the stress-hardening type, appear to be more resistant to rutting. The new approach is shown to be accurate in predicting the development of rut depth with repeated loads applied by a variety of different vehicles. A computer program is written to incorporate the complete analysis method.

As a result of increasing industrial and agricultural activities, heavier trucks and higher traffic volumes have accentuated the problem of load rating and zoning of various farm-to-market roads that have light pavement structures. In evaluating overweight vehicle permit applications, the present practice in Texas is to determine the gross allowable loads on the light pavement structure by performing Texas triaxial tests on cored samples (C. McDowell, Wheel Load Stress Computations Related to Texas Highway Department Triaxial Method of Flexible Pavement Design, unpublished report of the Texas Highway Department). A more efficient, nondestructive testing method of determining damage to pavements by overweight vehicles is needed.

The new approach is a computerized procedure that uses results obtained from the Dynaflect or the falling weight deflectometer (FWD) to determine the number of passes of a specified load that will cause a critical level of rut depth in a light pavement structure. Conversely, the maximum allowable load on a light pavement structure can be determined using rut depth as a criterion for unacceptability. Rut depths are caused by accumulating pavement deformation under repeated load applications. Each time a load passes, the pavement fails to rebound as much as it was deflected under load. Establishing the difference between the loading and the unloading path is critical to making a reliable prediction of rut depth. Some of the advantages of the new approach are

1. Nondestructive testing (NDT) will reduce the time and the manpower currently required to deter-

mine the maximum load allowed on a pavement, will expedite permit evaluation, and will reduce the costs of the overall process;

2. Estimating the maximum allowable number of applications of load on a pavement will assist in planning and budgeting decisions that are related to patterns of future development; and

3. The method will assist in evaluating the economic impact of load-intensive industries on the local road maintenance and rehabilitation budget.

DATA COLLECTION

This involved the nondestructive testing of 78 pavement sections from 12 farm-to-market roads using the Dynaflect and the falling weight deflectometer. In addition, construction drawings were used to determine the layer thickness of those sections tested and these were checked using a pavement dynamic cone penetrometer. These data formed the basis for the development of the determination of the load deflection model using the two nondestructive methods.

Location of Test Sites

The pavement sections tested are located in Brazos and Burleson Counties of District 17 in a climate where annual rainfall and evapotranspiration are nearly balanced and hard freezes rarely occur. The pavement sections are representative of some of the weaker subgrade conditions that occur in the state.

Test Sections

The test sections were chosen to be at mileposts (spaced 2 mi apart) along the farm-to-market roads. These sections represent a diverse sampling. Some were constructed or reconstructed as early as 1953 and as late as 1981. Table 1 gives the farm-to-market (FM) roads that were tested, the base course thicknesses, and the field-observed base course material type. Figure 1 shows typical cross sections of these roads. Base course thicknesses range from 4 to 14 in. Base course materials were found to consist of crushed stone, river gravel, sandstone, and iron ore. The surface courses or wearing courses, although originally intended to be only a surface treatment course, were measured to be about an inch thick. This is due to numerous seal coat applications.

The falling weight deflectometer and the Dynaflect were used on each section. Usually two or three sections spaced about 10 ft apart were tested at each of the selected mileposts. Measurements were made at points between the wheelpaths where the traffic is slight in order to obtain a more consistent evaluation of the overall integrity of the pavement.

TABLE 1 Relevant Construction Details of Test Sections in District 17

Road Name	Mile Post No.	Base Course Thickness (in.)	Field Identified Base Course Material Type
Burleson County			
FM 3058	2 to 10	6	Crushed stone (caliche)
FM 908	10	8	
FM 1361	6 to 10	8	
FM 2000	8 to 10	7	Crushed stone and sandstone
	12	6	Gravel
FM 2155	2 to 4	6	River gravel
FM 50	2 to 4	7.5	River gravel
	6 to 16	7.5	Crushed stone
Brazos County			
Old Spanish Road	2 to 4	14	Crushed stone (caliche)
FM 974	6 to 8	4	Crushed stone (iron ore)
FM 1179	4	6	Crushed stone and gravel
FM 1687	2	9	Gravel
FM 2038	8 to 10	10	River gravel
FM 2776	0 to 2	6	River gravel

Falling Weight Deflectometer

The Dynatest 8000 FWD test system (1,2) was used in this study. The FWD itself is a lightweight, trailer-mounted unit. It can deliver an impulse load of from 1,500 to 24,000 lb to a pavement. The impulse is essentially a half sine curve with a duration of 25 to 30 milliseconds. The load is transmitted to the pavement through a 12-in.-diameter loading plate that rests on a thick rubber pad that is in contact with the pavement surface. In principle, the force applied to the pavement is dependent on the mass of the drop weights used, the height of the drop, and the spring constant of the rubber pad as well as that of the overall pavement. In practice, however, the applied force is changed by varying the mass of the drop weights or the height of the drop, or both. The actual load relayed to the pavement is measured by the load cell located just above the loading plate. The deflection basin is obtained by monitoring the deflections at seven locations on the pavement surface using velocity transducers. One of these is located in an opening in the center of the loading plate.

In the tests the height of drop and the weight were adjusted to produce four different load levels: 9,000, 11,000, 15,000, and 23,000 lb, the exact magnitude of which was registered by the load cell. Figure 2 shows the locations of the deflection sensors and a set of typical deflection basins observed at the four different load levels.

Dynaflect

The Dynaflect (3) is the most commonly used NDT device in the United States for the purpose of pavement evaluation and design. This equipment is a dynamic force generator mounted on a covered trailer. The cyclic force is produced by a pair of counterrotating unbalanced flywheels, and this force oscillates in a sine-wave fashion with an amplitude of 500 lb at a frequency of 8 cycles per second. This force, together with the dead weight of the trailer, which is about 1,600 lb, is transmitted to the ground via two steel wheels placed 20 in. apart. The peak-to-peak deflections are measured by five geophones placed at 1-ft intervals with the first directly between the wheels. A typical deflection basin is shown in Figure 3.

DATA ANALYSIS

After it was verified that ILLI-PAVE with appropriately assumed material models can reproduce measured deflection basins, the computer program was used to generate deflection basins for four different load levels with different combinations of assumed material models for the base course and the subgrade; different thicknesses of base course were used. These finite element computations were made to simu-

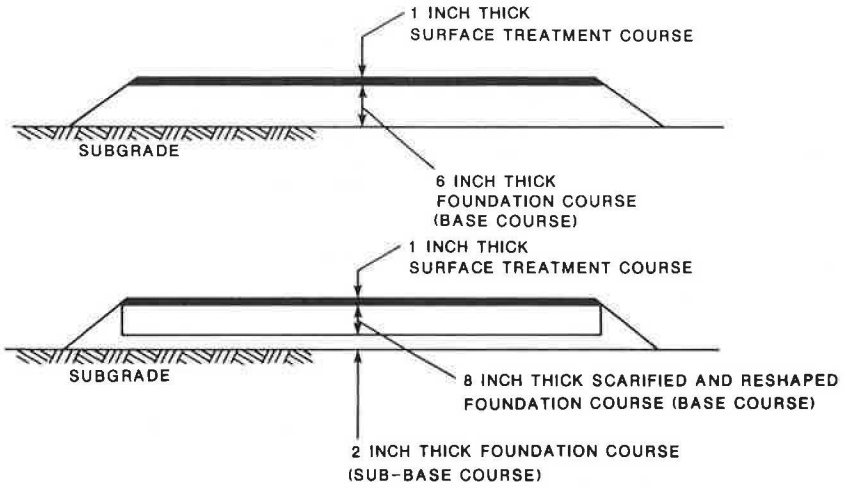

FIGURE 1 Typical cross sections of farm-to-market roads.

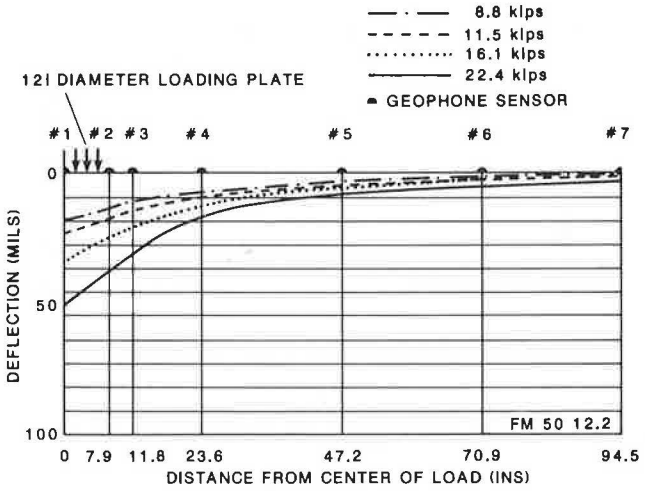

FIGURE 2 Typical deflection basin—falling weight deflectometer.

late tests done with an FWD. It was assumed that the last deflection sensor reading, which is 94.5 in. from the center of the loading plate, is related to subgrade material type.

After a procedure for identifying material models from FWD deflection sensor readings had been developed, a load deformation equation was formulated for each set of deflection sensor readings. A hyperbolic load deflection model was adopted and a means of determining the unknown coefficients was established.

The load rating or rutting model used is one that allows for a linear unloading path in the load deflection curve. The reloading path was assumed to be the same as the loading path. The gradient of the unloading path was determined from actual rut depth and the number of passes of a known load, or estimated from a formulation presented in this study, which was based on backcalculation from observed rut depths. Finally, on the basis of comparisons of deflection basins from the FWD and the Dynaflect, a correlation between the first and the last deflection sensor readings of both instruments was made.

The analytical approach adopted, the analytical tools used, and the assumptions made are discussed in the next section.

ILLI-PAVE: Finite Element Analysis

ILLI-PAVE (4,5) is a finite element program that models an asymmetrical solid of revolution as shown in Figure 4 and allows for linear as well as nonlinear stress-dependent elastic moduli for granular and fine-grained soils. This program has been shown

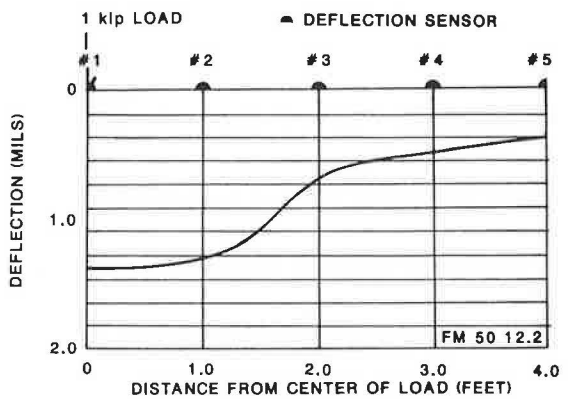

FIGURE 3 Typical deflection basin—Dynaflect.

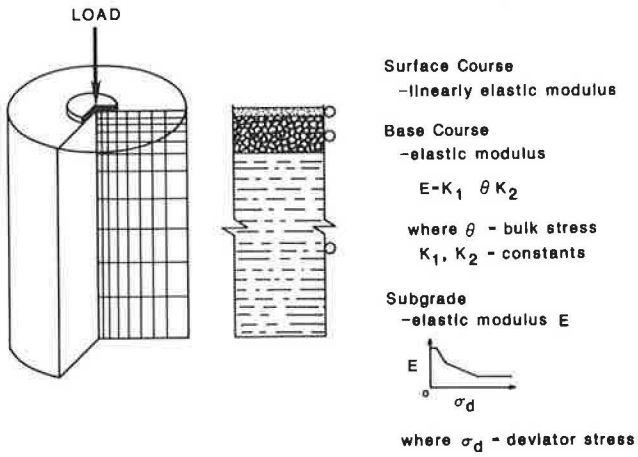

FIGURE 4 ILLI-PAVE model: finite element pavement analysis

to be adequate in predicting the response of flexible pavement to load (6).

For the analyses done in this study, a mesh of 121 elements was used. The elements were smallest nearest the pavement surface to allow for greater accuracy in computation. To allow for an adequate simulation of the boundary conditions, it was suggested (7) that the depth of the mesh be at least 50 times the radius of the circular loading plate of the FWD, which is 6 in., and that the horizontal extent be at least 12 times that radius away from the center of the loading plate. In this case, to accommodate the last FWD deflection sensor, a width of 96 in. was used. However, from the analyses made at about 11,000 lb loading, vertical stresses caused by the load input appear to be negligible beyond a depth of about 12 times the radius of the loading plate.

How ILLI-PAVE was used in this study and the material models that were input are described in the following subsections.

Pavement Material Models

The farm-to-market roads encountered generally have three distinct layers: a surface course, a base course, and a subgrade. Some older roads were found to have a subbase consisting of the old road base that was partly scarified and then overlaid with new base course material. The subgrade material was found to vary consistently along the road.

A pavement dynamic cone penetrometer (DCP) (8) was introduced to check the thickness of pavement layers by detecting when the stiffness changed. This device consists of a steel rod with a 60-degree cone of tempered steel at one end. A sliding hammer of about 17.6 lb falling from a height of 22.6 in. provided the consistent impact load required to penetrate the pavement. The penetration given as inches per blow gives an indication of the stiffness of the pavement layers. This instrument was found to be useful for comparing the stiffnesses of the base courses encountered in this study. Figure 5 shows the DCP.

The 1-in.-thick surface courses did not contribute much to the pavement in terms of rigidity but

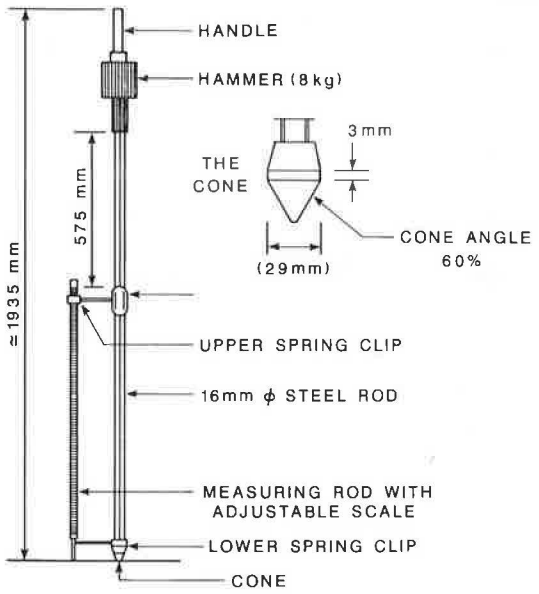

FIGURE 5 Dynamic cone penetrometer *(8)*.

were nevertheless included in the material modeling in recognition of their presence. An assumed modulus was used for this material in all of the analyses because the actual value of the modulus has virtually no influence on the results. The base course thicknesses used in the simulation were taken from construction drawings. However, the thicknesses found using the DCP differed from the design value by as much as 5 in. for an 8-in.-thick base course. However, in most cases the difference was much less. In the ILLI-PAVE analyses, the subbase course, if any, was considered as part of the base course because its material type did not appear to be different. As a point of interest, from the DCP data it appeared that most old pavements show a distinct interfacial layer between the base course and the subgrade. This might be due to infiltration of fines from the subgrade into the base course layer as well as to the presence of moisture.

Base course materials were found to be of the granular, unbound type. Using the DCP it was found that knowledge of the material hardness and shape is not sufficient to categorize its load deflection behavior. Figure 6 shows the rate of penetration of the DCP into a few pavements with different base course materials. It appeared that the major determining factor of the stiffness of the material is the unit weight, that is, the degree of compaction of the material. This had been realized earlier (9).

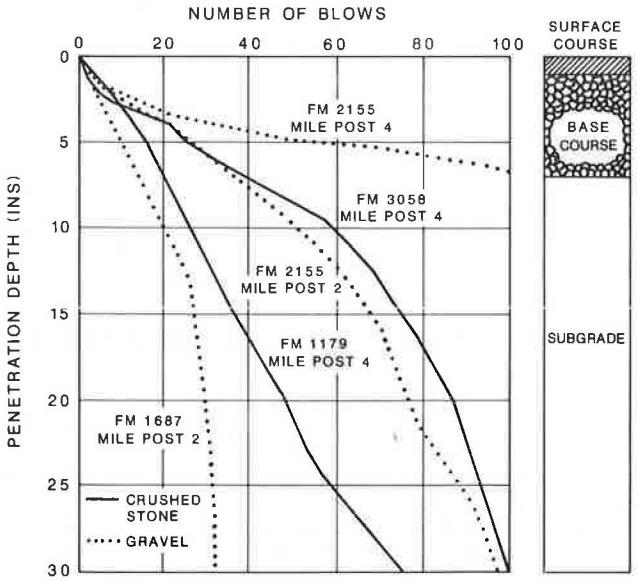

FIGURE 6 Comparison of pavement stiffnesses using the dynamic cone penetrometer.

The elastic modulus of the base course material was expressed as

$$E = K_1 \theta^{K_2} \quad (1)$$

where

θ = the bulk stress or the first stress invariant and
K_1 = the unknown coefficient defining the material.

This value shall be referred to as the K_1-value hereafter. The range of K_2-values was reported to be between 0.30 and 0.60 (10;11,pp.256-266). Most

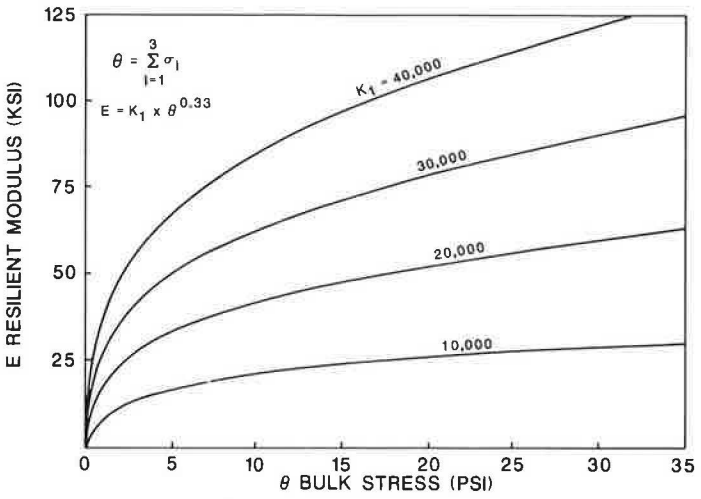

FIGURE 7 Base course material models.

analyses using ILLI-PAVE (4,10) adopt a range of from 0.30 to 0.33 for this value. For practical reasons, in this study a value of 0.33 was assumed. This reduces to one the number of factors to be identified in the base course material. Subsequent analyses showed that this is an adequate assumption. Figure 7 shows the assumed base material model.

Four nonlinear elastic moduli, shown in Figure 8, were used to describe the subgrade properties. They are for the very soft, soft, medium, and stiff subgrades. These models had been successfully used before ILLI-PAVE (4,10).

Table 2 gives a summary of the pavement material properties used in the analyses with ILLI-PAVE.

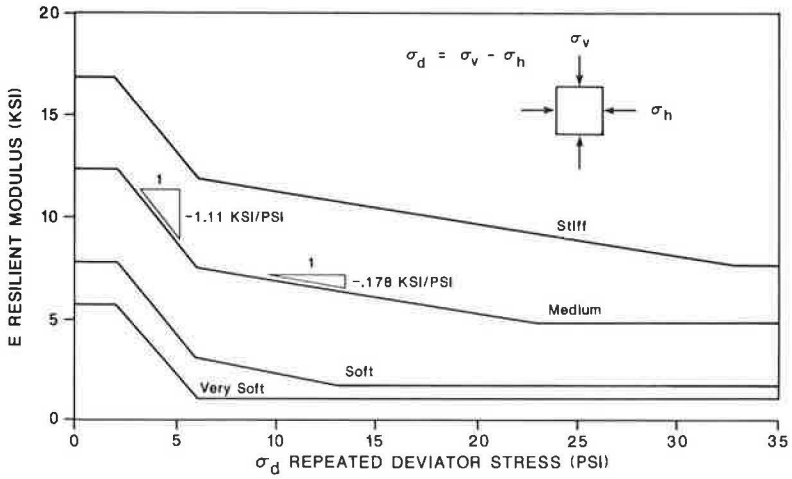

FIGURE 8 Subgrade soil material models.

TABLE 2 Material Properties Used in ILLI-PAVE

Property	Surface Course	Base Course	Subgrade			
			Stiff	Medium	Soft	Very Soft
Unit weight (pcf)	145.00	135.00	125.00	120.00	115.00	110.00
Lateral pressure coefficient at rest	0.87	0 60	0.82	0.82	0.82	0.82
Poisson's ratio		0.38	0.45	0.45	0.45	0.45
Unconfined compressive strength (psi)			32.80	22.85	12.90	6.21
Deviator stress (psi)						
Upper limit			32.80	22.85	12.90	6.21
Lower limit			2.00	2.00	2.00	2.00
Deviator stress at breakpoint (psi)			6.20	6.20	6.20	6.20
Initial elastic modulus (ksi)			12.34	7.68	3.02	1.00
Elastic modulus at failure (ksi)			7.605	4.716	1.827	1.00
Constant elastic modulus (psi)	30,000					
Elastic modulus model	Linear	See Figure 12	←		See Figure 13	→
Friction angle (degrees)		40.0	0.0	0.0	0.0	0.0
Cohesion (psi)		0.0	16.4	11.425	6.45	3.105

Generation of Deflection Basin Using ILLI-PAVE

To obtain enough load deflection data to cover a wide spectrum of light pavement structures with different materials, a series of finite element computer runs was made. These simulations included a combination of four subgrade types, that is, very soft, soft, medium, and stiff, and four base course material types with K_1-values of 10,000, 100,000, 200,000, and 300,000. In addition, four different base course thicknesses were used: 2, 6, 12, and 18 in. For all of these combinations, four FWD loadings of 80, 100, 140, and 200 psi were used. The corresponding loads were 8,765, 10,956, 15,339, and 21,913 lb. In addition to this framework, other combinations were used as necessary. The results of these simulations were found to form a more than adequate pool of data from which important correlations of various parameters were identified.

Matching the Measured Deflection Basin Using ILLI-PAVE

Previous study (6) had shown ILLI-PAVE to be adequate in predicting the response of flexible pavement to loads. That presupposes that appropriate material models are used to simulate the response of real pavements.

In this study, measured deflection basins of farm-to-market road sections were successfully matched to show further that the program and the material models used in it are valid. The procedure was to adjust the input for subgrade and base course material characteristics to obtain field-measured deflection basins. Some difference in the curvature of the deflection basin was observed and was probably due to the lack of homogeneity of the base and the subgrade materials. Table 3 gives the results obtained for two of the sections that were matched.

Load Deflection Model

A hyperbolic relationship between the load and the deflection of the light pavement structure was assumed. Because the hyperbolic stress-strain relationship is true of most soil materials (12-14) and because the light pavement structures considered are composed of soil materials, it is reasonable to adopt this as the load deflection model. The general equation is

$$P = \Delta/(A + B\Delta) \quad (2)$$

where

P = load and
Δ = deflections.

The constants A and B will hereafter be termed coefficient A and coefficient B.

Rewriting Equation 2 results in

$$\Delta/P = A + B\Delta \quad (3)$$

A plot of Δ/P versus Δ yields the straight line, shown in Figure 9, from which coefficients A and B are found. Equation 3 assumes a stress-softening behavior. However, extrapolation of field-measured maximum deflections for different loads showed that some pavements do stress harden. To allow for this, a modified hyperbolic load deflection equation was used. This expression is

$$P/\Delta = (1/A) + (1/C)P \quad (4)$$

where C is a constant.

TABLE 3 Comparisons of Measured Deflection Basins with ILLE-PAVE Results

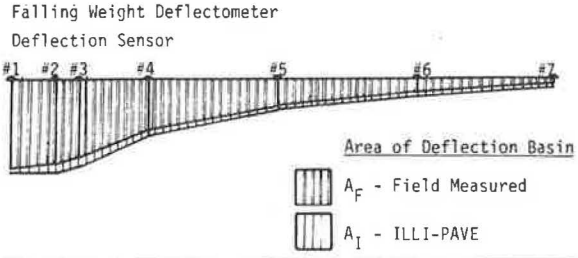

ROAD		FM50		FM3058	
MILEPOST		12		10	
SECTION		2		1	
FWD LOAD (LBS)		11473		11140	
DEFLECTION (MILS)		Field	ILLI-PAVE	Field	ILLI-PAVE
@ SENSOR NO.	1	26.57	26.99	55.75	55.60
	2	19.45	22.57	44.61	43.53
	3	16.02	19.96	33.50	35.70
	4	10.12	4.80	15.59	18.37
	5	4.57	2.40	5.71	5.72
	6	2.40	2.15	3.54	2.67
	7	2.17	1.58	2.74	2.07
RATIO OF A_I/A_F		1.07		1.01	
MEASURED BASE COURSE THICKNESS (INS)		13.5		7.5	
BASE COURSE MODEL WHERE θ = DEVIATOR STRESS (PSI)		$150000^{0.60}$		$200000^{0.33}$	
SUBGRADE MODEL		soft		very soft	

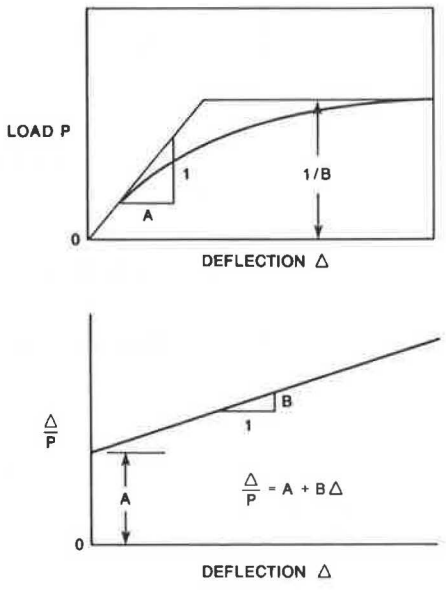

FIGURE 9 Load deflection model—stress-softening form.

A plot of P/Δ versus P yields a straight line as shown in Figure 10 from which A and C are found. Careful examination of the hyperbolic equation shows that by putting B = -A/C into Equation 2, a stress-hardening form of load deflection behavior results. Henceforth, these expressions are described as the stress-hardening and the stress-softening form of the hyperbolic load deflection equation for the pavements considered.

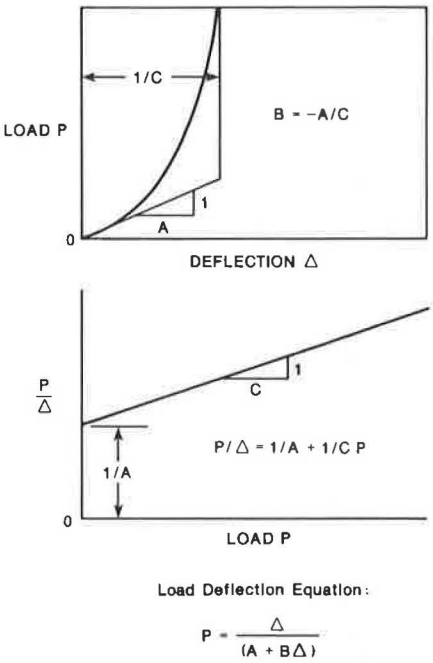

FIGURE 10 Load deflection model—stress-hardening form.

Load Rating and Rutting Model

A rut can be formally defined as (15) "a permanent deformation in and of the pavement layers or subgrades caused by consolidation or lateral movement of the materials due to traffic loads." Because the farm-to-market roads being considered do not contain much thickness of asphaltic material to move laterally under loads, rutting due to consolidation is the primary concern.

In considering the problem of rebound deformation under repetitive loading, the following information is of some relevance. In the loading and reloading of silica sand, Duncan and Chang (12) found that after the initial loading, the path of which was hyperbolic, the unloading and reloading path could be approximated with a high degree of accuracy as linear and elastic. In another study, Raad and Figueroa (16) observed that the resilient behavior of granular base and subgrade were maintained even after large deformations. Larew and Leonards (17) suggested that the rebound reached an equilibrium value after approximately 1,000 repetitions. Thompson and Robnett (18) thought that the size of the rebound was related to the moisture level.

For the purpose of developing a load rating model, the rutting models shown in Figure 11 were assumed. The Type I model shows a stress-softening load deflection behavior and the Type II a stress-hardening one. The unloading path was assumed to be linear. This path is expressed, using a multiplier, in terms of the initial slope or initial stiffness

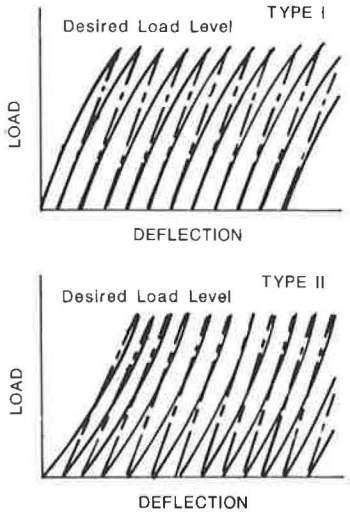

FIGURE 11 Load deflection model for repetitive loading (rutting) on pavement.

of the pavement. The multiplier is assumed to be independent of the load level and can be found if information about the measured rut depth caused by a known number of passes of a certain load is available. By using measured rut depths and the corresponding number of 18-kip equivalent single axle loads (ESALs) on farm-to-market roads obtained from a previous Texas Transportation Institute project (19), estimated values for the multiplier can be obtained. These are found to depend on the initial stiffnesses of the pavements, as will be shown later.

SUMMARY OF RESULTS

Description and Discussion of Load Rating Procedure

Two approaches to the load rating procedure were developed. One is for use with a falling weight deflectometer and the other, which is based on the first, is for use with a Dynaflect. The two approaches are presented in depth in the following sections. Although they are described as if all of the data reduction is done by hand, the entire process has been programmed and is done automatically.

Procedure Using the Falling Weight Deflectometer

1. Obtain the field-measured response of pavement to an FWD pressure of about 100 psi that corresponds to a load of about 10,956 lb. This loading will be referred to as the standard FWD load. The condition is necessary because much of this procedure was developed on the basis of that load level.
2. Adjust measured deflections at Sensors 1 and 7 to their equivalent values at the standard FWD load. This can be done by multiplying the values by the ratio of 10,956 lb over the registered load transmitted to the pavement. A linear variation can be assumed because the departure is not expected to be large. These corrected deflections will be referred to as the FWD deflections in the rest of the procedural outline.
3. Determine coefficient A of the load deflection equation. The stiffness of a pavement structure refers to the value obtained by dividing the applied load by the corresponding deflection at the point of loading. The overall stiffness is then the division

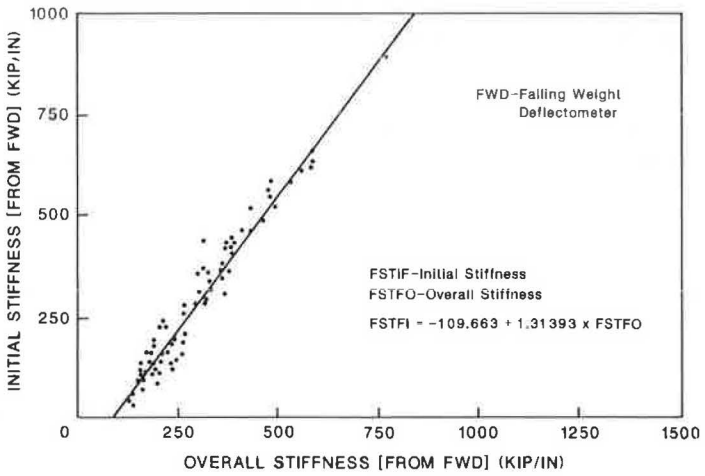

FIGURE 12 Determination of initial slope (stiffness) of load deflection curve.

of the standard FWD load by the maximum FWD deflection, which will be at Sensor 1. The initial stiffness, which is the slope of the load deflection curve near a zero load, is then read from Figure 12 and the inverse of this is the value of coefficient A. Figure 12 was derived from field-measured deflections.

4. Determine the type of subgrade. With the FWD deflection at Sensor 7, from Figure 13, the type of subgrade soil model can be determined. Figure 13 was based on field-measured deflections.

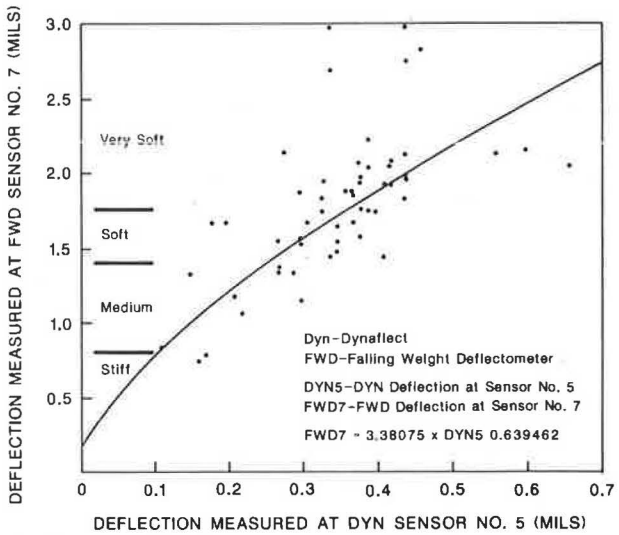

FIGURE 13 Determination of subgrade soil model from deflection.

5. Determine the standard deflection. This is the maximum deflection that will be obtained if the particular pavement structure is resting on a very soft subgrade and loaded with a standard FWD load. This value can be obtained from Figure 14. This correlation was derived from the ILLI-PAVE analyses and was found to match the field-measured values.

6. Determine the base course material model. By interpolating from the curves shown in Figure 15, the K_1-value of the base course material can be

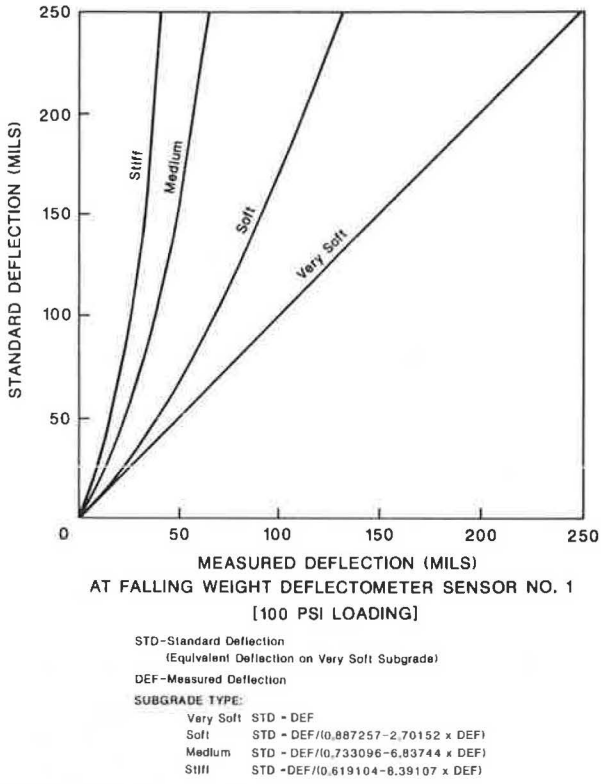

FIGURE 14 Determination of standard deflection.

found. Necessary inputs will be the base course thickness and the FWD deflection at Sensor 1. These curves were based on the ILLI-PAVE analyses.

7. Determine coefficient B of the load deflection equation. As can be seen from Figure 16, coefficient B is dependent on the K_1-value of the base course material and the subgrade type. The positive value can be interpolated from the curves shown in the figure. Difference scales for the value of coefficient B are given to adjust for the different subgrades encountered. This figure was based on ILLI-PAVE analyses. For the negative value of coefficient B, refer to Figure 17. This value is a linear function of the value of coefficient A of the load de-

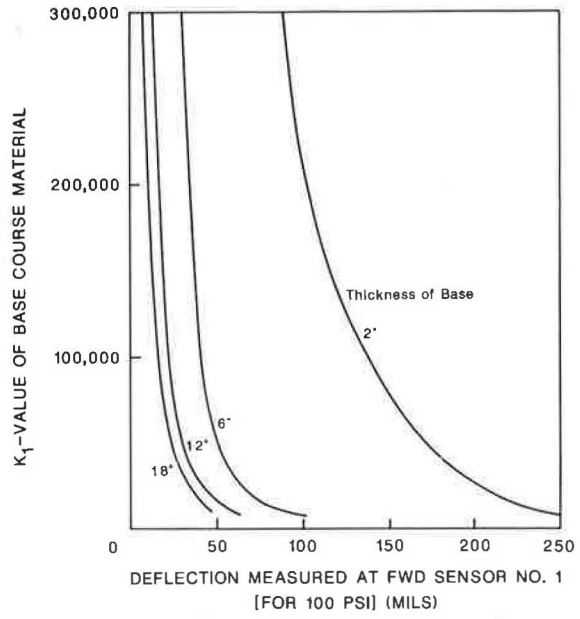

FWD-Falling Weight Deflectometer
STD-Standard Deflection
H-Base Course Thickness (ins)

$K_1 = CC \times STD^{CD}$

For $H \geq 5.0$ $CC = 10^{12.8778H^{-0.18345}}$

$CD = -2.95407e^{-0.017531H}$

For $H < 5.0$ $CC = 10^{16.1791H^{-0.349993}}$

$CD = -4.98760H^{-0.39432}$

FIGURE 15 Determination of base course material model from FWD deflection.

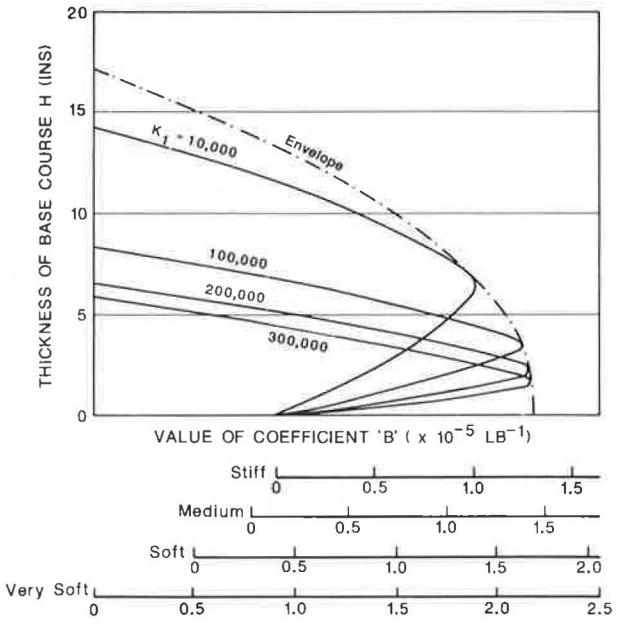

B-Coefficient 'B' of Load Deflection Equation
H-Thickness of Base Course
K_1-Coefficient for Base Course Material Model

$B = CE + CF \times H + CG \times H^2$

where $CE = 1.36543 \times 10^{-6} \times K_1^{0.185895}$

$CF = 3.15679 \times 10^{-6} + 3.24823 \times 10^{-11} \times K^1 - 1.05093 \times 10^{-16} \times K_1^2$

$CG = -1.74866 \times 10^{-7} + 1.00162 \times 10^{-11} \times K_1 + 2.3941 \times 10^{-17} \times K_1^2$

FIGURE 16 Determination of positive value of coefficient B.

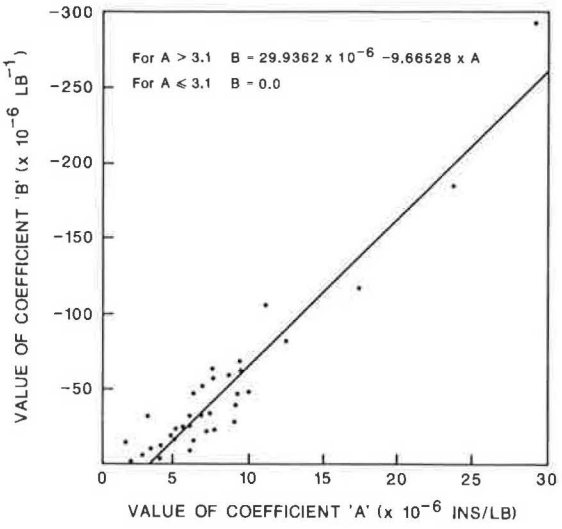

FIGURE 17 Determination of negative value of coefficient B.

flection equation. As a check, it was observed that for a positive value of coefficient B, if the calculated maximum deflection differs from the measured value by more than 20 percent, it should be replaced with a negative value that can be found from Figure 17. This step was always found to provide a satisfactory load deflection equation. Figure 17 shows a linear relation between the negative values of coefficient B and coefficient A, both of which were calculated from measured deflections.

8. Determination of the multiplier for the initial slope. This multiplier when applied to the initial slope (stiffness) of the load deflection curve is the slope of the unloading path describing the deflection of the pavement after the passage of a wheel load. Sixty-four light pavement sections from five farm-to-market (FM) roads, namely FM 418 and FM 365 in District 20, FM 665 in District 16, FM 612 in District 8, and FM 1381 in District 13, were used to backcalculate this multiplier. Values of this multiplier from these sections were found to vary from about 0.90 to 1.7. Figure 18 shows a method of estimating this value. However, if the rut depth and the number of passes of a known load are available for a particular road, the multiplier can be backfigured from the equation

$$\text{Multiplier} = \Delta P_m \, [A \, P_m/(1 - B \, P_m)] - \Delta_m \quad (5)$$

where

P_m = measured load and
Δ_m = measured rut depth and measured number of passes of P_m.

9. Determine the allowable number of passes. The number of passes of a desired load that will cause a specified rut depth can be easily found from the following expression:

$$N_x = R_x/[\Delta_N - (A \, P_{xi}/\text{Multiplier})] \quad (6)$$

where

N_x = allowable number of passes of a load equal to P_x,
R_x = specified rut depth,
P_x = specified load, and
$\Delta_N = AP/(1 - BP_x)$.

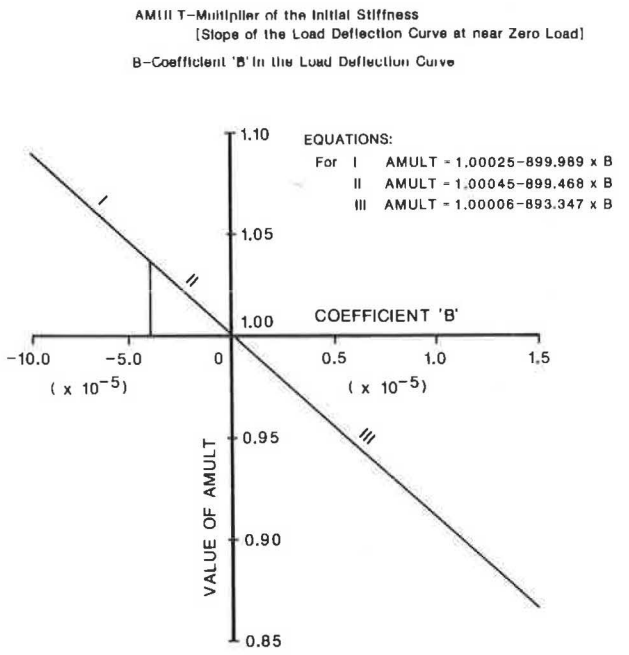

FIGURE 18 Determination of multiplier of the initial slope (stiffness) for the unloading path.

In the case of a set of different loads considered as a single pass, as for that of a multiple axle truck,

$$N_x = R_x / \left\{ \sum_{i=1}^{n} [\Delta_{N_i} - (A\,P_{xi}/\text{Multiplier})] \right\}$$

where n is the number of loads in the set.

Procedure Using the Dynaflect

1. Obtain field-measured response of pavement with a Dynaflect.
2. Determine the equivalent FWD deflection for the reading at Dynaflect Sensor 1. Because this approach is based on that described earlier for the FWD, the maximum Dynaflect deflection must be correlated with that of the FWD. Figure 19 shows the relationship between overall stiffness of pavement measured with a Dynaflect and that obtained from the FWD. The equivalent FWD deflection can be calculated from the following expression:

$$\text{FWD deflection} = -7.24474 + (29.6906 \times \text{Dynaflect deflection}) \quad (7)$$

3. Determine coefficient A of the load deflection equation. The equivalent FWD overall stiffness can be obtained from Figure 19. The initial stiffness, which is the slope of the load deflection curve near a zero load, is then read from Figure 12 and the inverse of this is the value of coefficient A.
4. Determine the type of subgrade. This is found from Figure 13 using the Dynaflect reading at Sensor 5.

The remainder of the procedure is identical to Steps 5 through 9 for the falling weight deflectometer.

Computer Program

A computer program, LOADRATE, written in FORTRAN, facilitates the load rating procedure developed in this study. This program can calculate the number of passes of a specified load that will cause a specified critical level of rut depth for every section for which a deflection basin is input and then give the average of the number of passes allowed for that particular road. The deflection basin can be that obtained using either a falling weight deflectometer or the Dynaflect. Figure 20 shows two computer outputs of a sample problem. It also is possible to print the material model of the base course and the subgrade for each section considered.

Evaluation of the Accuracy of the Procedure

In the correlation of data, regression analysis was used to get the best fit. The degree of accuracy of the simulated load deflection model can be seen in Figures 21-24. The figures compare the measured maximum deflections of the test sections with those obtained in the procedure at three different load levels using FWD readings. It can be seen that the best result was obtained at the 11,000-lb load level. This was because the material models for the

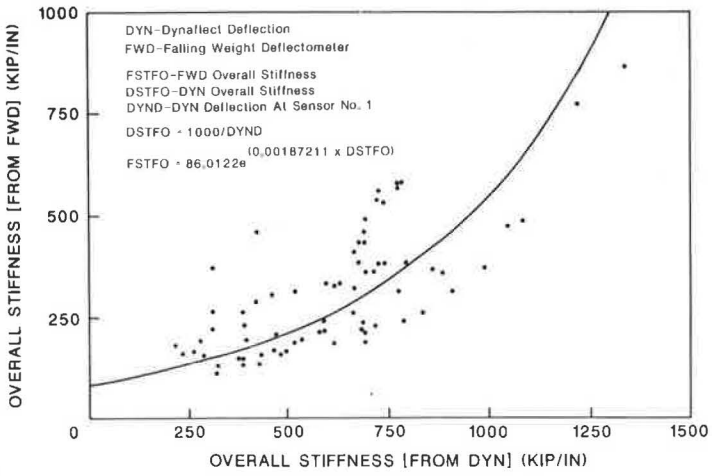

FIGURE 19 Determination of equivalent FWD overall stiffness from Dynaflect overall stiffness.

Using the Falling Weight Deflectometer

TEXAS HIGHWAY DEPARTMENT
LOAD RATING OF LIGHT PAVEMENT

JOB:SAMPLE PROBLEM 1 TYPE 2-S1-2 VEHICLE

DISTRICT: 17 COUNTY:BURLESON ROAD:FM2000
ALLOWABLE RUT(INS): 0.75

AXLE NUMBER	WHEEL LOAD(LBS)
1	4000.
2	9000.
3	9000.
4	9000.
5	9000.

RECORDED RUT(INS): 0.00 LOAD(LBS): 0. PASSES:0.0000D 00

DATE: 12/20/1982 FALLING WEIGHT DEFLECTOMETER

SECTION NO.	BASE THICKNESS (INS)	DEFLECTIONS (MILS) W1	W2	W3	W4	W5	W6	W7	LOAD (LBS)	NO. OF ALLOWABLE PASSES
8- 0	7.00	54.88	32.91	21.18	10.31	5.04	2.87	2.17	11108.	0.263D 03
8- 1	7.00	55.98	32.83	21.69	11.18	5.59	3.23	2.05	10981.	0.233D 03
10- 0	7.00	51.93	32.83	22.44	11.65	5.00	2.44	1.20	11616.	0.392D 03
10- 1	7.00	53.74	34.09	23.27	12.36	5.55	2.95	1.70	11696	0.350D 03
12- 0	6.00	31.53	19.29	13.54	7.21	4.02	2.60	1.30	11759.	0.181D 04
12- 1	6.00	32.24	18.74	12.83	7.01	3.90	2.44	1.20	11791.	0.170D 04

AVERAGE NUMBER OF PASSES TO CAUSE SPECIFIED RUT : 0.7908D 03

Using the Dynaflect

DATE: 3/ 1/1983 DYNAFLECT

SECTION NO.	BASE THICKNESS (INS)	DEFLECTIONS (MILS) W1	W2	W3	W4	W5	NO. OF ALLOWABLE PASSES
8- 0	7.00	2.13	1.53	1.14	0.87	0.60	0.287D 03
8- 1	7.00	1.89	1.50	1.14	0.86	0.66	0.456D 03
10- 0	7.00	1.41	1.08	0.74	0.55	0.39	0.386D 04
10- 1	7.00	1.47	1.14	0.74	0.53	0.35	0.161D 04
12- 0	6.00	3.30	1.14	0.78	0.54	0.22	0.958D 02
12- 1	6.00	1.47	1.08	0.78	0.54	0.40	0.168D 04

AVERAGE NUMBER OF PASSES TO CAUSE SPECIFIED RUT : 0.1332D 04

FIGURE 20 Computer printout for a sample problem.

base course and the subgrade were determined on the basis of a 100-psi loading from an FWD. At the 24,000-lb load level the deviations were more pronounced. At a lower load level the load deflection curve appears to closely match that obtained from the field data. It should be noted that the procedure presented uses only one deflection basin. The accuracy of the approach using the FWD is an indication of the accuracy of the approach using the Dynaflect because the latter was based on the former.

When evaluating the accuracy of the rutting model, it was observed that the analysis is quite sensitive to the value of the slope multiplier. Backcalculation of the number of passes for those sections used to derive the expression for the multiplier showed that, for certain cases, only the order of magnitude could be reproduced. This might be avoided if some rut history were available to compute the multiplier.

Sample Problem

To illustrate the use of this procedure in load rating light pavements, Figure 25 shows the results of the analysis with various types of trucks. Vehicles with weights at the current legal limits in Texas are compared with those proposed (20). It can be seen that the number of passes of a particular vehicle that will cause a certain rut depth, in this case 0.75 in., depends more on the load distribution on the axles than on the gross vehicle weight. Hence

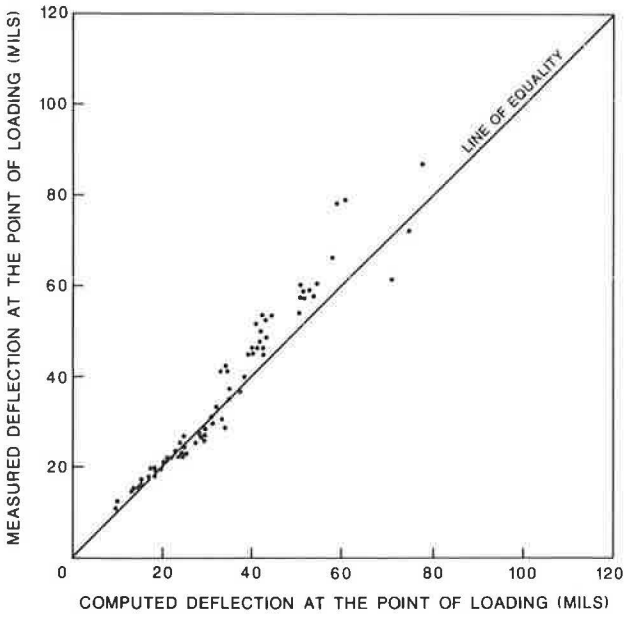

FIGURE 21 Comparison of measured deflections with computed deflections at about 9,000 lb loading.

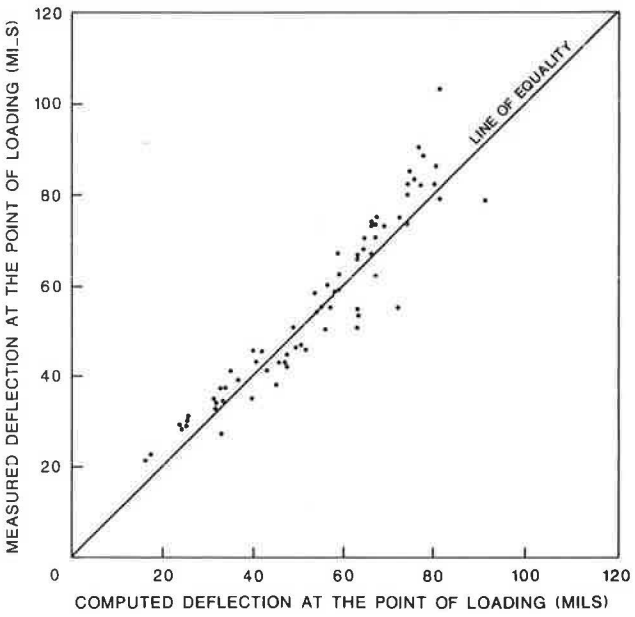

FIGURE 23 Comparison of measured deflections with computed deflections at about 15,000 lb loading.

it can be seen that, when a criterion or basis for measuring the level of damage is decided on, the procedure can be used as a tool for evaluation.

SUMMARY AND CONCLUSIONS

A new procedure for the load rating of light pavement structures using the falling weight deflectometer or the Dynaflect has been presented. A computer program was developed. In the course of the study, the following conclusions were drawn:

1. It was found that light pavement structures, such as those commonly found in the farm-to-market roads, show either a stress-softening form or a stress-hardening form of load deflection behavior.
2. It was shown that a hyperbolic stress-strain relationship or load deflection may be used to describe both the stress-softening and the stress-hardening form of load deflection characteristics of light pavements.
3. The ILLI-PAVE finite element pavement analysis program was again verified and shown capable of simulating deflection basins of flexible light pavement structures to match those measured in the field.
4. A procedure for determining the nonlinear elastic material models for the base course and the subgrade using the falling weight deflectometer or the Dynaflect was developed.

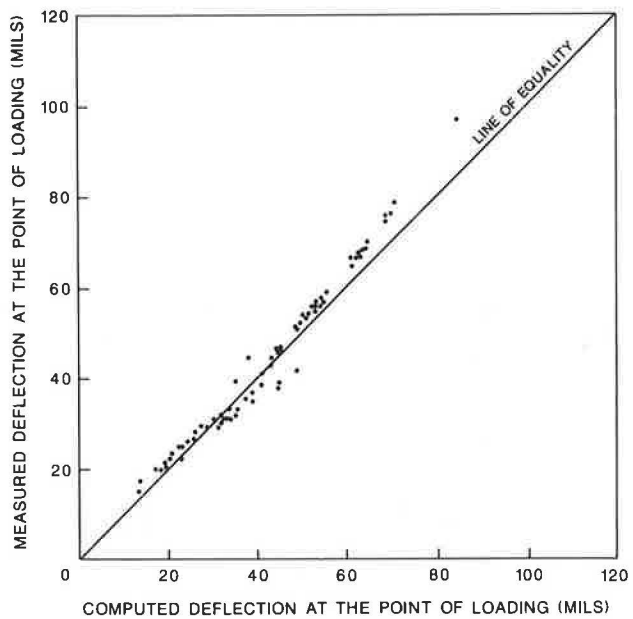

FIGURE 22 Comparison of measured deflections with computed deflections at about 11,000 lb loading.

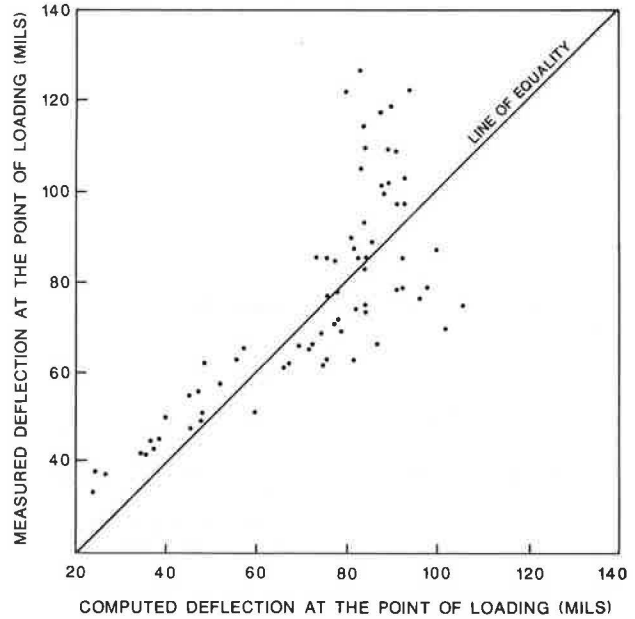

FIGURE 24 Comparison of measured deflections with computed deflections at about 23,000 lb loading.

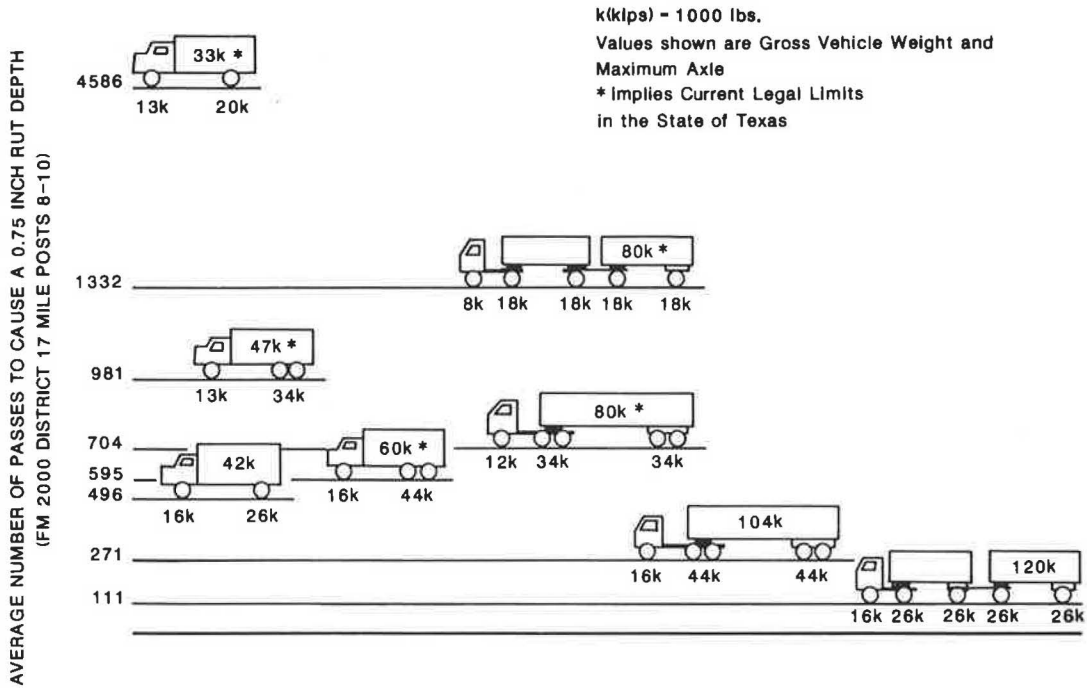

FIGURE 25 Comparison of damage that can be done by various overweight vehicles on a farm-to-market road.

5. A model of repetitive loading on pavements, which assumes a hyperbolic-shaped load deflection curve with a linear unloading path, was proposed. The slope of this unloading line was found to be smaller than the initial slope of the load deflection curve for the stress-softening type of pavement, but it was larger for the stress-hardening type.
6. Pavements with a thicker base course were usually found to show a stress-hardening form of load deflection behavior. This form is more resistant to rutting than is the stress-softening form.
7. It was shown that the proposed procedure is capable of reproducing the load deflection characteristics of the pavement sections tested.
8. The procedure calculates realistic rut depth histories for a variety of different vehicles.

ACKNOWLEDGMENT

This research was conducted in cooperation with the Federal Highway Administration, U.S. Department of Transportation. The authors are grateful for the funding support provided by the Texas State Department of Highways and Public Transportation under Research Project 2-8-80-284.

REFERENCES

1. R.C. Koole. Overlay Design Based on Falling Weight Deflectometer Measurements. In Transportation Research Record 700, TRB, National Research Council, Washington, D.C., 1979, pp. 59-72.
2. Dynatest 8000 FWD Test System. Dynatest Consulting, Inc., Ojai, Calif., 1982.
3. F.H. Scrivner, G. Swift, and W.M. Moore. A New Research Tool for Measuring Pavement Deflection. In Highway Research Record 129, HRB, National Research Council, Washington, D.C., 1966, pp. 1-11.
4. J.L. Figueroa and M.R. Thompson. Simplified Structural Analysis of Flexible Pavements for Secondary Roads Based on ILLI-PAVE. In Transportation Research Record 766, TRB, National Research Council, Washington, D.C., 1980, pp. 5-10.
5. ILLI-PAVE User's Manual. Transportation Facilities Group, Department of Civil Engineering, University of Illinois at Urbana-Champaign, May 1982.
6. M.L. Taylor. Characterization of Flexible Pavement by Non-Destructive Testing. Ph.D. dissertation. University of Illinois at Urbana-Champaign, 1978.
7. J.M. Duncan, C.L. Monismith, and E.L. Wilson. Finite Element Analysis of Pavements. In Highway Research Record 228, HRB, National Research Council, Washington, D.C., 1968, pp. 18-33.
8. E.G. Klegn, J.H. Maree, and P.F. Savage. The Application of a Portable Pavement Dynamic Cone Penetrometer to Determine in-situ Bearing Properties of Road Pavement Layers and Subgrades in South Africa. Proc., 2nd European Symposium on Penetration Testing, Amsterdam, The Netherlands, May 24-27, 1982, pp. 277-283.
9. W.A. Dunlap. Deformation Characteristics of Granular Materials Subjected to Rapid, Repetitive Loading. Research Report 27-4. Texas Transportation Institute, Texas A&M University, College Station, Nov. 1967.
10. M.S. Hoffman and M.R. Thompson. Backcalculating Nonlinear Resilient Moduli from Deflection Data. In Transportation Research Record 852, TRB, National Research Council, Washington, D.C., 1982, pp. 42-51.
11. E.J. Yoder and M.W. Witczak. Principles of Pavement Design. John Wiley & Sons, Inc., New York, 1975.
12. J.M. Duncan and C.Y. Chang. Nonlinear Analysis of Stress and Strain in Soils. Journal of the Soil Mechanics and Foundation Division, ASCE, Vol. 96, No. SM5, pp. 1629-1653.
13. R.L. Kondner. Hyperbolic Stress-Strain Re-

sponse: Cohesive Soils. Journal of the Soil Mechanics and Foundation Division, ASCE, Vol. 89, No. SM1, pp. 115-148.
14. R.L. Kondner. A Hyperbolic Stress-Strain Formulation for Sands. Proc., 2nd Pan-American Conference on Soil Mechanics and Foundation Engineering, Brazil, Vol. 1, 1963, pp. 289-324.
15. R.E. Smith, M.I. Darter, and S.T. Herrin. Highway Distress Identification Manual. Interim Report. FHWA, U.S. Department of Transportation, March 1979.
16. L. Raad and J.L. Figueroa. Load Response of Transportation Systems. Journal of the Transportation Engineering Division, ASCE, Vol. 106, No. TE1, 1980, pp. 111-128.
17. H.G. Larew and G.A. Leonards. A Strength Criterion for Repeated Loads. Proc., HRB, National Research Council, Washington, D.C., 1962, pp. 529-556.
18. M.R. Thompson and Q.L. Robnett. Resilient Properties of Subgrade Soils. Transportation Engineering Journal, Jan. 1979, pp. 71-89.
19. J.P. Mahoney and R.L. Lytton. Measurements of Pavement Performance Using Statistical Sampling Techniques. Research Report 207-2. Texas Transportation Institute, Texas A&M University, College Station, March 1978.
20. C.M. Walton, C-P. Yu, P. Ng, and S. Tobias. An Assessment of Recent State Truck Size and Weight Studies. Research Report 241-4. Center for Transportation Research, University of Texas at Austin, July 1982, pp. 113-116.

Publication of this paper sponsored by Committee on Strength and Deformation Characteristics of Pavement Sections.

In Situ Pavement Moduli from Dynaflect Deflection

SHAKIR HUSAIN and K. P. GEORGE

ABSTRACT

A complete pavement evaluation entails not only a condition survey, including load testing, but also in situ material characterization. With the simplifying, but justifiable, assumption that pavement materials are elastic under moving wheel loads, they are characterized by a modulus and Poisson's ratio. This study develops a methodology and computer program to determine the in situ elastic modulus for each layer in a multilayer flexible pavement. The surface deflection basin measured using the Dynaflect, or similar devices that employ five or more deflection sensors, would be the primary input data in the program. Points on a two-dimensional surface deflection basin are fitted to field data. Iteration is required to match the measured with the computed points by adjusting the assumed values for the layer moduli. The Chevron program is used to predict deflections. A computerized pattern search technique, the mainstay of the iteration, accomplishes the task of matching the deflections by minimizing the sum of squared errors. The usefulness of the method is illustrated by comparing the outputs of this program with those of the "standard" OAF program developed for FHWA. Results are presented to show that the present method gives far more reasonable results than does the OAF program. Suggestions for improving the solution procedure when dealing with erratic or inconsistent deflection readings, or both, are discussed. The feasibility of using deflection data of other devices, for example falling weight deflectometer, in the present method is illustrated by example problems.

A pavement undergoes deterioration with time and traffic; therefore, rehabilitation or even reconstruction is required to extend its useful life. In situ structural strength (i.e., remaining life of existing pavement), if properly evaluated and accounted for in the design procedure, aids in reducing rehabilitation construction expenses. A complete structural evaluation may determine the adequacy of the pavement and enables the engineer to predict its future service life with respect to the traffic using it. When pavement is found to be inadequate, the evaluation forms the basis for designing the improvements needed to provide service for a selected design period.

It is both useful and relevant for an engineer to have knowledge of the inherent mechanical properties of a pavement structure in order to calculate various responses (stresses and strains) throughout the

structure and to make a rational evaluation of its bearing capacity and useful structural lifetime in terms of traffic loading. Pavement response may be analyzed by the finite element method (1), elastic layer analysis based on Burmister's theory (2), the viscoelastic layer analysis (3), or other methods. One major difficulty in response analysis of pavement structures lies in having to determine the structural properties, such as elastic moduli, of pavement materials.

There are two possible methods for determining the elastic moduli of pavement materials. The first method is to conduct laboratory testing on either laboratory-compacted specimens or undisturbed samples taken from the pavement. Nondestructive testing is the second method. For example, surface deflections or deflection basins under known loading conditions, or both, have been widely used. Surface deflection basins may be determined using a Benkelman beam, Dynaflect, Road Rater, or other device. Because of its relatively higher degree of mobility, the Dynaflect is increasingly preferred for routine evaluation of highway pavements.

The question of how to estimate the material parameters in situ from surface deflections now arises. This problem is complicated because the material parameters are stress dependent. That is, the parameters estimated should preferably correspond to the magnitudes of stress or strain, or both, encountered under the actual loading condition the pavement is subjected to under wheel loads.

Theoretical solutions for determining elastic moduli of multilayer systems have been found (4,5); for purposes of discussion, these solution procedures are grouped as follows: those employing deflection data from Dynaflect or Road Rater (6-8) and those making use of such devices as a falling weight deflectometer (9,10). Because a large number of highway agencies in the United States rely on Dynaflect or Road Rater for pavement evaluation, a review of the various methods related to those two devices is presented.

Vaswani (11) proposed a structural design procedure based on Dynaflect maximum deflection (DMD). The method proposed by Jimenez (12) using Dynaflect deflections assumes that the elastic modulus of the asphalt concrete (AC) is known (if not, it is assumed). This requirement constitutes the major limitation of this approach. Majidzadeh et al. (13) reported a system (designated the Ohio moduli program) that employs various combinations of Dynaflect deflection data such as the first sensor deflection (w_1) plus the second sensor deflection (w_2), w_1 plus spreadability, and so on. He also presented a nomographic solution of in situ modulus calculations for two-layer flexible pavements. In the overlay design program called OAF, Majidzadeh and Ilves (7) employed a deflection matching technique for determining the in situ layer stiffnesses. The in situ asphalt modulus is compensated for temperature; and the base, subbase, and subgrade moduli are corrected for stress effects when test loads differ from design loads. While using field data to substantiate the applicability of the procedure, they experienced difficulties and commented, "The computed asphalt layer stiffness shows a large variation, and in a few cases the asphalt is stiffer than steel; nevertheless the values are reasonable in a great majority of the cases. . . ."

DMD data in conjunction with a series of curves were used in an FHWA study (14) to evaluate the stress-dependent subgrade moduli. That the asphalt materials need to be characterized in the laboratory is a major drawback of this method. Irwin (6) used multilayer elastic theory--the BISTRO computer program--in conjunction with Dynaflect deflection data to estimate the moduli of pavement layers. Because of the trial-and-error approach adopted, the basic algorithm used is inefficient to say the least. Following Irwin's approach, Kilareski and Anani (8), employing the Road Rater deflection basin, proposed a deflection matching procedure that requires the use of the BISAR computer program in conjunction with a successive approximation procedure. Kilareski and Anani, however, realized that many combinations of the elastic moduli yield deflections that match the observed ones. To obtain unique results, they introduced an additional condition of $E_1/E_2 = 0.7$ (E_1 and E_2 are moduli of first and second layers, respectively). Unfortunately, this ratio cannot be established a priori. Also, because the Dynaflect first sensor does not measure the deflection beneath the load, this program cannot be used with the Dynaflect.

Lytton and his coworkers (15) have developed another method, based on elastic layer theory, of predicting the layer moduli. This method makes use of an explicit expression for deflection, originally proposed by Vlasov and Leont'iev (16). The deflection equation is inverted by a nonlinear pattern search technique to determine the values of the layer moduli that would best fit the observed surface deflections. No doubt, the computer program using this approach in conjunction with Dynaflect deflections is as efficient as the authors claim. However, before it can be applied to other pavement sections, the user must develop several constants, five in all, for which no method exists as yet. Therefore, the applicability of this method is also quite limited.

To estimate the pavement material moduli, researchers have developed computer programs. As Majidzadeh et al. (7) concede, the OAF program incorporating the state of the art of deflection matching techniques has resulted in unsatisfactory modulus values, especially when the AC surfacing is underlaid by stiff cemented layers. The first objective of this study, therefore, is to develop a "general" procedure for estimating in situ pavement layer moduli. The procedure, as is customary, uses the deflection response of pavement as the primary input. The entire deflection basin, rather than deflections at discrete locations, is used, however. A second objective is to demonstrate, with illustrative examples, the versatility of the method compared with the OAF program developed for FHWA.

METHODOLOGY FOR DETERMINING IN SITU MODULI

No direct, analytical solution exists that can uniquely determine the elastic moduli for a multilayer system from surface deflection measurements alone. A reverse solution is thus necessitated wherein a set of initial modulus values is "guessed" and the pavement response (deflections) is calculated using these values in conjunction with the Chevron program. The solution procedure requires that the assumed moduli be adjusted so that the objective function, which is the sum of squared differences of measured and computed surface deflections, tends to be a minimum.

This is not exactly a simple process because a multilayer system has an infinity of elastic modulus combinations that can result in the same single surface deflection. As indicated by other researchers (7,8,14), the problem is further compounded because the moduli of asphalt concrete are temperature sensitive and those of granular and subgrade materials are stress dependent.

Details of the method developed in this paper are presented in the following paragraphs. The flowchart

in Figure 1 summarizes the important features of the method. The various steps have been rationalized and streamlined through the procedure, called the In-Situ Moduli Determination (IMD) program, described herein.

1. The pavement section is modeled by layers of uniform thickness (thickness preferably determined from construction or coring data), the lowest of which is the semi-infinite subgrade. The upper layer is typically either asphalt bound or concrete, and the two intermediate layers can be either cement bound or granular material, though this is not an exclusive structural makeup.

2. A set of initial modulus values must be assumed. Although the initial values can be arbitrarily chosen, the closer the assumed values are to the correct moduli, the faster the convergence will be. Limiting the range of predicted moduli for each layer within certain plausible constraints assures the uniqueness of the solution. Poisson's ratio of various layers is assumed from laboratory test data or a knowledge of the materials involved, or both.

3. Employing the elastic layer theory (Chevron) and the assumed values of the moduli, the deflection values $\hat{w}_i$ ($\hat{w}_1$, $\hat{w}_2$, $\hat{w}_3$, $\hat{w}_4$, and $\hat{w}_5$) can be calculated. An error function is obtained by subtracting the predicted value of deflection ($\hat{w}_i$) from the observed value (w_i). The square of the errors of all the sensor deflections results in the expression

$$e^2 = \sum_{i=1}^{5} (w_i - \hat{w}_i)^2 \quad (1)$$

To minimize the sum of squared errors, a computerized pattern search in conjunction with the general gradient technique, as proposed by Lytton et al. (15), is used. Had the deflection been an explicit function of the moduli, the error function of Equation 1 could have been minimized by least square

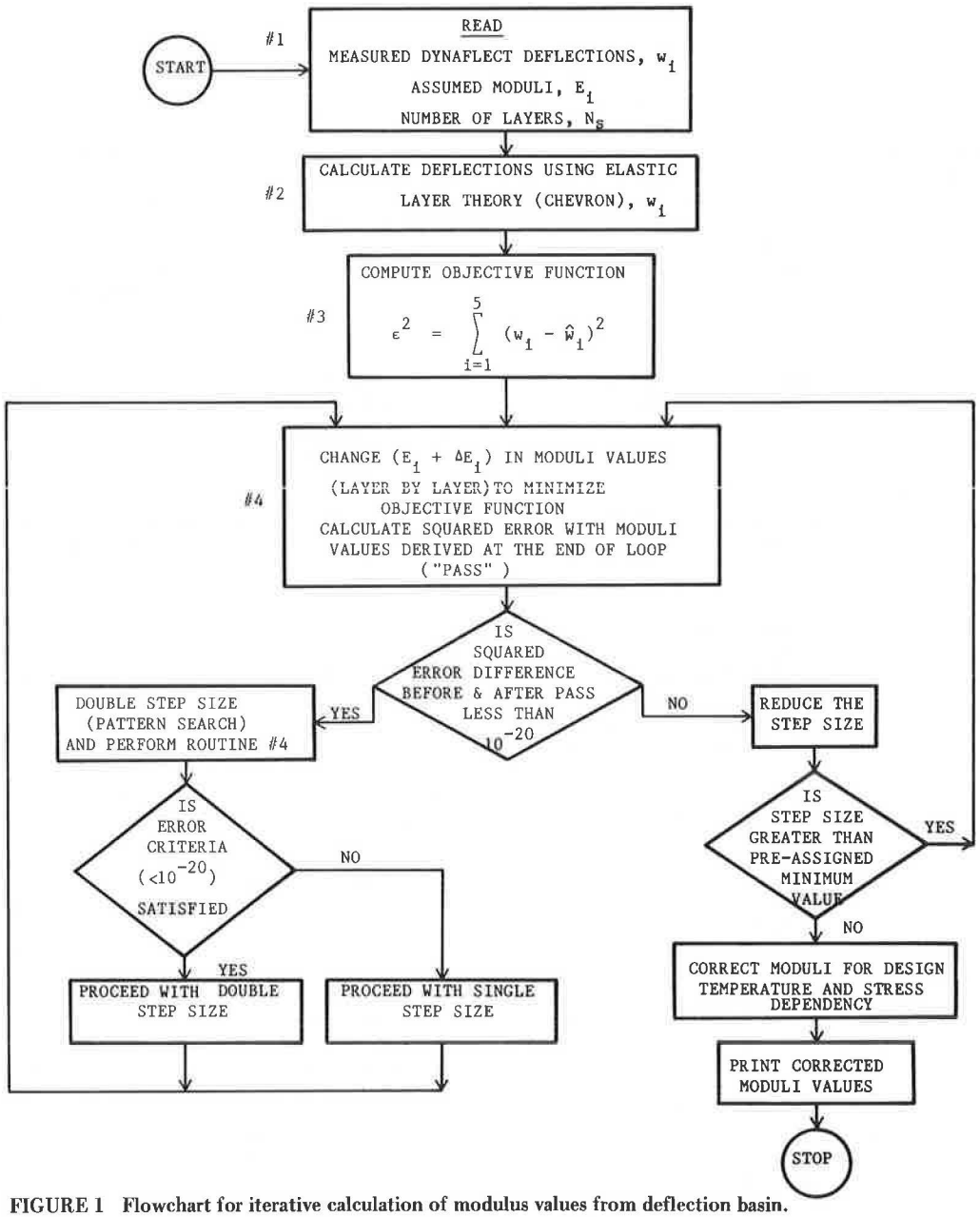

FIGURE 1 Flowchart for iterative calculation of modulus values from deflection basin.

techniques. The pattern search, replacing the simple least square analysis, therefore, permits the use of more realistic nonlinear equations that relate the observed values of deflection to the independent variables, modulus values in this instance.

The program starts with the initial set of moduli and modifies these initial estimates by a preassigned value, designated as "step size," in subsequent iterations. Unlike other programs (8,10), the IMD program starts from the surface layer and proceeds to the subgrade; when through once, it is said to have completed a pass. For each modification of a given layer modulus, the square of error is calculated and compared with the error calculated in the preceding step; if it is smaller than the previous error, it replaces the earlier one and the corresponding change in the layer modulus is incorporated. On completing a pass, if the difference in squared error before and after the pass falls below a specified criterion ($<10^{-20}$ in the algorithm), the program resorts to a pattern search whereby the step size is doubled. Alternatively, a step size reduction is instituted should the criterion for squared error not be satisfied. Whether the doubled step size, according to the pattern search, is acceptable or not is governed by the squared error criterion. Step size is decreased as the solution procedure advances, eventually terminating the program when the step size reaches a small preassigned value desired by the programmer. A relevant flow diagram and other details of this calculation routine can be found elsewhere (17). The set of values thus obtained is the "best" estimate of the in situ layer moduli for given loading and environmental conditions. To reduce them to the standard conditions, however, some corrections must be made.

Temperature Correction

The temperature of the pavement fluctuates with diurnal and seasonal temperature variations. It is known that the modulus of AC decreases (consequently the deflection increases) with increase in pavement temperature (18). For the modulus values calculated at various temperatures to be comparable, they should be adjusted to a standard temperature, usually designated as the design temperature, conveniently chosen at 60°F in this study.

Determination of the average temperature of the AC layer during field measurements is a prerequisite to making the corrections. Graphs (Figures 2a and 2b) developed by Southgate (19) are recommended for this purpose. Figure 2a should be used for AC layers thicker than 2 in. and Figure 2b for AC layers 2 in. or less thick.

The AC modulus at the test temperature is modified so that at the design temperature [60°F (15°C)], with the simplifying assumption, the deteriorated asphalt concrete exhibits a temperature dependency identical to that of the original AC mix. Typical moduli-temperature relationships of AC mixtures are shown in Figure 3. Making use of Figure 3, effective modulus at design temperature can be obtained using the following equation:

$$E_1 = \hat{E}_1 \cdot EDES/EEXP \quad (2)$$

where

E_1 = effective AC modulus at design temperature of 60°F (15°C),
$\hat{E}_1$ = effective AC modulus at test temperature,
EDES = modulus of original AC at design temperature, and
EEXP = modulus of original AC at test temperature.

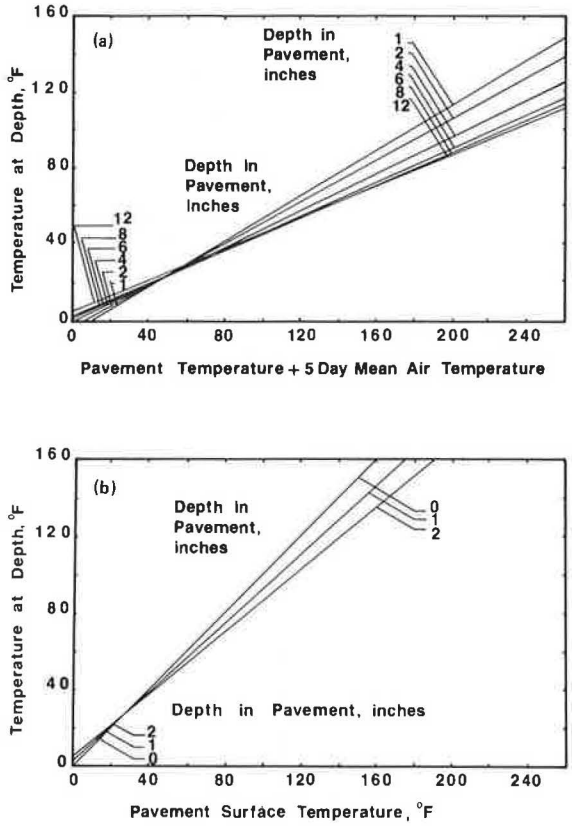

FIGURE 2 Temperature prediction graphs: (a) pavements more than 2 in. thick; (b) pavements equal to or less than 2 in. thick *(19)*.

Correction for Stress Dependency

Because the moduli of subgrade materials and granular bases are stress dependent, the modulus computed with Dynaflect deflection basin tends to be larger than that under a 9-kip (40-kN) wheel load. To overcome this apparent limitation of the Dynaflect, the calculated subgrade modulus is corrected for stress dependency. The relationships generally applicable for granular base (subbase) and subgrade materials are, respectively,

$$E_{B(SB)} = A_1(A_2)\theta^{B_1(B_2)} \quad (3)$$

$$E_S = A_s\sigma_d^{-B_3} \quad (4)$$

where

E_B, E_{SB}, E_S = moduli of base, subbase, and subgrade;
A_1, B_1 = material constants for granular base;
A_2, B_2 = material constants for granular subbase;
A_3, B_3 = material constants for the subgrade;
θ = $(\sigma_1 + \sigma_2 + \sigma_3)/3$ in situ bulk stress; and
σ_d = $\sigma_1 - (\sigma_2 + \sigma_3)/2$ in situ deviatoric stress, in which σ_1, σ_2, and σ_3 are in situ principal stresses.

The weight of overlaying layers and the static load of the deflection measuring device constitute the in situ stress at a point.

After the layer moduli have been determined, the Chevron program is used to compute the stress σ_d and

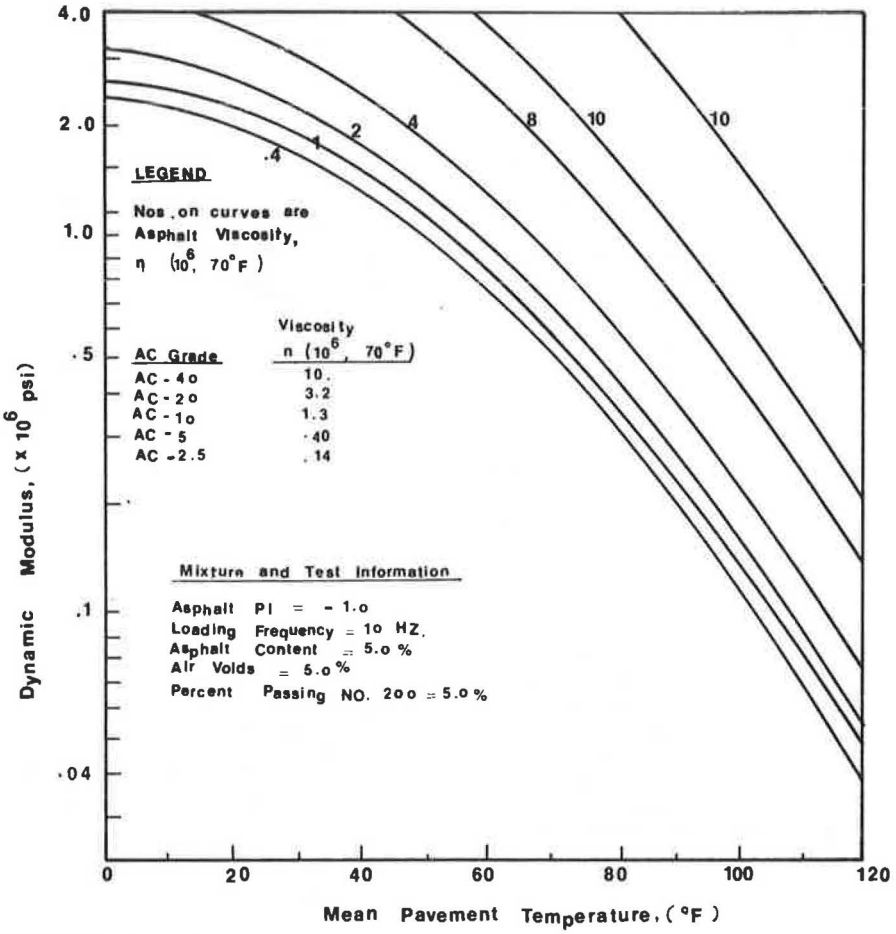

FIGURE 3 Estimation of the asphalt concrete dynamic modulus as a function of mean pavement temperature.

θ for the Dynaflect loading so that the constants A_1, A_2, and A_3 can be determined. Note that the constants B_1, B_2, and B_3 should be known and are, therefore, a known input to the program.

The layer theory occasionally predicts tensile bulk stresses; in that event Equation 3 is not defined; consequently, A_1 and A_2 cannot be determined. (Note that compressive stresses are assumed to be positive.) The base and the subbase moduli may then be corrected using the following empirical relationship (7):

$$E_{B(SB)} = A_1(A_2)(0.99 + 0.01\theta) \quad (5)$$

Input Data for IMD Program

Data, primarily material properties and response deflections, constitute the input for the IMD program. Pavement layer thickness and material characteristics that include the "guessed" modulus values, Poisson's ratio, and the unit weights of each layer are the required material properties. Representative sensor deflections (five in all) comprise the remaining input data. A step-by-step procedure to prepare the input data and a sample input-output of an example problem can be found elsewhere (17).

In summary, the IMD program uses a deflection matching technique to derive the in situ moduli of pavement layers. The computed AC modulus is subsequently corrected for temperature, and the base, subbase, and subgrade moduli, as applicable, are corrected for stress dependency.

COMPARATIVE STUDY OF IMD PROGRAM

The IMD program, as envisioned in this paper, enables the engineer to estimate the mechanistic properties of a pavement system employing pavement deflection data. This section is intended to provide at least partial verification of the program. Also illustrated are the application of the program and its use in evaluating pavement layer moduli employing input data from devices such as the Dynaflect or the falling weight deflectometer (FWD). Several IMD solutions are obtained from Dynaflect data ascertained from various sources. The following comparisons and evaluations establish the applicability of the program:

1. Comparing the IMD solution with the "standard" OAF program output;
2. Adjusting field deflection data to improve the solution procedure; and
3. Adapting the IMD program to other deflection data, for instance those from the FWD.

Comparison of IMD and OAF Solutions

Five sets of Dynaflect data (7), given in Table 1, are analyzed for layer moduli using the IMD as well

TABLE 1 Measured Dynaflect Deflection Data *(7)*

Section No.	Location	Layer Thickness (in.)		Type of Data	Deflection (mils) for Radial Distance of				
		Surface	Base		10.00 in.	15.62 in.	26.00 in.	37.36 in.	49.03 in.
1	Abondale, Arizona								
	Before overlay	4.0	8.0 (gravel)	Measured	1.458	0.990	0.690	0.456	0.334
				Adjusted	1.450	1.100	0.690	0.456	0.310
	After overlay	4.0 + 2.0-in. overlay	8.0 (gravel)	Measured	0.926	0.748	0.576	0.354	0.252
				Adjusted	0.926	0.800	0.550	0.380	0.260
2	Benson, Arizona								
	Before overlay	7.75	4.0 (gravel)	Measured	1.180	0.668	0.430	0.249	0.140
				Adjusted	0.950	0.668	0.430	0.250	0.160
	After overlay	7.75 + 1.75-in. overlay	4.0 (gravel)	Measured	0.742	0.562	0.314	0.198	0.131
				Adjusted					
3	Dead River, Arizona								
	Before overlay	7.25	6.0 (cement treated)	Measured	1.458	1.206	0.876	0.692	0.524
				Adjusted	1.520	1.206	0.910	0.660	0.524
	After overlay	7.25 + 3.25-in. overlay	6.0 (cement treated)	Measured	0.750	0.712	0.600	0.508	0.356
				Adjusted	0.820	0.750	0.620	0.480	0.356
4	Lupton, Arizona								
	Before overlay	4.0	6.0 (cement treated)	Measured	1.152	0.912	0.664	0.524	0.358
				Adjusted	1.142	0.960	0.730	0.524	0.358
	After overlay	4.0 + 3.5-in. overlay	6.0 (cement treated)	Measured	0.642	0.534	0.456	0.372	0.302
				Adjusted	0.622	0.564	0.456	0.362	0.302
5	Crazy Creek, Arizona								
	Before overlay	4.0	6.0 (cement treated)	Measured	1.597	1.300	0.890	0.580	0.426
	After overlay	4.0 + 2.5-in. overlay	6.0 (cement treated)	Measured	0.860	0.718	0.598	0.470	0.333

Note: 1 in. = 25.4 mm; 1 mil = 0.0254 mm.

as the OAF solutions, and the results are given in Table 2. Moduli before and after overlay also are compared in the table. Columns 6 and 10 list the effective thicknesses (h_{eff}) calculated in accordance with the following equation, which was originally proposed by Odemark (20):

$$h_{eff} = \sum_{i=1}^{k-1} h_i (E_i/10{,}000)^{1/3}$$

where k is the number of layers and E_i is the modulus of the ith layer. For comparison purposes a 10,000-psi (69-MN/m²) (21) subgrade is adopted in calculating the effective thickness.

The OAF program consistently failed to predict the moduli of the cement-treated base (CTB) layer of a stabilized pavement. Without exception, the IMD program did predict reasonably accurate modulus values for the CTB layer. For gravel base pavements, also, the IMD program predicted moduli far better than those predicted by the OAF program. For example, the OAF program predicted moduli of 5,779,000 psi (39 846 MN/m²) and 4,200 psi (29 MN/m²), respectively, for AC surface and gravel base compared with IMD-estimated values of 70,000 psi (483 MN/m²) and 91,400 psi (630 MN/m²). The reasonableness of the solutions is further assessed by comparing the effective thickness of a given pavement before and after overlay. It is gratifying to note that the difference between before and after effective thicknesses is approximately equivalent to the overlay thickness as listed in column 2 of Table 1. Effective thicknesses calculated in accordance with the OAF program do not meet this requirement, however. The foregoing results suggest that the IMD program can provide reasonable engineering solutions for flexible pavement systems of all types: full depth, gravel base, or cemented base.

TABLE 2 Comparison of IMD and OAF Solutions

Section No.	Location	Overlay	IMD Solution				OAF Solution			
			Surface Modulus (psi)	Base Modulus (psi)	Subgrade Modulus (psi)	h_{eff} (in.)	Surface Modulus (psi)	Base Modulus (psi)	Subgrade Modulus (psi)	h_{eff} (in.)
1	Abondale, Arizona	Before	70,000	91,400	6,300	24	5,779,000	4,200	11,700	39
		After	250,000	45,100	6,800	31	239,000	77,900	7,600	33
2	Benson, Arizona	Before	70,000	12,700	7,800	19	100,000	15,700	8,500	21
		After	83,800	42,700	10,300	26	443,000	5,100	16,100	37
3	Dead River, Arizona	Before	462,800	102,200	5,100	39	117,000		5,100	
		After	162,000	499,900	7,300	49	412,000		7,400	
4	Lupton, Arizona	Before	500,000	264,000	6,900	33	241,000		7,100	
		After	271,900	500,000	9,400	45	458,000		10,400	
5	Crazy Creek, Arizona	Before	174,900	89,900	4,900	23	109,000		5,400	
		After	500,000	292,900	8,800	45	350,000		8,200	

Note: 1 psi = 6.89 kPa and 1 in. = 25.4 mm.

Adjusting Field Deflection to Improve Solution

Although the IMD program is a valuable tool for assessing pavement condition, in the event that inconsistent data (deflection readings describing the deflection basin) are input to the program, it can produce completely misleading results that could lead to erroneous conclusions. In the case of pavements, the deflection data are often subject to fairly wide ranges of interpretation simply because the engineer is working with materials that have been altered in varying degrees by the forces of nature. Therefore, it should be emphasized, as with most other types of numerical analysis, that the final results are as valid as the data used as input to the computations.

To even out systematic measurement errors, it is advised that several (no fewer than 10) sets of deflection readings be ascertained from the field with the mean values serving as input data for the IMD program. Nonetheless, the engineer should attempt a quick check of the reasonableness of the sensor deflections. The sensor readings defining a deflection basin might be satisfactory provided that (a) the deflection basin conforms to a concave (upward) surface in a log-log plot and (b) the rim of the basin (defined by sensor deflections w_5 and w_4 with or without w_3) approaches a straight line in the same plot.

To illustrate the correction procedure, reference is made to Table 1, in which the raw deflection data, as well as the same data after adjustment in accordance with the foregoing discussion, are given. How the raw data of sections 3 and 4 are adjusted is graphically shown in Figure 4. The modulus values computed using the IMD program, with the raw and adjusted deflection basin, are given in Table 3. It is encouraging to note that slight adjustments in the deflection bowl have improved the predicted modulus values of AC surface and gravel or the cement-treated layer of pavements, 1(B), 2(B), 2(A), and 3(B). Several other results derived from deflection data (7), though not reported here in the interest of brevity, suggest that smoothing of the deflection bowl causes a decrease in the AC modulus with a corresponding increase in the modulus of the cement-treated layer; the effective thickness remains nearly the same.

As revealed by the results in Table 3, the modulus value of cement-treated base layer is increased after overlaying. This increase may be attributed to the enhancement of structural integrity of the pavement.

Layer Moduli Using IMD Program with FWD Data

Whether deflection data, other than Dynaflect-generated data, can be input in the IMD program is examined in this section. Due in part to its versatility, the falling weight deflectometer is chosen for comparison. Recent investigations (10) have

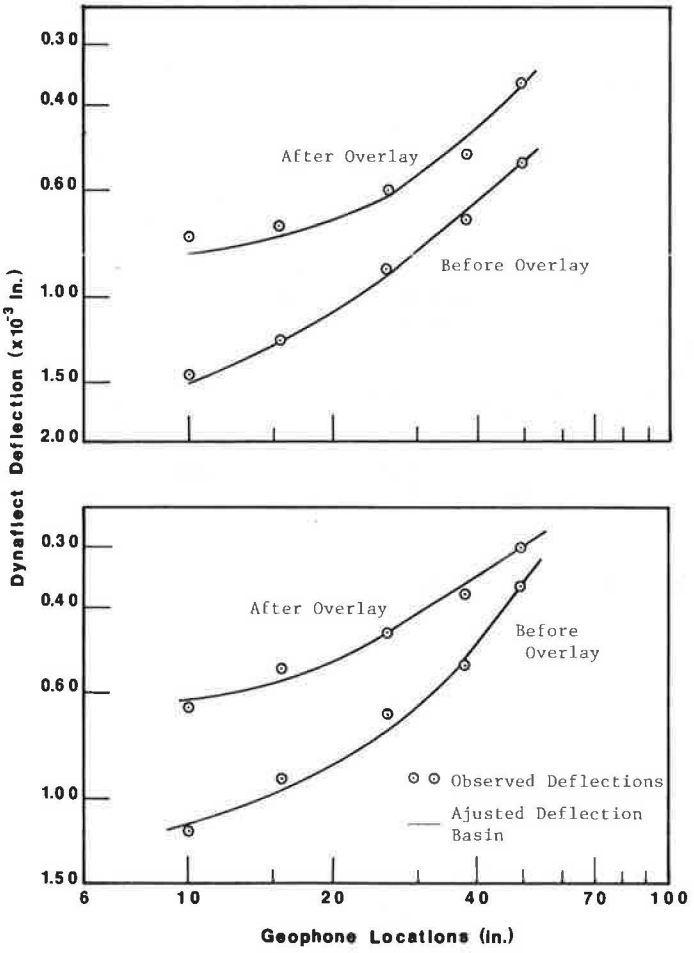

FIGURE 4 Comparison of Dynaflect deflection readings with the adjusted deflection basin.

TABLE 3 Improving In Situ Moduli by Modifying Deflection Basin

Section No.	Location	Overlay	IMD Solution for Measured Deflection Data: Surface Modulus (psi)	Base Modulus (psi)	Subgrade Modulus (psi)	h_{eff} (in.)	IMD Solution for Adjusted Deflection Data: Surface Modulus (psi)	Base Modulus (psi)	Subgrade Modulus (psi)	h_{eff} (in.)
1	Benson, Arizona	Before	70,000	12,700	7,800	19	70,000	57,900	8,800	22
		After	83,800	42,700	10,300	26				
2	Dead River, Arizona	Before	463,000	102,000	5,100	39	208,800	90,000	4,800	32
		After	162,000	500,000	7,300	49	332,000	90,000	7,100	46
3	Lupton, Arizona	Before	500,000	264,000	6,900	33	330,600	499,500	6,800	35
		After	272,000	500,000	9,400	45	300,000	500,000	9,400	45

Note: 1 psi = 6.89 kPa and 1 in. = 25.4 mm.

shown that the FWD loading system simulates the effect of a moving 9-kip (40-kN) wheel load and does so in terms of load intensity and, to a lesser extent, duration or time of loading (for a specific point on the pavement). To use the FWD deflection data in the IMD program, however, one modification must be made; that is, substitute the appropriate FWD load for the Dynaflect load.

The FWD data, as given in Table 4 (10), are input in the IMD program and in situ moduli are calculated and are given in Table 5. Tabulated for comparison purposes are the moduli calculated using the in situ stress-dependent elastic moduli, four-layer (ISSEM 4) program of Dynatest (10). The AC modulus of 875,900 psi (6038 MN/m²) at 64.4°F (18°C) better corroborates the results reported elsewhere (13), including those of the authors of the ISSEM 4 program (10). Only AC modulus is temperature dependent, as indicated by the data in Table 5. The moduli of the layers, which include the base, subbase, and subgrade, however, are poorly predicted by the IMD program. See the first column of Table 4 for each temperature. As has been discussed in the previous section, the deflection basin is smoothed by slightly correcting the last sensor deflection (Table 4) with substantial improvement in the entire output (Table 5). Further improvement is sought by treating the pavement as a three-layer problem. It is encouraging to note that all of the IMD-predicted moduli, with the AC modulus approaching the published values (13), show good agreement with those of the ISSEM 4 solution. The near equality of the effective thicknesses estimated with the two sets of modulus values (compare columns 6 and 11 of Table 5) may be offered as further proof of the overall agreement between the two solution procedures.

CONCLUDING REMARKS

A methodology and algorithm (the IMD program) for the evaluation of in situ moduli of individual pavement layers on the basis of measured Dynaflect deflections were presented. The algorithm is based on a deflection matching technique in conjunction with a multilayer elastic analysis such as Chevron. The deflection equation is inverted by a nonlinear pattern search technique to determine the values of the layer moduli that would best fit the observed surface deflections.

The applicability of the program is illustrated by comparing solutions with those of the standard OAF program (7). Several comparisons, of which only a few are reported here, suggest that the IMD program predicts more realistic modulus values than does the OAF program. In addition, the IMD program

TABLE 4 Falling Weight Deflectometer Data for AC Surface = 7.0 in., Lime Rock Base = 10.43 in., and Subbase = 12.20 in. *(10)*

Temperature (°F)	Falling Weight Deflectometer Data	Radial Distance (in.) 0.00	12.00	17.72	29.50	47.24
64.4	Deflection (mils)	8.070	5.905	4.645	3.031	1.614
		8.070[a]	5.905[a]	4.645[a]	3.031[a]	2.000[a]
80.6	Deflection (mils)	7.047	4.173	3.149	2.027	1.181

[a]Adjusted deflections.

TABLE 5 Layer Moduli Using IMD Program with Falling Weight Deflectometer Data Listed in Table 4

Temperature (°F)	Layer Moduli (IMD Solution): Surface Modulus (psi)	Base Modulus (psi)	Subbase Modulus (psi)	Subgrade Modulus (psi)	h_{eff} (in.)	Layer Moduli (ISSEM 4 Solution): Surface Modulus (psi)	Base Modulus (psi)	Subbase Modulus (psi)	Subgrade Modulus (psi)	h_{eff} (in.)
64.4	875,000	89,100	9,200	63,000	65	1,027,000	68,000	29,000	29,000	70
	757,400	87,500	20,000	39,300	67[a]					
	753,000	70,000		33,200	68[b]					
80.6	566,000	67,100	59,600	66,300	69	586,400	91,000	49,000	45,000	69
	544,400	79,600		52,400	69					

Note: 1 in. = 25.4 mm, 1 psi = 6.89 kPa, and °C = (F - 32) (5/9).
[a]Four-layer solution with adjusted deflections.
[b]Three-layer solution.

is amenable to solution by deflection data from the falling weight deflectometer.

A few pointers may help to improve the solution procedure. First, the deflection data, if erroneous, should be corrected; and second, special attention should be paid to modeling the pavement. A set of consistent sensor readings would have the deflection basin conform to a concave (upward) surface in a log-log plot, and the rim of the basin approaches a straight line in the same plot. Experience also indicates that problems arise when the first and second sensor deflections are nearly equal, perhaps because of erroneous field data. Thin wearing surfaces do not contribute substantially to the strength of the pavement structure. For this reason, a wide range of modulus values may fit to satisfy deflection; therefore, this layer may be combined with an adjacent layer of similar characteristics. Finally, many pavement systems of more than three layers may well be solved using a three-layer model. For pavements of four or more layers the authors suggest reducing the system initially to a three-layer model; if it does not lend itself to solution, a four-layer model may be tried.

ACKNOWLEDGMENT

This paper is a part of a research study entitled "Overlay Design and Reflection Cracking Analysis for Pavements" sponsored by the Mississippi State Highway Department and the Federal Highway Administration, U.S. Department of Transportation. The authors acknowledge the suggestions and continued support offered by J.P. Sheffield and A.B. Crawley of the Highway Department.

REFERENCES

1. J.M. Duncan, C.L. Monismith, and E.L. Wilson. Finite Element Analysis of Pavements. In Highway Research Record 228, HRB, National Research Council, Washington, D.C., 1968, pp. 18-34.
2. D.M. Burmister. The General Theory of Stresses and Displacements in Layered Soil Systems I. Journal of Applied Physics, Vol. 16, 1945.
3. F. Moavenzadeh and J.E. Ashton. Analysis of Stresses and Displacements in a Three-Layer Viscoelastic System. Research Report 67-31. Department of Civil Engineering, Materials Research Laboratory, Ohio State University, Columbus, 1967.
4. F.H. Scrivner, C.H. Michilak, and W.M. Moore. Calculation of the Elastic Moduli of a Two-Layer Pavement System for Measured Surface Deflections. In Highway Research Record 431, HRB, National Research Council, Washington, D.C., 1973, pp. 12-25.
5. W.H. Cogill. The Utilization of the Results of the Measurements of Surface Deflection Profiles as a Means of Estimating the Stiffness of Pavement Materials. Proc., Australian Road Research Record, Vol. 6, Part 4, 1972, pp. 142-149.
6. L.H. Irwin. Determination of Pavement Layer Moduli from Surface Deflection Data for Pavement Performance Evaluation. Proc., Fourth International Conference on Structural Design of Asphalt Pavements, University of Michigan, Ann Arbor, 1977, pp. 831-840.
7. K. Majidzadeh and G.J. Ilves. Flexible Pavement Overlay Design Procedures. Report FHWA/RD-81/032. FHWA, U.S. Department of Transportation, Vol. 1, 1981.
8. W.P. Kilareski and B.A. Anani. Evaluation of In-Situ Moduli and Pavement Life from Deflection Basins. Proc., Fifth International Conference on Structural Design of Asphalt Pavements, Delft, The Netherlands, 1982, pp. 349-365.
9. P. Ullidtz. Overlay and Stage by Stage Design. Proc., Fourth International Conference on Structural Design of Asphalt Pavements, University of Michigan, Ann Arbor, 1977, pp. 722-735.
10. R.N. Stubstad and J. Sharma. Deriving Mechanistic Properties of Pavement Layers from Surface Deflections. International Conference on Computer Applications in Civil Engineering, Roorkee, India, 1979.
11. N.K. Vaswani. Design of Flexible Pavements in Virginia Using AASHO Road Test Results. In Highway Research Record 291, HRB, National Research Council, Washington, D.C., 1969, pp. 89-103.
12. R.A. Jimenez. Pavement-Layer Modular Ratios from Dynaflect Deflections. In Transportation Research Record 671, TRB, National Research Council, Washington, D.C., 1978, pp. 23-28.
13. K. Majidzadeh. Dynamic Deflection Study for Pavement Condition Investigation. Ohio Department of Transportation, Columbus, 1974.
14. H.J. Treybig. Mechanistic Method of Pavement Overlay Design. In Transportation Research Record 700, TRB, National Research Council, Washington, D.C., 1979, pp. 72-77.
15. R.L. Lytton, C.H. Michalak, and T. Scullion. The Texas Flexible Pavement Design System. Proc., International Conference on Structural Design of Asphalt Pavements, Delft, The Netherlands, 1982.
16. V.Z. Vlasov and N.N. Leont'iev. Beams, Plates, and Shells on Elastic Foundation (translated from Russian). Israel Program for Scientific Translations, Jerusalem, 1966.
17. S. Husain. In-Situ Pavement Moduli Using Dynaflect Deflection. M.S. thesis. University of Mississippi, University, 1984.
18. M.W. Witczak. Development of Regression Models for Asphalt Concrete Modulus for Use in MS-1 Study. The Asphalt Institute, College Park, Md., 1978.
19. H.F. Southgate. An Evaluation of Temperature Distribution Within Asphalt Pavements and Its Relationship to Pavement Deflection. Department of Transportation of Kentucky, Frankfort, 1968.
20. N. Odemark. Investigations as to the Elastic Properties of Soils and Design of Pavements According to the Theory of Elasticity. Staten Vaeginstitut, Stockholm, Sweden, 1949.
21. A.A.A. Molenaar and Ch.A.P.M. VanGurp. A Pavement Management System for Provincial Roads in The Netherlands. Proc., International Conference on Structural Design of Asphalt Pavements, Delft, The Netherlands, 1982.

The opinions, findings, and conclusions expressed in this paper are those of the authors and not necessarily those of the Mississippi State Highway Department or the Federal Highway Administration. This paper does not constitute a standard, specification, or regulation.

Discussion

Waheed Uddin*

Determination of in situ Young's moduli of pavement layers based on dynamic deflection basins is an area of growing interest for researchers involved in non-

*7201 Hart Lane, Apt. 2085, Austin, Tex. 78731

destructive testing of pavements. At the TRB 64th Annual Meeting, two other papers (1,2) were presented that were also based on the inverse application of layered linear elastic theory to match measured deflection basins. A summary of different self-iterative computer programs is presented by Uddin et al. (1).

As pointed out by Uddin et al. (1), nearly all procedures require "guess" moduli in input data. The IMD program described by the authors is no exception and will produce user-dependent results. The moduli determined by the authors are apparently reasonable compared with OAF solutions but are not necessarily unique. The criterion selected by the authors for assuring uniqueness is "to limit the range of predicted moduli for each layer within certain plausible constraints." In other words, the proposed criterion for uniqueness is itself user dependent. It is interesting to examine the range of moduli selected by the authors for their example problems of Tables 2, 4, and 5.

Some other aspects that would be of interest in this self-iterative procedure are reproducibility of results if the limits of modulus ranges are changed, an example of the validity of the procedure for a pavement of known material properties, and an example for applicability to rigid pavements. A discussion of these points by the authors is warranted. In the IMD program, temperature correction for the AC layer is applied before stress sensitivity is taken into account. In the writer's opinion, it is not appropriate to call the final moduli in situ moduli if the test temperature is different from the design temperature. A logical approach is to determine in situ moduli at test temperature before correcting AC modulus to the standard temperature (1).

The authors apparently believe the misconception that a Dynaflect basin will result in higher moduli than those expected under a heavier design wheel load. This belief is not supported by any definitive field evidence. Bush and Alexander (2) describe results of a comparative study of a Dynaflect and several heavy load falling weight deflectometers. For almost all test areas, the subgrade moduli determined from the Dynaflect basin are comparable to the values evaluated for other heavier NDT devices. The writer's research experience at the University of Texas at Austin also does not show any definite trend of higher subgrade moduli predicted for a Dynaflect compared to those for a heavier falling weight deflectometer. The stress sensitivity approach for correction of Dynaflect moduli is based on laboratory resilient modulus (M_R) relationships. In general, the effects of loading mode and device dependency are ignored in this approach. A reasonable and rational method for deriving effective moduli of pavement layers is to perform an equivalent linear analysis based on the approach of strain sensitivity (1,3). This approach eliminates any laboratory M_R tests to determine material constants, and the problem of tensile bulk stress does not arise.

The moduli determined from FWD basins (Table 5) are yet another example of the nonuniqueness of IMD solutions. For the first FWD basin, the IMD program produced widely scattered moduli (33,200, 39,300, and 63,000) for the subgrade. The IMD program is designed for a semi-infinite subgrade. In the case of a rock layer at a shallow depth, this assumption will result in an overpredicted subgrade modulus (4).

The Dynaflect system has been subjected to accuracy checks and repeatability tests in numerous studies and has been found a reliable device. It is unexpected that measuring 10 basins and smoothing the resulting average basin for IMD analysis, as recommended by the authors, will be favored by any agency for routine use. It appears that the authors have experienced considerable variations and significant repeatability errors in their deflection basin data. Malfunctioning of the NDT device or its deflection measuring system could result in erroneous data. In the opinion of the authors, nearly same values of Sensor 1 and Sensor 2 deflections (low values of SCI) indicate erroneous field data. However, experience in Texas (4) shows that very small and even zero values of SCI are possible on rigid pavements.

Any smoothing or adjustment in a measured deflection basin should be avoided in the writer's opinion. The computer program could easily be modified to converge on a smoothed basin. The shape of a deflection basin is an important feature of pavement response and an indicator of the structural integrity of pavement layers. Figure 5 shows examples of different basin shapes based on the Dynaflect data.

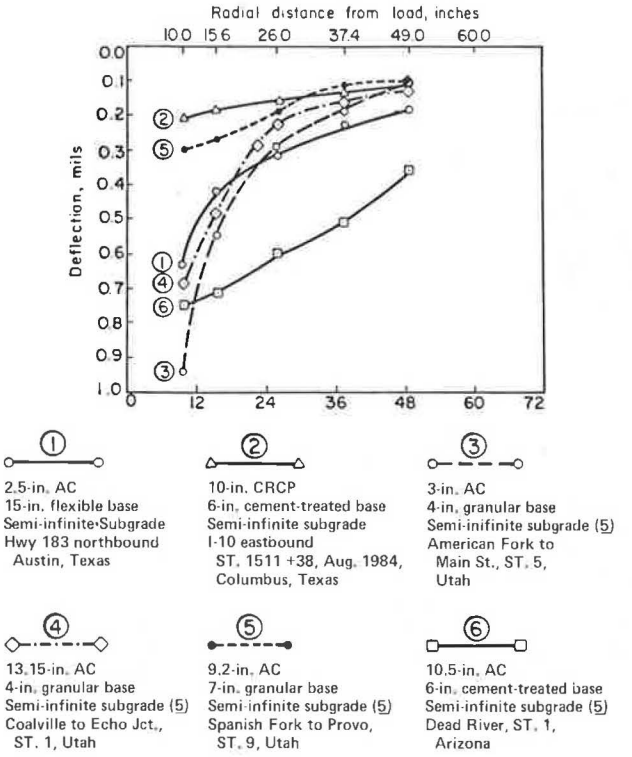

FIGURE 5 Examples of variations in deflection basin shapes (Dynaflect).

These basins are unique responses of these pavements and any alteration in measured deflections is not justifiable. Figure 4 would definitely be more useful if the authors had also plotted theoretical deflections corresponding to the iteration in which the IMD program converged in each case.

REFERENCES

1. W. Uddin, A.H. Meyer, W.R. Hudson, and K.H. Stokoe II. Project-Level Structural Evaluation of Pavements Based on Dynamic Deflections. In Transportation Research Record 1007, TRB, National Research Council, Washington, D.C., 1985, pp. 37-45.
2. A.J. Bush III and D.R. Alexander. Pavement Evaluation Using Deflection Basin Measurements and Layered Theory. In Transportation Research Rec-

ord 1022, TRB, National Research Council, Washington, D.C., 1985, pp. 16-25.
3. W. Uddin, A.H. Meyer, and W.R. Hudson. A Flexible Pavement Structural Evaluation System Based on Dynamic Deflections. Presented at the 1985 Annual Meeting of the Association of Asphalt Paving Technologists, San Antonio, Tex., Feb. 1985.
4. A. Taute, B. Arthur, F. McCullough, and W.R. Hudson. Improvements to the Material Characterization and Fatigue Life Prediction Methods of the Texas Rigid Pavement Overlay Design Procedure. Research Report 249-1. Center for Transportation Research, The University of Texas at Austin, March 1981.
5. K. Majidzadeh and G.J. Ilves. Flexible Pavement Overlay Design Procedures. Report FHWA/RD-81/032. FHWA, U.S. Department of Transportation, Vol. 1, 1981.

Authors' Closure

The authors wish to thank Uddin for his interest in the paper and offer the following comments.

In Uddin's interesting discussion, the authors are asked to examine the range of moduli selected initially for example problems of Tables 2, 4, and 5. It is significant to report that despite the values assumed in the routine, the IMD program predicted more or less the same in situ moduli. Another point concerns the reproducibility of results if the limits of modulus ranges are changed. The purpose of setting limits is to prevent the solution procedure from entering a nonfeasible region. As and when this happened, the program printed out a message to this effect. If limits are set, however, this problem is altogether eliminated. Concerning the validity of the IMD program, the authors wish to indicate that the program has been verified for pavements of known material properties.

The discusser's comment that the corrected moduli should be designated as the final moduli has some merit. The authors, however, contend that the name "in situ moduli" is appropriate because these moduli are truly field values.

The discusser asserts that the subgrade modulus determined from Dynaflect basin is comparable to the values evaluated by other heavier NDT devices including the falling weight deflectometer. Several previous studies have suggested (1,2), and the authors concur with them, that subgrade modulus of resilience is stress dependent. To the discusser's comment that strain sensitivity should be preferred to stress sensitivity relations to correct the moduli of particulate materials, the authors offer the explanation that the latter approach has a proven record of providing satisfactory results.

Citing different moduli obtained from four- and three-layer solutions, the discusser comments that IMD solutions may not be unique. The authors do recommend a three-layer solution as a first choice for any problem. The example cited in the paper serves to reinforce this contention because the three-layer solution resulted in a modulus of 33,200 psi, which compares well with the ISSEM 4 modulus of 29,000 psi.

Whether a zero SCI value can be observed in flexible pavements is another question raised by the discusser. The authors wish to reaffirm their contention that, unlike in rigid pavements, SCI in flexible pavements is neither zero nor very small as suggested by the discusser.

The smoothing of the deflection basin proposed by the authors has as its sole purpose detecting and delineating erroneous sensor readings. Modifying the computer program to converge on a smoothed basin, as suggested by the discusser, is certainly a viable alternative.

REFERENCES

1. K. Majidzadeh and G.J. Ilves. Flexible Pavement Overlay Design Procedures. FHWA/RD-81/032. FHWA, U.S. Department of Transportation, Vol. 1, 1981.
2. H.T. Treybig, B.F. McCullough, F.N. Finn, and R. McComb. Design of Asphalt Concrete Overlays Using Layer Theory. Fourth International Conference on Structural Design of Asphalt Pavements, University of Michigan, Ann Arbor, 1977.

Publication of this paper sponsored by Committee on Strength and Deformation Characteristics of Pavement Sections.

Use of Dynamic Analysis in Predicting Field Multilayer Pavement Moduli

MICHAEL S. MAMLOUK

ABSTRACT

The response of a multilayer pavement system to dynamic loading excitations is discussed and compared with the static response. Field Road Rater deflection data previously obtained at the Pennsylvania Transportation Research Facility are used to backcalculate pavement layer stiffnesses using the elastodynamic technique. Sets of layer moduli and fundamental frequencies are developed for five sections of the test track. The amount of error associated with the use of the static analysis commonly used is also evaluated. The dynamic analysis incorporates the inertial effect (radiation damping and resonance) of the pavement structure that cannot be included within static analyses. Simply replacing the Young's modulus in a static analysis by the resilient modulus or the dynamic modulus does not change it to a dynamic analysis. Unless the inertia of the system is considered in the interpretation of the dynamic response of pavements, misleading results may develop.

Surface deflection measurements of pavements have gained wide acceptance in the past few decades. Unlike laboratory testing, the deflection measurement technique is fast and relatively accurate and can be used to evaluate the structural condition of a pavement system with a minimum of disturbance and cost. In this technique a load is applied to the pavement and the surface deflection is measured. With the exception of Benkelman beam and California continuous deflectometer, most of the deflection measurement devices are dynamic in nature. Among such devices are the Dynaflect, the Road Rater, various vibrators, and the falling weight deflectometer. The first three devices impart steady-state (harmonic) loading with either constant or variable frequencies, and the latter device imparts impulsive (transient) loading. In the case of harmonic loadings, peak-to-peak deflections are measured at several distances from the load from which the envelope of the surface movement is determined.

Mechanistic analyses of the data obtained from dynamic loading devices have hitherto been based on elastostatic and viscoelastostatic models (1-6) in which, obviously, the inertia of the pavement plays no part. Several computer programs are currently used in analyzing the dynamic response of pavement. These programs are based on static analyses such as Chevron, VESYS, BISTRO, BISAR, and so forth. Thus it is tacitly assumed that the dynamic response of pavement structures is similar (if not identical) to the static response.

The stress-strain relations of isotropic elastic materials are expressed in terms of moduli (Young's modulus, shear modulus, etc.). Stress-strain moduli such as the resilient modulus and the dynamic modulus are sometimes used to interpret the inelastic and time-dependent response of materials. The resilient modulus represents the stress-strain relationship after many load repetitions (i.e., current modulus of the material, which is normally different from the initial value). On the other hand, the dynamic modulus is a frequency-dependent parameter obtained from dynamic loading tests on a finite specimen.

The governing differential equations of elastodynamics include the inertial effect (radiation damping and resonance) of the pavement structure that cannot be incorporated within static analyses. Simply replacing Young's modulus in a static analysis by the resilient modulus or the dynamic modulus is insufficient to recover the elastodynamic equations.

Backcalculated material properties are sensitive to minor changes in surface deflections. Thus use of an erroneous static analysis in backcalculating the material properties from dynamic surface deflections may result in large error magnifications. Although nonlinear elastic models of pavement structures (3) likely offer some improvement over linear elastic models, more significant modeling errors may result from neglecting the inertial response of pavements.

The objective of this study is to use the elastodynamic analysis in backcalculating the stiffnesses of various layers of an actual pavement structure (Pennsylvania Transportation Research Facility). Field surface deflections, which were previously obtained using the Road Rater, are reanalyzed in the present study using dynamic analysis. The resonant frequencies of various pavement sections are determined. A comparison of static and dynamic analyses is presented.

CONCEPT OF DYNAMIC ANALYSIS

The governing equation for steady-state elastodynamics is the Helmholtz equation (7):

$$\mu u_{i,jj} + (\lambda + \mu)\, u_{j,ij} + \rho\omega^2 u_i = 0 \qquad (1)$$

where

λ, μ = Lame's constants that are related to Young's modulus and Poisson's ratio,
ρ = mass density,
ω = circular frequency of excitation, and
u_i = ith cartesian component of the displacement vector.

In Equation 1 cartesian indicial notation, in which the subscripts range from 1 to 3, is assumed; addition is implied over repeated subscripts; and a comma

denotes differentiation with respect to the space variable (i.e., $u_{i,j} = \partial u_i/\partial x_j$). Also, the displacements are assumed to be time harmonic.

The usual assumptions of material linearity and isotropy are invoked. Soil and pavement layers are assumed to be unbounded laterally but are underlaid by a rigid bedrock or incompressible layer at a finite depth. Full interface bonding (no slip) conditions are assumed at the layer interfaces.

In addition to the usual elastic constants (Young's modulus and Poisson's ratio) and the mass density, a fourth constant (damping ratio) may be specified to characterize the material damping (internal energy dissipation) of each layer (8). In other words, the viscoelasticity of the pavement materials is considered through the use of the damping ratio. A typical value of 5 percent was assumed in this study (8). The damping of the materials can also be indirectly considered through the use of the complex modulus rather than the dynamic modulus without the viscous term.

It should be noted that the material damping is virtually negligible because by far the major component of energy dissipation in continua results from radiation (geometric) damping; that is, the dispersion of energy from the source of excitation to the far field. The radiation damping is implicitly incorporated in the elastodynamic solution.

The solution of Equation 1 for a point load in a half-space can be expressed in the form:

$$u_i(x, \omega) = G_{ij}(x, \xi, \omega) P_j(\xi, \omega) \quad (2)$$

where

u_i = the ith displacement component,
G_{ij} = Green's function (a mathematical solution used to reduce the order of integration if the boundary values are known),
P_j = the jth load component,
x = coordinates of field point,
ξ = coordinates of load point, and
ω = circular frequency of excitation.

Analytical integration of the point load solution yields the disk load solution. However, no closed-form solutions are available for excitation of layered systems. Therefore solutions must be obtained by numerical means.

Kausel and Peek (9) have recently proposed a numerical technique that renders the elastodynamic problem of layered systems tractable. The solution is based on the assumption that the displacement field is linear in the direction of layering between adjacent interfaces. Thus sufficiently thin layers must be specified to ensure the validity of this representation. In practice, artificial sublayers may be introduced to satisfy this requirement. More details about the dynamic behavior of materials are found elsewhere (7-11).

FIELD MEASUREMENTS

Field measurements were obtained in March 1976 at the Pennsylvania Transportation Research Facility by Anani (5). The facility is a 1-mi, single-lane, oval-shaped, full-scale experimental highway. The construction, instrumentation, and operation of the research facility are discussed elsewhere (12).

In the present study, five test sections were considered: 1c, 1d, 2, 7, and 9, which had similar surface temperature, moisture content, and cumulative equivalent axle loads (ΣEALs) at time of testing. Each pavement section consisted of four layers: surface, base, subbase, and subgrade, with material properties as given in Table 1. The layer thicknesses of the five test sections are given in Table 2. It should be noted that not enough information is available about the thickness of the compressible subgrade layer under the subbase and above the incompressible layer or the bedrock. A thickness of 20 ft was assumed.

TABLE 1 Material Properties of Test Sections of Pennsylvania Transportation Research Facility *(12)*

Layer	Material Type	Density (lb/ft³)
Surface	Bituminous concrete	145
Base	Bituminous concrete	141
Subbase	Crushed limestone	141
Subgrade	Predominantly A-7 soil	124

TABLE 2 Layer Thicknesses of Test Sections of Pennsylvania Transportation Research Facility *(12)*

	Thickness (in.)		
Section	Surface	Base	Subbase
1c	1.5	6	8
1d	1.5	6	6
2	2.5	6	8
7	1.5	8	8
9	2.5	4	8

Surface deflection measurements (5) were obtained using the Road Rater device, Model 400. The Road Rater had two loading plates (4 in. x 7 in. each) and four deflection measurement sensors (geophones) 1 ft apart as shown in Figure 1. The Road Rater was operated to provide a simple harmonic loading with a frequency of 25 Hz and a peak-to-peak contact pressure of 13 psi under each plate in addition to a static pressure of approximately 27 psi. The peak-to-peak deflections were measured at each of the four geophone locations. Two sets of deflection readings obtained under approximately the same conditions from each test section were analyzed in the present study.

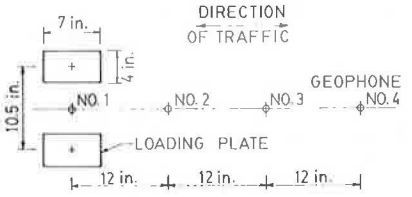

FIGURE 1 Schematic diagram of the Road Rater.

The surface temperature at the time of the measurements was 64°F and the moisture content ranged between 20.1 and 20.7 percent. The cumulative equivalent axle load experienced by the pavements before the measurements ranged between $1,296 \times 10^3$ and $1,336 \times 10^3$. The Road Rater deflection readings ($RR\delta_1$, $RR\delta_2$, $RR\delta_3$, and $RR\delta_4$) measured in an outward

direction in addition to other associated data are given in Table 3.

BACKCALCULATION OF LAYER STIFFNESSES

The inverse problem of determining material properties from the response of the pavement structure to surface loading (from nondestructive deflection testing) is not easy to solve. No direct theoretical solution is available in the literature to determine the material properties of a multilayered system if the surface deflections and the layer thicknesses are known. Therefore it is necessary to employ iterative schemes based on the fact that surface deflections remote from the loaded area are primarily governed by the stiffness of the deeper layers. This has been indicated in several previous sensitivity analyses (5,6).

TABLE 3 Road Rater Deflection Measurements and Associated Data *(5)*

Section	Deflection Measurements ($\times 10^{-6}$ in.) RR δ_1	RR δ_2	RR δ_3	RR δ_4	Surface Temperature (°F)	Moisture Content (%)	ΣEAL (x 1,000)
1c	645	457	285	167	64	20.1	1,296
	555	427	265	168	64	20.7	1,336
1d	801	543	311	167	64	20.1	1,296
	661	474	266	162	64	20.7	1,336
2	423	340	253	166	64	20.1	1,296
	446	355	247	182	64	20.7	1,336
7	410	333	247	177	64	20.1	1,296
	405	343	250	187	64	20.7	1,336
9	817	558	266	140	64	20.1	1,296
	795	517	245	138	64	20.7	1,336

Using the iteration technique, the number of unknown parameters must be less than or equal to the number of the measured surface deflections. Because there are only four geophones in the Road Rater used, the maximum number of unknown material properties that may be determined is four. If Poisson's ratios and material damping factors are assumed, the material stiffnesses of the four layers may be calculated. The procedure, however, can be easily adapted for pavement systems with more than four layers if more sensors are used in each Road Rater run.

An iterative process was used in this study to backcalculate the in situ layer moduli for the pavements at the Pennsylvania Research Transportation Facility. The iterative procedure used here is similar to the procedure followed by Kilareski et al. (6), except that the dynamic analysis is used. A computer program, DYNAMIC, was developed for this purpose (see flow chart in Figure 2). The program starts with input of the Road Rater data ($RR\delta_1$, $RR\delta_2$, $RR\delta_3$, and $RR\delta_4$). Initial layer moduli (E_1, E_2, E_3, and E_4) are assumed to represent the moduli of surface, base, subbase, and subgrade materials, respectively. Poisson's ratios of 0.35, 0.4, 0.4, and 0.45 are assigned to the four layer materials, respectively. Surface deflections consistent with the assumed material properties are computed using the procedure developed by Kausel and Peek (9). The loading platens of the Road Rater device are idealized by twin flexible circular plates (28 $in.^2$ each) spaced 10.5 in. center to center.

The calculated deflections (δ_1, δ_2, δ_3, and δ_4) are compared with the Road Rater deflection measurements ($RR\delta_1$, $RR\delta_2$, $RR\delta_3$, and $RR\delta_4$). The differences between the calculated and the measured deflections are assumed to be entirely due to incorrectly assumed E-values. The correction starts with the outermost reading and the lowest layer (subgrade), with the assumption that the difference between δ_4 and $RR\delta_4$ is primarily due to an erroneous assumption for the subgrade modulus (E_4). A new value of E_4 is calculated for the next iteration as follows:

$$E_{i(new)} = E_{i(old)} \times [(RR\delta_i + \delta_i)/2]/RR\delta_i \quad (3)$$

where

$RR\delta_i$ = measured deflection,
δ_i = calculated deflection, and
i = 4.

This method of correction adjusts only one-half of the discrepancy to assure a gradual convergence. This correction will reduce the value of E_4 if the calculated deflection is too small, which implies that the assumed value of E_4 is too large.

The correction of E_4 will influence all other calculated deflections, so the next interation produces a new set of δ-values. Using the newly computed values of δ, the subbase modulus (E_3) is adjusted using $RR\delta_3$ and δ_3 using Equation 3 with i = 3. A new set of deflections is then computed using the new E_3 value and previous E_1, E_2, and E_4 values. The value of E_2 is then adjusted followed by E_1 using similar procedures. Thus, after four calculations have been made, a new set of moduli has been generated. This interative process is followed until the differences between the calculated and the measured deflections for all geophones are within a predetermined tolerance (δ_{tol}) of 4 percent, which was found to provide reasonably accurate results. The percentage differences in deflection measurements [$\%\delta_{i(diff)}$] are calculated as follows:

$$\%\delta_{i(diff)} = ABS\,[(RR\delta_i - \delta_i)/RR\delta_i] \times 100\% \quad (4)$$

where i takes values of 1, 2, 3, or 4, representing the deflection points under consideration. To reduce unnecessary computer calculations, some limitations were imposed as shown in Figure 2.

RESULTS AND ANALYSIS

Because the Road Rater deflection measurements were obtained at an operating frequency of 25 Hz in the field, that frequency was incorporated in the backcalculation process. Using the aforementioned procedure, a set of layer moduli is obtained for each section of the test road analyzed. In addition to the dynamic analysis, a static analysis (with a frequency of zero) is used to backcalculate the layer moduli of the same sections using the same field deflection measurements obtained at 25 Hz. The main reason for the static analysis was to estimate the amount of error made when using the static analysis in analyzing the dynamic response of pavements. The average moduli of various pavement sections obtained using static and dynamic analyses, as well as the amount of error, are given in Table 4.

As the data in Table 4 indicate, the static analysis resulted in higher moduli for the upper two layers than those obtained from the dynamic analysis with average errors of 9 and 11 percent for the two layers, respectively. On the other hand, the static analysis resulted in a smaller subgrade modulus with an average error of 12 percent. The ratios of modulus values using dynamic analysis to modulus values using static analysis for individual road sections and various layer materials are shown in Figure 3. A careful look at this figure would show that the mod-

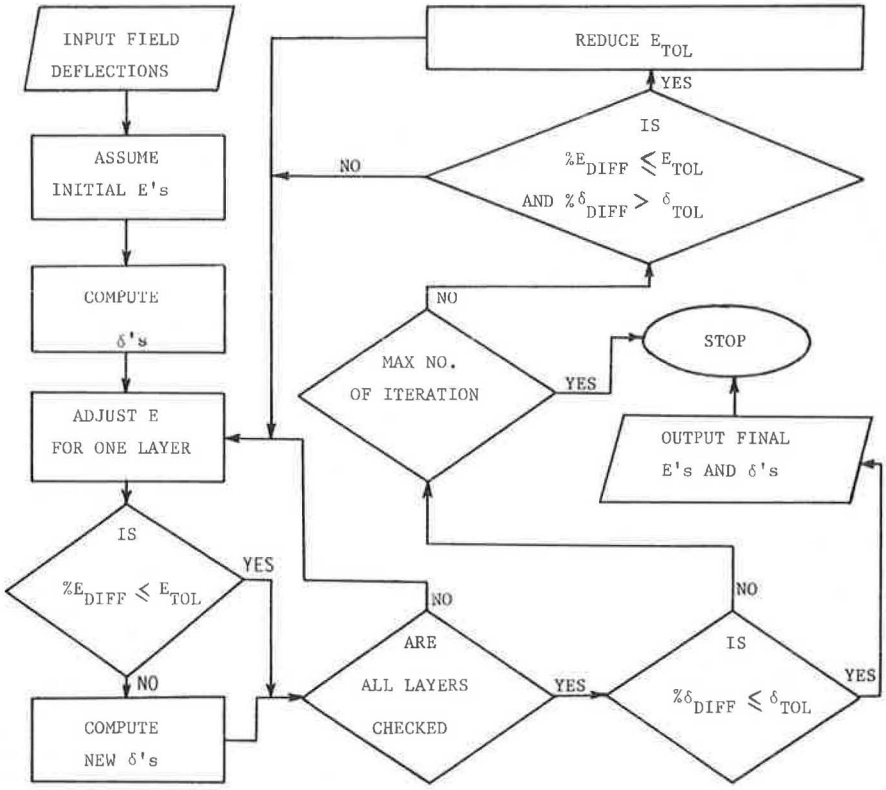

Notes: E_{DIFF} = absolute difference between new and old E values

δ_{DIFF} = absolute difference between measured and calculated δ values.

E_{TOL} and δ_{TOL} = tolerances in E and δ values (%)

FIGURE 2 Flow diagram for the DYNAMIC computer program.

TABLE 4 Average Moduli (ksi) of Various Layers Using Static and Dynamic Analyses

Layer	Analysis		Percentage Error
	Static	Dynamic	
Surface	707	647	9
Base	845	762	11
Subbase	15	15	0
Subgrade	29	33	-12

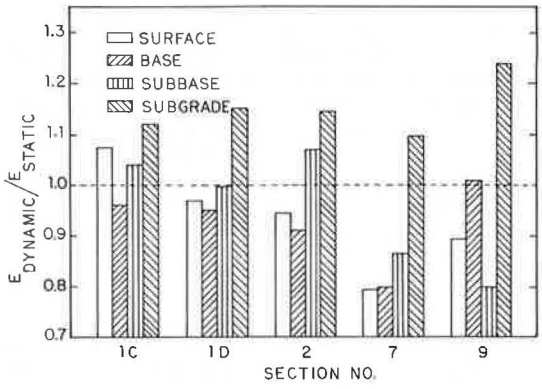

FIGURE 3 Ratios of modulus values obtained using dynamic and static analyses for various road sections.

uli of the top three layers were overestimated in some road sections and underestimated in other sections using static analysis, with no consistent trend. The modulus for the subgrade material, however, was always underestimated when static analysis was used. The largest amount of modulus overestimation due to the use of static analysis was obtained for the surface of Section 7 with an average error of 21 percent, and the largest amount of modulus underestimation was obtained for the subgrade of Section 9 with an average error of 24 percent. No general conclusion can be derived to evaluate the amount of error when static analysis is used because this error is a function of several factors including layer thicknesses, material stiffnesses, and the Road Rater operating frequency. Although the amount of error due to the use of static analysis appears to be relatively small in this study, a more serious situation might occur if the operating frequency of the deflection measurement device were close to the natural vibration frequency of the pavement system as discussed in subsequent paragraphs.

In the second step of the analysis the average layer moduli estimated from the two Road Rater measurements for each road section using the dynamic analysis were considered. Using these moduli, the dynamic responses of various road sections were evaluated at different Road Rater operating frequencies ranging from zero to 50 Hz. The ratios of dynamic surface deflection to static surface deflection for various road sections are shown in Figures 4-8, respectively. In each figure, four curves are shown

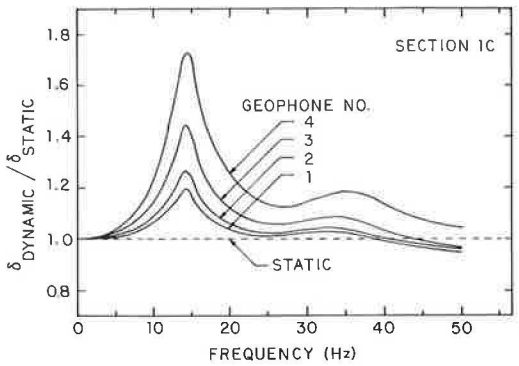

FIGURE 4 Dynamic-to-static deflection ratio for Section 1c at various frequencies and geophone locations.

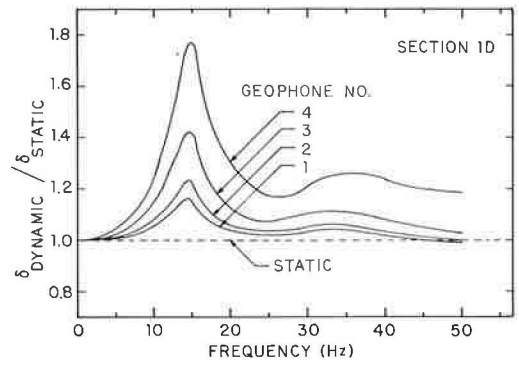

FIGURE 5 Dynamic-to-static deflection ratio for Section 1d at various frequencies and geophone locations.

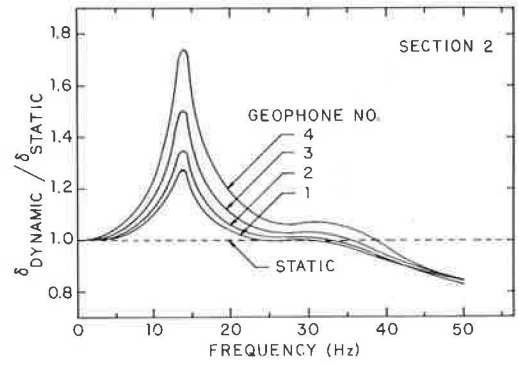

FIGURE 6 Dynamic-to-static deflection ratio for Section 2 at various frequencies and geophone locations.

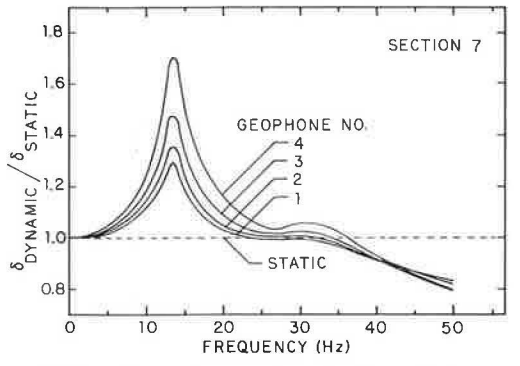

FIGURE 7 Dynamic-to-static deflection ratio for Section 7 at various frequencies and geophone locations.

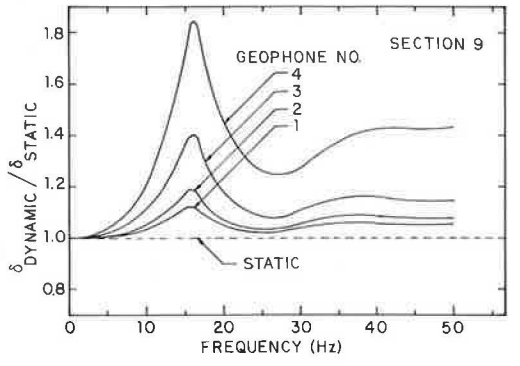

FIGURE 8 Dynamic-to-static deflection ratio for Section 9 at various frequencies and geophone locations.

for various geophones of the Road Rater. From these figures it can be concluded that the dynamic responses of the pavement system are more apparent when the distance from the load is increased. This is indicated by the gradual increase in the dynamic-to-static deflection ratio from geophone 1 through geophone 4 in all road sections. Therefore the amount of error made using static analysis in evaluating the dynamic response of pavement gets large when the deflection is measured at a large distance from the center of the load.

A more serious finding is that the natural vibration frequencies (fundamental frequencies) fall within the common range of the operating frequency of the Road Rater. This is indicated by the large ratio of dynamic-to-static deflections (large magnification factors). The resonant response of the pavement system occurs when the frequency of the applied load is equal to a natural vibration frequency of the pavement system. Note that for any pavement system there is a series of natural vibration frequencies, namely first fundamental frequency, second fundamental frequency, and so forth. The first fundamental frequency can be defined as the lowest frequency at which the magnification factor reaches a local maximum. The subsequent fundamental frequencies can be obtained at frequencies equal to the first fundamental frequency multiplied by certain factors that are functions of shear moduli, densities, Poisson's ratios, and thicknesses of various layers (8). The first fundamental frequency is usually the most important one because the magnification factor is high at that frequency. In this study, the first fundamental frequencies of various road sections ranged between 13 and 16 Hz, and the second fundamental frequencies ranged between 30 and 42 Hz as given in Table 5. The fundamental frequencies of each road section are slightly changed at different geophone locations, especially the second fundamental frequency as indicated by the ranges given in Table 5.

If the Road Rater is operated at or close to any fundamental frequency of the pavement system, especially the first one, a resonant response will occur that might be detected by the unsteady geophone readings resulting from the large vibration amplitudes of the pavement surface. This resonant response

TABLE 5 Natural Frequencies (fundamental frequencies) of the Test Road Sections (Hz)

Section	Fundamental Frequency	
	First	Second
1c	14	34-35
1d	14	34-35
2	14	31-32
7	13	30-31
9	16	36-42

was reported by some researchers [e.g., Sharpe et al. (1)]. It should be noted that the actual field resonant frequencies of Pennsylvania Transportation Research Facility sections might be slightly different from those obtained in this study because of the assumption of a subgrade thickness of 20 ft above a rigid layer. Other factors that might affect the resonant response include temperature, moisture content, random variation in material properties, and existence of cracks in asphalt concrete layers as well as various experimental errors.

A large amount of error may occur when the deflection measurement device has only one operating frequency. The Dynaflect is such a device with a typical frequency of 8 Hz. If the natural frequency of the pavement system is equal or close to the operating frequency of the deflection measurement device, a resonant condition will occur. Unless dynamic analysis is used, misleading results may develop.

Typical surface deflections were examined to further compare static and dynamic pavement responses. Figure 9 shows surface deflection under static and dynamic loads for Section 9. For the static case (using the dynamic solution with zero frequency), a stress of 6.5 psi was used on each Road Rater plate; a stress of ±6.5 psi was used in the dynamic case as well as in the field study. It is noted that the difference between static and dynamic responses is not large for that road section.

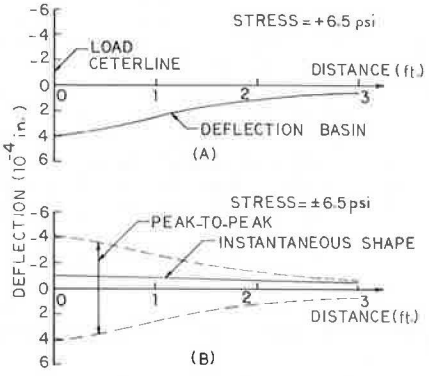

FIGURE 9 Surface deflections for Section 9 under (A) static load condition and (B) steady-state vibrating load condition at 25 Hz.

This happened because, accidentally, the magnification factor at 25 Hz is close to unity as shown in Figure 8. Larger amounts of error might occur due to the use of static analysis in other cases if the magnification factor were largely different from unity. This situation might occur at some combinations of layer thicknesses, material stiffnesses, and loading frequency.

Furthermore, if a static load is applied to the pavement system, the pavement response will be in phase with the load. However, if a vibrating (harmonic) load is superimposed on an initial static load, the instantaneous pavement response will be generally out of phase with the load because of both geometric and material dampings. In this case, the pavement surface at a point may be moving upward when the vibrating load is being increased. Indeed, the pavement surface takes a wave form propagating away from the load. When a Road Rater with two loading plates is used, the surface waves will be similar to waves produced on a smooth surface of water when two stones are simultaneously thrown into it. With the Road Rater geophones, only the peak-to-peak surface deflections are recorded and no information is obtained regarding the instantaneous pavement response or the out-of-phase condition. The dynamic response of the pavement can be represented by a complex number in which the real part represents the in-phase response and the imaginary part represents the 90-degree out-of-phase response. Resonance occurs when the response of the pavement system is 90 degrees out of phase with the applied load and, consequently, the applied load is exactly balanced by the damping force (10).

The phase angles at various geophone locations for Section 9 at 25 Hz are given in Table 6. This indicates that the instantaneous deflection lags the instantaneous load, and this lag is different from one location to another. The instantaneous shape of the pavement surface when the load is zero and increasing is shown in Figure 9. The instantaneous shape fluctuates between the peak-to-peak limits. It should be noted that the wave length of the instantaneous surface shape for Section 9 is about 11 ft, which is longer than the 3-ft distance considered in the present study. Thus no wave shape appears in Figure 9.

TABLE 6 Phase Angles at Various Geophone Locations for Test Section 9 at 25 Hz

Geophone	Phase Angle (degrees)
1	-14.4
2	-19.3
3	-33.3
4	-57.2

SUMMARY AND CONCLUSIONS

In this study, the concept of dynamic response of the pavement is discussed and compared with the static response. Field Road Rater data that were obtained at the Pennsylvania Transportation Research Facility during a previous study (5) are used in the present study to backcalculate the pavement layer moduli using elastodynamic analysis. Static analysis was also used and the associated error was evaluated. The resonant frequencies of the different sections of the test track are estimated. The following conclusions are obtained:

1. The dynamic response of a multilayer pavement system is materially different from its static response. Dynamic analysis incorporates the inertial effect (radiation damping and resonance) of the pavement structure, which cannot be incorporated within static analyses. Simply replacing Young's

modulus in a static analysis by the resilient modulus or the dynamic modulus is insufficient to recover the elastodynamic equations.

2. If the operating frequency of the deflection measurement device (e.g., 25 Hz for the Road Rater and 8 Hz for the Dynaflect) coincides with one of the fundamental frequencies of the pavement system, a resonant condition will occur and a large magnification of the deflection measurements will result. Unless dynamic analysis is used in the interpretation of the dynamic response of the pavement system, misleading results may develop. Although the amount of error resulting from using the static analysis in this study did not exceed 24 percent, larger amounts of error may result in other cases with different operating frequencies of the deflection measurement device, different layer thickness, or different material properties (which might occur at different temperatures or moisture contents for the same materials). No simple relation between static and dynamic pavement responses exists.

3. No "direct" mechanistic solution is currently available to backcalculate material properties from surface deflection data obtained by either static or dynamic loading. Iterative processes are usually used for this purpose.

4. The number of deflection measurements for one run of the deflection measurement device should at least equal the number of unknown material properties. Because the material properties obtained are sensitive to any error in the deflection measurements, a larger number of deflection data points may provide more accurate results.

5. Further research is needed to study the transient loading of the pavement systems obtained from the path of vehicles or from the use of the falling weight deflectometer.

ACKNOWLEDGMENTS

The author wishes to acknowledge E. Kausel at MIT for providing the computer program used in this study. Thanks are extended to T.G. Davies and R. Sen at the State University of New York at Buffalo for their instructive advice during the study. The Pennsylvania Transportation Institute and the Pennsylvania State University are also acknowledged for providing information pertaining to the research facility and the deflection measurements.

REFERENCES

1. G.W. Sharpe, H.F. Southgate, and R.C. Deen. Pavement Evaluation by Using Dynamic Deflections. In Transportation Research Record 700, TRB, National Research Council, Washington, D.C., 1979, pp. 34-46.
2. B.F. McCullough and A. Taute. Use of Deflection Measurements for Determining Pavement Material Properties. In Transportation Research Record 852, TRB, National Research Council, Washington, D.C., 1982, pp. 8-14.
3. M.S. Hoffman and M.R. Thompson. Backcalculating Nonlinear Resilient Moduli from Deflection Data. In Transportation Research Record 852, TRB, National Research Council, Washington, D.C., 1982, pp. 42-51.
4. R.N. Stubstad and B. Connor. Use of the Falling Weight Deflectometer to Predict Damage Potential on Alaskan Highways During Spring Thaw. In Transportation Research Record 930, TRB, National Research Council, Washington, D.C., 1983, pp. 46-51.
5. B.A. Anani. An Evaluation of In-Situ Elastic Moduli from Surface Deflection Basins of Multilayer Flexible Pavements. Ph.D. dissertation. Pennsylvania State University, University Park, 1979.
6. W.P. Kilareski and B.A Anani. Evaluation of In-Situ Moduli and Pavement Life from Deflection Basins. Proc., Fifth International Conference on the Structural Design of Asphalt Pavements, Delft, The Netherlands, Vol. 1, Aug. 1982, pp. 349-366.
7. A.C. Eringen and E.S. Suhubi. Elastodynamics, Vol. 2: Linear Theory. Academic Press, New York, 1975.
8. F.E. Richart, Jr., R.D. Woods, and J.R. Hall. Vibrations of Soils and Foundations. Prentice-Hall, Inc., Englewood Cliffs, N.J., 1970.
9. E. Kausel and R. Peek. Dynamic Loads in the Interior of a Layered Stratum: An Explicit Solution. Bulletin of the Seismological Society of America, Vol. 72, No. 5, Oct. 1982, pp. 1459-1481.
10. R.W. Clough and J. Panzien. Dynamics of Structures. McGraw-Hill Book Co., New York, 1975.
11. S. Prakash. Soil Dynamics. McGraw-Hill Book Co., New York, 1981.
12. E.S. Lindow et al. The Pennsylvania Pavement Research Facility, Vol. 2: Construction, Instrumentation, and Operation. Interim Report, Research Project 71-7, Report PTI 7505. The Pennsylvania Transportation Institute, Pennsylvania State University, University Park, Feb. 1973.

Discussion

Waheed Uddin*

Formulation of a dynamic response analysis for interpretation of dynamic deflection basins is a significant contribution to the state of the art. In addition to the author's paper, two more papers on this subject were presented during the 64th Annual Meeting of the Transportation Research Board (1,2). The author's elastodynamic analysis has been used only on Road Rater Model 400 deflection basins. The basic constitutive law in this analysis is still linear elasticity. Pavement materials and subgrade in the real world do not exhibit linear elastic behavior. Therefore caution should be exercised in applying the findings from the Road Rater study to other vibratory devices. The dynamic response of a pavement system is device dependent in addition to its known dependency on frequency and loading mode effects. Several aspects of the study need further elaboration:

1. The author's static analysis is based on the formulation of his dynamic analysis at zero frequency. How good is the static analysis? It can be judged only if the author provides a comparison with the well-established layered elastic theory. A comparison with responses predicted by ELSYM5 or BISAR programs should be included. These programs have been validated in several studies by comparison with measured responses (3).

*7201 Hart Lane, Apt. 2085, Austin, Tex. 78731

2. The paper lacks any documentation of the validity of the proposed dynamic analysis. An appropriate way to validate the author's procedure is to check the backcalculated moduli with some independent measurements of in situ dynamic moduli such as the SASW method (4).

3. A companion paper by the author (2, Figure 6) shows static deflection to be larger than dynamic deflection for a similar Road Rater study. This is contrary to the findings in this paper. Moreover, material damping can be quite significant for subgrade soils (5), which the author has totally ignored.

4. The selection of subgrade thickness appears to be arbitrary. A subgrade of 20 ft in thickness is assumed in this paper and 12.5 ft was assumed elsewhere (2). Both dynamic and static responses are significantly influenced if a rigid bottom is assumed at a shallow depth. The resonance condition discussed by the author will probably be insignificant if a deeper subgrade is assumed.

5. Several aspects of the backcalculation procedures need further clarification: (a) The procedure is user dependent because "guess" moduli are required as input. How is the uniqueness of derived moduli ensured? (b) What typical values of tolerance in E were used? (c) What is the validity of the procedure for a pavement with known properties?

6. The peak-to-peak force generated by this model of Road Rater is smaller than the 1,000-lb force of a standard Dynaflect. Therefore shear strains in granular subbase-base and subgrade for Road Rater loading will be of low amplitude and the backcalculated moduli of these materials are maximum dynamic moduli. Determination of effective moduli corresponding to standard design load conditions will require a procedure such as an equivalent linear analysis (6). This method is based on a strain sensitivity approach used in earthquake engineering.

7. It has been emphasized in this paper and elsewhere (2) that any NDT device operating at a frequency close to the fundamental frequency of pavement will result in large magnification of surface deflections. How were the natural frequencies of the test pavements established? It is observed from the data in these two papers and related publications that the first natural frequency of pavements is generally above 10 Hz. The discussions in this paper and elsewhere (2) imply that the Dynaflect is inferior because it operates at a fixed frequency of 8 Hz. A device operating at a lower frequency (e.g., Dynaflect) should not be susceptible to resonance condition.

8. It turns out that the low excitation frequency is a merit and provides a rational justification for using static analysis to interpret the Dynaflect deflection basins. Uddin (7) has shown that, for all practical purposes, a static analysis of Dynaflect deflection basins using layered theory is a reasonable approach because the peak-to-peak harmonic force of a Dynaflect can be considered as an equal pseudostatic force. This is further confirmed by the results of an earlier study of the Texas Transportation Institute (8). The TTI study showed that the Dynaflect deflections measured at the surface are independent of the frequencies in the range of 6 to 10 Hz.

REFERENCES

1. J.M. Roesset and K.-Y. Shao. Dynamic Interpretation of Dynaflect and Falling Weight Deflectometer Tests. In Transportation Research Record 1022, TRB, National Research Council, Washington, D.C., 1985, pp. 7-16.
2. T.G. Davies and M.S. Mamlouk. Theoretical Response of Multilayer Pavement Systems to Dynamic Nondestructive Testing. In Transportation Research Record 1022, TRB, National Research Council, Washington, D.C., 1985, pp. 1-7.
3. R. Haas and W.R. Hudson. Pavement Management Systems. McGraw-Hill Book Co., Inc., New York, 1980.
4. S. Nazarian, K.H. Stokoe II, and W.R. Hudson. Use of Spectral Analysis of Surface Waves Method for Determination of Moduli and Thickness of Pavement Systems. In Transportation Research Record 930, TRB, National Research Council, Washington, D.C., 1983, pp. 38-45.
5. F.E. Richart, Jr., R.D. Woods, and J.R. Hall. Vibrations of Soils and Foundations. Prentice-Hall, Inc., Englewood Cliffs, N.J., 1970.
6. W. Uddin, A.H. Meyer, W.R. Hudson, and K.H. Stokoe II. Project-Level Structural Evaluation of Pavements Based on Dynamic Deflections. In Transportation Research Record 1007, TRB, National Research Council, Washington, D.C., 1985, pp. 37-45.
7. W. Uddin. A Structural Evaluation Methodology for Pavements Based on Dynamic Deflections. Ph.D. dissertation. The University of Texas at Austin, 1984.
8. W.H. Cogill. Analytical Methods Applied to the Measurements of Deflections and Wave Velocities on Highway Pavements, Part I: Measurements of Deflections. Research Report 32-14. Texas Transportation Institute, Texas A&M University, College Station, March 1969.

Author's Closure

The author would like to thank the discusser for his instructive comments on the paper. It should be noted that in this study, the term "deflection basin" was not used because, when a harmonic load is applied to pavements, the pavement surface takes on a wave form. Currently, only the peak-to-peak deflections are measured and no information is obtained regarding the instantaneous basin deflections. Replies to the discusser's comments follow in order:

1. Although not reported in the paper, pavement Section 9 of the Pennsylvania Transportation Research Facility was analyzed using the computer program with zero frequency and using the Chevron computer program (with a very stiff semi-infinite layer underlying the subgrade). The deflections of the two programs did not differ by more than 5 percent. This is to be expected because the Helmholtz equation reduces to Navier's equation when the frequency is reduced to zero. The latter equation is, of course, the governing differential equation of elastostatics.

2. The validity of the dynamic analysis has been established by Kausel and Peek (1). Verification of the applicability of the analysis to pavement systems by the methods proposed by the discusser would be welcome. However, it should be pointed out that whereas dynamic analysis can easily reproduce real loading conditions, analyses and testing of a seismic nature will necessarily involve extrapolation to field conditions (as noted by the discusser, comment 6).

3. The dynamic deflection can be either smaller or larger than the corresponding static deflection depending on several factors such as the operating frequency of the loading device, material properties, layer thicknesses, number of layers, and depth to bedrock. Note that the author has not "totally ig-

nored" material damping. A material damping ratio of 5 percent was used (see discussion between Equations 1 and 2). Further, radiation damping is believed to be more significant than material damping during dynamic vertical translation.

4. That the pavement response is significantly influenced by the depth to bedrock has been discussed elsewhere (2,3).

5. In the backcalculation procedure, the initial modulus values affect the number of iterations required to reach a certain accuracy. In both static and dynamic analyses, there is no guarantee that the solutions are unique although the range of admissible solutions may be relatively narrow. A 3 percent tolerance in E was used in this study. Within the constraints of the assumed model (linearity), the solutions are thought to have greater validity than do those of models that ignore the dynamic effect.

6. The author agrees with the discusser that test loading conditions should correspond as closely as possible with field conditions and that some appropriate method should be used to extrapolate test data in cases in which field conditions are not replicated. However, this latter procedure is difficult to implement because many factors influence the response of a pavement system (as distinct from a single soil sample tested in the laboratory) including, for example, cyclic loading, pavement layer thicknesses and stiffnesses, and subgrade material properties. Thus the best procedure appears to be to test pavement systems under design loads and analyze these data directly. The author's analysis is not restricted to low loading levels.

7. The natural frequencies of pavements are functions of material properties: layer thicknesses, number of layers, and depth to bedrock. The first natural frequency of typical pavement sections can be below 10 Hz as demonstrated by Hoffman and Thompson (4). For example, field tests (4) showed that the first natural frequency of "Sherrard" section with 4 in. of asphalt concrete surface and 14 in. of crushed stone base and an AASHTO A-4(6) subgrade is between 8 and 10 Hz, whereas "Viola" section (Stations 13 and 18) with a 9-in. bituminous aggregate mixture surface and a 6-in. AASHTO A-6(9) subgrade has a first natural frequency of 8 Hz. These examples show clearly that the Dynaflect may result in resonating the pavement system, and unless dynamic analysis is used, misleading results may develop. The natural frequencies of the pavement sections in the current study were determined by running the computer program for various frequencies. By definition, the frequencies that resulted in relatively large deflections are the resonant frequencies.

8. As discussed before, resonance may occur at low excitation frequencies under certain conditions. That these conditions were not encountered by Uddin (5) and Cogill (6) does not mean that they do not occur in practice [see Hoffman and Thompson (4)].

In conclusion, true dynamic analysis has a most useful role to play in pavement evaluation. It is the only means whereby the resonant condition can be predicted. Further, it shows clearly the range of validity of purely static analyses and thus serves to warn the user of such analyses of the conditions under which error may result. Of course, it is not proposed that the present analysis can cope with all the complexities of pavement response, but, in regard to one important factor (pavement inertia under dynamic loading), it is, the author hopes, a step forward.

REFERENCES

1. E. Kausel and R. Peek. Dynamic Loads in the Interior of a Layered Stratum: An Explicit Solution. Bulletin of the Seismological Society of America, Vol. 72, No. 5, Oct. 1982, pp. 1459-1481.
2. J.M. Roesset and K.-Y. Shao. Dynamic Interpretation of Dynaflect and Falling Weight Deflectometer Tests. In Transportation Research Record 1022, TRB, National Research Council, Washington, D.C., 1985, pp. 7-16.
3. T.G. Davies and M.S. Mamlouk. Theoretical Response of Multilayer Pavement Systems to Dynamic Nondestructive Testing. In Transportation Research Record 1022, TRB, National Research Council, Washington, D.C., 1985, pp. 1-7.
4. M.S. Hoffman and M.R. Thompson. Nondestructive Testing of Flexible Pavements--Field Testing Program Summary. Transportation Engineering Series 31. University of Illinois at Urbana-Champaign; Illinois Cooperative Highway and Transportation Research Program Series 188, June 1981.
5. W. Uddin. A Structural Evaluation Methodology for Pavements Based on Dynamic Deflections. Ph.D. dissertation. The University of Texas at Austin, 1984.
6. W.H. Cogill. Analytical Methods Applied to the Measurements of Deflections and Wave Velocities on Highway Pavements, Part I: Measurements of Deflection. Research Report 32-14. Texas Transportation Institute, Texas A&M University, College Station, March 1969.

Publication of this paper sponsored by Committee on Strength and Deformation Characteristics of Pavement Sections.

Pavement Thickness Designs Using Low-Strength (Pozzolanic) Base and Subbase Materials

GARY W. SHARPE, ROBERT C. DEEN, HERBERT F. SOUTHGATE, and MARK ANDERSON

ABSTRACT

Information is presented on combining laboratory test data for pozzolanic base and subbase materials with elastic layer theory and a limiting strain criterion to determine thickness designs equivalent to conventional asphaltic concrete and crushed stone pavement structures. A summary of laboratory testing in Kentucky is also presented. An example thickness design determination is given that includes an economic comparison of alternative designs with the conventional asphaltic concrete and crushed stone thickness design.

The use of pozzolans in cementing materials antedates recorded history. Ancient Egyptians used a cement composed of calcined impure gypsum. The Greeks and Romans used calcined limestone and later developed pozzolanic cements by grinding together lime and a volcanic ash. The term pozzolana has been extended to include not only natural volcanic materials but diatomaceous earths and other highly siliceous rocks and artificial products. Pozzolans are defined as siliceous materials, even though they are not cementitious in themselves, because they contain constituents that will combine with lime in the presence of water at ordinary temperatures to form compounds that possess cementing properties.

With the escalating costs of materials and construction for highways and streets, many agencies charged with the responsibility of designing and constructing highways are using byproduct pozzolanic materials. Low-strength (pozzolanic) materials have been used fairly extensively in some areas of the United States as well as abroad. Until recently, the use of pozzolanic materials in highway and street construction in Kentucky was not often economically competitive with abundant supplies of high-quality aggregates. However, as costs of producing and processing aggregate materials have increased, so has the feasibility of using stabilized bases, particularly pozzolanic base materials. To date, pozzolanic bases in Kentucky have been used primarily in low-volume traffic situations. Mixtures that have been considered recently and evaluated to some degree include (a) lime kiln dust, fly ash, and dense-graded aggregate; (b) byproduct lime and dense-graded aggregate; (c) lime kiln dust, fly ash, dense-graded aggregate, and sand; (d) lime kiln dust, fly ash, and limestone mine screenings (waste material from limestone quarrying operations); and (e) "scrubber sludge," quicklime, and dense-graded aggregate or pond ash.

Pozzolanic base or subbase materials have been used on an experimental basis for a number of Lexington, Kentucky, street projects. Two projects for the Kentucky Transportation Cabinet also are being evaluated. Performance experience currently is limited but evolutionary. Modifications in the designs presented in this paper may be required to reflect additional field experience.

Current thickness design procedures for both rigid and flexible pavements in Kentucky have been developed using elastic layer theory matched with pavement performance histories. Flexible thickness design procedures (1,2) are supported by more than 40 years of pavement performance experience and also have been related to AASHO Road Test data. Rigid pavement design procedures (3-5) have been related to performance experience embodied in design procedures of the Portland Cement Association (6) and the AASHO Road Test (7,8).

Thickness designs in Kentucky (both flexible and rigid) are based on limiting strain criteria. A strain-repetitions to failure criterion for flexible pavements was developed by matching theoretically computed strains with repetitions determined from historic pavement performance data and previous empirical thickness design procedures. For rigid pavements a limiting strain criterion was developed and related to the merged fatigue criteria of the Portland Cement Association and AASHTO thickness design procedures.

LOW-STRENGTH BASE AND SUBBASE MIXTURES

Materials

Kentucky specifications (9) currently require pozzolanic mixtures used as base components of pavement structures to have unconfined compressive strengths greater than 600 psi at 7 days when specimens are prepared and cured in accordance with ASTM C 593. Mixtures used for bases normally have three components: fly ash, a source of lime (hydrated lime, quicklime, or lime kiln dust), and an aggregate. Cement or cement kiln dust have been substituted for the lime source.

Pozzolanic mixtures used as subbases are not generally required to have strengths as great as those for bases. There are no strength requirements in Kentucky for subbase applications. Recent experience on one project resulted in compressive strengths on the order of 300 psi at 7 days when cured according to ASTM C 593. Two mixtures that have potential as a subbase material have been investigated in the laboratory: (a) scrubber sludge, aggregate, and some form of lime and (b) aggregate stabilized with baghouse lime. Compressive strengths of 300 to 600 psi at 7 days when cured according to ASTM C 593 have been obtained.

Fly Ash

The properties of fly ash will vary depending on sources and properties of coal burned at the specific facility under consideration. The range of typical properties of fly ash are illustrated elsewhere (10). The fly ash is silt-sized spherical particles 0.015 to 0.050 mm in diameter.

Sources of Lime

Commercial sources of lime for use as a stabilizing material include quicklime and hydrated lime. Most highway agencies specify that lime materials shall meet requirements of ASTM C 207, Type N. Typical properties of limes used for stabilization are summarized elsewhere (10,11).

The characteristics of lime and cement kiln dusts may vary significantly, depending on specifics for each producing location. Typical ranges of composition and physical properties of cement and lime kiln dusts are reported elsewhere (12). Lime kiln dusts used in Kentucky for laboratory and field analyses were within those typical ranges.

Scrubber sludge is a waste material obtained with the use of scrubbers to remove fly ash and residue from coal-burning processes of electric generating power plants. Scrubber sludge (flue gas desulfurization sludge) consists of fly ash and a lime dust slurry filter cake material. The filter cake is a compound of calcium sulfate and calcium sulfite. Quicklime or hydrated lime normally is added to the sludge for stabilization. Stabilization reactions begin almost immediately after the combination of fly ash and lime with the dewatered sludge.

Aggregates

Aggregates for both base and subbase pozzolanic mixtures that have been investigated included dense-graded limestone aggregates, limestone mine screenings (byproduct of limestone quarrying operations), river sand, slag, and gravels. In addition, pond ash waste material has been evaluated in the laboratory and may be an appropriate aggregate for a subbase. The predominant aggregate in Kentucky has been dense-graded limestone.

Two types of aggregate--dense-graded limestone aggregate, which meets Kentucky specifications (13), and pond ash (also called bottom ash)--have been used to prepare sludge-aggregate mixtures. Gradation tests as well as a slake durability test (Kentucky method) (14) were performed on the pond ash. The slake durability test resulted in 5 percent loss. Gradation specifications for dense-graded aggregate as well as gradations and characteristics of a pond ash material from one facility in Kentucky are shown in Figure 1. There was a disproportionate amount (outside specifications for compacted base) of plus-1-in. material in the pond ash. The large size of the coarse particles is an indication that the pond ash might be more suitable as a subbase material than as a base material.

Specimen Preparation

All specimens for this study were prepared in general accordance with ASTM C 593(79) in 4-in.-diameter by 4.6-in. molds. Deviations from that method involved the use of a 5.5-lb hammer and a 12-in. free-fall instead of the specified 10-lb hammer and 18-in. drop. Moisture-density relationships were determined in accordance with ASTM D 698(79) instead of ASTM D 1557(79). Maximum dry density and optimum moisture content were determined using a polynomial curve-fitting procedure. A smoothing technique was used to eliminate localized changes in concavity.

Initial mixtures contained high percentages of fine particles, and compaction procedures were varied from those specified in ASTM C 593(79), which are more applicable to coarse mixes. Even though subsequent specimens involved coarser mixes, compaction techniques were kept constant so direct comparisons of engineering properties could be made.

All specimens prepared for or obtained from base course mixtures were submerged in water for 4 hr be-

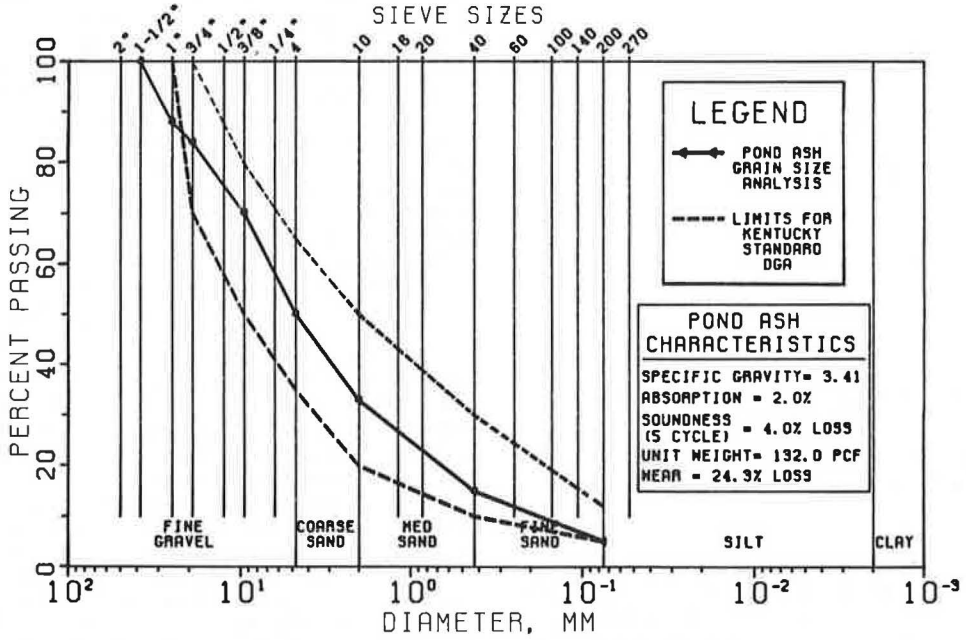

FIGURE 1 Gradation curves—dense-graded limestone aggregate and pond ash material.

fore testing for compressive strengths, as required by ASTM C 593(79). If slaking occurred, the materials or mixture proportions, or both, were eliminated from consideration as pavement components.

The only deviations from ASTM C 593(79) occurred when aggregate-scrubber sludge mixtures were tested. It was not possible to submerge sludge specimens, because some began to slake immediately on submergence. Slaking also prevented vacuum saturation or freeze-thaw testing. Strength testing of scrubber sludge was performed without submergence. This deficiency, although considered acceptable for material proposed as a subbase where confinement is provided by base and pavement layers, is not appropriate for base course construction. ASTM C 593(79) also specifies accelerated curing at 100°F in a sealed container. Other curing conditions included ambient curing and combinations of accelerated and ambient curing. Certainly, additional research is necessary to develop specifications and variations thereof to adequately reflect needed characterizations of materials for specific applications.

Testing

Unconfined compressive strength tests [ASTM C 39(72)], splitting tensile strength tests [ASTM C 496(71)], and tests for static-chord modulus [ASTM C 469(65)] were performed. During compressive strength tests, additional information was obtained by measuring deformation with deflection dial gauges. A four-point least-squares fitting technique was developed to calculate and plot the static-chord modulus of elasticity (Figure 2) from axial load and axial deformation data.

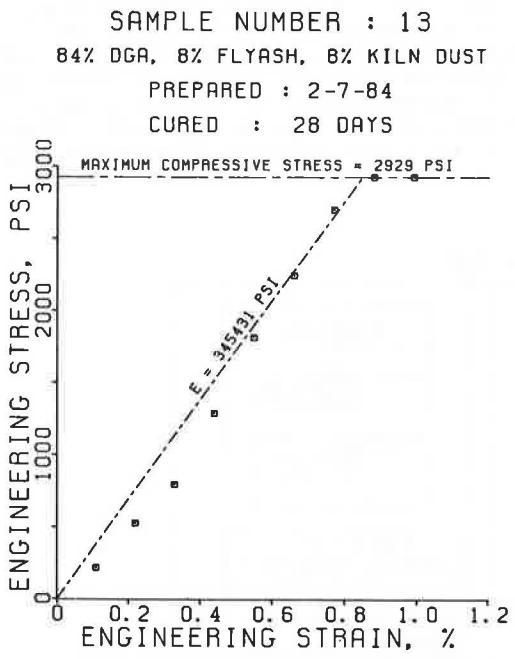

FIGURE 2 Example determination of static-chord modulus.

Attempts were made to measure lateral deformation during compressive strength testing for the purpose of obtaining data from which Poisson's ratio could be estimated. Poisson's ratio was estimated from the ratio of the slopes of the axial stress-axial strain curve and the axial stress-lateral strain curves. Techniques used to measure lateral strains, however, did not produce consistent and reliable results. Therefore, the literature was searched to determine the experience of others (10,15). Values from 0.08 to 0.3, depending on stress level as a percentage of the ultimate, were indicated. A Poisson's ratio of 0.15 was assumed for all pozzolanic base mixtures (16) until sufficient reliable test data for Kentucky mixtures could be accumulated. A summary of results of recent laboratory analyses in Kentucky is given in Table 1.

PAVEMENT THICKNESS DESIGN

Design Methodologies

Structural Number

Other agencies have developed layer coefficients for pozzolanic base materials for use with the AASHTO interim guide for flexible pavement design (7). A review of the literature has indicated considerable variability among suggested layer coefficients for pozzolanic materials (10,17,18). The range of suggested coefficients varies from 0.20 to 0.44 with most recommendations on the order of 0.28 to 0.30 for pozzolanic base mixtures. Lesser values for structural coefficients are recommended for lower strength materials used as subbases.

Stress Ratio

Other thickness design procedures (19) use a failure criterion relating the ratio of flexural strength to modulus of rupture as a function of repetitions to failure. Flexural strength and modulus of rupture are determined from laboratory tests and analyses.

Elastic Modulus for Pozzolans

Early thickness designs using pozzolans in Kentucky were restricted to low-volume city street applications (20) and related well to other design methodologies. The same evaluations using thickness design procedures (based on static-chord modulus) for low-fatigue city street applications resulted in somewhat unrealistic thickness requirements when applied to high-fatigue design levels. Comparisons with other design methodologies also indicated reasonable correlations at low fatigue levels but wide variations for high-fatigue applications. However, there was concern that elastic layer parameters determined from some laboratory and field analyses did not completely account for the characteristics of pozzolanic materials.

A literature review indicated a wide range of elastic moduli for low-strength base and subbase materials depending on specific procedures used to determine the parameters. All studies reviewed indicated increasing elastic moduli for pozzolanic materials proportionate to increases in compressive strength or tensile strength, or both. However, magnitudes of elastic moduli did vary considerably for similar compressive strengths.

Initial estimates of elastic moduli in this study were determined by the static-chord method [ASTM C 469(65)] and generally were relatively low (30,000 to 300,000 psi) (Figure 3). Elastic moduli for lime-fly ash mixtures reported elsewhere (10) were on the order of 100,000 to 500,000 psi for similar levels of compressive stresses (see Figure 3). Even greater magnitudes of elastic moduli (1,600,000 to 3,300,000 psi) have been reported by others (12).

TABLE 1 Strength Parameters for Various Pozzolanic Mixtures and for Various Curing Conditions

MIXTURE COMPONENTS (percent)							OPTIMUM MOISTURE CONTENT (percent)	MAXIMUM DRY DENSITY (pcf)	MIXTURE SOURCE (a)	CURING CONDITION (b)	UNCONFINED COMPRESSIVE STRENGTH (psi)	MODULUS OF ELASTICITY (psi)	SPLITTING TENSILE STRENGTH (psi)
FLY ASH	LIME KILN DUST	BY-PRODUCT LIME	SCRUBBER SLUDGE	RIVER SAND	DENSE-GRADED AGGREGATE	POND ASH							
--	--	--	10	--	--	90	11.8	126.2	field	No. 1	186	14,453	---
--	--	--	10	--	--	90	11.8	126.2	field	No. 7	557	83,836	---
--	--	--	15	--	--	85	9.5	143.6	field	No. 1	309	24,185	---
--	--	--	15	--	--	85	9.5	143.6	field	No. 7	670	37,526	---
--	--	--	20	--	--	80	11.7	133.5	field	No. 1	264	18,067	---
--	--	--	20	--	--	80	11.7	133.5	field	No. 7	560	29,029	---
--	--	--	30	--	--	70	12.4	128.3	field	No. 1	211	14,302	---
--	--	--	30	--	--	70	12.4	128.3	field	No. 7	393	58,306	---
--	--	--	100	--	--	--	43.7	71.6	field	No. 3	71	9,564	---
--	--	--	100	--	--	--	43.7	71.6	field	No. 1	98	11,430	---
--	--	--	100	--	--	--	43.7	71.6	field	No. 6	166	21,369	---
--	--	--	100	--	--	--	43.7	71.6	field	No. 7	130	10,814	---
--	--	--	100	--	--	--	43.7	71.6	field	No. 11	155	21,007	---
--	--	--	10	--	--	90	10.3	150.5	lab	No. 1	99	8,870	13
--	--	--	10	--	--	90	10.3	150.5	lab	No. 7	826	77,471	62
--	--	--	10	--	90	--	9.9	133.7	lab	No. 1	153	7,159	4
--	--	--	10	--	90	--	9.9	133.7	lab	No. 7	286	26,124	10
--	--	--	15	--	--	85	11.2	151.4	lab	No. 1	160	10,285	7
--	--	--	15	--	--	85	11.2	151.4	lab	No. 7	646	59,187	68
--	--	--	15	--	85	--	10.9	130.6	lab	No. 1	189	7,782	6
--	--	--	15	--	85	--	10.9	130.6	lab	No. 7	275	17,700	12
--	--	--	20	--	--	80	11.0	132.9	lab	No. 1	196	15,512	12
--	--	--	20	--	--	80	11.0	132.8	lab	No. 7	617	55,834	9
--	--	--	20	--	80	--	11.8	124.9	lab	No. 1	168	10,080	9
--	--	--	20	--	80	--	11.8	124.9	lab	No. 7	254	17,576	---
--	--	--	100	--	--	--	50.4	65.2	lab	No. 1	107	9,508	---
--	--	--	100	--	--	--	50.4	65.2	lab	No. 7	207	14,955	---
--	--	12	--	--	88	--	6.5	142.1	lab	No. 1	646	35,038	---
--	--	12	--	--	88	--	6.5	142.1	lab	No. 2	738	44,431	---
--	--	16	--	--	84	--	7.3	140.6	lab	No. 1	636	23,295	---
--	--	16	--	--	84	--	7.3	140.6	lab	No. 2	515	25,157	---
--	--	20	--	--	80	--	6.8	135.8	lab	No. 1	315	11,589	---
--	--	20	--	--	80	--	6.8	135.8	lab	No. 2	232	6,377	---
8	8	--	--	--	84	--	5.6	134.3	field	No. 1	1,192	87,545	---
8	8	--	--	--	84	--	5.6	134.3	field	No. 4	922	74,445	---
8	8	--	--	--	84	--	---	----	cores	No. 9	585	62,980	---
8	8	--	--	--	84	--	---	----	cores	No. 10	1,570	216,524	---
8	8	--	--	--	84	--	7.4	139.6	lab	No. 1	1,987	166,618	226
8	8	--	--	--	84	--	7.4	139.6	lab	No. 2	2,403	202,027	---
8	8	--	--	--	84	--	7.4	139.6	lab	No. 4	897	96,608	---
8	8	--	--	--	84	--	7.4	139.6	lab	No. 6	3,222	259,895	387
8	8	--	--	--	84	--	7.4	139.6	lab	No. 8	308	----	---
5	5	--	--	--	90	--	7.5	139.2	lab	No. 1	1,291	94,669	---
5	5	--	--	--	90	--	7.5	139.2	lab	No. 2	1,526	150,962	---
5	5	--	--	--	90	--	7.5	139.6	lab	No. 4	228	----	---
5	5	--	--	--	90	--	7.5	139.6	lab	No. 5	280	18,314	---
6	4	--	--	--	90	--	6.4	146.3	lab	No. 1	488	37,634	---
10	10	--	--	--	80	--	8.0	133.1	lab	No. 1	296	17,619	---
8	4	--	--	--	88	--	6.9	142.1	lab	No. 1	1,116	----	---
8	6	--	--	--	86	--	8.1	150.8	lab	No. 1	1,290	----	---
8	8	--	--	10	74	--	7.5	141.0	lab	No. 1	1,255	----	---
8	8	--	--	10	74	--	7.5	141.0	lab	No. 2	280	----	---
8	8	--	--	10	74	--	7.5	141.0	lab	No. 3	134	----	---
8	8	--	--	10	74	--	7.5	141.0	lab	No. 4	136	----	---
8	8	--	--	25	59	--	7.6	138.7	lab	No. 1	1,272	----	---
8	8	--	--	25	59	--	7.6	138.7	lab	No. 2	356	----	---
8	8	--	--	25	59	--	7.6	138.7	lab	No. 3	82	----	---
8	8	--	--	25	59	--	7.6	138.7	lab	No. 4	123	----	---
8	8	--	--	50	34	--	7.1	135.6	lab	No. 1	923	----	---
8	8	--	--	50	34	--	7.1	135.6	lab	No. 2	157	----	---
8	8	--	--	50	34	--	7.1	135.6	lab	No. 3	105	----	---
8	8	--	--	50	34	--	7.1	135.6	lab	No. 4	79	----	---
10	10	--	--	80	--	--	10.1	110.9	lab	No. 1	89	9,139	---
8	8	--	--	42	42(c)	--	7.0	138.1	lab	No. 1	349	14,956	---
8	8	--	--	32	52(d)	--	6.6	137.5	lab	No. 1	157	4,237	---
8	8	--	--	--	84(e)	--	8.0	135.1	lab	No. 6	1,317	127,193	---
8	8	--	--	42	42(e)	--	7.2	133.6	lab	No. 1	1,194	----	---
8	8	--	--	42	42(e)	--	7.2	133.6	lab	No. 2	69	----	---
8	8	--	--	42	42(e)	--	7.2	133.6	lab	No. 3	439	----	---

a. "Lab" refers to samples mixed from dry components in the laboratory, "field" refers to samples mixed in the laboratory with components from a field situation, "cores" refers to samples obtained by coring an existing pavement.

b. Curing conditions :
   - No. 1 -- 7 days at 100 F in a sealed container (ASTM C 593-79)
   - No. 2 -- 7 days at 100 F in a sealed container and then 7 days at room temperature in air
   - No. 3 -- 7 days at room temperature in a sealed container
   - No. 4 -- 14 days at room temperature in air
   - No. 5 -- 21 days at room temperature in a sealed container
   - No. 6 -- 28 days at 100 F in a sealed container
   - No. 7 -- 7 days at 100 F in a sealed container and then 21 days at room temperature in air
   - No. 8 -- 28 days at room temperature in air
   - No. 9 -- 49 days ambient curing (field conditions) followed by a 14 day soaking period
   - No. 10 -- 132 days ambient curing (field conditions) followed by a 14 day soaking period
   - No. 11 -- 62 days at room temperature in air

c. No. 11 aggregate substituted for dense-graded aggregate.

d. Aggregate substituted for dense-graded aggregate consists of 32% No. 11, 20% aggregate meal.

e. Mines screenings substituted for dense-graded aggregate.

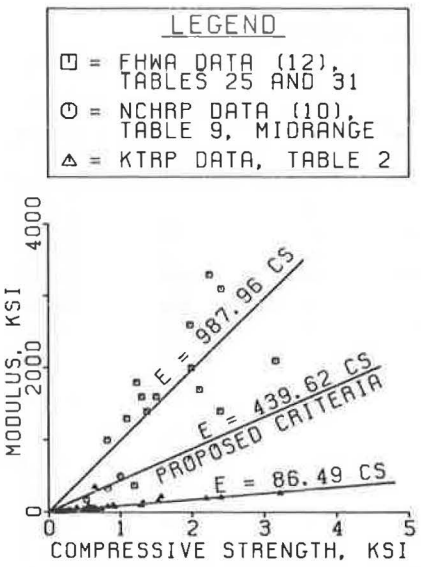

FIGURE 3 Modulus of elasticity versus compressive strength for various data sources.

Least-squares regression analyses were used to evaluate trends of modulus of elasticity versus unconfined compressive strength and tensile strength for the various sources of data (Figure 3). The Kentucky relationship (for the static-chord modulus) is most conservative and was developed for a number of pozzolanic base mixtures evaluated in Kentucky. Resilient moduli presented in the FHWA report showed the greatest rate of change of modulus per unit of compressive stress whereas data from the NCHRP report indicated a somewhat lesser rate of change. Data presented in the FHWA report (12) are resilient moduli determined by repeated load testing for a range of fly ash-kiln dust ratios and also a variety of sources of fly ash and kiln dusts (lime and cement kiln dusts). Figures 3 and 4 show trends of resilient modulus as a function of unconfined compressive strength and splitting tensile strength for all data. Additional plots have been developed for specific mixture proportions or components. Elastic moduli presented elsewhere (10, Table 9) were determined from plate load tests. Median moduli and compressive strengths were used to develop the relationship shown in Figure 3. The relationship of compressive strength versus modulus of elasticity based on data reported in the NCHRP synthesis was selected as a "middle-of-the-road" criterion to determine design elastic moduli. Additional research is necessary to verify and refine this design criterion.

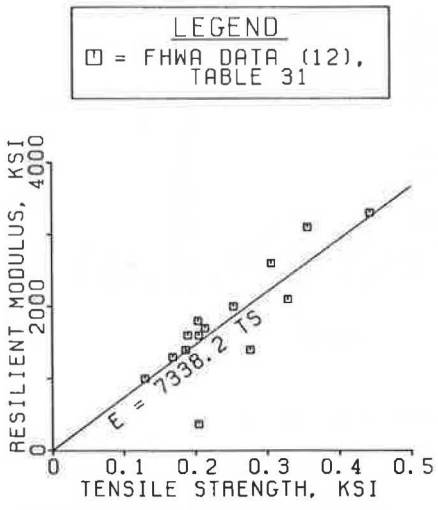

FIGURE 4 Resilient modulus as a function of splitting tensile strength.

Kentucky laboratory analyses were based on ASTM C 469(65) and resulting values were essentially static moduli of elasticity. A Model 400 Road Rater was used to obtain deflection measurements from in-service pozzolanic pavements. Deflection data indicated considerable variability and are currently being evaluated in more detail. However, preliminary analyses indicate backcalculated moduli of 1 million to 3 million psi.

Ahlberg and Barenburg (15) reported flexural moduli of elasticity from 1,500,000 to 2,500,000 psi. Resilient moduli reported by Collins and Emery (12) varied from 370,000 to 3,300,000 psi. Others (10) have reported ranges of moduli from 100,000 psi at a compressive strength of 400 psi to a modulus of 500,000 psi at a compressive strength of 1,000 psi.

The modulus of elasticity of asphaltic concrete varies as a function of temperature and frequency of loading (21,22). On the other hand, granular cohesionless materials have relatively constant moduli for frequencies of 0.1 to 50 Hz (23). For a soil that may be considered to behave as a linear viscoelastic solid, the elastic modulus is a function of frequency (24). Hardin and Black (25,26) have demonstrated dramatic variations of elastic moduli of cohesive soils at low frequencies (less than 0.1 Hz) because of creep phenomena. This partly explains observed variations in elastic moduli from static and dynamic tests. Furthermore, it also has been demonstrated that modulus varies as a function of strain amplitude (23,25,26), which varies considerably among test procedures.

Static moduli were not considered representative of actual traffic loading conditions. Resilient moduli are determined on the basis of repeated load tests at 1 to 2 Hz. Road Rater deflections were obtained at 25 Hz using a 600-lb-force dynamic load and a 1,670-lb-force static load. Others (15) estimated elastic moduli from tests for flexural strength. In view of the significant variations of both frequency and strain amplitude of actual traffic loadings, the need at this time for conservative design moduli is apparent. In addition, Kentucky thickness design procedures, although predicated on a limiting strain-repetitions criterion, were verified initially by Benkelman beam deflection behavior where rebound deflections were obtained at low (creep) vehicle speeds (0.5 to 1.0 Hz) for an 18,000-lb axle load and were matched with theoretical deflections calculated using the Chevron N-layer program (27). Thus an interim criterion relating compressive strength and modulus of elasticity is shown in Figure 3.

Suggested Design Methodology

Thickness design procedures (flexible and rigid) in Kentucky have been developed on the basis of limiting strain-repetitions criteria. The flexible pavement criterion limits vertical compressive strains at the top of the subgrade and the tensile strain at the bottom of the asphaltic concrete (1,2,28). The rigid pavement design criterion is an expression of a stress-ratio fatigue criterion (3-5) in terms of tensile strain versus repetitions for various combinations of modulus of elasticity and modulus of rup-

ture. The same approach was used to develop a tensile strain-repetitions criterion for pozzolanic base materials (Figure 5).

For the pozzolanic material, the ratio of flexural stress to compressive stress at failure was estimated to be 0.25 at the ultimate compressive strength (15). Based on current Kentucky specifications of a minimum compressive strength of 600 psi, the flexural stress for pozzolanic base materials is

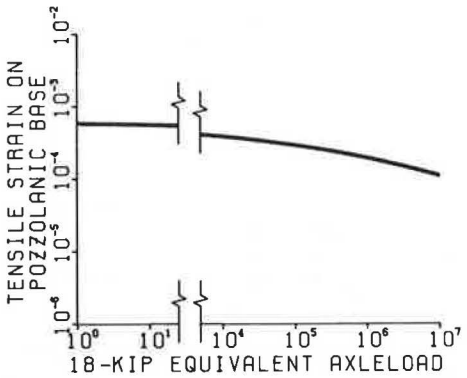

FIGURE 5 Limiting tensile strain at bottom of the pozzolanic base versus repetitions of an 18,000-lb axle load.

150 psi. The minimum design modulus of elasticity from Figure 3 is 250,000 psi. The assumed Poisson's ratio of 0.15 for pozzolanic materials (16) is near the value used to develop rigid pavement designs in Kentucky. The shape of the fatigue envelope used by the Portland Cement Association (6) for portland cement concrete pavements was applied to pozzolanic materials and defines the relationship of ratio of allowable tensile stress to repetitions of an 18,000-lb single axle load (3-5). The allowable tensile stress versus repetitions relationship for pozzolanic materials is the Portland Cement Association curve shifted according to the following relationship:

Tensile strain = (Flexural strength) x (Stress ratio) ÷ (Modulus of elasticity)

where the stress ratio value corresponds to a specific value for repetitions of an 18,000-lb equivalent axle load. More specifically, for pozzolanic base mixtures,

Tensile strain = (150 psi) x (Stress ratio) ÷ (250,000 psi)

These equations convert the ratio of allowable stress ratio to allowable tensile strain at the bottom of the pozzolanic base (see Figure 5). The resulting criterion, compared to one proposed by Thompson (19), is slightly more conservative. Experience with pozzolanic pavements in Kentucky has been limited; the proposed criterion also may be adjusted on the basis of field performance.

Recent studies (3-5) have involved the application of work and energy principles to combine all strain components into a single resultant. Strain energy density is the energy at a point in a body to resist the energy imposed on that body by an outside load and is equal and opposite to the work at that point, as defined by classical physics (29,30). The strain energy density for each point in the pavement structure must be summed (integrated) to obtain the total strain energy, which would equal the total work caused by the external force. Strain energy density, or work, at a given location within the structure may be used as the basis of design instead of using a single strain, such as the vertical compressive strain, as the criterion. Recent investigations of both flexible and rigid pavements have used concepts of equal work as the basis of thickness designs.

To develop a design procedure that uses pozzolans in the pavement structure, the elastic layer theory embodied in the Chevron N-layer computer program (27) was used first to determine thickness requirements for conventional designs (1/3 asphaltic concrete and 2/3 crushed stone base) using traditional materials (1,2,28). Work at critical locations--bottom of the asphaltic concrete or top of the subgrade, or both--was determined and used as the controlling fatigue value for the respective materials at their critical locations.

Elastic layer theory then was used to determine strains and work for a matrix of thicknesses of pozzolanic base (of varying moduli of elasticity) combined with several thicknesses of asphaltic concrete surfacing. Results of those analyses were used to develop a series of graphs similar to Figures 6 and 7.

Determination of an equivalent structural thickness design that uses pozzolans may be achieved by matching the critical strains and work for a conventional pavement design with companion work and strains for some combination of thicknesses of asphaltic concrete surfacing and pozzolanic base. The work and the vertical compressive strain at the top of the subgrade for the control (conventional) pavement were used in combination with Figures 6 and 7 (and other similar graphs) to determine thicknesses of pozzolanic bases corresponding to specific elastic moduli and various thicknesses of asphaltic concrete surfacing. Thicknesses of pozzolanic bases will be slightly increased using a criterion based on work compared to vertical compressive strain. Resultant thicknesses of pozzolanic bases were used to develop Figure 8. The specific thickness of pozzolanic base may then be determined depending on the desired modulus of elasticity and the desired thickness of asphaltic concrete surfacing. Modulus of

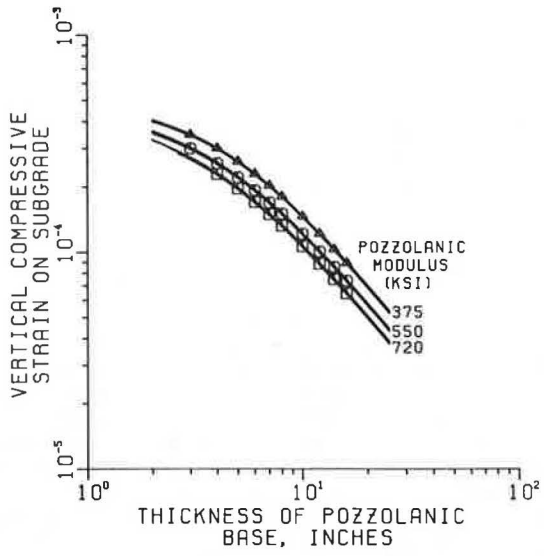

FIGURE 6 Vertical compressive strain at top of subgrade versus thickness of pozzolanic base for constant modulus of elasticity of pozzolanic base and constant thickness of asphaltic concrete surfacing.

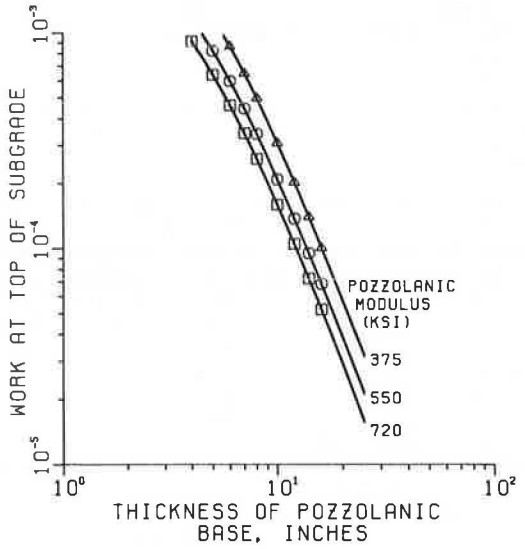

FIGURE 7 Work at top of subgrade versus thickness of pozzolanic base for constant modulus of elasticity of pozzolanic base and constant thickness of asphaltic concrete surfacing.

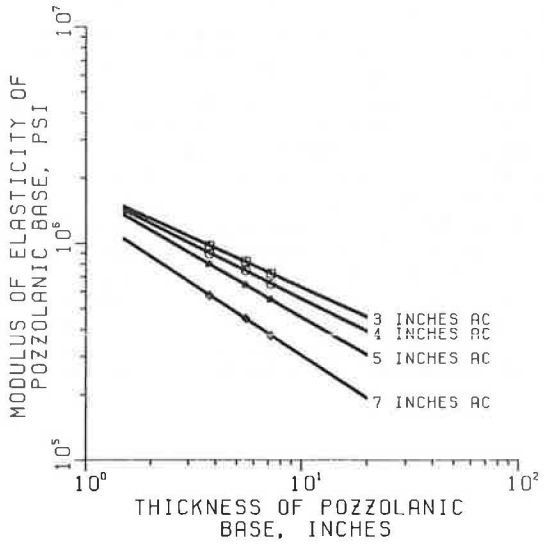

FIGURE 8 Equivalent thickness designs using pozzolanic base for varying thicknesses of asphaltic concrete and moduli of pozzolanic base materials.

elasticity may be related to compressive strength by Figure 3.

Design thicknesses (based on the work at the top of the subgrade) were checked against the limiting tensile strain criterion (1,2,28) at the bottom of the asphaltic concrete and the limiting tensile strain at the bottom of the pozzolanic base (Figure 5) to verify that fatigue of the asphaltic concrete and pozzolanic base was not controlling. Experience in Kentucky has shown that tensile strain at the bottom of the asphaltic concrete layer is normally not the controlling design criterion because the relatively "stiff" moduli of pozzolanic bases limit the magnitude of tensile strains at the interface between asphaltic concrete and pozzolanic base.

EXAMPLE DESIGN

Phase 1 of the design procedure involves the determination of thickness requirements for a conventional asphaltic concrete pavement. Consider, for example, the following design conditions:

Design 18-kip equivalent axle loads (EALs) = 5 million

Design subgrade = California bearing ratio (CBR) 9

Using Kentucky thickness design curves, a conventional asphaltic concrete pavement would be as follows:

Asphaltic concrete surface or base, or both = 7 in.

Dense-graded aggregate base = 14 in.

In Phase 2, structurally equivalent designs using pozzolanic base materials are determined. Critical strains and work for conventional designs are determined using the Chevron N-layer computer program (Figures 6 and 7). Limiting strains corresponding to those of conventional structures may be used to determine thickness requirements for pozzolanic bases for a constant thickness of asphaltic concrete. Analyses of a number of asphaltic concrete thicknesses may be used to develop Figure 8. The specific thickness design is based on estimated elastic modulus obtained from an analysis of compressive strength data (Figure 3).

The major benefit associated with the use of a pozzolanic base is the substitution of a less expensive material for a portion of a more expensive component of the pavement structure. Pozzolanic bases may be especially advantageous as alternatives to very thick conventional asphaltic concrete pavements or thick full-depth asphaltic concrete pavements for which deep rutting may be a potential problem. Pozzolanic bases also may be a cost-effective alternative to some rigid pavements. This, however, has not been considered in Kentucky.

OTHER FACTORS

Effects of Curing

Effects of curing were detected in the field by deflection measurements. Table 2 gives a summary of deflection data obtained directly on a 6-in. layer of lime kiln dust-fly ash-dense-graded aggregate base for three city street projects. Design proportions for Sites 1 and 2 were the same: 8 percent lime kiln dust, 8 percent fly ash, and 84 percent dense-graded aggregate. Design proportions for Site 3 were 6 percent lime kiln dust, 6 percent fly ash, and 88 percent dense-graded aggregate. Field deflection measurements were obtained at similar ages for

TABLE 2 Road Rater Deflections on 6-in. Pozzolanic Bases

	Deflections (in. x 10^{-5}) at Sensor Number		
Project No.	1	2	3
1	53.8	29.8	15.1
2	118.5	46.0	24.8
3	147.2	56.9	24.3

all sites: 7 to 9 days after placement. Prior laboratory and field data indicated that subgrade conditions were similar for the three projects (CBR 4).

Site 1 was placed in mid-August and curing conditions were favorable--temperatures ranged from 60°F to 80°F and the bituminous curing membrane was in good condition. Site 2 was placed in early November when air temperatures were much cooler (40°F to 60°F). The bituminous curing membrane was not placed immediately after compaction. Site 3 was placed in early May. Air temperatures were unseasonably cool and rainfall was record setting. Site 3 was drenched immediately after placement of the bituminous curing membrane, and the membrane was washed away in some locations. In those areas, the surface of the base course was unbound or poorly bound. The site also was subjected to significant rainfall during the initial 7-day curing period. It is apparent from the deflection data that greater strengths resulted from more favorable curing conditions. Deflection data also indicated the influence of the bituminous curing membrane on proper curing and associated strength gains.

Both laboratory (Table 1) and the field data (Table 2) indicated that high temperatures and moisture retention are primary contributors to good curing and associated gains in strength. Thus placement of pozzolanic base materials is recommended when air temperatures are expected to be above 60°F for at least 7 days. Placement of a bituminous curing membrane is apparently essential for the development of high early strengths.

Autogenous Healing

Another aspect associated with low-strength pozzolanic base materials is the potential for reflective cracking of the overlying asphaltic concrete surfacing. It is anticipated that greater amounts of cracking will occur during curing of higher strength pozzolans.

Results of the deflection testing of the three test sites stimulated additional interest in the effects of curing and autogenous healing. A series of lime kiln dust-fly ash-dense-graded aggregate mixtures was prepared in 6-in.-diameter by 12-in. cylinders and cured at room temperature for 28 days. Compressive strengths of those specimens were 231 psi for Mixture A and 209 psi for Mixture B. The aggregate portion for Mixture A consisted of 84 percent dense-graded limestone; Mixture B contained 42 percent sand and 42 percent limestone mine screenings. The fine portions of both mixtures contained 8 percent each of fly ash and lime kiln dust. That was considerably less than for specimens compacted and cured according to ASTM C 593 (4-in.-high by 4.6-in.-diameter cylinder cured at 100°F for 7 days). Compressive strengths in those cases were 1,501 psi for Mixture A and 1,194 psi for Mixture B. The 6- by 12-in. cylinders tested for compressive strengths at 7 days were not destroyed but were sealed in plastic bags and cured to an age of 240 days. The cylinders were again subjected to compressive testing. Compressive strengths at that time were 870 psi for Mixture A and 1,367 psi for Mixture B. Significant strength gains may be partly attributable to long-term strength gain characteristics of pozzolanic materials and also to autogenous healing of the initial failure locations.

Autogenous healing apparently occurs in pozzolanic base specimens if they are left undisturbed and curing conditions remain favorable. However, conditions in the field may not be duplicated by laboratory conditions. Autogenous healing of cracks in field installations may be slowed by stressing under traffic loadings. Field curing conditions (temperature and moisture) also may vary considerably.

CLOSING COMMENTS

Experience in Kentucky with the performance and life-cycle costs of pozzolanic pavements has been almost nonexistent. Thickness design procedures for pozzolanic pavements have been developed by other agencies for other regions, but the extent to which Kentucky conditions are represented could not be determined at this time. This paper represents initial efforts to develop a thickness design methodology for pozzolanic pavements that is related to performance histories in Kentucky as well as to laboratory test data characterizing the properties of pozzolans. It is anticipated that the procedures presented herein may be the nucleus for the development of a complete set of thickness design curves using pozzolanic or other low-strength base materials.

Additional research on and experience with life-cycle costs, durability of materials, fatigue-shear strain relationships, and pavement performance will be necessary to refine procedures and methodologies for thickness design. Pavement sections are currently in place and are being monitored to provide such data for future analyses and refinements. Economic analyses apparently indicate competitiveness with other materials for initial construction.

A major criticism of pozzolanic pavements relates to reflective cracking of overlying asphaltic concrete layers associated with shrinkage cracking in the pozzolanic base. Additional evaluations are currently ongoing. One technique involves the use of stress-relief layers between the pozzolanic and the asphaltic concrete layers. Benefits are yet to be determined.

REFERENCES

1. J.H. Havens, R.C. Deen, and H.F. Southgate. Design Guide for Bituminous Concrete Pavement Structures. Research Report UKTRP-81-17. Kentucky Transportation Research Program, University of Kentucky, Lexington, Aug. 1981.
2. H.F. Southgate, R.C. Deen, and J.H. Havens. Development of a Thickness Design System for Bituminous Concrete Pavements. Research Report UKTRP-81-20. Kentucky Transportation Research Program, University of Kentucky, Lexington, Nov. 1981.
3. H.F. Southgate, J.H. Havens, R.C. Deen, and D.C. Newberry, Jr. Development of a Thickness Design System for Portland Cement Concrete Pavements. Research Report UKTRP-83-5. Kentucky Transportation Research Program, University of Kentucky, Lexington, Feb. 1983.
4. H.F. Southgate and R.C. Deen. Thickness Design Curves for Portland Cement Concrete Pavements. Research Report UKTRP-84-3. Kentucky Transportation Research Program, University of Kentucky, Lexington, Feb. 1984.
5. H.F. Southgate and R.C. Deen. Thickness Design Procedure for Portland Cement Concrete Pavements. Research Report UKTRP-84-6. Kentucky Transportation Research Program, University of Kentucky, Lexington, March 1984.
6. Thickness Design for Concrete Pavements. Portland Cement Association, Skokie, Ill., 1966.

7. Interim Guide for Design of Pavement Structures. American Association of State Highway and Transportation Officials, Washington, DC, 1972 and 1981.
8. The AASHO Road Test: Report 5--Pavement Research. Special Report 61E. HRB, National Research Council, Washington, D.C., 1962.
9. Fly Ash Stabilized Bases. Special Provision 83(70). Kentucky Transportation Cabinet, Frankfort.
10. Lime-Fly Ash-Stabilized Bases and Subbases. NCHRP Synthesis of Highway Practice 37. TRB, National Research Council, Washington, D.C., 1976.
11. Chemical Lime Facts. Bulletin 214, 3rd ed. National Lime Association, Arlington, Va., 1973.
12. R.J. Collins and J.J. Emery. Kiln Dust-Fly Ash Systems for Highway Bases and Subbases. Report FHWA/RD-82/167. FHWA, U.S. Department of Transportation, Sept. 1983.
13. Standard Specifications for Road and Bridge Construction. Kentucky Transportation Cabinet, Frankfort, 1983.
14. Slake Durability Index Test. Method KM-64-513-76. Kentucky Transportation Cabinet, Frankfort, 1976.
15. H.L. Ahlberg and E.J. Barenburg. Pozzolanic Pavements. Bulletin 473. Engineering Experiment Station, University of Illinois, Urbana, 1965.
16. E.J. Barenburg. Lime-Fly Ash-Aggregate Mixtures in Pavement Construction. National Ash Association, Washington, D.C., 1974.
17. M. Gomez and M.R. Thompson. Structural Coefficients and Thickness Equivalency Ratios. University of Illinois, Urbana, June 1983.
18. T.D. Larson and E.S. Lindow. An Evaluation of Pennsylvania's Flexible Pavement Design Methodology. Pennsylvania Transportation Institute, Pennsylvania State University, State College, Dec. 1974.
19. M.R. Thompson. Concepts for Developing a Nondestructive Testing Based Asphalt Concrete Overlay Thickness Design Procedure. University of Illinois, Urbana, June 1982.
20. G.W. Sharpe, H.F. Southgate, and R.C. Deen. Development of Pavement Thickness Designs Using Pozzolanic Base Materials. Research Report UKTRP-83-25. Kentucky Transportation Research Program, University of Kentucky, Lexington, Oct. 1983.
21. B.F. Kallas and J.C. Riley. Mechanical Properties of Asphalt Pavement Materials. Proc., Second International Conference on the Structural Design of Asphalt Pavements, University of Michigan, Ann Arbor, 1967.
22. J.F. Shook and B.F. Kallas. Factors Influencing Dynamic Modulus of Asphaltic Concrete. Proc., Association of Asphalt Paving Technologists, Vol. 38, 1969.
23. V.P. Drnevich and J.P. Jent. Response of Saturated Sands to Cyclic Shear at Earthquake Amplitudes. Water Resources Research Institute Report 87. University of Kentucky, Lexington, Oct. 1975.
24. F.E. Richart, Jr., J.R. Hall, Jr., and R.D. Woods. Vibrations of Soils and Foundations. Prentice-Hall, Inc., Englewood Cliffs, N.J., 1970.
25. B.O. Hardin and W.L. Black. Vibration Modulus of Normally Consolidated Clay. Journal of the Soil Melchanics and Foundation Division, ASCE, Vol. 94, No. SM2, March 1968.
26. B.O. Hardin and W.L. Black. Closure to Vibration Modulus of Normally Consolidated Clay. Journal of the Soil Mechanics and Foundation Division, ASCE, Vol. 95, No. SM6, Nov. 1969.
27. J. Michelow. Analysis of Stresses and Displacements in an N-Layered Elastic System under a Load Uniformily Distributed on a Circular Area. Chevron Research Corporation, Richmond, Calif., Sept. 1963.
28. R.C. Deen, H.F. Southgate, and J.H. Havens. Structural Analysis of Bituminous Concrete Pavements. Research Report 305. Division of Research, Kentucky Department of Highways, Lexington, May 1971.
29. I.S. Sokolnikoff. Mathematical Theory of Elasticity. 2nd ed. McGraw-Hill Book Co., New York, 1956.
30. R.C. Deen, H.F. Southgate, and J.G. Mayes. The Effect of Truck Design on Pavement Performance. Proc., Association of Asphalt Paving Technologists, Vol. 49, 1980.

Publication of this paper sponsored by Committee on Strength and Deformation Characteristics of Pavement Sections.

Deformation Characteristics of Granular Base Course in Flexible Pavements

SAFWAN KHEDR

ABSTRACT

The results of a triaxial test program performed on untreated granular crushed limestone base course material are presented. Triaxial tests were performed with time-variable confining pressure that varied simultaneously with the vertical dynamic loading. The test setup was designed to simulate the traffic-induced stress state on the granular base in flexible pavements. Various levels of stress state were applied to samples of different moisture contents and relative densities. The analysis of permanent deformation results revealed that a power relationship existed between the rate of permanent strain accumulation and the applied number of loading cycles. Further, the exponential parameter m in the relationship was found to vary over a limited range for all tested samples. The intersection parameter A, which expressed the rutting susceptibility of the material, was found to be most sensitive to stress state and resilient modulus. Parameter A was expressed in a power relationship to the octahedral stress ratio and the resilient modulus. The resilient modulus variation was investigated and found to depend mainly on the stress state. For deviator stress higher than 10 psi, the resilient modulus had a power relationship with the first stress invariant. Furthermore, the exponent of that relationship is linearly interrelated with the logarithm of the intersection coefficient of the same relationship.

A granular base course has a significant effect on the resilient deflection as well as on the residual deformation of a flexible pavement system (1). The degree of significance depends on pavement design structure and environmental conditions. One example is incorporating a free-draining base course to facilitate proper drainage for the pavement. A free-draining granular base, which contains a very low percentage of fines, may contribute to both resilient and residual deformation of the pavement.

The response of granular material under dynamic loading that simulates traffic is different from that under static loads. Therefore it should be tested under dynamic stresses of a magnitude expected in a pavement structure in order to characterize the material for the evaluation of pavement response under traffic. This has been recognized by researchers since 1958 (2). Several investigators have reported experimental results obtained from such tests (3-5). In these and other studies, efforts were directed toward resilient or residual characterization, or both, of granular material.

Barksdale (6) pioneered comprehensive experimental research to investigate the plastic deformation of a variety of granular materials. Ten different materials and blends were tested under constant confining pressure and uniaxial dynamic stress of triangular loading function. In his study Barksdale presented many conclusions that explained various points about deformations of granular materials and served as the basis for further refining research in the field. Some of these conclusions were:

1. Plastic strain accumulated approximately logarithmically with the number of load applications.
2. Threshold deviator dynamic stress existed beyond which the rate of strain accumulation tended to increase with the number of load repetitions.
3. Plastic strain was almost proportional to deviator dynamic stress at static confining pressure for small values of deviator stress.
4. Plastic and elastic strains were strongly dependent on confining pressure, undergoing a significant decrease with increasing confining pressure.
5. The plastic stress-strain curves exhibited a typical nonlinear response similar to those in monotonic stress conditions. A hyperbolic expression was suggested to describe the curves:

$$\epsilon_a = [(\sigma_1 - \sigma_3)/(k\sigma_3^n)]/\left(1 - \left\{[(\sigma_1 - \sigma_3)R_f(1 - \sin\phi)] \div (2c\cos\phi + \sigma_3\sin\phi)\right\}\right) \quad (1)$$

where

ϵ_a = axial strain,
$k\sigma_3^n$ = relationship defining the initial tangent modulus as a function of the confining pressure (σ_3) (k and n are constants),
c = cohesion,
ϕ = angle of internal friction, and
R_f = a constant relating compressive strength to an asymptotic stress difference.

Equation 1 was suggested at a particular number of loading repetitions. However, in applying Equation 1 in a particular estimation of rut depth with pavement performance life, an extensive testing program would be needed to calculate the parameters in the equation at various numbers of load repetitions.

Allen (4) conducted a series of experiments on nine samples of granular material in which both time-variable and constant confining pressures were applied. Although his study was not intended to investigate permanent deformation, he made the general comments that plastic strain decreased with increasing material density and that crushed stone speci-

mens experienced less plastic strain than the gravel specimen, which suffered the most plastic strain under the same stresses.

A laboratory dynamic triaxial test was conducted by the National Crushed Stone Association (NCSA) (7) to study the characteristics of plastic deformation of graded aggregates. Kalcheff (7) reported that the plastic strains were greatly dependent on the degree of consolidation for the same gradation, the amount and type of fines in the gradation, the stress sequence and magnitude, and the moisture content for some types of fines. In keeping with Barksdale's observation, Kalcheff noted that plastic strain accumulated approximately logarithmically with the number of load repetitions.

In the flexible pavement model VESYS II (8), it was suggested that the permanent deformation in flexible pavement layers be represented in the format

$$\epsilon_a = IN^S \tag{2a}$$

$$\epsilon_p = ISN^{S-1} \tag{2b}$$

$$F(N) = MN^{-\alpha} \tag{2c}$$

where

ϵ_a = permanent strain at N cycles,
I = intercept coefficient,
S = slope coefficient,
ϵ_p = permanent strain due to the Nth loading,
F(N) = fraction of total strain due to the Nth loading that is permanent,
M = IS/ϵ_r,
α = 1 - S, and
ϵ_r = resilient strain.

The system incorporated Equations 2a, 2b, and 2c in a predictive technique that used the similarity between the permanent strain cumulative curve and the static creep curve.

Numerous research efforts in the 1970s were devoted to the study of resilient deformations in granular materials as an element in flexible pavements (4,5,7,9,10). Hicks (5) and Allen (4) have reached, in separate efforts, similar conclusions about the resilient characteristics of granular materials. Some of these conclusions were

1. The resilient response of granular materials was independent of the stress pulse duration (for a duration time range of 0.1 to 0.2 sec).
2. The resilient response of granular material was significantly affected by the applied stress history. However, the response was fairly steady and stable after approximately 100 cycles of constant stress-amplitude dynamic loading.
3. Higher density material exhibited higher resilient modulus.
4. The stress level and condition were the factors with most influence on the resilient properties of granular materials. They found that either

$$M_R = k_1 \theta^{k_2} \tag{3}$$

or

$$M_R = k_3 \sigma_3^{k_4} \tag{4}$$

where

M_R = resilient modulus,
k_1, k_2, k_3, k_4 = regression constants,
σ_3 = confining pressure, and
θ = sum of principal stresses = $\sigma_1 + 2\sigma_3$

would represent the modulus-stress state relationship. Allen, however, found that Equation 3 had a higher correlation coefficient in the regression analysis.

5. Allen observed that the constant confining pressure (CCP) tests generally overestimated the resilient Poisson's ratio compared with the results of the dynamic confining pressure (DCP) tests. He also observed that the resilient modulus calculated from CCP tests exceeded that computed from the DCP test. However, this conclusion was not verified for all nine samples tested. Therefore he concluded that the continued use of the CCP triaxial test as a means of characterizing granular materials was justified.

The elastic layered solution has been frequently used as a technique for analyzing a flexible pavement system that contains untreated granular base or subbase, or both. However, because of the unrealistic tensile radial stresses calculated in these granular layers, and also because of the unrealistically low radial pressures calculated when using elastoplastic theory in the finite element method, it can be seen that no model has been established that would describe and account for the behavior of such material as part of a flexible pavement system under real traffic loading (11). All models in use characterize the granular layer as a continuum. It should instead be investigated as an assembly of oriented particles. The granular material can resist a certain amount of radial tensile stresses through the interparticle friction forces that are proportional to the normal stresses at the particles' interfaces. The development of these frictional forces will increase the material's tendency to slip. Therefore passive pressure due to adjacent overburden will be mobilized and, consequently, the confining pressure will increase, causing higher strength (i.e., higher modulus) (11). Because of the cohesionless nature of the untreated granular material, it should be tested under confinement pressure. Except for a few studies (4,10), the confining pressure was kept constant during the dynamic deviator loading in previous research efforts. Such a stress arrangement (CCP) has the following disadvantages:

1. It does not simulate the in situ condition in which lateral pressure changes simultaneously with vertical pressure as a function of time (12).
2. The role of the confining pressure in that stress arrangement is limited to conditioning stress and is not a direct reaction to vertical wheel loading.
3. In triaxial testing, there are two types of procedure:
   - Preconsolidate the sample under confining pressure before applying the dynamic vertical load, thus neglecting the effect of confining pressure on permanent deformation, and
   - Apply dynamic vertical loading simultaneously with the constant confining pressure (σ_3) and thus overestimate the effect of σ_3.
4. In a triaxial cell, the confining pressure is applied on the sample in all directions, which means inducing unrealistic static overburden pressure in the vertical direction.

There has been no report of a complete constitutive equation that would describe permanent deformation in untreated granular material during pavement life. The residual characteristics of granular material have not been investigated in experimentation that involved applying dynamic confining pressure that varied simultaneously with the axial pressure on a time scale to avoid the disadvantages previously mentioned.

The objectives of this study were to investigate the deformation mechanism of untreated granular material in an experimental program that involved applying stress conditions compatible with those expected in flexible pavements. Analysis of the experimental results should lead to the development of a constitutive equation to describe the dynamic creep of the material. Such a constitutive equation would be used in schemes for predicting rutting of flexible pavements.

EXPERIMENTAL PROGRAM

A crushed limestone aggregate obtained from Franklin County, Ohio, with a maximum size of 3/4 in. and limestone fines, was subjected to a dynamic testing program. Figure 1 shows the material gradation used. The fines in the aggregate had a liquid limit of 15 percent and nonplastic properties. The specific gravities measured were 2.57 and 2.64 for the coarse and fine portions, respectively. The compaction curves for the aggregate used are shown in Figure 2.

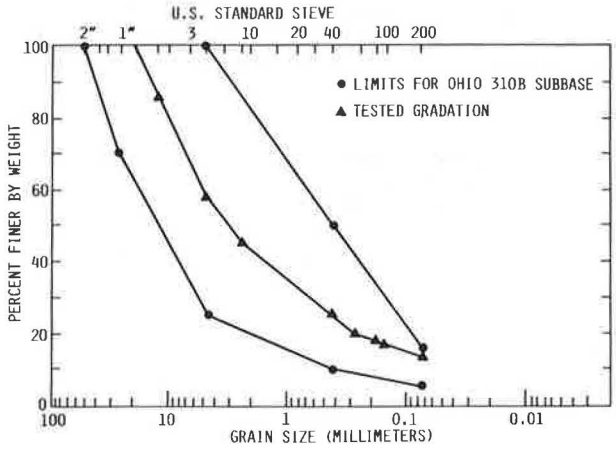

FIGURE 1 Aggregate gradation and gradation bands for Ohio 310B subbase.

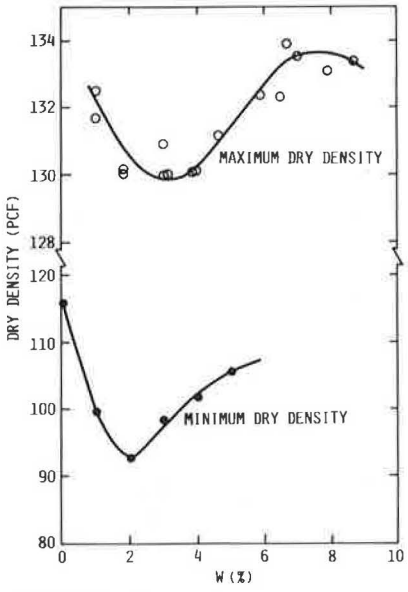

FIGURE 2 Compaction curves for tested aggregates.

Standard compaction procedure, employing the modified compaction energy, was used in determining the maximum dry density curve. The minimum dry density test was run in accordance with AASHTO T19-70. The samples involved in the testing program were 4 in. in diameter and 7.5 in. in height, compacted at 0, 4, or 6 percent water contents to approximately constant dry density of 130± pcf.

The dynamic testing involved applying simultaneous time-variable confining and deviator stresses on the aggregate samples. The tests were carried out in a triaxial cell. Figure 3 shows a schematic of the cell setup. The stresses were applied using two electronically connected material testing systems (MTSs) as shown in Figure 4. The first applied variable confining pressure with stroke control through a hydraulic setup and an oil-water interface. The second applied the required deviator stress with load control synchronized with the confining pressure. A haver-sine loading function was applied in both the vertical and the horizontal direction. The load frequency was one cycle per second with load duration of 0.125 sec. However, the cycle duration was somewhat longer for the lateral pressure because of the pressure transfer mechanism from the MTS to the triaxial cell. The static components of the ver-

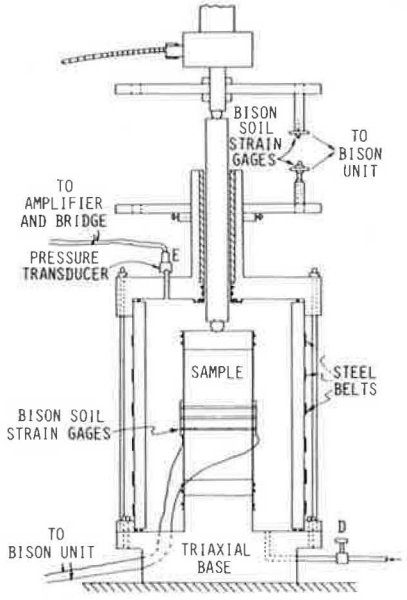

FIGURE 3 Triaxial testing arrangement.

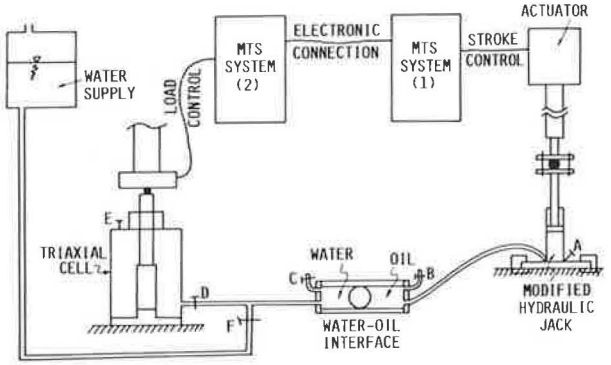

FIGURE 4 Base course testing arrangement.

TABLE 1 Physical and Ultimate Properties of Aggregate Samples

Sample No.	W (%)	γ_d (pcf)	γ_r (relative density)	Height (in.)	Static Modulus (psi)	ϕ^o
11	7.6	132.0	0.95	8.2		
21	4.6	130.0	0.92	6.75		
31	4.0	130.0	0.95	7.28	10,935	53.4
41	4.04	130.0	0.95	7.28		55.6
51	4.0	130.0	0.95	7.28	28,134	51.6
61	3.93	130.1	0.96	7.28	10,900	54.7
62	3.93	130.1	0.96	7.28	10,900	54.7
71	4.03	130.0	0.95	7.28	31,936	57.4
81	3.95	130.1	0.96	7.28	34,959	51.1
91	5.96	130.1	0.87	7.28	24,981	64.3
101	6.00	130.0	0.87	7.28	28,457	57.8
111	5.90	130.1	0.87	7.28	22,420	59.5
121	7.00	128.8	0.82	7.28	21,656	59.0
131	4.19	132.3	1.03	7.28	23,695	63.4
141	5.9	130.1	0.87	7.28	16,388	64.4
142	5.9	130.1	0.87	7.28	16,388	64.4
151	0	131.1	0.92	6.94	10,840	54.4
152	0	131.1	0.92	6.94	10,840	54.4
161	0	130.0	0.85	7.75	9,390	52.4
171	0	130.0	0.85	7.50	20,638	53.8
172	0	130.0	0.85	7.50	20,638	53.8
181	0	130.9	0.91	7.45	13,196	49.0
182	0	130.9	0.91	7.45	13,196	49.0
191	0	130.0	0.85	7.50	17,618	56.0
192	0	130.0	0.85	7.50	17,618	56.0
201	0	130.0	0.85	7.50	22,921	54.8
211	0	130.0	0.85	7.50	16,970	56.3
213	0	130.0	0.85	7.50	16,970	56.3
221	4.12	129.9	0.94	7.50	21,018	55.4
222	4.12	129.9	0.94	7.50	21,018	55.4
231	3.86	130.2	0.97	7.50	20,619	61.7
232	3.86	130.2	0.97	7.50	20,619	61.7
233	3.86	130.2	0.97	7.50	20,619	61.7
241	3.73	130.3	0.98	7.50	26,850	55.5
242	3.73	130.3	0.98	7.50	26,850	55.5

tical and confining pressures were continuously maintained throughout the test.

The dynamic tests were performed at dynamic deviator stress levels of 0, 5, 10, and 20 psi with dynamic confining pressures of 5, 10, and 15 psi applied to each group of samples having a specific water content.

The permanent and elastic deformations were monitored during every test for at least 4,000 load repetitions. All deformations were recorded using Bison soil strain gauge coils (1- and 2-in. diameters) mounted on a Plexiglas measuring assembly.

ANALYSIS OF RESULTS

Residual Deformation

Table 1 gives the physical and ultimate properties of the 24 tested samples. Table 2 gives the stress state at which each sample was tested for dynamic creep as well as its mechanical properties. Figure 5 shows two typical examples of dynamic creep results expressed in the form log ($\epsilon p/N$) versus log (N), where ϵp is the permanent strain after N load repetitions. Linear statistical regression of these results indicated the following equation:

$$\epsilon p/N = AN^{-m} \quad (5)$$

where m is material parameter and A is material and stress-state parameter.

Equation 5 was found to be applicable to all tested samples with correlation coefficients quite close to unity (correlation coefficients ranged from

TABLE 2 Stress State and Mechanical Properties of Aggregate Samples

Sample No.	Lateral Pressure (psi)		Deviatoric Pressure (psi)		Octahedral Stress (psi)		Poisson's Ratio υ	M_R (psi)	A ($\times 10^{-4}$)	m
	Static	Dynamic	Static	Dynamic	Normal σ_o	τ_o Shear				
11	10.0	0	0.96	21.0			0.45	44,000	2.597	0.688
21	1.33	8.25	2.87	18.10	14.28	8.85	0.45	21,300	5.349	0.817
31	1.08	4.10	2.46	10.78	7.69	5.08	0.473	20,200	5.146	0.903
41	4.94	0.0	1.69	24.30			0.45	30,600	8.448	0.899
51	4.84	0.0	1.67	21.42			0.44	36,400	8.05	0.908
61	1.73	4.07	1.35	1.16	4.46	0.55	0.5	13,000	0.1395	0.608
62	2.12	4.60	2.11	20.54	11.45	9.68	0.5	28,300	6.632	0.900
71	2.00	8.07	2.60	10.33	11.51	4.87	0.374	30,700	2.188	0.838
81	1.90	11.76	3.33	19.95	18.41	9.41	0.337	38,500	2.664	0.831
91	1.13	4.28	2.25	20.30	11.05	9.57	0.46	25,300	5.483	0.812
101	2.06	14.81	3.40	18.84	21.09	8.88	0.406	35,100	0.5938	0.725
111	1.88	10.30	2.68	19.96	16.95	9.41	0.409	34,200	3.716	0.827
121	1.96	10.02	2.48	11.20	13.75	5.28	0.528	24,500	4.666	0.859
131	1.08	5.11	2.38	11.02	8.78	5.19	0.55	14,800	4.521	0.864
141	0.99	5.08	2.63	0	5.08	0	0.453	45,200	0.08049	0.559
142	1.03	4.85	2.69	4.71	6.42	2.22	0.453	20,500	3.984	0.909
151	0.95	5.29	2.55	0	5.29	0	0.54	6,800	0.6455	0.743
152	1.00	5.03	2.86	4.83	6.64	2.28	0.34	9,890	1.990	0.765
161	1.06	5.00	2.26	10.95	8.65	5.16	0.716	17,100	8.367	0.767
171	1.95	14.00	2.68	0	14.00	0	0.445	35,000	0.4432	0.806
172	2.07	15.10	2.66	18.48	21.26	8.71	0.445	29,600	3.368	0.814
181	1.80	10.44	2.25	0	10.44	0	0.387	45,000	6.435	0.902
182	2.02	9.71	2.24	9.50	12.88	4.48	0.387	30,300	3.555	0.743
191	0.95	5.00	2.32	0	5.00	0	0.80	7,260	6.278	0.705
192	1.06	5.13	2.26	20.17	11.85	9.51	0.80	17,800	13.756	0.746
201	2.03	10.20	2.12	0	10.20	0	0.287	79,940	0.4303	0.861
202	2.04	10.80	2.07	18.66	17.02	8.80	0.287	34,500	4.277	0.777
211	0.89	5.10	2.29	0	5.10	0	0.522	1,550	4.414	0.903
213	1.01	5.16	2.27	19.46	11.65	9.17	0.56	27,000	37.663	0.873
221	1.95	10.15	2.14	0	10.15	0	0.442	29,400	1.759	0.875
222	2.13	10.12	2.56	9.55	13.30	4.50	0.442	33,000	0.5702	0.741
231	0.30	12.35	2.46	0	12.35	0	0.59	23,500	0.4911	0.671
232	1.00	5.21	2.29	4.38	6.67	2.07	0.59	24,300	0.2192	0.725
233	1.08	5.13	2.27	19.78	11.72	9.32	0.59	34,100	2.488	0.800
241	1.98	10.40	2.86	0	10.40	0	0.452	50,000	1.133	0.822
242	2.12	10.21	2.79	8.96	13.20	4.22	0.452	30,500	0.3279	0.699

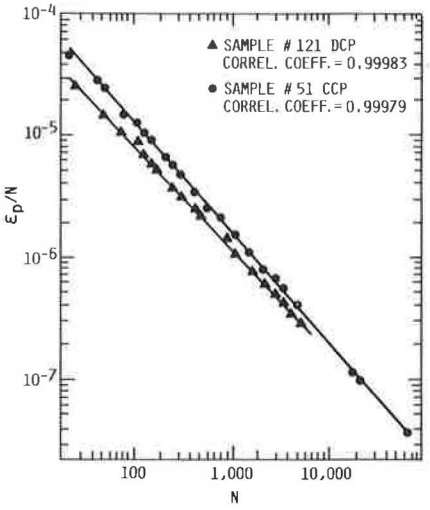

FIGURE 5 Rate of permanent strain accumulation versus number of load repetitions.

0.93 to 1.0). It should be pointed out that the results shown in Figure 5 are for Sample 121, which was tested under dynamic confining pressure (DCP), and for Sample 51, which was tested under constant confining pressure (CCP). The indicated high values of the correlation coefficients and the extremely high values of the statistic F* for the test results strongly suggest that Equation 5 accurately represents dynamic creep for granular material. However, a closer look at the regression residuals suggested that the data points on the log ($\varepsilon p/N$) versus log (N) graph tended to form a very flat convex curve that could be approximated by a straight line. A schematic (Figure 6) magnifies this trend. Nevertheless, this observation does not reduce the significance of Equation 5 accurately describing the test results. Data obtained by Chou (11) and Barksdale

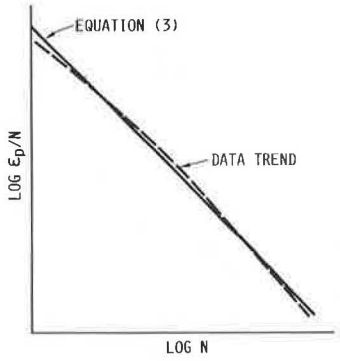

FIGURE 6 Data trend and model representation.

(6) were analyzed and found to be consistent with the same conclusion. Equation 5 verified the VESYS (8) suggestion presented in Equation 2.

In general, permanent deformation was found to increase with increasing deviator stress and decreasing confining pressure, resilient modulus, water content, static initial modulus, angle of internal friction, and relative density within the ranges considered in this study. Resilient Poisson's ratio had no apparent effect on permanent deformation.

Similar trends were observed for samples tested under zero deviator stress, defined in this paper as dynamic consolidation, except that higher dynamic confining pressure resulted in more sample consolidation. Permanent deformation cumulation was observed even for those samples the resilient Poisson's ratios of which were larger than 0.5. The dynamic consolidation followed Equation 5 as well. However, the mechanism of dynamic creep, which is mainly due to shear straining, was different from that of dynamic consolidation, which was attributed to volumetric changes. Because dynamic consolidation was of no practical significance to pavement performance, it was not investigated any further.

From Equation 5, a complete evaluation of parameters m and A should be sufficient to characterize the residual behavior of the granular material. Table 2 gives the values of m and A for each sample. They were calculated using linear regression analysis of test data. Samples 11, 41, and 51, which were tested under CCP and were not included in the analysis, are discussed in the following sections.

Parameter m in Equation 5 is the slope of the linear relationship between log ($\varepsilon p/N$) and log (N). It was found to vary within the general range of 0.7 to 0.9 (Figure 7). The overall average value of m is 0.804 with a standard deviation of 0.067.

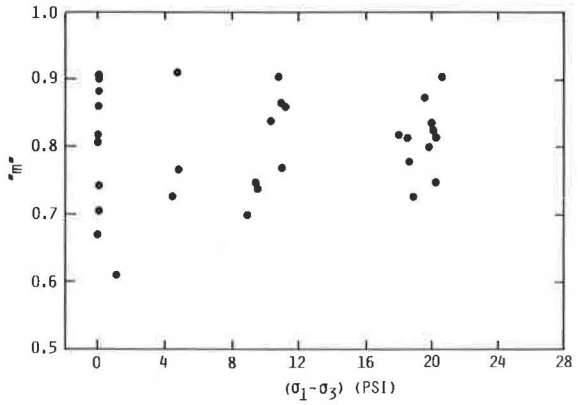

FIGURE 7 Parameter m versus deviator stress.

Multiple regression analysis of m versus resilient modulus (M_R), deviator stress ($\sigma_1 - \sigma_3$), confining pressure (σ_3), octahedral shear [$\tau_o = (2^{1/2})(\sigma_1 - \sigma_3)/3$], octahedral normal [$\sigma_o = (\sigma_1 + 2\sigma_3)/3$], water content (w), relative density (γ_r), and angle of internal friction (ϕ) revealed that m did not show a particular correlation with any of these variables. No specific trend was observed for m variation.

Figure 7 shows m variation with the applied deviator stress ($\sigma_1 - \sigma_3$). It can be seen from the figure that parameter m varied within a relatively narrow range. Therefore it could be considered constant for practical design purposes. Figure 8 shows that the confidence level of the actual mean of parameter m would lie within the shaded zone, assuming a normal distribution variation for the obtained m values.

Parameter A can be defined as the residual strain after the first load cycle is applied on the sample. Although the consideration of m as a constant is not

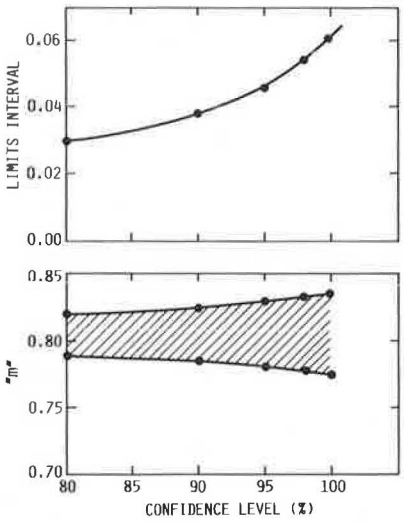

FIGURE 8 Predicted statistical range for parameter m.

strictly justified, useful information relative to the dependency of residual strains on various independent parameters may be gained by considering m a constant. In such a case, parameter A should reflect the residual behavior of the granular material (Equation 5). Statistical analysis of the test results revealed that parameters A and m were not interrelated.

Stepwise regression analysis in the power form was conducted between A and all physical and mechanical variables considered in the analysis of m variation. Only the data set with $(\sigma_1 - \sigma_3) > 0$ (i.e., dynamic creep) was considered in the analysis. The correlation array is given in Table 3. In general, parameter A had a positive correlation with $(\sigma_1 - \sigma_3)$, τ_o, σ_o, principal stress ratio $[R_p = (\sigma_1 - \sigma_3)/\sigma_3]$, and octahedral stress ratio $(R_o = \tau_o/\sigma_o)$; it had negative correlation with w, γ_r, initial static modulus (E_s), M_R, ϕ, and σ_3. It appeared to be highly dependent on either principal or octahedral stress ratio.

TABLE 3 Correlation Coefficients for Factors Affecting Parameter A and Resilient Modulus M_R

Factor	A	M_R
$(\sigma_1 - \sigma_3)$	0.637	0.552
τ_o	0.637	0.553
σ_3	-0.149	0.648
σ_o	0.241	0.731
$(\sigma_1 - \sigma_3)/\sigma_3$	0.777	0.080
τ_o/σ_o	0.798	0.130
M_R	-0.215	1.000
E_s	-0.198	0.627
tan ϕ	-0.049	0.051
w	-0.274	0.250
γ_r	-0.414	0.096

Note: All variables except w expressed in logarithm form.

Several forms of multiple regression were applied to the test results. The following expressions are examples of such forms:

$$A = c_1(\sigma_1 - \sigma_3)^{c2}(\sigma_3)^{c3} \quad (6)$$

$$A = c_4(\sigma_1 - \sigma_3)^{c5}(\sigma_3)^{c6}(M_R)^{c7} \quad (7)$$

$$A = c_8(\sigma_1 - \sigma_3)^{c9}(\sigma_3)^{c10}(M_R)^{c11}\exp(c_{12}w) \quad (8)$$

$$A = c_{13}(R_p)^{c14}(M_R)^{c15} \quad (9)$$

$$A = c_{16}(R_p)^{c17}(M_R)^{c18}\exp(c_{19}w) \quad (10)$$

where c_i are regression constants. The analysis of these regression models was done in three phases incorporating principal stresses as shown in Expressions 6-10, incorporating octahedral stresses instead of principal stresses, and finally incorporating the relative density instead of the water content. It was found that including either the relative density or the water content in the analysis would yield essentially the same results. That is, the third phase did not significantly affect the analysis.

The results of the first two phases are given in Table 4. Comparison of the correlation coefficient and the statistic F* of the different models revealed the significance of various variables for parameter A. Incorporating the octahedral stresses appeared to improve the correlation. Regression Expression 9 would then become

TABLE 4 Results of Multiple Regression Analysis of Parameter A

Model	Correlation Coefficient	F*	F
Phase 1—Incorporating Principal Stresses			
6	0.777	13.72	3.57
7	0.836	13.10	3.21
8	0.857	11.02	3.02
9	0.800	15.99	3.57
10	0.844	14.00	3.21
Phase 2—Incorporating Octahedral Stresses			
6	0.801	16.15	3.57
7	0.844	14.06	3.21
8	0.867	12.14	3.02
9	0.830	20.00	3.57
10	0.865	16.81	3.21

$$A = s_1(R_o)^{s2}(M_R)^{s3} \quad (11)$$

where s_1, s_2, and s_3 are regression constants. The values of these constants for the data presented are 0.0358, 2.135, and -0.304, respectively. Equation 11 was suggested to describe the variation of parameter A in a less-complicated form. Figure 9 shows the relationship of A versus R_o for all tested samples. It was not practically possible to control sample preparation and stress state of the dynamic test in order to produce controlled values of resilient modulus. The results shown in Figure 9 were divided into two groups that have values of resilient modulus below and above 25,000 psi, respectively.

Substituting Equation 11 into Equation 5 results in

$$\epsilon p/N = s_1(R_o)^{s2}(M_R)^{s3}N^{-m} \quad (12)$$

Equation 12 is the constitutive equation that describes the permanent strain of granular material as a function of its resilient modulus, which reflects material strength, stress state, and number of loading cycles. It can be used to predict permanent de-

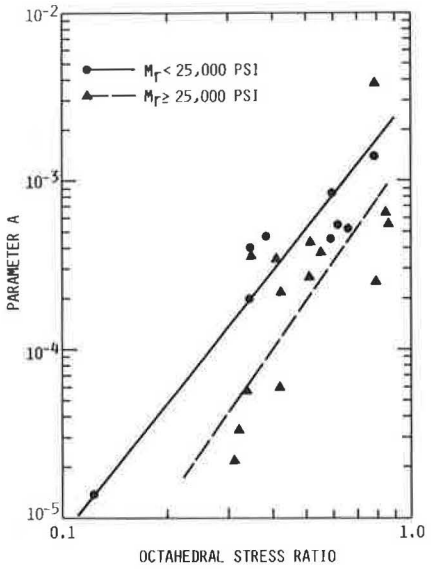

FIGURE 9 Parameter A versus octahedral stress ratio.

formation in an untreated base course along with pavement life.

Resilient Deformation

Figure 10 shows typical results of the resilient modulus versus number of loading cycles (N). The granular material reached a stable condition after 100 cycles beyond which the modulus did not vary significantly.

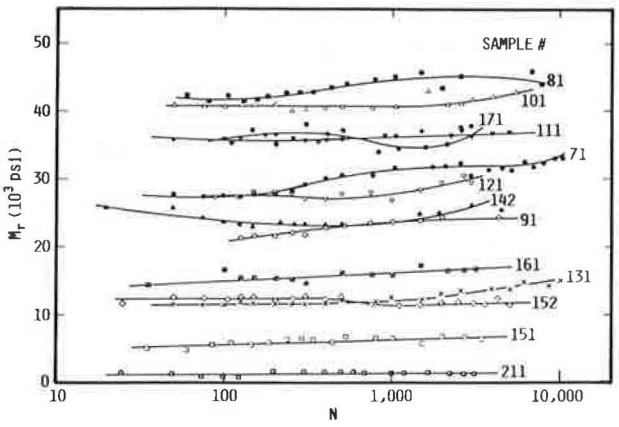

FIGURE 10 Resilient modulus versus number of load repetitions.

Table 3 gives the correlation array of the resilient modulus versus different variables. The modulus was most sensitive to changes in stress state. It increased with dynamic deviator stress as well as dynamic confining pressure. In some samples, however, the modulus decreased with increasing deviator stress for low values of deviator stress (less than 10 psi). At high stress levels, the modulus reached a stable maximum value. The measured results from Samples 82, 22, and 240 were compared to predictions from Equation 3 and verified this equation satisfactorily. However, only the results from Sample 82 for a stress level $(\sigma_1 - \sigma_3)$ above 10 psi agreed with Equation 3 (Figure 11). Table 5 gives the results of statistical analysis of the data.

A logarithmic relationship was observed between the constants k_1 and k_2 in Equation 3 (10). The

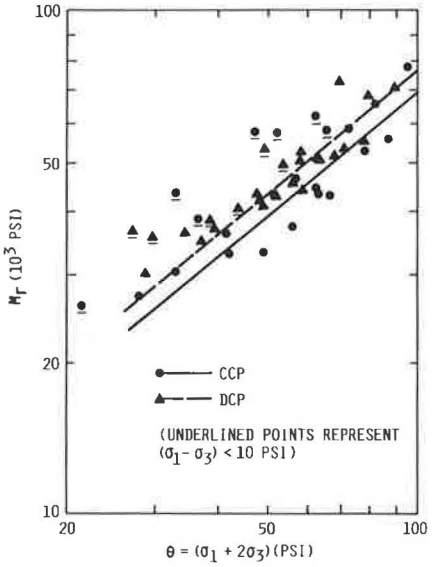

FIGURE 11 M_R versus θ for sample 82.

TABLE 5 Regression Results of Equation 2

Sample No.	Test Type	k_1	k_2	Correlation Coefficient
82[a]	CCP	1.704×10^3	0.802	0.949
	DCP	2.790×10^3	0.703	0.953
22	DCP	5.450×10^3	0.526	0.860
240	DCP	1.760×10^3	0.749	0.953

[a]Only points with $(\sigma_1 - \sigma_3) > 0$ were included.

data obtained by Allen (4) for DCP and CCP tests and by Hicks (5) for dry and wet samples are plotted in Figure 12. The linear relationship on the semilog plot between k_1 and k_2 is apparent in that figure. The relationship could be expressed as

$$k_2 = H_1 - H_2 \log k_1 \quad (13)$$

where H_1 and H_2 are regression constants. Values of H_1 and H_2 for the presented data are shown in Figure 12. It should be mentioned that Hicks' data presented in Figure 12 were for different materials, gradations, and fines contents. Apparently Equation 13 holds regardless of these factors. That is, H_1 and H_2 are dependent only on the type of testing (CCP or DCP).

A final comment should be made on the effect of static stresses on which dynamic stresses were superimposed. The static stresses were necessary to assure proper sample seating and conditioning in the vertical direction and to avoid negative confining pressure from occurring during the test. It was found that changing static confining pressure within 3 psi did not affect the resilient modulus significantly. On the other hand, the deviator static

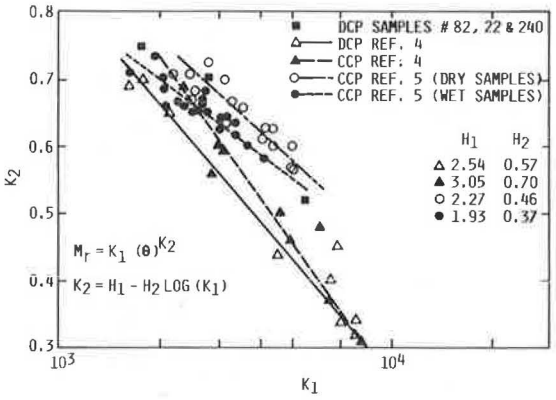

FIGURE 12 Interrelationship between k_1 and k_2.

stress had significant effect on the modulus (Figure 13). Doubling the value of the static deviator stress from 3 to 6 psi could increase the resilient modulus by 50 percent or more. In any standardization of the dynamic test procedure on granular material, this factor should be taken into account. That is, a standard seating static stress should be assigned in order to assure reproducible and comparable test results.

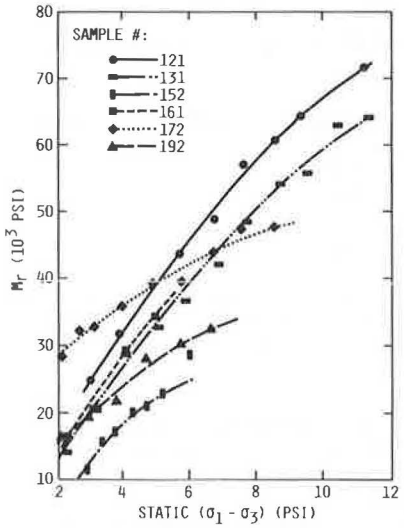

FIGURE 13 Resilient modulus versus static vertical stress.

SUMMARY AND CONCLUSIONS

A triaxial test program that applied time-variable confining pressure synchronized with deviator dynamic stress application was designed and performed on untreated granular base course material. Both residual and resilient characteristics were investigated during the program. Analyses of the results led to the following conclusions:

1. The rate of permanent strain accumulation decreases logarithmically with the number of load repetitions with excellent correlation. This is expressed in Equation 5.
2. Parameter m in Equation 5 was found to vary in the range of 0.7 to 0.9 for the material tested, with a mean value of 0.804.
3. Parameter A in Equation 5 was expressed in a power form as a function of octahedral stress ratio and resilient modulus, Equation 11.
4. The resilient modulus for granular material was found to be most sensitive to stress state. Equation 3 was verified in most of the test results.
5. Constants k_1 and k_2 in Equation 3 were intercorrelated through a logarithmic relationship, Equation 13.
6. The resilient modulus of granular material was found to be sensitive to seating static vertical stress. This should be considered when standardizing the dynamic testing process for granular material.
7. Further studies are needed to validate the applicability of these conclusions to other types and conditions of base course materials.

REFERENCES

1. The AASHO Road Test: Report 5--Pavement Research. HRB Special Report 61E. HRB, National Research Council, Washington, D.C., 1962.
2. H. Seed and C. Chan. Effect of Stress History and Frequency of Stress Application on Deformation of Clay Subgrades Under Repeated Loading. Proc., HRB, National Research Council, Washington, D.C., Vol. 37, 1958.
3. P. Pell and S. Brown. The Characteristics of Materials for the Design of Flexible Pavement Structures. Proc., Third International Conference on the Structural Design of Asphalt Pavements, London, England, 1972.
4. J. Allen. The Effect of Non-Constant Lateral Pressures of the Resilient Response of Granular Materials. Ph.D. dissertation. University of Illinois at Urbana-Champaign, 1973.
5. R. Hicks. Factors Influencing the Resilient Properties of Granular Materials. Ph.D. dissertation. University of California, Berkeley, 1970.
6. R. Barksdale. Laboratory Evaluation of Rutting in Base Course Materials. Proc., Third International Conference on Structural Design of Asphalt Pavements, London, England, 1972.
7. I. Kalcheff. Characteristics of Graded Aggregates as Related to Their Behavior Under Varying Loads and Environments. Presented at Conference on Graded Aggregate Base Material in Flexible Pavements, Oak Brook, Ill., 1976.
8. J. Rauhut, J. O'Quin, and W. Hudson. Sensitivity Analysis of FHWA Structural Model VESYS II, Vol. 1: Preparatory and Related Studies. Report FHWA-RD-76-23. FHWA, U.S. Department of Transportation, March 1976.
9. J. Morgan. The Response of Granular Materials to Repeated Loading. Proc., Third Conference of the Australian Road Research Board, 1966.
10. S. Khedr. Residual Characteristics of Untreated Granular Base Course and Subgrade Soils. Ph.D. dissertation. Ohio State University, University Park, 1979.
11. Y. Chou. Analysis of Permanent Deformations of Flexible Airport Pavements. Report FAA-RD 77-6. U.S. Army Engineer Waterways Experiment Station, Vicksburg, Miss.
12. S. Brown, B. Brodrick, and C. Bell. Permanent Deformation of Flexible Pavements. Research Report to ERO. U.S. Army, University of Nottingham, United Kingdom, 1977.

Publication of this paper sponsored by Committee on Strength and Deformation Characteristics of Pavement Sections.

Seasonal Load Limits Based on Rut Depth

AMIR F. BISSADA and HASAN AL-SANAD

ABSTRACT

In hot climates, the prevention of excessive rutting failures in flexible pavements often requires limits on the allowable axle loads on such pavements during periods of high temperature and moisture. A rational approach for selecting this load limit to ensure a uniform rate of rutting failure throughout a typical year is discussed. The approach selected is based on the use of mechanical methods for determining the effects of seasonal changes in temperature and moisture on the pavement's response to load. The rate of rutting failure with traffic is regarded as the performance variable with traffic. The concept of pavement performance relates the rate of change of rutting damage units with traffic divided into straight-line segments for each season. The performance variable is predicted for each season, allowing for consideration of seasonal pavement behavior and traffic conditions. The validity of the method has been verified by determining the seasonal load limit for a typical road pavement under a particular set of seasonal environmental conditions, pavement materials, and axle load distributions in Kuwait. If a seasonal load limit based on the rutting damage criterion were adopted, pavement service life would be significantly extended.

Highway managers recognize that the load carrying capability and the rate of decrease of useful service life of asphalt pavement vary during the year. Under uniform traffic, these variations reflect seasonal changes such as temperature and moisture content in the physical characteristics of various layers of pavement materials. The application of normally acceptable heavy axle loads during critical periods when the pavement materials are in their weakened condition leads to an accelerated deterioration rate and premature failure.

In cold regions seasonal temperature changes cause poor spring-thaw performance as a result of differences in the response of materials to freezing and moisture changes. In nonfrost regions, however, environmental factors, such as temperature of the asphalt layers and moisture within granular layers and subgrade, have an overriding influence on the performance behavior of the pavement structure. The seasonal variations in temperature and moisture conditions are sometimes more important than the stress states because most of the permanent shear deformation observed occurs when the pavement material is subjected to high temperatures or moisture (1,2).

The surface curvature index (SCI) measured on asphalt pavements 150 to 300 mm thick during the high-temperature summer period in Kuwait was found to exceed two to three times the normal SCI values (3,4). This explains the relatively high reduction in the load carrying capacity of the asphalt layers during the high-temperature summer season.

In current practice decisions concerning the magnitude of seasonal load limits, the dates of their imposition, and the duration of the restricted period are usually made on the basis of local experience based on seasonal observations of pavement surface deflections. The method described in NCHRP Synthesis 26 (5) and Report 76 (6) is typical of these approaches. It directly accounts for seasonal changes in pavement performance by measuring SCI and deflections at both normal and peak periods of a year.

Recently, other methods of pavement response analysis and materials testing have been used in a more rational mechanical approach and applied to the problem of selecting the spring-thaw load limit. The fatigue-based criterion (7) and the uniform failure rate criterion (8), which predicts pavement distress in terms of fatigue cracking, rutting, and roughness, are among the recent criteria developed for this purpose.

The objective of this study is to develop a rational seasonal load limit procedure based on the rutting damage potential of the pavement layers. Because shear strength of a layer material is a function of the state of stress and its level in the pavement structure, resulting changes in rutting damage depend mainly on seasonal axle loads and environmental conditions. The method is demonstrated with an application to an in-service asphalt pavement road in Kuwait.

RUTTING DAMAGE CRITERION

Justification of the use of the rutting damage-based criterion as a basis for selecting the critical season load limit follows.

Asphalt pavement failures in hot climatic regions are mainly due to excessive permanent deformations or rutting of asphalt-bound and granular layers as well as of subgrade soil. Rutting damage occurs in these layers in the form of cumulative permanent deformation or inadequate stability. Both distress modes are related to the shear strength of the layer material.

The allowable shear stress (q_f) can be calculated from the single-load shear strength as $q_f = (\sigma_1 - \sigma_3)/2$, where $(\sigma_1 - \sigma_3)$ is the failure deviator stress obtained from a triaxial test at a confining pressure value (σ_3) equal to that computed in the pavement layer under a standard dual wheel load system during a given period.

Shear failure in any layer of a pavement subjected to the standard dual wheel load system is assumed to occur when the maximum shear stress attains the shear strength of the material under triaxial loading condition. The factor $F = q_i/q_f$ indicates the

relative probability of failure for the ith pavement layer, where q_i denotes the maximum shear stress developed within the ith layer.

The computer algorithm relevant to the layered elastic theory coupled with the seasonal values of the elastic response parameters of the pavement are used for calculating stresses and strains at three specific points: (a) directly under the centerline of one wheel, (b) at the edge of one wheel, and (c) at the centerline of the dual wheels. All these points are located at the middepth of each pavement layer and at the surface of subgrade as shown in Figure 1.

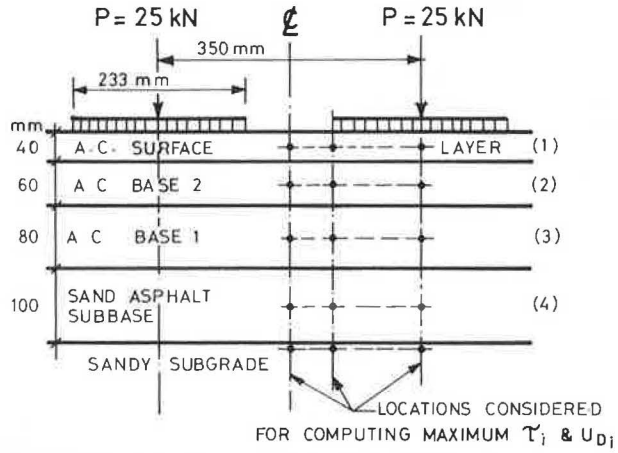

FIGURE 1 Asphalt pavement structure analyzed for a standard dual wheel load system.

The rutting damage potential (RD) of each pavement layer is assessed from the permanent deformation curves, relating the magnitude of permanent strain (ε_p) to the number of deviator stress repetitions (N). A typical curve presented in a double-logarithmic scale, as shown in Figure 2, can be developed for each layer material under specific environmental conditions. Changes in the deviator stress (q) would produce results that would follow parallel lines. These linear relationships are the result of extensive laboratory tests carried out on different asphaltic and granular paving materials (9-11). On the other hand, changes in mix characteristics, environmental conditions (such as temperature or moisture), and experimental conditions (such as degree of confinement or frequency of loading) would change the slope of these linear relationships. Consequently, for a certain permanent strain value, the rutting damage potential of the ith layer material during a given period j is defined as follows:

$$RD_{ij} = (N_f/N_i)_j = (q_i/q_f)^c_j \quad (1)$$

where

q_f = half the failure deviator stress, which is taken as a limit for the range of linearity. Above this stress level, the rate of permanent strain is greatly accelerated and eventually leads to failure (Figure 3).

N_f = number of applications of the deviator stress level (q_f), assumed to be equal to 1 in the criterion proposed here (i.e., one single application of half the failure deviator stress would produce the maximum permissible permanent strain).

q_i = an applied deviator stress level equaling the maximum shear stress computed in the ith pavement layer.

N_i = number of applications of the deviator stress level (q_i), which produces the maximum permissible permanent strain.

c = a coefficient that characterizes the susceptibility of the layer material to rutting damage. Its value depends on the properties and mix composition of the material and environmental and experimental conditions.

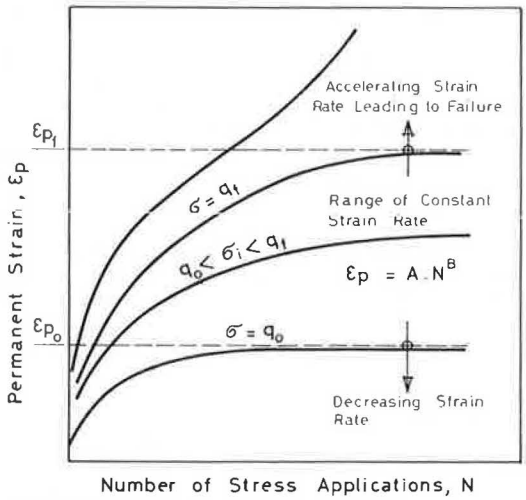

FIGURE 3 Relationship between permanent strain and applied stresses.

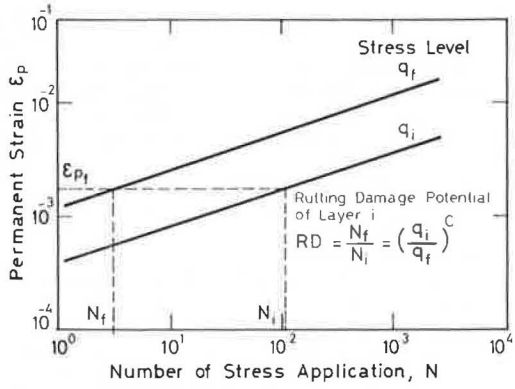

FIGURE 2 Equivalent rutting damage in asphalt pavement layer at different stress levels.

For asphalt paving mixtures, the c-value was found to range from 5 to 8 (11,12), so that higher values are more appropriate to finer gradation mixtures with high bitumen content tested at relatively high temperatures. For unbound granular materials and sandy subgrade soils, c-values range from 8 to 14 depending on grain size distribution and moisture content (10).

The permanent deformation within a pavement layer is assumed to be a function of the elastic volume change calculated in the same layer (13). Accordingly, the rutting damage potential for the whole pavement structure during period j is determined by averaging the weighted rutting damage for each pave-

ment layer with respect to the value of strain energy of distortion (U_{D_i}) absorbed by each layer as follows:

$$RD_j = \Sigma_i (RD_i \times U_{D_i})/\Sigma_i U_{D_i} \quad (2)$$

The daylight hours in each season are divided into environmental periods to allow prediction of changes in rutting damage due to variable temperature gradients in the pavement structure. This is especially important in seasons with a mean air temperature higher than 20°C and where a nonuniform distribution of traffic loading possibly exists during daylight hours. The accumulated rutting damage potential for a pavement structure during the daylight hours of season S is then determined as follows:

$$RD_s = \Sigma_j RD_j \times W_j \quad (3)$$

where RD_S is the accumulated rutting damage potential for season S and W_j is the percentage of load applications while the pavement is in the jth period.

The maximum axle load permitted during the critical season should be restricted to one which produces a rate of rutting damage with traffic ($\Delta RD/\Delta T$) not exceeding 1.5 times the average value produced for the whole year by the maximum legal axle load. The objective of such a criterion is to maintain a uniform rate of pavement distress throughout the year and consequently extend the service life of the pavement.

APPLICATION OF THE LOAD LIMIT PROCEDURE

To evaluate the load limit approach, the following experimental analysis and statistical study of the necessary input parameters were carried out on a section of a highway in Kuwait that is subjected to heavy traffic loading throughout a typical year. The pavement structure consists of 18-cm-thick asphalt concrete layers and a 10-cm-thick sand-asphalt base layer constructed on a sandy subgrade desert soil.

Experimental Investigations and Assessment of Existing Pavement

Field surveys and sampling programs were carried out to evaluate the pavement section and its condition during three different temperature seasons of the year. The following parameters were collected:

- Visual aspect of the bituminous pavement including rut depth measurements using a 1.20-m straightedge;
- Dynamic deflection measurements using Dynaflect;
- The type and thickness of the asphalt pavement layers, properties of subgrade soil, and its water content;
- Information about past service period and maintenance provided; and
- Laboratory testing program to determine resilient moduli of the pavement and subgrade materials and the failure deviator stress at different confining pressures within the range of seasonal temperatures.

The response of the pavement to the maximum legal axle load applied locally was determined using the BISAR layered elastic computer program (14). The stresses and strains in the pavement structure and subgrade due to a dual wheel load of 50 kN spaced at 350 mm between centers were calculated. The maximum shear stress and the strain energy of distortion in each pavement layer and on the top of the subgrade were calculated for each season at four different temperature gradients corresponding to 6:00 a.m., 10:00 a.m., 2:00 p.m., and 6:00 p.m., respectively.

The laboratory testing and the computer analysis necessary to complete the procedure are well established and described elsewhere (9,11,15-17). The general information concerning the road section tested and the principal assessment data are given in Table 1.

Pavement Temperature Distribution

Temperature distribution in the bituminous pavements has been recorded in a real scale model and the re-

TABLE 1 Pavement Material Properties and Assessment Data Used in Seasonal Rutting Damage Analysis[a]

Depth of Pavement Layer (mm)	Season of the Year	E-Modulus (N/mm^2)	Poisson's Ratio	Maximum Shear Stress, q_i (N/mm^2)	Strain Energy of Distortion ($U_D \times 10^{-4}$)	Failure Stress, q_f (N/mm^2)	Deviator $(\sigma_1 - \sigma_2)/2$ at σ_3 (N/mm^2)	Exponential c, 1/log slope of ϵ_p – N curve
Asphalt	1	2120	0.40	0.162	0.024	1.80	0.40	5
Concrete	2	180	0.45	0.152	1.089	0.75	0.30	6
Surface 0-40	3	28	0.45	0.148	9.897	0.50	0.30	7
Asphalt	1	2810	0.40	0.083	0.039	2.30	0.30	5
Concrete	2	520	0.40	0.098	0.165	1.05	0.20	6
Base 1 40-100	3	60	0.45	0.100	1.119	0.62	0.20	7
Asphalt	1	3120	0.40	0.089	0.037	2.80	0.10	5
Concrete	2	1300	0.40	0.067	0.044	1.40	0.10	6
Base 2 100-180	3	280	0.45	0.059	0.166	0.85	0.10	7
Sand	1	3400	0.40	0.162	0.124	1.40	0.00	5
Asphalt	2	1800	0.40	0.138	0.167	0.80	0.00	7
Subbase 180-280	3	520	0.45	0.103	0.323	0.40	0.00	7
Silt	1	110	0.45	0.046	0.361	0.43	0.40	6
Sand	2	110	0.45	0.068	0.556	0.32	0.30	7
Subgrade	3	130	0.45	0.093	0.870	0.21	0.20	10

[a]For the period 12:00 p.m. to 16:00 p.m.

sults of this investigation have been published (18). On the basis of this experimental work the following approximate temperature frequency function has been established:

$$f(T°C) = 1/[(2\pi)^{1/2}]\ (10) \exp[-0.005\ (T - 35)^2] \quad (4)$$

where T°C is the temperature of the pavement surface.

The probability that the temperature of the pavement is lower than T_1 is given by

$$P(T < T_1) = 1/[(2\pi)^{1/2}]\ (10) \int_{-\infty}^{T_1} \exp[-0.005\ (T - 35)^2]\ dT \quad (5)$$

The cumulative histogram of the pavement surface temperature is shown in Figure 4. This histogram indicates three seasonal conditions for the pavement surface temperatures in Kuwait as follows:

Season 1: $8 < T°C < 25$ for 25 percent of the year,

Season 2: $25 < T°C < 45$ for 50 percent of the year, and

Season 3: $45 < T°C < 67$ for 25 percent of the year.

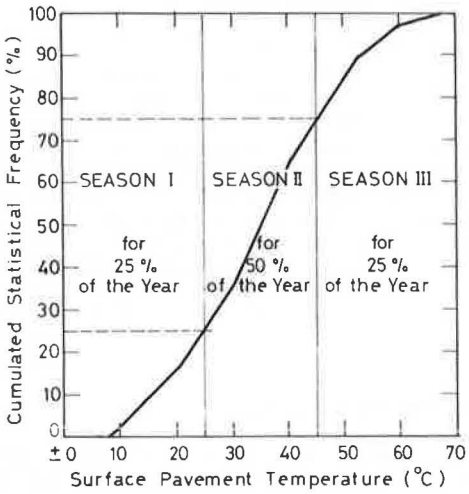

FIGURE 4 Cumulative histogram of pavement temperatures.

Traffic Load Distribution

Previous statistical investigations (15,19), carried out in the development of the local asphalt pavement design method, have permitted characterization of the daily traffic pattern of commercial vehicles on the main roads in Kuwait and the associated axle load distribution. These are shown in Figure 5.

To assess the impact of the axle load limits on pavement failure, an axle load distribution model with a gamma density function is developed to estimate the axle frequency response to variable axle load limits as suggested by Saccomanno and Abdel Halim (20):

$$f(x) = \beta(x - \theta) \exp[-\psi(X - \theta)] \quad (6)$$

where

- $f(x)$ = proportion of axle loads with a load value of x kN;
- θ = smallest axle load observed in the truck fleet = 20 kN; and
- β, ψ = calibration parameters, which vary with limiting legislation and other jurisdictional factors.

The cumulative number of axles up to an axle load limit of X_m can be expressed as

$$F(x) = \int_{\theta}^{X_m} \beta(x - \theta) \exp[-\psi(x - \theta)]\ dx \quad (7)$$

and the total payload (L) carried by the pavement can be expressed as

$$L(x) = \int_{\theta}^{X_m} \beta(x - \mu)(x - \theta) \exp[-\psi(x - \theta)] \quad (8)$$

where μ is the average weight per axle of an empty truck = 20 kN.

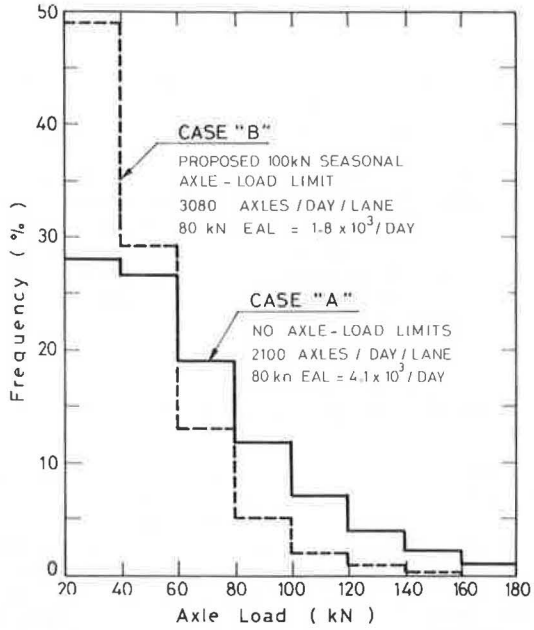

FIGURE 5 Axle load distribution for a constant payload (11,330 ton/day).

In Kuwait as well as in many other developing countries, the usual lack of enforcement and a low response rate to legislation suggest that it would be more appropriate to use the upper limit (i.e., $X_m = \infty$) in the preceding definitions. In the case of the road section analyzed in this study, the observed number of axle passes (greater than 20 kN) was 2,110 per day per lane. The adjusted parameter values of β and ψ for the axle load distribution shown in Figure 5 were taken to be 300 and -0.370, respectively.

The total payload (L) carried by the observed number of axle passes was calculated with Equation 8 to be 11,330 tons per day. On the basis of this, the number of axle passes would increase if an axle load limit were enforced. In Figure 5 a new axle load distribution is shown for the same payload and with the assumption that legislation is enforced. This distribution reduces the axle load limit from $X_m = \infty$ to $X_m = 100$ kN. This axle load restriction would result in an increase in the number of axle passes from 2,110 to 3,080, if it were to be enforced during the critical season. Converting the axle load applications of x kN to an equivalent standard axle load (EAL) of 80 kN, using the fourth power damage

function, a reduction in the 80-kN EAL from 4.1 x 10^3 to 1.8 x 10^3 per day is obtained as a result of the axle load distribution under the new axle load limit.

Seasonal Rutting Damage Rate

The implications of a critical seasonal load limit are analyzed in terms of its effect on rutting damage to the pavement studied. The effects of both temperature and moisture variations on the strength of layer materials and consequently on the rutting damage potential have been considered for the three seasons of the year. Due to the slight seasonal changes in moisture content of the sandy subgrade under the pavement section (2 to 4 percent), the effect of temperature variations on the rutting damage rate was dominant. For each season, the 16 daylight hours are divided into four equal periods from 4:00 a.m. to 8:00 p.m. to account for the effect of variation in both temperature gradient and traffic load distribution.

An example of the effect of temperature gradient on the unit rutting damage corresponding to the three seasons is shown in Figure 6. The distribution of the rutting damage rate within the pavement layers during the period from 12:00 p.m. to 4:00 p.m. is calculated according to the mechanical approach introduced in this paper. As seen in Figure 6, the 40-mm-thick surface asphalt concrete layer has the highest rutting damage potential because its temperature during this period of the day compared to the underlying base layers is highest. However, due to the relatively low shear strength value of the sand-asphalt subbase at zero confining pressure, the rutting damage potential of this layer is almost of the same order as that for the surface asphalt concrete layer.

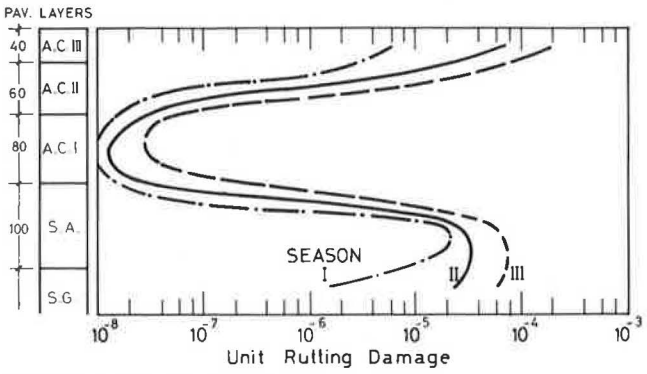

FIGURE 6 Distribution of rutting damage rate within pavement layers during the period 12:00 noon to 4:00 p.m.

The pronounced effect of the variable moisture content on the failure deviator stress of the sandy subgrade soil and consequently on the rutting damage potential is shown in Figure 6. There is no significant effect on the temperature gradient in the pavement on the rutting damage potential of the subgrade soil. However, the effect of seasonal temperatures was found to be extremely high. During Season 3 with the highest summer temperature, the rutting damage potential in the subgrade is 30 times greater than that for the winter temperature (Season 1) between 12:00 p.m. and 4:00 p.m.

The weighted average rutting damage rate for the whole pavement structure has been calculated for the different 4-hr periods considering the distribution of the traffic axle loads. The results are shown for the three different seasons in Figure 7. During Season 3 with the highest temperature, the predicted rutting damage rate for the pavement under study was found to be five times greater than that for Season 2 with the medium temperature range. This result indicates that if a uniform rutting damage rate criterion is used, a seasonal axle load limit should be imposed. Table 2 gives a summary of the resulting weighted average rutting damage rates for the three seasonal conditions. A maximum allowable axle load limit of 100 kN is proposed for the study pavement during the critical Season 3.

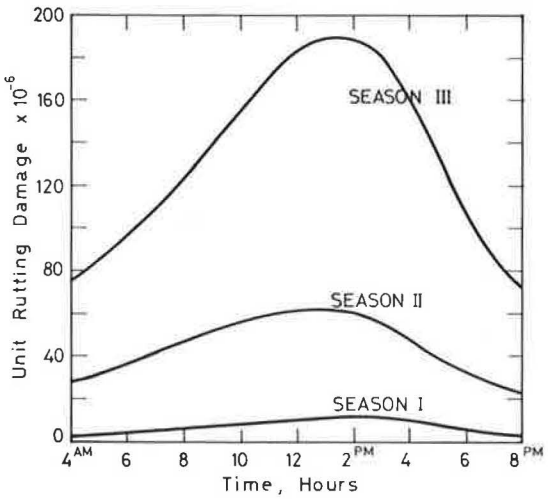

FIGURE 7 Unit rutting damage development during 1 day at different seasonal temperatures.

The change in the rutting damage resulting from the axle load limit was calculated under the assumption that the total payload remains constant. Figure 8 shows that $\Delta RD/\Delta T$ during the critical season decreases from 39.20 x 10^{-6} for the case of no axle load limit to 17.22 x 10^{-6} for the case of a 100-kN axle load limit. Accordingly, the annual rutting damage rate is decreased by 40 percent as the data in Table 2 indicate. Furthermore, the objective of the proposed criterion, to maintain a uniform rate of pavement distress throughout the year, is also met.

Alternative seasonal load limit policies could be analyzed in terms of their effects on the rate of rutting damage using the proposed procedure. However, an essential step in the economic analysis of alternative load limit policies is the determination of cumulative damage to the pavement or its remaining service life up to a certain maximum rutting value under each of the possible alternatives considered.

The annual rate of increase of rutting measured on the road pavement studied during the past 6 years was found to vary from one location to another depending on the frequency of the lateral distribution of wheelpaths as well as on the average traffic speed (1). Excluding the permanent deformations developed during the first 2 years after construction, the measured rate of increase of rutting varied between 2.5 and 5.0 mm annually. Accordingly, the equivalency of the calculated damage unit to a rut-

TABLE 2 Seasonal Rutting Damage Rate $\Delta RD/\Delta T$

Season	Ratio[b]	4:00 a.m.-8:00 a.m. .20 T[a]	8:00 a.m.-12:00 a.m. .35 T	12:00 p.m.-4:00 p.m. .30T	4:00 p.m.-8:00 p.m. .15 T	Seasonal $\Delta RD/\Delta T \times 10^{-6}$
1	.25 Y	0.7	1.3	1.4	0.4	3.8 x .25 = 0.95
2	.50 Y	5.4	11.2	12.0	3.6	32.2 x .50 = 16.10
3	.25 Y					
No axle load limit		29.4	56.0	56.4	15.0	156.8 x .25 = 39.20
Maximum axle load 100 kN		12.9	24.6	24.8	6.6	68.9 x .25 = 17.22

Note: Annual rutting damage rate: no seasonal axle load limit = 0.95 + 16.10 + 39.20 = 56.25 x 10^{-6}, with seasonal axle load limit of 100 kN = 0.95 + 16.10 + 17.22 = 34.27 x 10^{-6}, and percentage decrease in rutting damage rate = 40.
[a]Ratio to total daily traffic.
[b]Ratio to whole year.

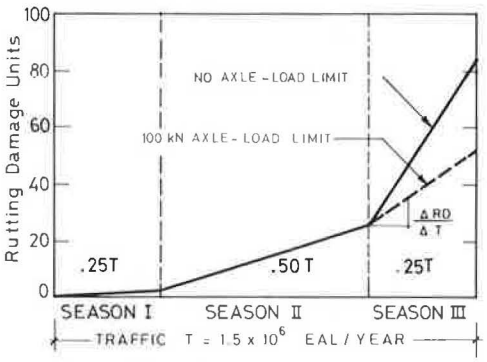

FIGURE 8 Effect of seasonal load limit on annual decrease in rutting damage units.

ting value of the pavement structure for each location could be estimated. Using these equivalency values, the implications of the alternative load limits are analyzed in terms of their effects on the remaining rutting life of the study pavement.

CONCLUSIONS

Previous studies have documented that rutting damage in pavements in the form of shear deformations in flexible pavement layers is experienced in hot climatic areas. Seasonal environmental effects, such as changes in temperature or moisture, or both, on the load-associated distress are considered in order to select a seasonal load limit that will provide a uniform rate of rutting damage. The results of the research described in this paper suggest the following conclusions:

1. The mechanical approach employed provides a rutting performance model. This model is based on the rutting damage potential of each pavement layer for any desired physical condition of the pavement provided that appropriate response parameters are used.
2. The performance variable is used to predict the rate of rutting damage with equivalent number of axle loads, thereby allowing the evaluation of seasonal variations in pavement conditions and axle load distributions.
3. The increased costs for pavement maintenance justify the use of the proposed mechanical procedure. Imposing a seasonal load limit will modify maintenance and rehabilitation costs by changing the time over which these expenditures are required.
4. Seasonal load limits will reduce rut depth and increase time before maintenance.

REFERENCES

1. A.F. Bissada. Analysis of High-Temperature Instability Failures of Heavily Trafficked Asphalt Pavements. Proc., Association of Asphalt Paving Technologists, Vol. 49, 1980.
2. C.R. Freeme, J.H. Maree, and A.W. Viljoen. Mechanistic Design of Asphalt Parameters and Verification Using the Heavy Vehicle Simulation. Proc., Fifth International Conference on the Structural Design of Asphalt Pavements, Delft, The Netherlands, Vol. 1, 1982.
3. S.N. Doshi, H.R. Guirguis, and M.S. Mesdary. The Influence of Temperature on Dynamic Deflections of Flexible Pavements. Proc., International Conference on Roads and Development, Paris, France, May 1984.
4. A.F. Bissada and H.R. Guirguis. Dynamic Deflection Measurements of Asphalt Pavements at High Service Temperatures. Proc., International Symposium on Bearing Capacity of Roads and Airfields, Trondheim, Norway, June 1982.
5. Roadway Design in Seasonal Frost Areas. NCHRP Synthesis of Highway Practice 26. TRB, National Research Council, Washington, D.C., 1974.
6. F.H. Scrivner, R. Peohl, W.M. Moore, and M.B. Phillips. Detecting Seasonal Changes in Load-Carrying Capabilities of Flexible Pavements. NCHRP Report 76. HRB, National Research Council, Washington, D.C., 1969.
7. J.H. Hardcastle, R.P. Lottman, and T. Buu. Fatigue-Based Criteria for Seasonal Load Selection. In Transportation Research Record 918, TRB, National Research Council, Washington, D.C., 1983, pp. 22-30.
8. M.S. Mamlouk. Seasonal Load Limit Using Failure Rate Criterion. In Transportation Research Record 954, TRB, National Research Council, Washington, D.C., 1984, pp. 58-63.
9. S.F. Brown and C.A. Bell. The Prediction of Permanent Deformation in Asphalt Pavements. Proc., Association of Asphalt Paving Technologists, Vol. 48, 1979.
10. L.D. Allen and R.C. Deen. Rutting Models for Asphaltic Concrete and Dense-Graded Aggregate from Repeated-Load Tests. Proc., Association of Asphalt Paving Technologists, Vol. 49, 1979.
11. S. Huschek. Zum Verformungsverhatten Von Asphaltbeton Unter Druck. Mitteilung 54. Institut fur Strassen-, Eisenbahn-und Felsbau, EDI, Zurich, Switzerland, March 1983.
12. P.J. Van De Loo. The Creep Test: A Key Tool in Asphalt Mix Design and in the Prediction of Pavement Rutting. Proc., Association of Asphalt Paving Technologists, Vol. 47, 1978.
13. S. Huscheck. Evaluation of Rutting Due to Viscous Flow in Asphalt Pavements. Proc., Fourth International Conference on the Structural De-

sign of Asphalt Pavements, Ann Arbor, Mich., Vol. 1, 1977.
14. D.L. De Jong, M.G.F. Peutz, and A.R. Korswagen. Computer Program BISAR, Layered Systems under Normal and Tangential Surface Loads. External Report AMSR.0006.73. Koninklijke Shell Laboratorium, Brussels, Belgium, 1973.
15. A.F. Bissada, S.K. Hamdani, and H.R. Guirguis. Design Criteria of Asphalt Pavement Structures at High Service Temperatures. Proc., Fifth International Conference on the Structural Design of Asphalt Pavements, Delft, The Netherlands, Vol. 1, 1982.
16. R.J. Schmidt. A Practical Method for Measuring the Resilient Modulus of Asphalt Treated Mixes. In Highway Research Record 404, HRB, National Research Council, Washington, D.C., 1972, pp. 22-32.
17. Test Procedures for Characterizing Dynamic Stress-Strain Properties of Pavement Materials. TRB Special Report 162. TRB, National Research Council, Washington, D.C., 1975.
18. A.F. Bissada. Asphalt Pavement Temperatures Related to Kuwait Climate. In Highway Research Record 404, HRB, National Research Council, Washington, D.C., 1972, pp. 71-85.
19. A.F. Bissada and A. Al-Abdulla. Asphalt Pavement Response to Excessive Axle-Loads in Kuwait. Presented at the International Road Federation Conference for the Middle East and North Africa, Cairo, Egypt, April 1978.
20. F.F. Saccomanno and A.O. Abdel Halim. Economic Analysis of Axle-Load Limits in Less-Developed Countries. In Transportation Research Record 898, TRB, National Research Council, Washington, D.C., 1983, pp. 357-364.

Publication of this paper sponsored by Committee on Strength and Deformation Characteristics of Pavement Sections.

Abridgment

Predicting Resilient Modulus: A Study to Determine the Mechanical Properties of Subgrade Soils

R. F. CARMICHAEL III and E. STUART

ABSTRACT

Extensive literature review, detailed regression studies, and limited laboratory testing were used to develop models for predicting subgrade resilient modulus. General models are proposed for cohesive soils and nonplastic or granular-type soils. These two models are provided in the new Forest Service Surfacing Handbook (FSH 7709.56a) to provide the practicing engineer with guidance in the absence of test results. More than 250 different soils, representing more than 3,300 modulus test points, were placed in a computerized data base for regression studies. Although these data come from a literature search and testing variations definitely existed, the final models provide a useful first estimate. However, it was strongly recommended that resilient modulus laboratory tests be obtained whenever feasible. The effect of an error in subgrade modulus estimation on the thickness obtained from the design procedure was also studied. Some laboratory tests were made for use in model verification.

Since 1972 the U.S.D.A. Forest Service has been developing a program to provide systematic pavement management for the design of Forest Service roads. As initially developed, this project-level design system uses the AASHO Interim Design Guides as the basic structural and performance model (1-3) for paved roads and a rut depth model developed by the U.S. Army Corps of Engineers for the design of aggregate-surfaced roads.

Recently the structural models in the Surfacing Design and Management System (SDMS) were modified to use the mechanistic approach for determining the thickness of the structural roadway section components (4). This work was basically a revision of Chapter 50 of the Forest Service Transportation Engineering Handbook (5). At this time, the Forest Service has decided to place the information in Chapter 50 in a separate handbook. The Surfacing Handbook, Forest Service publication FSH 7709.56a, will be the new equivalent to the existing Chapter

50 design procedure. The new mechanistic approach is based on elastic-layered theory and requires that the resilient modulus of the subgrade soil be input into the design procedure. Although this input can be determined with repetitive load triaxial testing of subgrade soil samples, such testing is not currently widely available to Forest Service field engineers. The need exists to develop a quick method for determining the resilient modulus from correlations with established or newly developed tests or procedures (6).

STUDY OBJECTIVE

The overall project objective was to develop correlations for predicting subgrade resilient modulus values from basic soil tests or newly developed tests or procedures. This study was undertaken so that a quick method for estimating subgrade resilient modulus would be available to practicing Forest Service engineers.

SCOPE OF STUDY

The project included three general work areas:

1. Collecting existing data from the literature,
2. Establishing correlation models using this data base, and
3. Testing several soils to help verify the new models.

The significant results of this study are the correlation equations summarized in this paper.

LITERATURE REVIEW AND DEVELOPMENT OF DATA BASE

A literature search was made on the Highway Research Information Service (HRIS) data base, and approximately 100 references were collected and reviewed for the establishment of a data base. Although it was initially hoped that extensive data would be reported in the literature for correlation testing between resilient modulus tests and other strength tests such as the California bearing ratio (CBR) test, such was not the case. Therefore resilient modulus test results were recorded in the data base along with more basic soil parameters such as the plasticity index (PI), water content (%W), and amount of material passing the No. 200 sieve. The data base contained more than 3,300 records of resilient modulus test results for more than 250 different soils at specific confining pressures and deviator stresses.

However, the literature study indicated that a more general form was needed for implementation in the Surfacing Handbook. Fortunately, other researchers (7) have proven that simpler relationships based on fundamental soil properties can be developed.

ESTABLISHMENT OF CORRELATION MODELS

Regression studies were initially made for individual soil types according to the unified soil classification (USC) system. Several problems with the data were encountered in the development of the regression equations, including (a) missing observations, (b) different test procedures, (c) lack of range in predictor values, (d) collinearity, (e) confounding of data, and (f) inconsistent sample sizes.

The data were divided according to individual soil types within the USC system and models were developed for each soil type for which data were available. The following symbols and units are used in the equations:

M_R = resilient modulus (ksi),
PI = plasticity index,
%W = percentage water,
CS = confining stress (psi),
DS = deviator stress (psi),
T = bulk stress (psi) (DS + 3CS),
DD = dry density (pcf),
S200 = percentage passing No. 200 sieve, and
SS = soil suction.

Using the best subsets of data found in the analysis of individual soil types, a general equation was sought that would encompass all soil types. Combining all the soil types to accomplish this objective did not yield reasonable results. It was decided to create two broad classes of soils: fine grained (Group 1) and coarse grained (Group 2). The coefficient for deviator stress tends to be negative for Group 1 and positive for Group 2. Specifically, Group 1 consisted of cohesive (fine-grained) soil types including CH, MH, ML, and CL, and Group 2 consisted of granular (coarse-grained) soil types GW, GP, GM, GC, SW, SP, SM, or SC. The following general equations were found after several trial combinations.

Cohesive Soils

The general model is as follows:

$$M_R = 37.431 - 0.4566(PI) - 0.6179(\%W) - 0.1424(S200) + 0.1791(CS) - 0.3248(DS) + 36.422(CH) + 17.097(MH)$$

where

CH = 1 for CH soil
= 0 otherwise (for MH, ML, or CL soil);
MH = 1 for MH soil
= 0 otherwise (for CH, ML, or CL soil);

and the other terms are as defined previously. Here,

$R^2 = 0.759$,
standard error (SE) = 5.277, and
N = 418 observations.

Ranges of the variables are given in the following table.

	Soil Type			
	CH	MH	ML	CL
PI	21-55	13	2-12	13-20
%W	11-36	37-51	6-24	9-21
S200	79-91	86	80-93	60-92
CS	2-20	2-6	0.5-4.5	2.5-40
DS	2-15	1-12	0.5-9.0	3.0-40

Granular Soils

The general model is as follows:

$$\log M_R = 0.523 - 0.0225(\%W) + 0.544(\log T) + 0.173(SM) + 0.197(GR)$$

where

SM = 1 for SM soils
= 0 otherwise;
GR = 1 for GR soils (GM, GW, GC, or GP)
= 0 otherwise;

TABLE 1 Soil Samples Tested for Resilient Modulus

Soil No.	USC[a]	Dry of Optimum Water Content (%)	Optimum Water Content (%)	Wet of Optimum Water Content (%)	Liquid Limit (%)	Plastic Limit (%)	Percentage Passing No. 200 Sieve
10607	GW-GM	4.48 (4.0)	5.21 (8.0)		NP	NP	5
10600	GW	19.53 (19.2)	25.22 (25.0)		39	35	20
10823	SP-SM	8.48 (8.5)	12.08 (13.3)		NP	NP	8
10799	SM		13.15 (15.0)	17.84&17.90 (19.0)	35	NP	28
10604	SC		14.58 (14.3)	16.63 (16.4)	35	21	43
10756	CL		13.36 (14.0)	16.05 (16.0)	40	16	68
10755	CL		12.07 (10.3)	11.4 (17.0)	44	14	81
10825	CH		19.78 (19.4)	20.07 (21.0)	61	15	91

Note: Laboratory compaction efforts were aimed at obtaining the water content shown in parentheses; the actual value obtained appears first.

[a]Unified soil classification system.

and the other terms are as defined previously. Here,

$R^2 = 0.836$,
SE = 0.1627, and
N = 583 observations.

Ranges of the variables are given in the following table.

	Soil Type		
	NP	SM	GR
%W	4.0-8.8	8.7-37.8	5.7-12.3
CS	1.0-20.0	1.0-23.0	1.0-20.0
DS	1.0-20.0	1.0-30.0	5.0-90.0
T	4.0-75.0	3.4-116.0	8.0-114.8

SOILS TESTING FOR MODEL VERIFICATION

The Forest Service provided the researchers with a number of soil samples of a range of material types collected at random by the Region 5 laboratory. Basic soil test results were provided by the Forest Service. Table 1 gives the soil samples, the USC classifications, and the water contents used for the M_R tests that were run.

The new AASHTO test method T274-82 for the resilient modulus of subgrade soils was used in testing. When the moisture-density relationship was known, laboratory test specimens were compacted to two density values selected for testing: (a) the maximum density at the optimum water content and (b) one other density either wet of optimum or dry of optimum. ARE, Inc., soil testing produced more than 300 M_R values for the different deviator stress and confining stress combinations. The actual values were compared with the predicted values from the two general equations (for cohesive soils and for granular or nonplastic soils). Figures 1 and 2 show the results of these comparisons. For the limited range of soils tested, the models do a fair job of estimating M_R. Although the scatter is broad, there do not appear to be any major trends in the data that would cause a rejection of the equations. Some of the scatter obviously could be attributed to the fact that before AASHTO T274-82 no standard procedure existed; hence the scatter or error of the "prediction." The engineer should always use these equations with engineering judgment.

The models presented have been adopted for use in the new Forest Service Surfacing Handbook (FSH 7709.56a). These models are the most applicable ones available at this time. Certainly, caution must be used when using these or any regression equations to ensure that the input information is within the inference space from which the equations were developed. By using these equations, the engineer can estimate subgrade strength as a function of moisture content for each season of the year. The Surfacing Handbook design procedure allows for such variations in subgrade modulus.

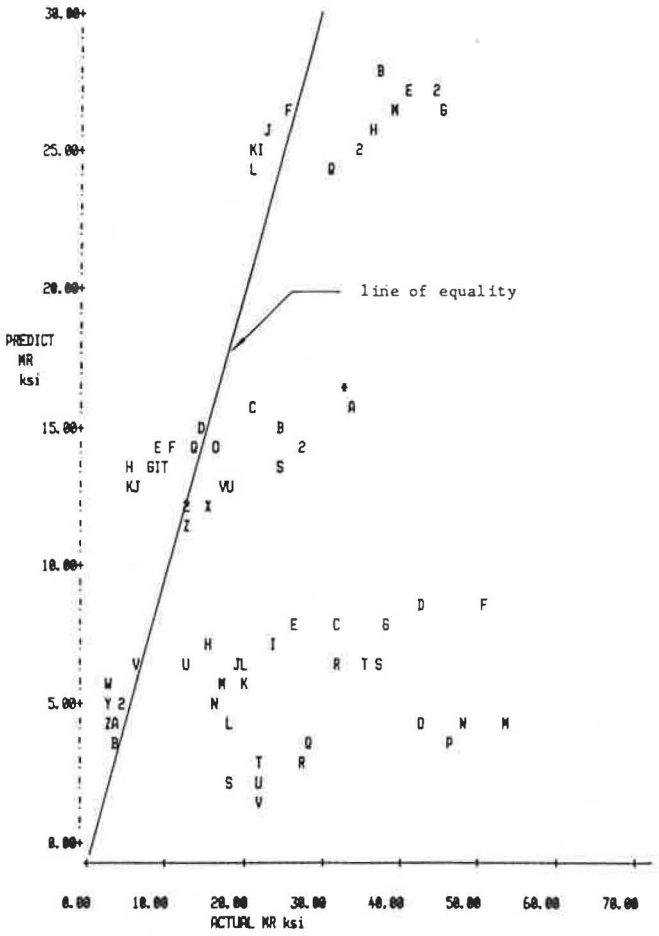

FIGURE 1 Modulus of resilience results from testing of cohesive soils versus predictions from general cohesive equation.

ACKNOWLEDGMENTS

The authors wish to acknowledge the funding and cooperation of the U.S.D.A. Forest Service for this project. The Region 5 laboratory collected soil samples and provided these samples to ARE, Inc., in an expeditious manner. Adrian Pelzner of the Washington

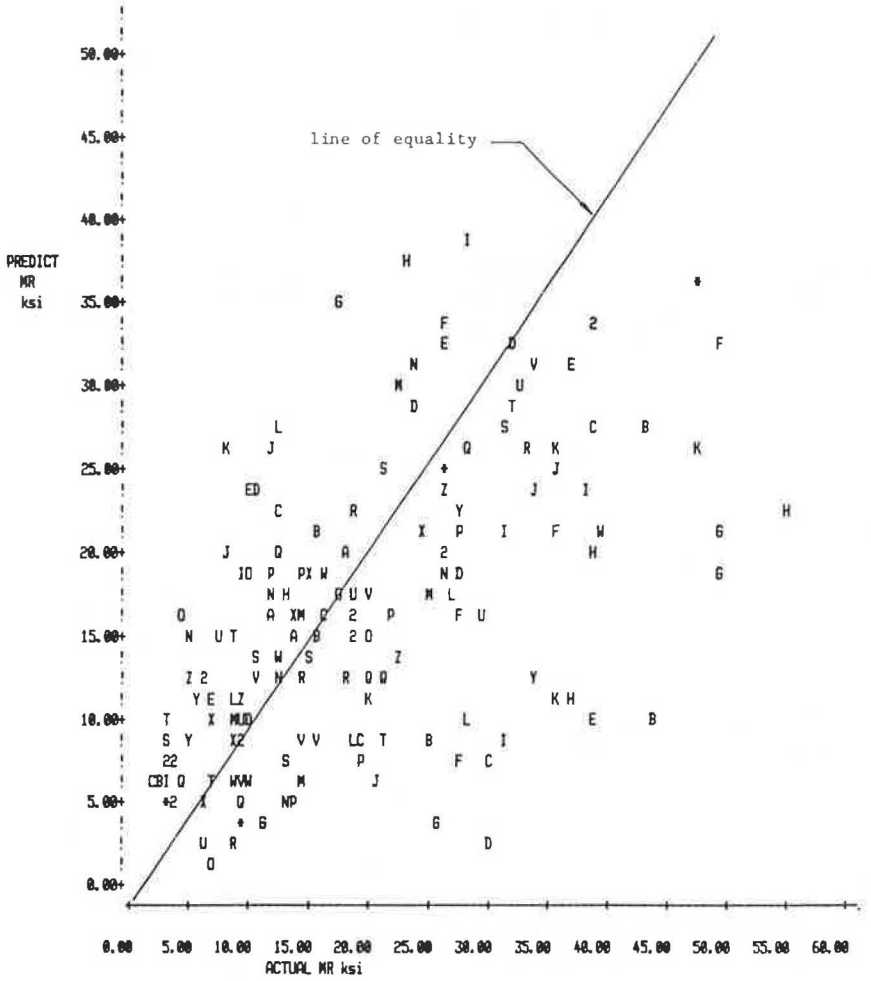

FIGURE 2 Modulus of resilience results from testing of granular soils versus predictions from general equation.

Engineering Staff Unit and Ken Inouye and Frederick Hsia of Region 5 provided the authors with a thorough and helpful review of these results.

REFERENCES

1. T.G. McGarragh and W.R. Hudson. A Pavement Design and Management System for Forest Service Roads--A Conceptual Study. Research Report 12. Council for Advanced Transportation Studies, The University of Texas at Austin, July 1974.
2. F.L. Roberts, B.F. McCullough, H.J. Williamson, and W.R. Wallin. A Pavement Design and Management System for Forest Service Roads--A Working Model. Research Report 43. Council for Advanced Transportation Studies, The University of Texas at Austin, Feb. 1977.
3. B.F. McCullough and D.R. Luhr. A Pavement Design and Management System for Forest Service Roads--Implementation. Research Report 60. Council for Advanced Transportation Studies, The University of Texas at Austin, Jan. 1979.
4. B.F. McCullough and D.R. Luhr. The New Chapter 50 Revisions to the Transportation Engineering Handbook and New Pavement Design and Management System. Draft Report Project FSH 7709.11. Center for Transportation Research, U.S. Department of Transportation; Forest Service, U.S. Department of Agriculture, Junc 1982.
5. Transportation Engineering Handbook, Chapter 50. Forest Service, U.S. Department of Agriculture.
6. U.S. D.A. Forest Service. Forest Service Geotechnical Workshop. EM7170-2. Proceeding of a Conference held in Denver, Colo., June 1982.
7. T.C. Johnson, D.G. Cole, and E.J. Chamberlain. Influence of Freezing and Thawing on the Resilient Properties of Silt and Soil. CRREL Report 78-23. U.S. Army Corps of Engineers, Sept. 1978.

Publication of this paper sponsored by Committee on Strength and Deformation Characteristics of Pavement Sections.

Pavement Response to Road Rater and Axle Loadings

M. C. WANG

ABSTRACT

The response of flexible pavements to 18-kip (80-kN) single axle and Road Rater loadings was investigated. A Benkelman beam was used to measure surface deflection under the axle loading; and a model 400 Road Rater was operated at 25-Hz frequency to monitor pavement deflection. The pavement deflection data were analyzed and the pavement layer moduli were evaluated. The modulus values, in turn, were used to analyze the critical response of the test pavements. Results of the study indicate that, at least for the conditions investigated, summer deflection measurements are as effective as spring season measurements for pavement condition evaluation. The layer modulus values evaluated from the Road Rater deflection basins are not necessarily equal to those obtained from the Benkelman beam deflection basins. Critical pavement response to axle loading can be estimated from the corresponding Road Rater data by using the developed relationships. These relationships and other data may provide a basis for the development of a generally accepted pavement evaluation criterion for use in pavement management programs.

Numerous devices are frequently used to evaluate the structural capacity and to predict the future performance of flexible pavements; these include Benkelman beam, Road Rater, Dynaflect, and falling weight deflectometer, among others. The Benkelman beam was available long before the other devices. Since its development, the Benkelman beam has been widely adopted for pavement evaluation. As a result, a wealth of Benkelman beam deflection data and various evaluation criteria have been developed (1-4). Other devices have also received considerable study, and different deflection criteria for evaluation of pavement performance have been proposed (5-8).

Although various evaluation criteria already exist, a generally accepted one has not yet been available. Primary reasons for this may be that (a) each study was conducted under its specific environmental and pavement conditions and (b) the test loading conditions varied considerably among these studies. In considering loading condition, it should be noted that these various testing devices employ different types of loading for testing. The Benkelman beam uses the actual axle loading, whereas the other devices use loadings that differ considerably among themselves and are smaller than the axle loading.

In the development of a generally accepted evaluation criterion, it is essential to have a fundamental understanding not only of the behavior of pavement response to each type of loading but also of the relationship among the pavement responses to the various loadings. Pavement response to one type of loading with respect to actual axle loading is of particular importance.

This study was undertaken to investigate pavement response to Road Rater and axle loadings. The deflection under axle loading was determined using a Benkelman beam. In this study, the deflection data were used to evaluate the pavement layer moduli, which, in turn, were employed to analyze critical pavement responses including the maximum tensile strain at the bottom of a stabilized base course and the maximum vertical compressive strain at the top of the subgrade. From all of these data, relationships between the Road Rater and the Benkelman beam (axle) loadings were developed for surface deflections, modulus values, and critical strains.

TEST PAVEMENTS AND MATERIALS

This study was conducted as a part of the research project undertaken at the Pennsylvania Transportation Research Facility. The research facility was constructed in 1972 and was composed of 17 test pavements. Of these pavement sections, one section (Section 8) was overlaid and three sections (Sections 10 through 12) were replaced by eight shorter sections in 1975. All pavements were 12 ft (3.7 m) wide.

The subgrade soil was a silty clay that had classifications ranging from A-4 to A-7 according to the AASHO classification and CL according to the unified soil classification. The subbase material was a crushed limestone. The base course materials were bituminous concrete, aggregate cement, aggregate-lime-pozzolan, aggregate bituminous, and crushed stone. In the aggregate-cement base course, three types of aggregate were used--limestone, slag, and gravel. The wearing surface was an ID-2A bituminous concrete.

The traffic on the research facility was provided by a conventional truck tractor pulling a semitrailer and one or two full trailers. A total of about 2.4 million and 1.3 million applications of 18-kip (80-kN) equivalent axle loads (EALs) have been applied to the pavements constructed in 1972 and 1975, respectively. More detailed information on the research facility can be found elsewhere (9).

MAXIMUM SURFACE DEFLECTION

Pavement surface deflections were measured biweekly in the wheelpaths by using a Benkelman beam and a Road Rater. Because spring season deflections are widely used for pavement evaluation, the deflection data obtained during the months of March, April, and May are selected and discussed first. It is neither possible nor necessary to present all of the spring season deflection data; thus, for the purpose of discussion, pavement sections that are more representative of each pavement group (in terms of base course material type) are selected. The pavement sections selected and their base course materials are those of Section 3 (aggregate-lime-pozzolan),

Scotion 5 (aggregate bituminous), Section 7 [bituminous concrete, 8 in. (203 mm) thick], Section 9 [bituminous concrete, 4 in. (102 mm) thick], Section 14 (full-depth bituminous concrete), A (limestone aggregate cement), D (gravel aggregate cement), and E (crushed stone). The maximum Road Rater deflections of these sections are plotted against 18-kip (80-kN) EALs in Figure 1. Note that the Road Rater used is a model 400, which has a vibrating mass of 160 lb (72 kg) and is operated at a frequency of 25 Hz.

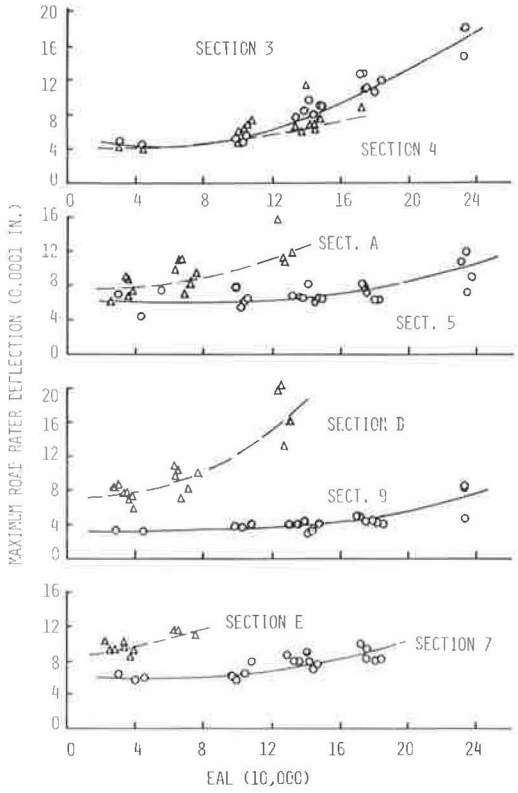

FIGURE 1 Variation of maximum Road Rater spring season deflection with equivalent axle load.

Figure 1 shows, as would be expected, that the maximum Road Rater deflections increase with increasing EAL; the rate of increase differs for different pavement sections. Also, for each pavement, the rate of increase becomes greater in the later stages of pavement service life. The increase in pavement deflection is primarily due to the progressive deterioration of the pavement structure as evidenced by the gradual decrease in the present serviceability index (PSI) of the pavement sections. The PSI data of all of the test pavements are documented in a research report (10) and are also summarized in an earlier paper (9). An attempt was made to establish relationships between the increased deflection and the dropped PSI; however, no apparent correlation between the two was found.

The maximum Benkelman beam deflections also increase with EAL in a manner similar to that of the maximum Road Rater deflections. Again, no correlation between the increase in deflection and the drop in PSI was found for Benkelman beam deflections.

The maximum Benkelman beam and Road Rater deflections are correlated in Figure 2, in which there are 137 data points for pavements with bituminous concrete base and 52 data points for other pavements.

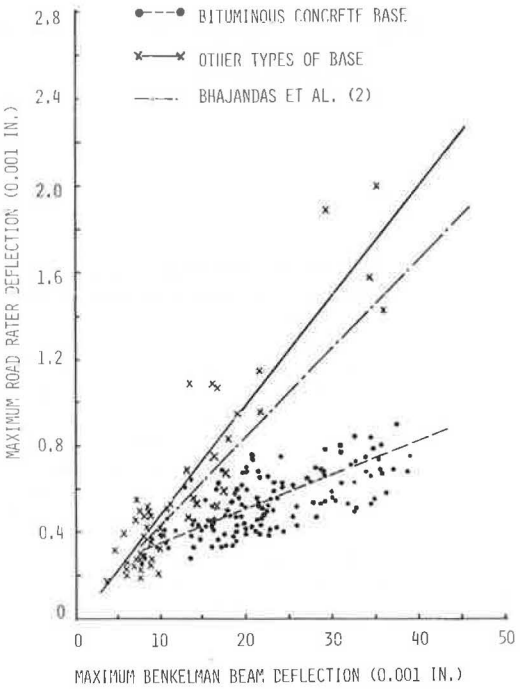

FIGURE 2 Correlations between maximum Road Rater and Benkelman beam deflections.

The correlation analysis was performed using the SAS computer program (11). Both linear and nonlinear relationships were considered in the analysis. It is interesting to note that the data points for pavements with bituminous concrete base form a distinct group and are located below the data points for other base course materials. Results of the analysis yield the following equations:

$$RRD = 0.15 + 0.018\ BBD \quad (1)$$

with $R^2 = 0.669$ and $\bar{R}^2 = 0.665$ for pavements containing bituminous concrete base courses, and

$$RRD = -0.04 + 0.051\ BBD \quad (2)$$

with $R^2 = 0.849$ and $\bar{R}^2 = 0.846$ for pavements containing other types of base course materials. In Equations 1 and 2, RRD designates Road Rater deflections and BBD stands for Benkelman beam deflections, both in units of 10^{-3} in., R^2 is the coefficient of determination, and $\bar{R}^2$ is the adjusted coefficient of determination for degree of freedom.

The trend of correlation shown in Figure 2 is quite clear. Due to the wide scatter of data points, however, the values of R^2 and $\bar{R}^2$ are low especially for the bituminous concrete pavements. The correlations indicate that when the deflection is large, the Road Rater deflection corresponding to a given Benkelman beam deflection is considerably smaller for pavements with bituminous concrete bases than for pavements with other types of base course materials. Although this could possibly be due to a viscous damping effect of the bituminous concrete under the vibratory Road Rater loading, exact causes for this effect are not clearly understood. The available correlation developed by Bhajandas et al. (5) between Road Rater deflections, which were determined at 25-Hz frequency, and Benkelman beam deflections is also included in Figure 2. Note that their correlation was developed on the basis of only 52

samples and no indication of the type of base course materials in the pavements was given. Their correlation is shown bracketed between the two developed in this study.

SURFACE DEFLECTION BASIN

Because of the seasonal change in pavement temperature and subgrade moisture content, it is expected that pavement deflections will vary with the seasons. Due to the low pavement temperature and subgrade moisture content in the winter, winter deflections are the smallest. However, the spring season deflections are not necessarily the largest as generally thought. A comparison of spring and summer Road Rater deflection basins is shown in Figure 3 and given in Table 1. The deflection basins are presented in terms of the readings at Sensors 1 (S_1, maximum deflection) and 4 (S_4), surface curvature index (SCI, which is the difference in readings between Sensors 1 and 2), and base curvature index (BCI, which is equal to $S_3 - S_4$). The ratio between the spring and the summer data is plotted against the spring data. The figure shows that for 15 of the 16 pavement sections containing bituminous concrete base course, S_1 values obtained in the spring (March, April, and May) are smaller than those determined in the summer (June, July, and August); this is in agreement with the findings of the AASHO Road Test (3). For other pavement sections, however, the spring season deflections are approximately equal to the summer data. The values of S_4 are greater in the spring than in the summer for the majority of the pavement sections regardless of the type of base course material. It also appears that the ratio of S_4 readings between spring and summer increases with increasing spring season values. The figure also shows that the SCI data generally follow the trend of S_1 data, whereas the BCI data resemble S_4 data.

The smaller S_1 values in the spring than in the summer for bituminous concrete pavements can be attributed to lower pavement temperature in the spring. Because bituminous concrete is temperature dependent, the higher pavement temperature in the summer decreases the material stiffness. As a result, the summer deflections are greater than those of the spring. Although the stiffness of the base course affects S_1 deflection greatly, its effect on S_4 deflection is not as great. Available information (12) has shown that S_4 deflection is influenced most by subgrade condition. Generally speaking, the softer the subgrade is, the greater the S_4 deflection will be. For the test pavements, the subgrade moisture content is significantly higher in the spring (approximately 20 percent) than in the summer (about 18 percent). Because the stiffness of the subgrade decreases with increasing moisture content, the greater moisture content in the spring will result in a lower subgrade stiffness. As a consequence, the S_4 deflections are greater in the spring than in the summer. Figure 3 also shows that the effect of pavement temperature on SCI is as significant as that of S_1. However, BCI values are less sensitive to subgrade moisture variation than are S_4 values.

Table 2 gives the ratio of spring to fall deflection data. The data indicate that a great majority of the ratios are greater than unity, which indicates that spring season deflections are greater than those in the fall. Because the pavement temperature in the fall is close to that in the spring, the greater deflection observed in the spring can be attributed to the higher subgrade moisture content.

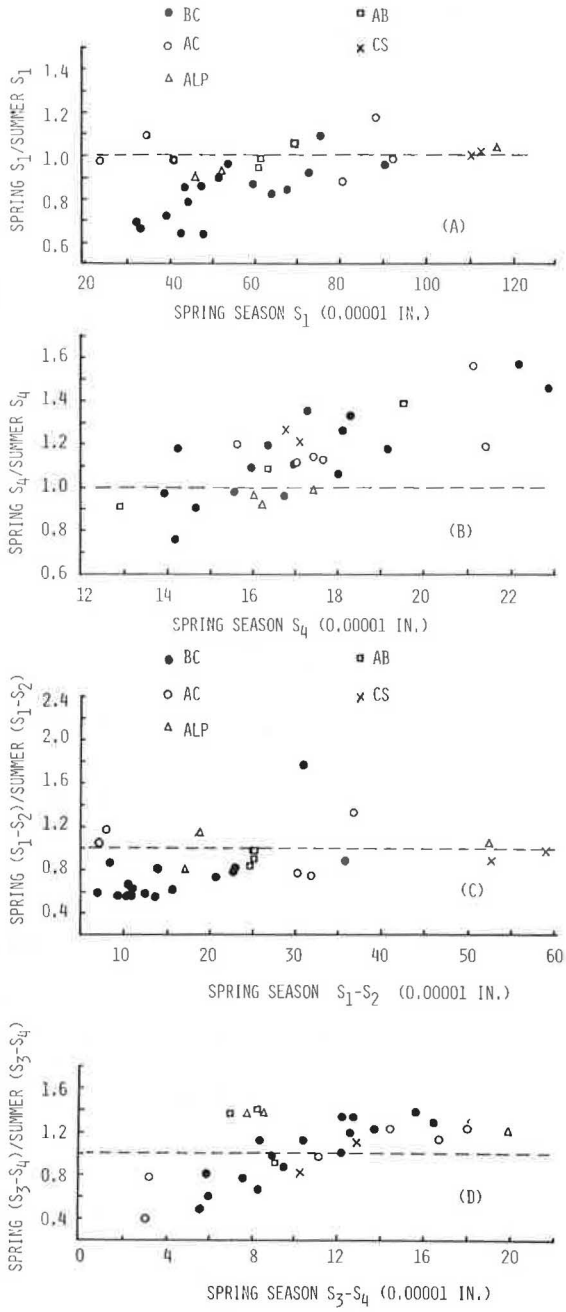

FIGURE 3 Average Road Rater deflections in spring and summer.

The available subgrade moisture data show that the moisture contents in the spring and fall are approximately 20 and 17 percent, respectively.

The maximum Benkelman beam deflection data show a similar trend of variation with seasons, but the difference between seasons is not as great as that of Road Rater deflection data. According to these observations, the deflection data obtained in the summer, which are greater than the spring season deflections, could be more effective for evaluation of fatigue life of bituminous concrete pavements. A primary reason for this is that, in the summer, the higher pavement temperature decreases the stiffness of bituminous concrete and therefore increases the tensile strain at the bottom of the bituminous con-

TABLE 1 Average Road Rater Deflection Data

Section No.	Base Course Material[a]	S_1			S_4			$S_1 - S_2$			$S_3 - S_4$		
		Sp[b]	Sp/Su[c]	Sp/F[d]	Sp	Sp/Su	Sp/F	Sp	Sp/Su	Sp/F	Sp	Sp/Su	Sp/F
1B	BC	44.24	0.78	0.99	17.28	1.36	1.11	11.02	0.63	1.11	10.42	1.12	1.41
		51.37	0.89	1.13	15.94	1.10	0.97	12.40	0.59	1.24	12.59	1.19	1.76
1C		42.70	0.63	0.90	18.00	1.06	1.07	10.44	0.56	0.91	9.51	0.87	1.33
		59.32	0.86	1.08	18.12	1.26	1.05	15.56	0.61	1.18	13.78	1.22	1.52
1D		47.96	0.62	0.92	19.16	1.18	1.25	13.54	0.55	0.89	8.25	0.66	1.11
		72.97	0.92	1.18	16.93	1.11	1.08	22.77	0.77	1.25	16.42	1.30	1.53
2		39.01	0.71	1.06	16.31	1.20	1.14	10.51	0.67	1.30	7.59	0.77	1.23
		53.69	0.96	1.31	18.51	1.33	1.11	13.89	0.82	1.86	12.19	1.01	2.17
6		31.77	0.69	1.03	16.71	0.95	1.05	8.33	0.85	1.69	5.86	0.81	1.26
		43.51	0.85	1.22	22.18	1.57	0.84	9.24	0.56	2.07	5.58	0.49	1.13
7		32.81	0.66	0.91	14.62	0.90	0.88	6.92	0.57	0.97	8.38	1.10	1.58
		47.50	0.85	1.13	22.89	1.45	1.24	10.95	0.56	1.29	5.97	0.60	1.18
8		67.25	0.83	1.00	13.89	0.97	0.91	23.22	0.84	0.97	12.22	1.34	1.40
		75.73	1.09		14.13	0.76		30.94	1.78		9.04	0.99	
9		60.70	0.81	1.05	14.20	1.18	1.02	20.62	0.74	0.97	12.70	1.34	1.82
		90.08	0.95	1.16	15.56	0.98	0.97	35.68	0.88	1.19	15.61	1.40	1.73
4	AC	23.13	0.97	0.87	15.61	1.20	1.05	7.50	2.12	1.57	3.20	0.78	0.89
		34.09	1.09	1.25	21.09	1.56	1.17	7.78	1.17	3.93	3.05	0.40	2.75
A		94.29	0.98	1.03	21.43	1.18	0.88	30.25	0.77	1.17	17.94	1.23	1.11
B		40.42	0.97	1.15	17.05	1.11	0.88	7.11	1.04	2.84	11.08	0.97	2.00
C		80.81	0.87	0.90	17.42	1.14	1.02	31.78	0.75	0.76	14.41	1.23	1.87
D		88.95	1.18	1.39	17.64	1.12	0.89	36.83	1.34	2.14	16.68	1.14	1.43
3	ALP	46.05	0.89	1.06	16.20	0.92	1.05	18.56	1.14	1.32	8.58	1.38	1.50
		52.14	0.93		16.07	0.96		17.18	0.80		7.76	1.36	
		116.52	1.04	1.35	17.46	0.99	0.81	52.33	1.04	1.87	19.93	1.21	1.38
5	AB	60.95	0.93	1.20	16.31	1.09	1.16	25.53	0.92	1.54	6.87	1.35	1.00
		61.05	0.98		12.87	0.90		24.85	0.86		8.24	1.40	
		69.32	1.05	1.42	19.51	1.38	1.21	25.09	0.96	2.23	9.16	0.94	1.22
E	CS	110.58	1.00	1.14	17.11	1.21	1.19	58.85	0.98	1.33	10.29	0.84	1.21
		112.55	1.02	1.21	16.77	1.27	1.17	52.70	0.90	1.25	12.92	1.11	1.40

[a] Base course materials: BC = bituminous concrete, AC = aggregate cement, ALP = aggregate-lime-pozzolan, AB = aggregate bituminous, CS = crushed stone.
[b] Sp = deflection data obtained in spring season in units of 10^{-5} in.
[c] Sp/Su = ratio of spring season to summer data.
[d] Sp/F = ratio of spring season to fall data.

TABLE 2 Layer Modulus Computed from Spring Season Road Rater Deflection Basins

Section No.	Layer Thickness[a] (in.)	Base Course Material[b]	EAL (10^6)	Layer Modulus (10^3 psi)			
				Surface	Base	Subbase	Subgrade
1C	1.5–6–8	BC	1.4	730	899	31	21
			1.8	708	952	36	24
			2.3	811	879	34	22
1D	1.5–6–6	BC	1.4	536	794	32	22
			1.8	480	544	31	36
			2.3	811	879	34	22
2	2.5–6–8	BC	1.4	774	809	42	25
			1.8	742	951	39	28
			2.3	940	902	38	23
7	1.5–8–8	BC	1.0	837	964	38	21
			1.4	664	740	34	28
			1.8	841	873	41	23
			2.3	647	768	43	26
9	2.5–4–8	BC	0.3	643	798	15	28
			1.4	443	619	16	29
			1.8	596	732	18	24
			2.3	538	509	14	21
3	2.5–8–8	ALP	0.3	200	500	100	34
			1.4	50	150	35	28
5	2.5–8–8	AB	0.3	150	100	117	35
A	2.5–4–8	AC	0.3	100	2,830	50	21
			0.6	60	1,455	60	21
			0.9	80	800	45	20
			1.3	20	100	40	20
C	2.5–6–8	AC	0.3	100	1,000	30	32
			0.6	300	470	22	32
			0.9	26	168	15	28
D	2.5–6–6	AC	0.3	300	504	15	30
			0.6	300	212	19	28
			0.9	70	100	18	26
			1.3	20	40	11	24
E	2.5–8–8	CS	0.3	220	45	30	40
			0.6	800	36	27	31
			0.9	500	45	24	26

[a] Thicknesses of surface, base, and subbase courses, respectively.
[b] Base course materials: BC = bituminous concrete, AC = aggregate cement, AB = aggregate bituminous, ALP = aggregate-lime-pozzolan, CS = crushed stone.

crete base. Because tensile strain is related to fatigue cracking in a power function, it is often used to evaluate the fatigue life of pavement structures.

For maximum surface deflection, the deflection basin also varies with EAL. The general trend of Road Rater deflection basin variation with EAL is shown in Figure 4. Figure 4 shows the Road Rater deflection basins at three levels of EAL for pavement Sections 3 and 5. It is seen that as EAL increases, the deflection basin becomes deeper and narrower, and the radius of curvature at the loading point becomes smaller. For the Benkelman beam deflections, the trend of deflection basin variation with EAL is not as well defined as is that for the Road Rater deflection basins. This is probably because the accuracy of Benkelman beam readings is not as high as that of the Road Rater readings. Note that the Benkelman beam readings were taken with a dial gauge, whereas the Road Rater readings were monitored using accelerometers.

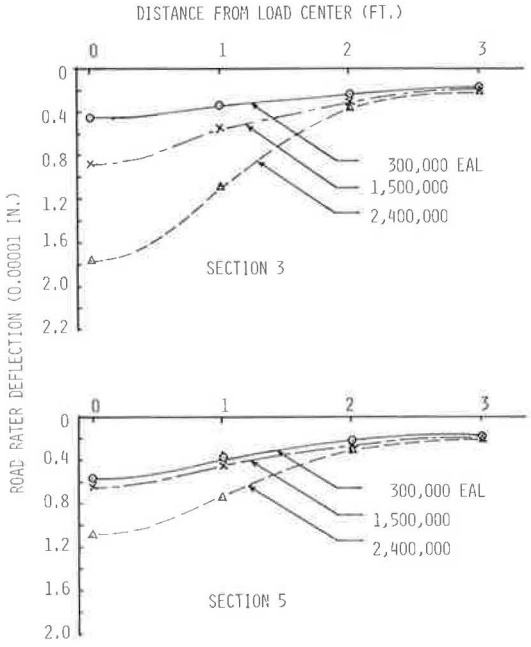

FIGURE 4 Road Rater deflection basins for Sections 3 and 5.

PAVEMENT LAYER MODULUS

The spring season deflection basin data were used to evaluate the modulus of each constituent pavement layer. The evaluation was made by using the computer program that was developed earlier based on the method of successive iteration (12,13). It should be noted that, for modulus evaluation, each of the four sensor readings of the Road Rater was plotted against EAL and smooth curves were drawn through the data points. From these curves, the deflection data at a desired level of EAL were read to obtain deflection basins for use as input to the computer program. In the computer analysis, the Poisson's ratios used were 0.45, 0.35, and 0.45 for the bituminous concrete surface, crushed limestone subbase, and silty clay subgrade, respectively; and 0.35, 0.30, 0.20, and 0.15 for the bituminous concrete, aggregate bituminous, aggregate cement, and aggregate-lime-pozzolan base courses, respectively. Also, the 4- x 7-in. (10.2- x 17.8-cm) loading plates of the Road Rater were approximated by two circular areas spaced 10.5 in. (26.7 cm) apart center to center; each has a 3-in. (7.6-cm) radius. The contact pressure under each plate is 13 psi (89.6 kPa).

For the Road Rater deflection basins thus obtained, layer modulus values at different EALs were evaluated for most of the test pavements and the results of evaluation are summarized in Table 2. The data in the table indicate that a great majority of the subgrade modulus values fall within 20,000 and 30,000 psi (138 and 207 MPa) with few fluctuating between 30,000 and 40,000 psi (207 and 276 MPa). This type of fluctuation is as would be expected; primary reasons are that (a) the subgrade material may not be uniform in terms of its soil composition and compaction conditions (including moisture content and dry density) throughout the entire test pavements and (b) it is difficult to obtain theoretical deflection basins (the basins computed from the theory of elasticity) that will fit perfectly to the measured deflection basins because of possible nonuniformity in pavement materials and layer thickness. Recall that the evaluation of modulus employed the procedure of successive iteration for which a set of layer moduli must first be assumed to compute deflection basins. The computed deflection basin is then compared with the measured one and the difference, if any, between the two deflection basins serves as the basis for adjusting the assumed modulus values. The adjustment is made by using the successive iteration procedure until the difference between the two deflections is less than 10 percent of the measured values.

Except for pavement Sections 3 and 5, the modulus of the subbase course of each pavement varies within a narrow range. Specifically, the subbase modulus fluctuates between 31,000 and 43,000 psi (214 and 297 MPa) for Sections 1C, 1D, 2, and 7; between 14,000 and 18,000 psi (97 and 124 MPa) for Section 9; between 40,000 and 60,000 psi (276 and 414 MPa) for Section A; between 15,000 and 30,000 psi (103 and 207 MPa) for Section C; between 11,000 and 19,000 psi (76 and 131 MPa) for Section D; and between 24,000 and 30,000 psi (166 and 207 MPa) for Section E. When the previously mentioned factors, which could possibly cause modulus variation, are considered, this range of variation in each section can be considered normal. However, for Section 3, the difference between the highest and the lowest values is as much as threefold. Also, the highest subbase modulus values for Sections 3 and 5 are considerably greater than those of other sections. This is rather unexpected and possible causes of this wide variation are not yet fully understood. One interesting trend of variation is that the subbase modulus appears to decrease with EALs for some sections (2, 3, C, and E). The data also show that the overall range of subbase modulus values is considerably broader than that of subgrade modulus values. There is no trend indicating how the subbase modulus variation is related to the type of base course material, however.

For the pavements containing bituminous concrete base course (Sections 1C, 1D, 2, 7, and 9), both the surface and the base course moduli fluctuate within an expected range. There is no apparent trend of variation of layer modulus with layer thickness. For other sections, except Sections 5 and E, the base course modulus decreases with EAL. The decrease in the base course modulus could possibly be attributed to progressive deterioration of the base course with traffic volume. The surface course modulus of these sections fluctuates randomly without a definite pattern. The data on Sections 3, A, and C indicate, as expected, that the aggregate-lime-pozzolan base, limestone aggregate cement base, and slag aggregate cement base courses have considerably greater moduli than does the bituminous concrete surface course.

TABLE 3 Layer Modulus Computed from Spring Season Benkelman Beam Deflection Basins

Section No.	Layer Thickness (in.)[a]	Base Course Material[b]	EAL (10^6)	Layer Modulus (10^3 psi)			
				Surface	Base	Subbase	Subgrade
1C	1.5–6–8	BC	1.4	25	300	10	29
1D	1.5–6–6	BC	1.4	20	100	8	21
2	2.5–6–8	BC	1.4	30	400	10	32
6	2.5–8–8	BC	1.4	40	300	10	28
7	1.5–8–8	BC	1.4	50	200	12	33
9	2.5–4–8	BC	1.4	50	200	10	20
3	2.5–8–8	ALP	1.4	85	100	18	20
5	2.5–8–8	AB	1.4	75	60	14	34
4	2.5–8–8	AC	1.4	500	750	16	58
A	2.5–4–8	AC	0.3	220	2,000	14	48
B	2.5–6–8	AC	0.3	500	1,000	10	51
C	2.5–6–8	AC	0.3	50	450	12	30
D	2.5–6–8	AC	0.3	150	500	12	49
E	2.5–8–8	CS	0.3	55	30	12	49

[a] Thickness of surface, base, and subbase courses, respectively.
[b] Base course materials: BC = bituminous concrete, AC = aggregate cement, AB = aggregate bituminous, ALP = aggregate-lime-pozzolan, CS = crushed stone.

Furthermore, the gravel base course has a smaller modulus than does the bituminous concrete surface, as indicated by Section E. Comparison of the modulus of the gravel base with that of the limestone subbase in Section E indicates that the base course material is slightly stiffer than the subbase course. This is as would be expected because the Road Rater loading induces greater confining pressures in the base course than in the subbase; the greater confinement causes higher stiffness for the gravel material.

For the Benkelman beam deflections, because fewer deflection basins are available and also because the variation of deflection basins with EAL is not as well defined as that of the Road Rater deflections, the analysis of layer modulus is made for only one level of EAL, which is 0.3 million for Sections A, B, C, D, and E and 1.4 million for the other sections. The deflection basins obtained at and near this level of EAL are averaged; for each averaged deflection basin, the deflection values at four locations--at the center of the dual loading tires and at 1, 3, and 5 ft (0.3, 0.9, and 1.5 m) off the center--are used as input to the computer program. The analysis is made for 18-kip (80-kN) single axle loading with dual tires each having 80 psi (552 kPa) tire pressure. Results of the analysis are summarized in Table 3.

The data in Table 3 show that both subgrade and subbase modulus values fluctuate without a definite pattern with respect to type of base course material. For each type of base course material, the base course modulus varies within a reasonable range. The modulus of surface course, which has the same material for all test pavements, appears to be smaller for pavements that contain a bituminous concrete base course. Reasons for this effect are not yet known.

For comparison of the modulus values evaluated from the Benkelman beam and the Road Rater deflection basins, the ratio between the two sets of values is plotted against the values obtained from the Road Rater deflections in Figure 5. Because the difference between the two sets of surface moduli is somewhat erratic, it is not included in the figure. Figure 5 demonstrates that the ratio of the two sets of subgrade modulus values fluctuates around unity, indicating that regardless of the type of base course material, the Benkelman beam and the Road Rater deflection basins give practically the same subgrade modulus. For the subbase modulus, however, the values obtained from Benkelman beam deflections

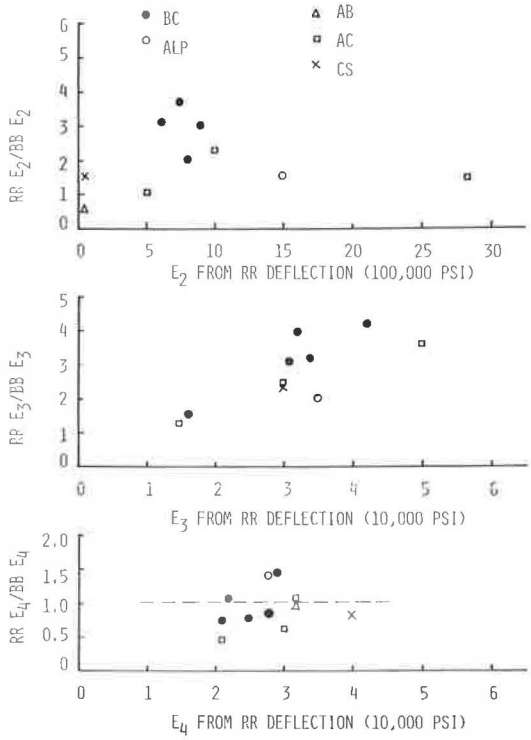

FIGURE 5 Ratio of layer modulus between Road Rater and Benkelman beam loadings.

are considerably lower especially for pavements containing a bituminous concrete base course. The difference between the two sets of base course moduli is not as great as is that for the subbase modulus. It appears that the modulus of bituminous concrete base computed from the Road Rater deflections is significantly higher than that computed from the Benkelman deflections, whereas the modulus of other base course materials is practically the same. Reasons for the observed modulus variations are not yet available. Additional study is needed to better understand the behavior of modulus variation.

The resilient modulus of each constituent pavement material was determined from laboratory repeated load tests on specimens 6 in. (152 mm) in diameter. The laboratory testing was conducted at a

room temperature of about 70°F (21°C). The test specimens for the surface, base, and subbase materials were prepared in the laboratory to the same composition and density as those in the field. For the subgrade soil, both undisturbed and remolded specimens were tested.

The repeated load had a frequency of 20 cycles per minute and a duration of 0.1 sec. The stationary confining pressure and cyclic deviatoric pressure used in the testing are given in Table 4. For each test condition, a minimum of three tests were performed. Resilient modulus values obtained from the laboratory testing are summarized in Table 5. Also included in Table 5 for comparison are the range and average values of layer modulus obtained from Tables 2 and 3.

TABLE 4 Confining and Deviatoric Pressures Used in Laboratory Repair Load Test

Test Material	Confining Pressure (psi)	Deviatoric Pressure (psi)
Surface	20, 30, and 40	10, 30, and 50
Base	10, 20, and 30	10, 25, and 40
Subbase	10 and 20	10, 20, and 30
Subgrade	5 and 10	5, 10, and 20

The data in Table 5 indicate that for the bituminous concrete surface, bituminous concrete base, and aggregate bituminous base course materials, the resilient modulus is practically equal to the layer modulus obtained from Benkelman beam deflection basins. The resilient modulus values for other base course materials are considerably greater than the layer modulus values. Also, the resilient modulus values are slightly greater for the limestone subbase and smaller for the silty clay subgrade compared with the layer modulus values. Although a slight difference between the two different sets of moduli can be expected, possible reasons for resilient modulus larger than layer modulus for one and smaller for the other are yet to be investigated.

Critical Pavement Response

The modulus values were used to analyze critical responses of the test pavements subjected to 18-kip (80-kN) single axle (Benkelman beam) loading and Road Rater loading. The analysis was made using the bituminous structures analysis in roads (BISAR) computer program; the critical responses analyzed included the maximum tensile strain at the bottom of a stabilized base course or maximum tensile strain at the bottom of a surface course for the pavement section containing crushed stone base course, and the maximum vertical compressive strain on top of the subgrade.

Because there are more data on the variation of Road Rater deflection basins with EAL, the maximum tensile strain (ε_t) at the bottom of a stabilized course (surface course for Section E and base course for other sections) and the maximum vertical compressive strain (ε_v) at the top of a subgrade are analyzed for the Road Rater deflection basins selected at different levels of EAL. Some of the results of the analysis are shown in Figures 6 and 7, which show the variation of vertical compressive

TABLE 5 Resilient Modulus and Layer Modulus

				Layer Modulus[a] (10^3 psi) from			
		Resilient Modulus (10^3 psi)		Road Rater Deflection		Benkelman Beam Deflection	
Layer	Material	Range	Average	Range	Average	Range	Average
Surface	Bituminous concrete	85–200	140	20–837	442	20–500	132
Base	Bituminous concrete	250–450	320	509–064	801	100–400	250
	Limestone aggregate cement	3,000–4,500	3,600	100–2,830	1,296	750–2,000	1,250
	Slag aggregate cement	2,500–4,000	3,200	168–1,000	546		450
	Gravel aggregate cement	2,000–3,800	2,500	40–504	214		500
	Aggregate-lime-pozzolan	1,500–3,500	2,400	150–500	325		100
	Aggregate bituminous	58–200	100		100		60
Subbase	Crushed limestone	42–64	48	11–117	35	8–18	12
Subgrade	Silty clay	6–20	8	20–40	26	20–58	36

[a]Values obtained from Tables 2 and 3.

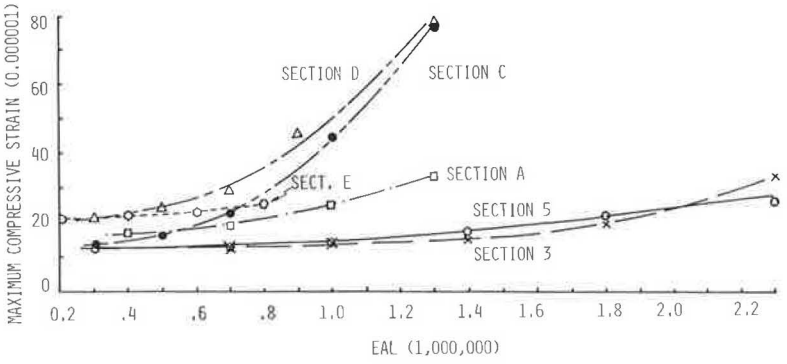

FIGURE 6 Variation of maximum vertical compressive strain at top of subgrade with EAL for Road Rater loading.

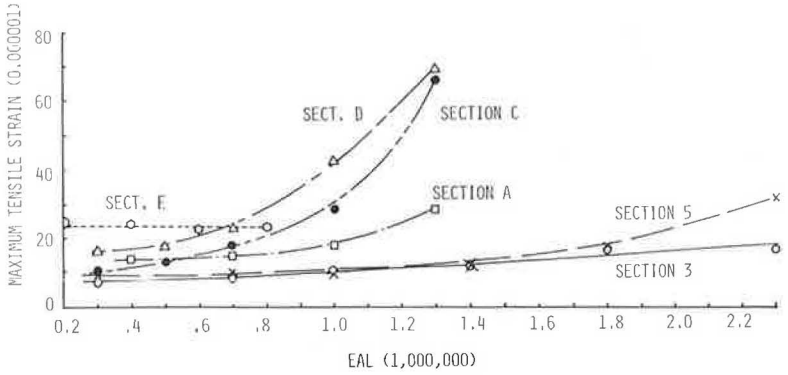

FIGURE 7 Variation of maximum horizontal tensile strain at bottom of stabilized course with EAL for Road Rater loading.

strain and horizontal tensile strain, respectively, with EAL. It is seen that, for most pavement sections, both strains increase with increasing EAL. The shape of the curve, generally speaking, follows that of the maximum surface deflection (Figure 1) except for Sections 3 and E. For Section 3, the rate of increase in strains is not as pronounced as is that of the surface deflection; and for Section E, the strains remain essentially constant throughout the entire range of EAL.

In addition to the results shown previously, each of the analyzed strain values is shown in Figure 8 in terms of the ratios between the two values, one obtained from the Benkelman beam and the other from the Road Rater ($BB\varepsilon_t/RR\varepsilon_t$ and $BB\varepsilon_v/RR\varepsilon_v$). The figure demonstrates that the ratio of maximum tensile strain ($BB\varepsilon_t/RR\varepsilon_t$) fluctuates around 20.0 for the data points of pavements containing bituminous concrete base courses and around 15.0 for the data points of the other types of base course materials. For the maximum vertical compressive strain, the ratio $BB\varepsilon_v/RR\varepsilon_v$ fluctuates around 10.0 regardless of the type of base course materials.

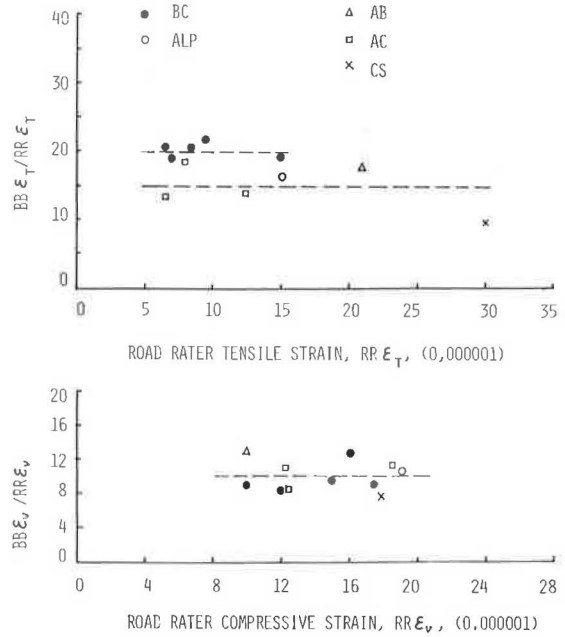

FIGURE 8 Ratio of critical strains between Road Rater and Benkelman beam loadings.

The results of computer analyses, which were discussed in an earlier report (14), indicated that for both maximum tensile and maximum vertical compressive strains, the values for Benkelman beam loading are 12.5 times those that occur under the Road Rater loading. It should be noted that the analysis was made for pavements containing bituminous concrete base courses only. Furthermore, in the analysis, the surface and base courses were treated as one layer, and the modulus values of the pavement layers were estimated on the basis of maximum surface deflection without consideration of the entire deflection basin. Because of these limitations, the current values of 20.0, 15.0, and 10.0 should be closer to the actual values and therefore should be more useful for practical applications.

SUMMARY AND CONCLUSIONS

The response of flexible pavements to two different types of loading--18-kip (80-kN) single axle and Road Rater loadings--was analyzed. The pavement response to the single axle loading on dual tires was measured using a Benkelman beam. The Road Rater used was a model 400, which was operated at 25-Hz loading frequency. The flexible pavements investigated contained different types of base courses including bituminous concrete, aggregate bituminous, aggregate cement, aggregate-lime-pozzolan, and crushed stone.

Pavement surface deflections obtained from these two types of loadings were analyzed; factors considered in the analysis were weather, base course materials, and cumulative axle load application. Also, the surface deflection basins were used to evaluate layer moduli, which in turn were used to analyze the maximum tensile strain at the bottom of the stabilized base course or at the bottom of the surface course of pavements without stabilized base courses and the maximum vertical compressive strain at the top of the subgrade.

Results of the analysis indicate that, for the conditions studied, spring season deflections are not necessarily the largest, as is generally thought, especially for pavements with bituminous concrete base courses. For other pavements, the spring season deflections are approximately equal to the summer data. For the spring season deflection data, the maximum surface deflection, maximum horizontal tensile strain, and maximum vertical compressive strain increase with increasing cumulative axle load applications as would be expected. From the results of the analysis, relationships between Road Rater and single axle loadings were established for layer modulus, maximum surface deflection, maximum

tensile strain, and maximum vertical compressive strain.

On the basis of the results of this study, it may be concluded that, at least for the conditions investigated, summer deflection measurements are as effective as, if not more so than, spring season deflection measurements for evaluation of pavement condition. The layer modulus values evaluated from the Road Rater deflection basins are practically the same as those obtained from the Benkelman beam deflection basins for the subgrade and base course materials. The subbase modulus obtained from the Road Rater deflection basins is considerably higher than that evaluated from the Benkelman beam deflection basins. For the surface course material, however, no definite trend in the relative magnitude between the two sets of layer modulus values is found. Furthermore, the resilient modulus obtained from the laboratory repeated load test is reasonably close to the layer modulus for most pavement layers except for aggregate cement and aggregate-lime-pozzolan base courses. For these base course materials, the resilient modulus is considerably greater than the layer modulus. Under 18-kip (80-kN) single axle loading, the maximum surface deflection, maximum horizontal tensile strain, and maximum vertical compressive strain can be estimated from the corresponding values caused by the Road Rater loading by using the developed relationships. These relationships and other data may provide a useful basis for the development of a generally accepted pavement evaluation criterion for use in pavement management programs.

REFERENCES

1. Proc., 41st Convention. Canadian Good Roads Association, 1960.
2. The AASHO Road Test: Part 2--Test Data, Analyses and Findings. HRB Special Report 22. HRB, National Research Council, Washington, D.C., 1955.
3. The AASHO Road Test: Report 5--Pavement Research. HRB Special Report 61E. HRB, National Research Council, Washington, D.C., 1962.
4. N.W. Lister. Deflection Criteria for Flexible Pavements. Report LR 375. Transport and Road Research Laboratory, Crowthorne, Berkshire, England, 1972.
5. A.C. Bhajandas, G. Cumberledge, and G.L. Hoffman. Flexible Pavement Evaluation and Rehabilitation. Journal of the Transportation Engineering Division, ASCE, Vol. 103, No. TE1, Jan. 1977.
6. M.S. Hoffman and M.R. Thompson. Nondestructive Testing of Flexible Pavements Field Testing Program Summary. Report UILU-ENG-81-2003. Civil Engineering Studies, University of Illinois, Urbana, June 1981.
7. R.C. Koole. Overlay Design Based on Falling Weight Deflectometer Measurements. In Transportation Research Record 700, TRB, National Research Council, Washington, D.C., pp. 59-72.
8. G.W. Sharpe, H.F. Southgate, and R.C. Deen. Dynamic Pavement Deflections. Journal of the Transportation Engineering Division, ASCE, Vol. 107, No. TE2, March 1981.
9. M.C. Wang. Performance Analysis for Flexible Pavements with Stabilized Base. In Transportation Research Record 888, TRB, National Research Council, Washington, D.C., 1982, pp. 70-76.
10. W.P. Kilareski, B. Anani, R.P. Anderson, M.C. Wang, and T.D. Larson. Remaining Life and Overlay Thickness Design for Modified Flexible Pavements. Interim Report PTI 7905. Pennsylvania Transportation Institute, Pennsylvania State University, University Park, Jan. 1979.
11. SAS User's Guide: Statistics. SAS Institute, Inc., Cary, N.C., 1982.
12. M.C. Wang and B.A. Anani. Evaluation of in situ Elastic Moduli from Road Rater Deflection Basin. In Transportation Research Record 810, TRB, National Research Council, Washington, D.C., 1981, pp. 54-57.
13. B.A. Anani. An Evaluation of In Situ Elastic Moduli from Surface Deflection Basins of Multilayer Flexible Pavements. Ph.D. dissertation. Pennsylvania State University, University Park, 1979.
14. M.C. Wang, T.D. Larson, A.C. Bhajandas, and G. Cumberledge. Use of Road Rater Deflections in Pavement Evaluations. In Transportation Research Record 666, TRB, National Research Council, Washington, D.C., 1978, pp. 32-39.

Publication of this paper sponsored by Committee on Strength and Deformation Characteristics of Pavement Sections.